Environmental and genetic correlates of neuropsychiatric diseases and the role of erythropoietin/hypoxia in the brain as potential treatment targets

DISSERTATION

for the award of the degree
Doctor rerum naturalium (Dr. rer. nat.)
of the Georg-August-Universität Göttingen

within the doctoral progam Neurosciences
of the Georg-August University School of Science (GAUSS)

submitted by

Agnes STEIXNER-KUMAR

born in Rum, Austria

Göttingen 2021

Doctoral thesis committee

Prof. Dr. Dr. Hannelore Ehrenreich (1st referee)
Clinical Neuroscience
Max Planck Institute of Experimental Medicine, Göttingen

Prof. Dr. Susann Boretius (2nd referee)
Functional Imaging Laboratory
German Primate Center, Göttingen

Prof. Dr. Klaus-Armin Nave
Department of Neurogenetics
Max Planck Institute of Experimental Medicine, Göttingen

Prof. Dr. Walter Paulus
Dept. of Clinical Neurophysiology
University Medical Center Göttingen

Members of the examination board

Prof. Dr. Dörthe Katschinski
Institute for Cardiovascular Physiology
University Medical Center Göttingen

Prof. Dr. Tiago Fleming Outeiro
Department of Experimental Neurodegeneration
University Medical Center Göttingen

Date of submission of thesis: 12.04.2021
Date of oral examination: 07.06.2021

"Our ambition should be to rule ourselves, the true kingdom for each one of us; and true progress is to know more, and be more, and to do more."

- Oscar Wilde

Acknowledgements

I am sincerely grateful for the guidance, mentoring, encouragement and support I received from my supervisor Prof. Dr. Dr. Hannelore Ehrenreich. Her constructive criticism and readiness to discuss projects at any stage, helped me to continuously improve my scientific work and to develop further as an academic researcher.

I also would like to thank the members of my thesis committee, who helped me shape my research projects and who always provided helpful feedback that contributed to my progress. Many thanks also to the members of my extended examination board for taking the time to evaluate my work.

Moreover, lots of thanks to my colleagues in the group, who made my PhD journey much more fun and interesting. It was very enjoyable to collaborate with all of you on various projects. Special thanks goes to Marina, who helped me getting started in this group on a professional and social level. Thanks to literally everyone else in the group, who was there all the way or just some parts of the journey. I learned from all of you and could not have wished for better colleagues.

Thank you also to the IMPRS Neuroscience program that provided me with extensive training and an excellent frame for pursuing my Master's and PhD studies.

A very big "Danke" to my parents, who made all this possible, who never questioned my - sometimes unusual - (study) decisions, and were simply there for me in every possible way and let me become the person I am today. Thanks to my siblings, from whom I have learned a lot and who definitely played a big part in shaping me. I would also like to thank my parents-in-law, who were always supportive and curious to see where my journey is going. And last, but certainly not least, thanks to the man by side, who has been an incredible support in all my endeavors, who believed in me, when I was in doubt, who helps me grow, encourages me to take a step outside my comfort zone and stands by me no matter what.

Simply put: Thanks to all the wonderful people who shared this exciting journey with me!

Contents

Abstract

Neuropsychiatric disorders are relatively frequent and present a considerable burden to affected individuals and society. Disease etiology is often complex and patients exhibit large heterogeneity regarding disease causing factors, presentation and progression. Available treatment options are often ineffective and/or linked to unwanted side-effects. On the other hand, availability of successful preventive actions is limited and requires a detailed study of risk factors for neuropsychiatric disease and its specific symptoms.

The first part of this thesis aimed to investigate environmental and genetic risk factors for polytoxicomania, i.e. multiple drug (ab)use, as a frequent comorbidity of schizophrenia. In a sample of ∼2000 schizophrenia/schizoaffective patients, we addressed the question if the exposure to accumulated environmental risk in early life increases susceptibility to polytoxicomania. Indeed, the accumulation of environmental risk was strongly associated with polytoxicomania throughout life and in particular in pre-adulthood. Moreover, the development of a novel GWAS-PGAS approach led to the identification of 41 common genetic variants potentially conferring risk to preadult polytoxicomania.

The objective of the second part of this thesis work was to further investigate brain-directed effects of hypoxia and erythropoietin (EPO) - a central hypoxia-inducible gene - as potential treatment option for neuropsychiatric disorders. Using a hypoxia reporter mouse line (CAG-CreERT2-ODD::R26R-tdTomato), we showed that both inspiratory hypoxia and motor-cognitive challenge, which causes endogenous hypoxia as a result of extensive neuronal activation (termed "functional hypoxia"), increased the number of hypoxic cells in the brain and the expression of hypoxia-inducible genes in the hippocampus. Interestingly, cell types showed variable responsivity to hypoxia: While neurons and endothelial cells were frequently labelled, hypoxia-labelling in microglia was entirely absent. Technical artifacts explaining this phenomenon were excluded by comparing construct mRNA levels across all cell types. Hexokinase 2 (Hk2) was identified as a mediator of cell type-specific hypoxia responsivity.

In addition, we report rapid effects of EPO on adult neurodifferentiation in the CA1 (6 hours after injection). Enhanced neuronal differentiation continued under EPO treatment, driving immature neurons (*Tbr1+*, *Tle4+* and later *Zbtb20+*) towards maturity, and resulted in ∼20% more neurons in the CA1 after 3 weeks of treatment. Simultaneously, the number of microglia in this region declined by an initial wave of apoptosis, followed by attenuated proliferation. This reduction was necessary for the increase in new neurons. Expression data further indicated that the microglial-neuron balance was maintained by signalling of microglial Colony-Stimulating Factor 1 Receptor (CSF1R) and its neuronally expressed ligand Interleukin 34 (IL34).

List of Abbreviations

DSM	**D**iagnostic and **S**tatistical **M**anual of Mental Disorders
PGC	**P**sychiatric **G**enomics **C**onsortium
GWAS	**G**enome-**W**ide **A**ssociation **S**tudies
SNP	**S**ingle-**N**ucleotide **P**olymorphism
OR	**O**dds **R**atio
DNA	**D**eoxyribo**N**ucleic **A**cid
ncRNA	**n**on-**c**oding **R**ibo**N**ucleic **A**cid
GRAS	**G**öttingen **R**esearch **A**ssociation for **S**chizophrenia (GRAS)
EPO	Erythro**PO**ietin
EPOR	Erythro**PO**ietin **R**eceptor
rhEPO	**r**ecombinant **h**uman Erythro**PO**ietin
GABA	**G**amma **A**mino-**B**utyric **A**cid
BrdU	5'-**B**romo-**d**eoxy**U**ridine
VEGF	**V**ascular **E**ndothelial **G**rowth **F**actor
HIF	**H**ypoxia-**I**nducible **F**actor
ODD	**O**xygen-**D**ependent **D**egradation
PHD	Prolyl-**H**y**D**roxylase
VHL	**V**on **H**ippel-**L**indau
PGAS	**P**henotype-based **G**enetic **A**ssociation **S**tudy
scRNA-Seq	**s**ingle-**c**ell **RNA**-**Seq**uencing
CA	**C**ornu **A**mmonis
fMRI	**F**unctional **M**agnetic **R**esonance Imaging
HK2	**H**exo**K**inase **2**
CRW	**C**omplex **R**unning **W**heel
DCX	**D**ouble**C**ortin
TBR1	**T**-Box **BR**ain transcription factor **1**
TLE4	**TLE** Family Member **4**, Transcriptional Corepressor
CTIP2\BCL11B	BAF Chromatin Remodeling Complex Subunit **BCL11B**
CSF1R	**C**olony **S**timulating **F**actor **1** **R**eceptor
CSF1	**C**olony **S**timulating **F**actor **1**
IL34	**I**nter **L**eukin **34**

1 Introduction

1.1 Neuropsychiatric diseases - causes and consequences

Neuropsychiatric disorders are relatively frequent and present a considerable burden to affected patients and their families. Life prevalence for any DSM-IV classified disorder is close to 50%. The majority of patients diagnosed have an early disease onset already during teenage or early adulthood (Kessler et al., 2005). This, and the lack of effective treatments for several of these disorders, increases the negative impact such disorders have on the lives of affected individuals with regard to social, emotional, economic and overall well-being. Therefore, identification of disease cause and underlying mechanisms is crucial to develop successful treatment strategies and thereby enable improvements in the quality of life of these patients.

During the last decades, large global efforts have been made to gain better insight into genetic underpinnings of neuropsychiatric diseases, e.g. by the Psychiatric Genomics Consortium (PGC). Whereas these efforts confirmed the high underlying genetic complexity of psychiatric diseases and contributed to a better understanding of the shared genetic roots of many of the neuropsychiatric disorders (Lee et al., 2019; Ruderfer et al., 2018; Solovieff et al., 2013; Visscher and Yang, 2016; Watanabe et al., 2019), so far they contributed little towards a truly causal understanding of disease origin or the development of new therapeutic strategies. Although such genome-wide association studies (GWAS) identified thousands of common genetic variants, also known as single-nucleotide polymorphisms (SNPs), that confer risk to certain psychiatric disorders, the identification of these risk loci has been of limited therapeutic use for several reasons: Firstly, the effect size of each individual variant is usually small with odds ratios (OR) typically <1.1. Secondly, the actual causal variant remains often unknown owing to the intricate linkage structure of variants in close proximity to each other. An additional layer of complexity is added by the potential interplay of individual risk (or protective) variants. This interplay of an individual's millions of SNPs may eventually determine the very unique risk load of each individual. Hence, even under the (idealized) assumption that all disease risk is exclusively conferred by SNPs, reliable individualized disease prognosis and the translation of genetic findings to therapeutic strategies appear still far away.

In addition, there is another aspect that crucially determines the onset, severity, duration and general risk to develop certain psychiatric diseases: the environment. This term in itself is of massive complexity. It includes *in utero*, peri- and postnatal influences, as well as social and socio-economic factors, exposure to stress, toxins, noise and air pollution, violence/abuse, infections and many others. Evidence supporting the notion that

environmental effects on psychiatric disease development and progression is abundant, e.g. age at onset of schizophrenia (Stepniak et al., 2014), risk for schizophrenia and psychosis (Agid et al., 1999; Varese et al., 2012), bipolar disorder (Agid et al., 1999), major depression (Agid et al., 1999; Kessler et al., 1997), anxiety disorders (Kessler et al., 1997), substance abuse disorder (Kessler et al., 1997; LeTendre and Reed, 2017). These environmental risks in turn shape the epigenetic landscape, thereby altering the way genetically encoded information is eventually "read out" and how it affects the function of body and mind. Epigenetic changes include changes in histone modifications or DNA methylation and increased/decreased abundance of specific non-coding RNAs (ncRNA) and have been suggested to be associated with schizophrenia and other psychotic disorders (Smigielski et al., 2020). Yet, the question, if these changes reflect cause or consequence of disease and associated risk factors, remains to be answered.

It has become increasingly apparent that the comprehensive assessment of the genetic constitution of individuals in form of "deep genotyping", which has become relatively easily accessible and affordable thanks to next-generation sequencing, is in many cases not sufficient to obtain a thorough understanding of the etiology of complex diseases. The extensive characterization of the phenotypical presentation, which can be analogously termed "deep phenotyping", of an individual as well as her/his environmental exposures is at least equally important for progress in this field. However, the acquisition of these data is much more laborious and often expensive and thus currently still rarely performed. Such data, as for example collected in the Göttingen Research Association for Schizophrenia (GRAS) (Ribbe et al., 2010) data base, are therefore extremely valuable. It allows not only a more detailed assessment of phenotypic differences and similarities within and across disease classifications, but also permits an in-depth investigation of the genotype-phenotype relationship. This opens avenues for the development of novel approaches that make full use of the genetic and phenotypic information available (see Project I).

In summary, genetic and environmental influences modify an individual's risk or resilience to develop neuropsychiatric disorders. In order to achieve a better understanding of disease contributing factors as well as disease presentation itself, an extensive evaluation of genetic, phenotypic and environmental components is key. The combination of these data will help to further disentangle the vast heterogeneity within psychiatric diseases and aid to gain better understanding of risk factors for disease. This will eventually allow more precise insights into etiology and effective treatment options for neuropsychiatric disorders.

1.2   Treating neuropsychiatric disorders

Treatment options for neuropsychiatric disease are as diverse as the disorders them-selves. They range from psychotherapeutic approaches over pharmacological interventions to physical treatments. They have varying efficacy and differ in their targeted disease domains, e.g. manic or depressive episodes, psychotic symptoms, cognitive function. While some treatments can alleviate symptoms of disease, neuropsychiatric disorders, including schizophrenia, Alzheimer's disease and dementia and autism, to date remain without cure. Schizophrenia, for example, is a debilitating condition that affects about 1% of the population across cultures (McGrath et al., 2004; McGrath et al., 2008). Despite its frequency, currently available treatments are of limited success and treatment-resistance is common (~12-40%) (Dammak, 2013; Mizuno et al., 2020). Current first-line antipsychotics target the dopaminergic system (McCutcheon et al., 2020) through antag-onism of the D2-receptor. Unfortunately, even in well-responding patients only positive symptoms of schizophrenia (such as hallucinations and delusions) show improvements, whilst negative symptoms (including anhedonia, social withdrawal, blunted affect, and cognitive impairments) are not recovered (McCutcheon et al., 2020). This highlights the need for more effective therapeutics that also target negative and cognitive symptoms adequately.

1.3   Erythropoietin in the brain - endogenous function and therapeutic potential

Erythropoietin (EPO) - originally known for its hematopoietic effects - exhibits neuropro-tective, neurotrophic, angiogenic, anti-inflammatory and anti-apoptotic functions in the brain (Noguchi et al., 2007). Not surprisingly, it has therefore been suggested as a po-tential agent to support neuroregeneration and to improve cognitive function (Brines and Cerami, 2005; Ehrenreich et al., 2004; Ehrenreich et al., 2007a; Ehrenreich et al., 2007b; Hasselblatt et al., 2006; Sirén et al., 2009). In fact, positive outcomes for stroke patients as well as structural and cognitive improvements in schizophrenia, major depression, bipolar disease and multiple sclerosis patients have been repeatedly reported (Ehrenre-ich et al., 2007a; Ehrenreich et al., 2007b; Miskowiak et al., 2010; Miskowiak et al., 2015; Miskowiak et al., 2014a; Miskowiak et al., 2014b).

   EPO is a glycoprotein which is mainly produced in the kidney, (fetal) liver and the brain and is stimulated by the hypoxia-inducible factor (HIF)-axis under hypoxia, i.e., lowered oxygen levels. The protein is primarily bound by the EPO receptor (EPOR) and activates a complex signalling cascade that involves the JAK-STAT pathway, MEK-ERK, PI3K-AKT as well as NFkB signalling (Noguchi et al., 2007). In the brain, neurons and as-trocytes have been found to be the main producers of brain-EPO (Bernaudin et al., 2000). EPOR is expressed by several brain cell types, including neurons, astrocytes, oligoden-drocytes, endothelial cells and microglia (Bernaudin et al., 1999; Hasselblatt et al., 2006; Juul et al., 1998; Morishita et al., 1996; Ott et al., 2015; Sirén et al., 2001; Sugawa et al.,

2002). Since EPO expression is conserved across mice, monkeys and humans (Digicayli-
oglu et al., 1995; Liu et al., 1997; Marti et al., 1996), a critical role for EPO in brain devel-
opment and function can be assumed. Indeed, EPO has been shown to be mediator of
neurogenesis and neuronal differentiation during development as well as in adulthood
(Hassouna et al., 2016; Park et al., 2006; Tsai et al., 2006; Yu et al., 2002) and is a driver of
oligodendrocyte and astrocyte differentiation and maturation (Hassouna et al., 2016; Iwai
et al., 2010; Lee et al., 2004; Sugawa et al., 2002). These features make the EPO-system an
attractive target for treating neuropsychiatric and neurodegenerative diseases.

1.4 Effects of erythropoietin on neurons

EPO and EPOR are strongly expressed during embryogenesis and early development in
mouse and human (Noguchi et al., 2007) and have been shown to be important drivers
of neurogenesis, cortical migration and laminarization during this period (Chen et al.,
2007; Constanthin et al., 2020; Tsai et al., 2006). EPO and EPOR continue to be ex-
pressed at lower levels in the adult nervous system (Noguchi et al., 2007). Several stud-
ies provided better understanding of the mechanisms that underlie the cognitive im-
provement observed after EPO administration in adulthood. For example, Adamcio et
al. (2008) showed that EPO enhances long-term potentiation in the CA1 and concomi-
tantly improves hippocampal memory. Moreover, 3-weeks of intraperitoneal adminis-
tration of recombinant human EPO (rhEPO) results in a ~20% increase in the number
of pyramidal cells in the CA1 (Hassouna et al., 2016). Interestingly, this numerical in-
crease was attributable to boosted neurodifferentiation, rather than accelerated prolifer-
ation of neuronal precursors as shown via 5'-bromo-deoxyuridine (BrdU) staining. Sim-
ilarly, in a more recent study (Project III, Wakhloo et al., 2020), we confirmed the rise in
newly formed neurons after 3-weeks of EPO treatment and found evidence for increased
neuronal differentiation and maturation in the CA1 as early as 6 hours after a single
EPO injection. Importantly, EPO does not only affect excitatory neuron populations, but
also facilitates inhibitory synapse density and transmission and augments maturation of
gamma-aminobutyric acid (GABA)ergic neurons in the CA1 postnatally (Khalid et al.,
2021).

1.5 Effects of erythropoietin on microglia

As mentioned above, EPO has the potential to target various cell populations. Although
not frequently investigated, EPO has also been observed to modulate microglial function
and activity. For example, EPO can reduce microglial activation and inhibit phagocyto-
sis of neurons by microglia (Chong et al., 2003; Mitkovski et al., 2015). Moreover, EPO
reduces the inflammatory response after brain injury and in neurodegenerative settings
(Ghezzi and Brines, 2004; Hellewell et al., 2013; Villa et al., 2003; Wang et al., 2007), pos-
sibly via reduction in microglial proliferation (Chong et al., 2003). *In vitro*, EPO has also
been shown to have an anti-apoptotic effect on microglia that were isolated from the rat

brain (Vairano et al., 2002). To date, microglial response to hypoxia has almost exclusively studied in terms of inflammatory and pathological context, e.g. in ischemic injury and inflammatory models (Kiernan et al., 2016; Kiernan et al., 2019; McRae et al., 1995; Yao et al., 2013). Yet, the responsiveness of certain microglial populations to vascular endothelial growth factor (VEGF) - a hypoxia-induced gene - suggests that microglial activation, number and function possibly is also modulated by hypoxia (Kreisel et al., 2019). This modulation may not only take place in pathophysiological situations, but likely allows microglia also in healthy conditions to react to physiological alterations in oxygen levels. Given the important role of microglia in brain homeostasis in health and disease (Prinz et al., 2021) as well as their generally tight interaction with neuronal development and connectivity (Pósfai et al., 2019), further investigations of effects of EPO and mild/physiological hypoxia on microglia appear worthwhile (Project III), as they will reveal additional insights into mechanisms related to their therapeutic potential.

1.6   Hypoxia - friend or foe?

As mentioned above, expression of EPO is triggered by hypoxic conditions. Such a hypoxic environment can develop either under physiological or pathophysiological conditions. Pathophysiological hypoxia can arise due to cardiac problems, apnea, anemia, ischemia, premature birth, perinatal complications or exposure to extreme heights with low oxygen pressure ("altitude sickness"). These conditions can lead to severe impairments of cellular function and even irreparable cell damage and death. In contrast, physiological hypoxia occurs under normal, healthy conditions and is beneficial as well as required for certain cellular functions. Physiological hypoxia acts as an important player during embryogenesis (Dunwoodie, 2009), in hypoxic niches such as the renal medulla (production site of EPO, Nangaku and Eckardt, 2007), areas of adult neurogenesis, e.g. dentate gyrus (Chatzi et al., 2015), the bone marrow (Parmar et al., 2007) or the heart (stem and progenitor cell maintenance; Kimura et al., 2015).

Hypoxia-inducible factor-1 (HIF-1) - in its heterodimeric form together with stably expressed aryl hydrocarbon receptor nuclear translocator (ARNT/HIF1B) - is a central coordinator of the hypoxic response under physiological as well as pathological conditions. This transcription factor contains an oxygen-dependent degradation (ODD) domain that makes it susceptible to degradation or stabilization depending on the oxygen level present within a cell. Under normoxic conditions degradation follows after hydroxylation of the ODD via prolyl-hydroxylases (PHDs) that recruit von Hippel-Lindau protein (VHL). This protein tags HIF for subsequent proteasomal degradation (Strowitzki et al., 2019, Figure 1). In response to HIF stabilization, targeted transcriptional programs are activated that alter various metabolic and functional processes in cells and tissues, e.g. shift from oxydative phosphorylation to glycolysis ("Warburg effect"), autophagy, apoptosis, inflammation, stemness and self-renewal (Dengler et al., 2014; Semenza, 1998).

In the brain, hypoxia has recently gained attention for its beneficial effects on neurogenesis and neuronal differentiation (Fagel et al., 2006; Santilli et al., 2010; Vieira et al.,
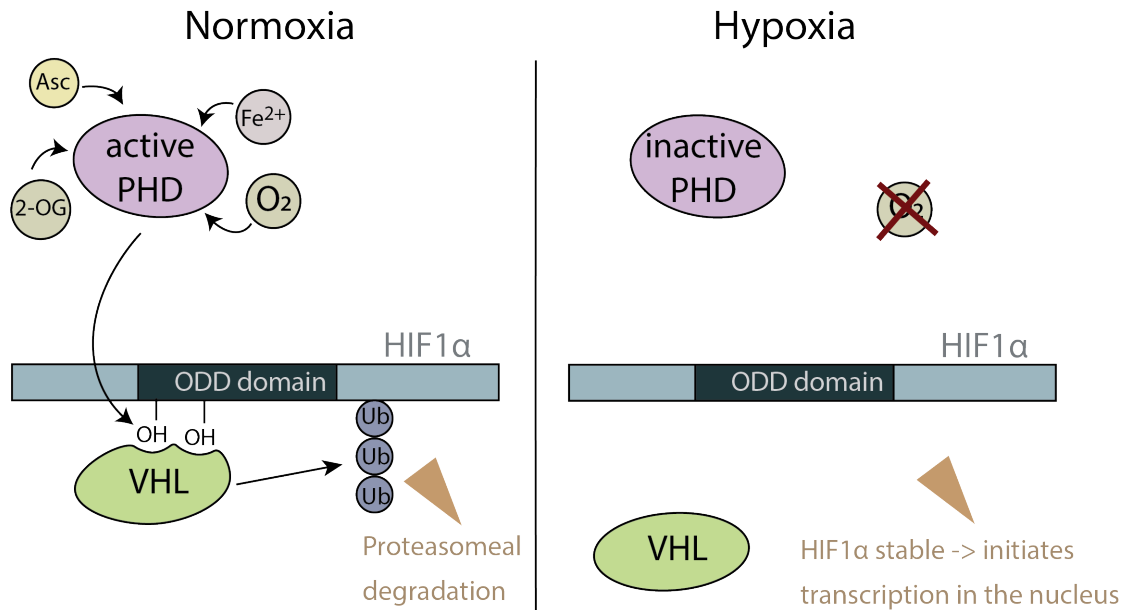
FIGURE 1: **HIF1α degradation pathway under normoxic and hypoxic conditions**. Under normoxic conditions and in the presence of co-substrates O_2, 2-oxaloglutarate (2-OG), iron (Fe^{2+}) and ascorbate (Asc) the PHDs hydroxylate the ODD domain of HIF1α. This recruits VHL which tags HIF1α via ubiquitilation for proteosomal degradation. Under hypoxia, PHDs remain inactive. Thus, HIF1α is stabilized and can initiate transcription by binding to hypoxia-responsive elements in the promoter regions of its target genes after dimerization with HIF1β subunits.

2011; Zhu et al., 2005; Zhu et al., 2010). While previously often investigated in negative and pathological contexts, it has become evident that physiological hypoxia not only is required for the function and integrity of certain brain areas but can also have positive effects on brain and cognitive function. The major difference between detrimental and beneficial hypoxia application lies in the treatment scheme applied: Severe and/or permanent anoxic or hypoxic conditions generally result in cellular damage (Doyle et al., 2008; Gorgias et al., 1996; Rybnikova et al., 2005), whereas mild to moderate hypoxia, applied over defined, relatively short, periods of time, can be largely beneficial (Mateika et al., 2015; Santilli et al., 2010; Wang et al., 2020; Wu et al., 2021).

2 Scope of the thesis

2.1 Aims of Project I

Project I investigated contributing risk factors for multiple drug (ab)use, also known as polytoxicomania, in a cohort of deeply-phenotyped schizophrenia and schizoaffective patients. This project aimed

1. to understand the effect of environmental risk factors (individually and upon accumulation) on the development of polytoxicomania throughout life as well as specifically in early life and adulthood.

2. to gain first insight into genetic associations with preadult polytoxicomania by applying a newly developed GWAS-PGAS approach to our relatively small, but well characterized sample of schizophrenia/schizoaffective patients.

2.2 Aims of Project II

Project II focused on the effects of exogenous (=inspiratory) and endogenous (=physiological "functional") hypoxia in the brain. The main goal was to study these effects by the use of a refined reporter mouse line that permanently labels hypoxic cells in the brain. Single-cell RNA sequencing (scRNA-Seq) was used to verify ubiquitous construct expression and to gain better insight into the hippocampal hypoxia-response.

2.3 Aims of Project III

Project III was designed to further explore how (exogenous or endogenous) hypoxia and peritoneal administration of erythropoietin - one of the major genes activated by hypoxia - affect hippocampal function and in particular processes of neuronal differentiation and maturation in the *cornu ammonis 1* (CA1). Moreover, we addressed the question to what extend erythropoietin and hypoxia modulate microglial function and abundance and if such changes alter the cross-talk between neurons and microglia thereby modifying processes of neuronal differentiation.

3 Project I: Preadult polytoxicomania – strong environmental underpinnings and first genetic hints

3.1 Overview of Project I

Polytoxicomania or multiple drug (ab)use, i.e., the use of ≥ 3 drugs within a defined time period, is a frequent comorbidity of schizophrenia and other psychiatric disorders (Alaja et al., 1998; Mueser et al., 2000; Toftdahl et al., 2016). It is associated with various negative outcomes with regard to behavior as well as mental and physical health (Connor et al., 2014; Hjorthøj et al., 2015). Like many psychiatric disorders, polytoxicomania often starts already during adolescence and possibly contributes to aggravation of existing mental health problems. In view of the potential deleterious consequences of this behavior, its high prevalence among teenagers (8-18%; Conway et al., 2013; Moss et al., 2014; White et al., 2013) is particularly alarming.

Whereas a large body of previous literature focused on genetic as well as environmental risk factors for single drug use and related disorders (Agrawal et al., 2018; Agrawal et al., 2011; Bierut et al., 2007; Cheng et al., 2018; Clarke et al., 2017; Furberg et al., 2010; Gelernter et al., 2014; Hancock et al., 2018; Hawkins et al., 1992; Kapoor et al., 2014; Moustafa et al., 2018; Qian et al., 2017; Treutlein et al., 2009), research on polytoxicomania is less abundant (Bailey et al., 2019; Collins et al., 1998; Jongenelis et al., 2019). Therefore, to date, its contributing risk factors remain widely unknown, and, accordingly, the grounds for possible preventive measures are weak. In order to systematically investigate effects of environmental risk exposure, extensive phenotyping of individuals and their environment is required. Apart from the individual effect of specific environmental risk factors, this allows to evaluate how an aggregation of different risk exposures affects the outcome of interest. Especially during early life, i.e., in pre-adulthood, the accumulation of environmental risk has been repeatedly shown to be a potent predictor of diverse health-related outcomes and behaviors, including age at schizophrenia onset (Stepniak et al., 2014), reduced global functioning and higher severity of psychopathology (Begemann et al., 2020; Lederbogen et al., 2011), boosted violent-aggressive behavior (Mitjans et al., 2019), unfavorable child development (Evans et al., 2013), enhanced use of tobacco, alcohol and other drugs as well as delinquency and suicidal behavior in students (Adelmann, 2005; Racz et al., 2016). Thus, the current project set out to exploit the GRAS data collection of ~2000 schizophrenia/schizoaffective patients to study if the exposure to a defined

set of environmental risk factors, including physical and sexual abuse, migration, urbanicity, problematic alcohol use and cannabis consumption, in early life (before age 18 and onset of schizophrenia) is associated with polytoxicomania. Risk factors were chosen based on our previous work on environmental risk accumulation in violent aggressive behavior (Mitjans et al., 2019). Alcohol and cannabis use have special status as predictors in context of polytoxicomania: Firstly, they are often considered to be "secondary risk factors", i.e., they themselves are the consequence of other risk factors. Secondly, mounting evidence suggest that alcohol and cannabis act as "gateway drugs". Such gateway drugs are considered to temporally precede and "open the door" to the use of other (illicit) drugs (Fergusson and Horwood, 2000; Fergusson et al., 2006a; Fergusson et al., 2006b; Hall and Lynskey, 2005; Kandel and Kandel, 2015; Lynskey et al., 2003; Olthuis et al., 2013; Secades-Villa et al., 2015).

In the current study (Steixner-Kumar et al., 2021), we indeed found a strong association of these gateway drugs with polytoxicomanic behavior. On an individual level, other environmental risk factors were associated with polytoxicomania to varying degrees. However, a striking effect of risk factor accumulation was observed: The more risk factors individuals were exposed to in early life, the higher was the percentage of individuals that developed polytoxicomania throughout life. A particularly strong association was found when individuals were stratified by onset of polytoxicomania. Amongst individuals with preadult onset of polytoxicomania ORs were >200 (extreme group comparisons 0 versus $\geq$3 risk factors). Importantly, the pattern of increasing propensity to develop polytoxicomania with increasing environmental risk accumulation was retained after removal of the two gateway drugs from the model. Inclusion of tobacco use as additional risk factor did not improve the model further. Overall, risk load in preadult polytoxicomanic individuals was high ($\sim$50% experienced $\geq$3 risk factors in early life), intermediate in adult (34% with $\geq$3 risk factors) and lowest in non-polytoxicomanic individuals (12% with $\geq$3 risk factors). We also observed a reduced premorbid intelligence and lower age at schizophrenia onset in the group of preadult polytoxicomanics.

Given the strong association of environmental risk accumulation with polytoxicomania and previously shown violent aggression (Mitjans et al., 2019), we asked the question whether such risk accumulation generally predicts behavioral outcomes and traits. To this end, we first tested the association of environmental risk factors with suicidal behavior as a form of auto-aggression and found risk factor accumulation to be associated with suicidal behavior. Nonetheless, this association appeared to be mainly driven by individuals with concurring hetero-aggression (compare Mitjans et al., 2019). In contrast, autistic traits in adulthood were not associated with the accumulation of a defined set of environmental risks previously proposed to be associated with autistic behaviors.

Apart from the exploration of environmental risks, another central goal of Project I was to obtain first insights into the genetic underpinnings of preadult polytoxicomania. Existing literature primarily focused either on genome-wide associations with single drugs or - in the rare case that multiple drug consumption was investigated - single

candidate genes only (Mallard et al., 2018). However, no GWAS on preadult polytoxico-mania has been available to date. As mentioned in the introduction, SNP effect sizes are often small and thus require large samples to ensure sufficient power to reveal signals. Hence, in smaller, yet extensively characterized samples with high quality information, genetic studies prove challenging. Therefore, a novel genetic approach (multiple GWAS-PGAS approach) that allows to extract genetic association signals from such samples was developed in the frame of this project. This approach yielded 41 SNPs found to be associated with preadult polytoxicomania. An additional gene-based analysis resulted in identification of another 11 potentially polytoxicomania-associated genes. Several of the identified genes, in which the risk-conferring SNPs were located, have previously been associated with substance use disorders as well as psychiatric disease and behavioral patterns known to be associated with substance use. Unfortunately, at the time of writing, suitable independent samples for the replication of findings were not available.

In summary, this project enhanced the understanding of contributing factors to the development of polytoxicomania and provided a in-depth characterization of affected individuals in terms of risk factor presentation, phenotypic outcomes including premorbid intelligence and age at schizophrenia onset, and drug use patterns. Moreover, with the generation of a novel GWAS-PGAS approach, first insights into genetic factors associated with preadult polytoxicomania were possible. These findings will hopefully provide a basis to advance preventive measures against this deleterious condition.

3.2   Original publication

Steixner-Kumar A.A. et al. (2021). Preadult polytoxicomania – strong environmental underpinnings and first genetic hints. Molecular Psychiatry, 1-12.

Personal contribution

I was involved in creating the study design, performed phenotypic and genotypic data curation, quality control of SNP array data as well as GWAS-PGAS and all other statistical analyses. I also contributed to interpretation of the results. Together with my supervisor I designed and created display items and wrote the manuscript draft.

ARTICLE

Preadult polytoxicomania—strong environmental underpinnings and first genetic hints

Agnes A. Steixner-Kumar [1] · Vinicius Daguano Gastaldi[1] · Jan Seidel[1] · Albert Rosenberger [2] ·
Martin Begemann[1,3] · Hannelore Ehrenreich [1]

Abstract

Considering the immense societal and personal costs and suffering associated with multiple drug use or "polytoxicomania", better understanding of environmental and genetic causes is crucial. While previous studies focused on single risk factors and selected drugs, effects of early-accumulated environmental risks on polytoxicomania were never addressed. Similarly, evidence of genetic susceptibility to particular drugs is abundant, while genetic predisposition to polytoxicomania is unexplored. We exploited the GRAS data collection, comprising information on N~2000 deep-phenotyped schizophrenia patients, to investigate effects of early-life environmental risk accumulation on polytoxicomania and additionally provide first genetic insight. Preadult accumulation of environmental risks (physical or sexual abuse, urbanicity, migration, cannabis, alcohol) was strongly associated with *lifetime* polytoxicomania ($p = 1.5 \times 10^{-45}$; OR = 31.4), *preadult* polytoxicomania with OR = 226.6 ($p = 1.0 \times 10^{-33}$) and *adult* polytoxicomania with OR = 17.5 ($p = 3.4 \times 10^{-24}$). Parallel accessibility of genetic data from GRAS patients and N~2100 controls for genome-wide association (GWAS) and phenotype-based genetic association studies (PGAS) permitted the creation of a novel multiple GWAS–PGAS approach. This approach yielded 41 intuitively interesting SNPs, potentially conferring liability to preadult polytoxicomania, which await replication upon availability of suitable deep-phenotyped cohorts anywhere world-wide. Concisely, juvenile environmental risk accumulation, including cannabis and alcohol as starter/gateway drugs, strongly predicts polytoxicomania during adolescence and adulthood. This pivotal message should launch more effective sociopolitical measures to prevent this deleterious psychiatric condition.

Introduction

Substance use disorders and multiple drug consumption are frequent in the general population and recurrent comorbidities of schizophrenia and other neuropsychiatric disorders

✉ Hannelore Ehrenreich
 ehrenreich@em.mpg.de

1 Clinical Neuroscience, Max Planck Institute of Experimental Medicine, Göttingen, Germany

2 Department of Genetic Epidemiology, University Medical Center, Georg-August-University, Göttingen, Germany

3 Department of Psychiatry and Psychotherapy, University Medical Center, Georg-August-University, Göttingen, Germany

[1–3]. Multiple drug use, also called polytoxicomania (the preferred term throughout this manuscript), is defined as the use of ≥3 drugs in a given period and associated with a range of negative behavioral, physical and mental health outcomes. These comprise higher psychological distress, impaired neuropsychological function, increased anxiety and depression, unsafe sexual behavior, greater risk for infectious diseases, and enhanced mortality, including suicides [4, 5]. Considering the large societal and personal costs and suffering associated with polytoxicomania, its high prevalence in teenagers (8–18%) [6–8] is alarming. Yet, its underlying causes are largely unknown. Previous studies have proposed that different individual (e.g., gender, school grades, ethnicity, depression, personality traits), familial (e.g., parental monitoring, inner-family conflicts), and other social factors (e.g., connectedness, drug use by peers) can increase the risk for polytoxicomania [9–12], but systematic investigations of a broader spectrum of risk factors, especially in large samples, are rare.

The preadult accumulation of environmental risk factors is a potent predictor of various health outcomes and negative behaviors, including earlier age at schizophrenia onset [13], reduced global functioning and higher severity of psychopathology [14, 15], boosted violent-aggressive behavior [16], unfavorable child development [17], enhanced use of tobacco, alcohol and other drugs as well as delinquency and suicidal behavior in students [18]. The predisposing risks for polytoxicomania have mostly been studied in isolation, and reports on how cumulative risk affects polytoxicomania are scarce (e.g., [19, 20]). Therefore, the current study investigates for the first time effects of preadult environmental risk accumulation on polytoxicomania based on the unique high-quality deep-phenotyping data of GRAS (Göttingen Research Association for Schizophrenia) [21].

Moreover, we aimed at shedding first light on possible genetic risk factors predisposing to polytoxicomania by exploiting the extensive genotyping information of GRAS. Past studies focused on genetic associations with single drugs (e.g., [22–24]). Few reports addressed any genetic underpinnings of polytoxicomania, concentrating on single genes, or performing genome-wide association studies (GWAS) on lifetime drug experimentation [25–27]. Even though twin studies suggest genetic liability to substance use disorders in adolescence [28], no study has explored preadult polytoxicomania on a genome-wide level likely due to world-wide missing databases on this condition which impedes any kind of replication study. Therefore, our novel multiple GWAS–PGAS (phenotype-based genetic association studies) approach utilizes extensive phenotyping information to improve the confidence with which genetic signals from single nucleotide polymorphisms (SNPs) in relatively small ($n < 3500$), but deep-phenotyped samples, can be identified.

We show here that environmental risk accumulation, including physical abuse, sexual abuse, migration, urbanicity, and the use of gateway drugs, cannabis, and alcohol [29, 30], strongly promotes polytoxicomania. Further, we support existing evidence that preadult polytoxicomania induces aggressive and criminal behavior later in life. Finally, we deliver first hints for a genetic susceptibility to preadult polytoxicomania, which ultimately require independent replication upon availability of suitable cohorts anywhere worldwide.

Subjects and methods

Subjects

The extended GRAS data collection consists of N~2000 schizophrenic and schizoaffective subjects

(according to DSM-IV-TR). Ethics Committees of Georg-August-University, Göttingen, and participating centers across Germany approved GRAS, complying with Helsinki Declaration. All patients (and/or legal representatives) gave written informed consent. For genetic association analyses, also healthy blood donors ($N = 2111$; age 33.68 ± 12.21 years, 58.46% males) were included. Complete phenotypical information was available for $N = 1904$ schizophrenia/schizoaffective patients (40.28 ± 13.11 years, 66.02% males), complete genotype information for $N = 1718$ individuals (40.44 ± 13.07 years, 66.94% males) after exclusion of individuals due to relatedness, ancestral outlier status, and missing phenotype data. We note that individuals were only included in phenotypic or genetic analyses if unambiguous information on environmental risk, drug use/autistic traits/suicidal behavior was obtainable, explaining some N number variation.

Phenotyping

Environmental risk

Environmental risk factors, including physical abuse, sexual abuse, migration, urbanicity, cannabis use and problematic alcohol use before age of 18 years and onset of schizophrenia, were operationalized as described in detail earlier [13, 16]. Additional environmental risk factors (for evaluation of autistic traits only) included perinatal complications, season of birth, early neurotrauma, paternal age, number of infections (positive serology) [13, 16].

Polytoxicomania

Medical reports and SCID-I allowed assessment of current and previous drug use. Drug classes included cocaine, opioids, hallucinogens, amphetamines, ecstasy, barbiturates, benzodiazepines, and inhalants. In the environmental risk study, use of ≥3 drugs was coded as polytoxicomania, use of ≤2 drugs as non-polytoxicomanic behavior. For the multiple GWAS–PGAS approach, exact definitions of polytoxicomania for each GWAS are provided in display items. Note that caffeine was not considered as "drug".

Other outcomes

Premorbid intelligence was measured by Mehrfachwahl–Wortschatz–Intelligenztest-B (MWT-B [31]), corrected for age and medication (CPZ; chlorpromazine equivalents) using standardized residuals from linear regression. *Suicidality*: Suicide attempts served as readout. *Autistic traits*: PANSS Autism Severity Score (PAUSS) [32] was used to assess severity.

Genotyping

Genotyping was performed using a semi-custom Axiom® myDesign™ genotyping array (Affymetrix, Santa Clara, CA, USA), based on a CEU (Caucasian residents of European ancestry from Utah, USA) marker backbone including 518,722 SNPs, and a custom marker set including 102,537 SNPs (described in detail [33]). A total of 530,316 autosomal variants passed quality control, had minor allele frequency (MAF) > 0.05, were in Hardy–Weinberg equilibrium (HWE; $p > 0.001$) and therefore included in genetic analyses.

Genetic association analysis

From each pair of related individuals (second to third-degree relatives, PIHAT > 0.185) one individual was randomly excluded. In healthy blood donor-patient pairs, priority was given to patient samples. Ancestral outliers were excluded based on principal component analysis (PCA; principal component1 (PC1 ± 3 SD) and PC2 ± 5 SD). PCs were calculated on LD-pruned marker set (long-range LD-regions removed) of 96,836 autosomal SNPs. In all association tests (SNP test: logistic regression; gene-based test: PC regression), sex and first 10 PCs were entered as covariates to control for population stratification.

Human expression data

Human tissue expression data (standardized) was downloaded from Harmonizome [34] (https://maayanlab.cloud/Harmonizome/dataset/GTEx+Tissue+Gene+Expression+Profiles, accessed 23/11/2020).

Statistical analysis

Calculations of relatedness, principal components, genetic association analyses, and LD-based clumping (index variant p value threshold=0.01) of GWAS results were performed in PLINK v1.90 [35], gene-based association tests in MAGMA v1.07b [36]. Chi-square tests and Fisher's exact tests were applied to test for categorical associations. Cochran–Armitage or Jonckheere–Terpstra tests (permutations $n = 20,000$) were employed for trends. Levene's test was used to assess homogeneity of variances. In case of homoscedasticity, Welch's, Games–Howell test, or Welch's ANOVA (R-package "onewaytests") were applied for group comparisons and post-hoc tests with continuous outcomes (Bonferroni-corrected). In all instances where mathematical assumptions could have been violated, robust statistical tests were carried out to exclude a negative impact of such violations on statistical outcomes. Calculation of variance inflation factors (VIF) assured absence of multicollinearity between predictor variables (all VIF < 1.2), except when smoking was included (thus rejecting it as predictor). Odds ratio (OR) was calculated using R-package "DescTools" or exact logistic regression with permutation (PROC LOGISTIC) when cell count was equal to 0 (SAS 9.4). Except for OR calculations, all statistical tests and workflows were performed in R v3.5.2 [37] or IBM SPSS Statistics for Windows, Version 25.

Results

Preadult polytoxicomania and aggressive behavior

We first explored the predictive potential of individual illicit drugs for aggressive behavior using a violent aggression proxy (Fig. 1A) [16]. The proportion of violently aggressive individuals increased step-wise with the number of illicit drugs consumed before age 18 years (Fig. 1B): Nearly 50% of individuals consuming ≥4 drugs in early life, i.e., who were clearly polytoxicomanic at a young age, showed violent aggression as compared to just 15% in the group of individuals, who did not use any illicit drug before age 18 (extreme group comparison OR = 5.3, 95% CI [3.4–8.3]).

Contrasting drug use in non-polytoxicomanic and polytoxicomanic individuals

A comparison of lifetime patterns of illicit drug use amongst non-polytoxicomanic (<3 drugs) and polytoxicomanic (≥3 drugs) individuals showed a highly diverse drug use in the latter group (Supplementary Table 1). While the vast majority of non-polytoxicomanic individuals never had contact with illicit/hard drugs in their life (>95% for any drug), the majority of polytoxicomanic individuals had used most of the respective drug classes at least once, e.g., only 13% and 24% did not have any contact with cocaine or ecstasy, respectively. Furthermore, frequency of use in polytoxicomanic individuals varied substantially between drug classes, e.g., although only 18% never tried hallucinogens, a minority of individuals (~3%) report using it (almost) daily. This combination makes it difficult to entirely exclude certain drug preferences at the individual level. Overall, however, polytoxicomanic individuals in our sample displayed a highly diverse and frequent use of drugs, without systematic preference. This clearly discriminates them from individuals classified here as non-polytoxicomanic.

Accumulated preadult environmental risk predicts polytoxicomania

Next, we evaluated the prognostic value of individual preadult environmental risks for polytoxicomania. Whereas
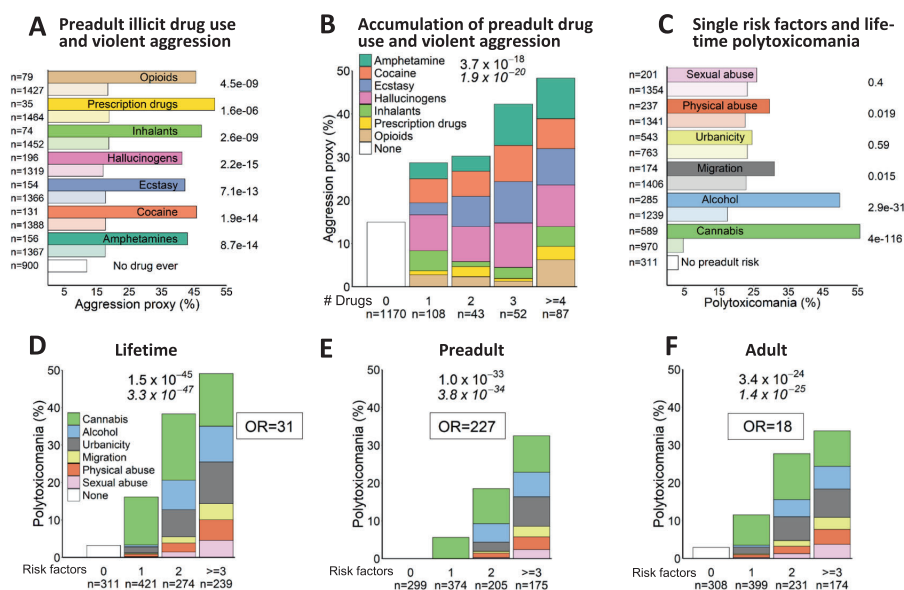
Fig. 1 Environmental influence on behavioral phenotypes. A Associations of preadult illicit drug use with violent aggressive behavior as measured by an aggression proxy (developed in Mitjans et al. [16]). Columns in dark colors denote preadult users of the respective drug; light colors indicate non-users of this specific drug. Note that drug use shown is not exclusive, i.e., a person that consumed opioids might also have used inhalants and thus appear in both columns as user; a person that used cocaine but not ecstasy will appear as non-user for ecstasy. Group "No drug ever" refers to lifetime non-consumption of any illicit drug. Left side: *N* numbers. Right side: *P* values (Chi²-test, two-sided) comparing users and non-users. Note that in this panel, cannabis, alcohol, nicotine and caffeine are not considered. **B** Step-wise increase in aggression proxy with the number of drug classes used in early life. Colors in bars represent respective drug classes. **C** Associations of single preadult environmental risk factors and lifetime polytoxicomania. Columns in dark colors denote individuals exposed to respective risk factor, light colors refer to individuals not exposed to this specific risk (not necessarily devoid of any risk at all). Note that risks shown are not exclusive, i.e., many individuals carry more than 1 risk factor. **D–F** Accumulation of preadult environmental risk factors leads to stepwise increase in lifetime polytoxicomania (**D**), exclusive preadult polytoxicomania (**E**) and polytoxicomania appearing exclusively later in life (**F**). Colors indicate respective risk factors (**B**), (**D–F**): *n* numbers below bars, (**A**), (**B**) on left side. Chi²-test *p* values (two-sided) on top of graph (**B**), (**D–F**) or right side (**A**), (**B**); Cochran–Armitage test *p* values (two-sided) (**B**, **C**), (**E**) underneath in italics. OR: Odds Ratio.

all factors by themselves showed some tendency, our "secondary" environmental risks, alcohol, and cannabis, revealed already here their expected role as gateway/starter drugs (Fig. 1C). The following accumulation analysis showed that the higher the number of preadult risk factors, the higher the likelihood of polytoxicomania over lifetime (extreme group comparison OR = 31.4, 95% CI [15.9–61.9]) (Fig. 1D). We next stratified by preadult polytoxicomania (≥3 drugs consumed before age 18 years/ onset of schizophrenia, Fig. 1E) and adult polytoxicomania (≥3 drugs consumed throughout life, but after age 18 years/ onset of schizophrenia, Fig. 1F). This resulted in extreme probabilities for developing polytoxicomania preadult with OR = 226.6 (extreme group comparison; 95% CI [50.8–∞]) and adult with OR = 17.5 (extreme group comparison; 95% CI [8.4–36.4]), strongly pointing to a causal relationship between preadult environmental risk and polytoxicomania.

Preadult environmental risk accumulation predicts polytoxicomania also without inclusion of starter drugs in the model

To alleviate concerns of potential circularity when including the starter drugs cannabis and alcohol as secondary environmental risks of polytoxicomania, we omitted them on a trial basis, using only 4 risk factors as predictors (urbanicity, migration, physical abuse, sexual abuse) (Supplementary Fig 1A–C). Reassuringly, the overall pattern of risk accumulation predicting polytoxicomania remained identical even though the effect was expectedly less pronounced.

Lack of evidence of an appreciable role of tobacco as gateway drug

Smoking prevalence in our sample was very high, with 85% of individuals reporting to have smoked at least once in their life. Of those, 80% started before age 18 and onset of
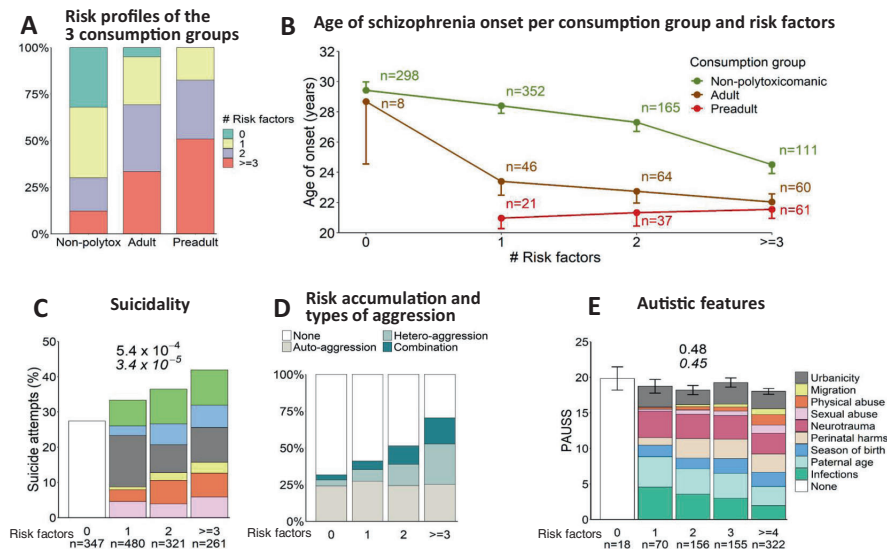
Fig. 2 Environmental risk load and behavioral consequences. A Risk factor distribution in the 3 different consumption groups: non-polytoxicomanic individuals (lifetime), exclusively adult polytoxicomanic, and exclusively preadult polytoxicomanic individuals, shows a clearly elevated risk load in (preadult) polytoxicomanic individuals. **B** Relation of number of preadult environmental risk factors and drug consumption behavior with age at schizophrenia onset. Mean±SEM. **C** Stair pattern increase in percentage of individuals who attempted to commit suicide with number of preadult environmental risk factors; legend of risk factors as in (Fig. 1D). **D** Distribution of auto- and heteroaggressive behavior shows that auto-aggression (suicide attempts) increases with the number of risk factors only in individuals who show heteroaggressive behavior as well. **E** Not all behavioral traits increase with environmental risk: No association of preadult environmental risk factors and autistic features in adulthood as quantified by PAUSS (developed in Kästner et al. [32]). Colors indicate respective risk factors. Mean±SEM (**C**), (**E**): *n* numbers below bars. Chi²-test (**C**) or one-way ANOVA (**E**) *p* values (two-sided) on top of graph; two-sided Cochran–Armitage (**C**) and Jonckheere–Terpstra trend tests (**E**) underneath in italics.

schizophrenia. Thus, although nicotine may be often consumed before other drugs, due to its high prevalence (and thus "non-specificity") its predictive value for use of illicit or hard drugs is rather limited. For example, whereas 37% and 34% of our individuals, who consumed cannabis (mostly also smokers) or had problematic alcohol use (either in isolation or in combination with other risk factors) in preadulthood, respectively, developed preadult polytoxicomania, "only" 19% of young smokers (including those with a combination of tobacco with cannabis and possibly other risk factors) progressed to preadult polytoxicomania.

Of note, multicollinearity excluded smoking as valid predictor. In fact, there was a very strong relationship between tobacco and cannabis use (cannabis is mostly smoked with tobacco). In our sample only 2.5% of individuals, who used cannabis at young age, never smoked before age 18 and onset of schizophrenia. They consumed cannabis in cookies or similar. Vice versa, 53% of all preadult smokers in our sample also report usage of cannabis. Nonetheless, when including smoking in a purely exploratory fashion as additional risk factor, the accumulation

model expectedly does not improve (Supplementary Fig 1D–F). Interestingly, when smoking was the only risk factor an individual was exposed to, it did not increase the probability of being polytoxicomanic, questioning a substantial role of tobacco by itself as starter drug.

Risk load comparison in individuals with or without polytoxicomania and role of cannabis and alcohol as starter drugs re-visited

Risk load in preadult polytoxicomanic subjects was immense (Fig. 2A). Nearly 50% of all individuals showing preadult polytoxicomania had experienced ≥3 risk factors before the age of 18 years/onset of schizophrenia. In the group of adult polytoxicomania, 34% had ≥3 risk factors in contrast to only 12% of individuals without polytoxicomania. All preadult polytoxicomanic individuals (100%) experienced at least 1 risk factor in early life. Likewise, in the adult polytoxicomanic group, only 5% of individuals had no risk factor before adulthood. In contrast, 32% of individuals in the non-polytoxicomanic group were "risk-free" (Fig. 2A).

Table 1 Prevalence of individual risk factors stratified by consumption group and number of risks.

Group	# Risk factors	n (%) Cannabis	Alcohol	Urbanicity	Migration	Physical abuse	Sexual abuse
Preadult	1	21 (100.0)	0 (0.0)	0 (0.0)	0 (0.0)	0 (0.0)	0 (0.0)
Adult		32 (69.6)	2 (4.3)	7 (15.2)	1 (2.2)	3 (6.5)	1 (2.2)
Non-polytox		52 (14.7)	31 (8.8)	191 (54.1)	12 (3.4)	30 (8.5)	37 (10.5)
Preadult	2	38 (100.0)	20 (52.6)	10 (26.3)	2 (5.3)	5 (13.2)	1 (2.6)
Adult		56 (87.5)	21 (32.8)	29 (45.3)	7 (10.9)	9 (14.1)	6 (9.4)
Non-polytox		79 (47.3)	38 (22.8)	105 (62.9)	28 (16.8)	47 (28.1)	37 (22.2)
Preadult	≥3	61 (100.0)	42 (70.0)	43 (81.1)	20 (32.8)	22 (36.1)	16 (26.7)
Adult		55 (91.7)	35 (59.3)	41 (73.2)	19 (31.7)	24 (40.0)	22 (36.7)
Non-polytox		77 (68.1)	57 (50.4)	98 (88.3)	44 (38.6)	63 (55.3)	44 (38.9)
Total[a]		**471 (38.3)**	**246 (20.0)**	**524 (43.1)**	**133 (10.8)**	**203 (16.5)**	**164 (13.3)**
p (χ^2)		***4.59e−93 (425.23)***	***1.72e−26 (118.65)***	*0.58 (1.08)*	***0.001 (13.61)***	***0.042 (6.35)***	*0.421 (1.73)*

Bold values indicate significant differences ($p < 0.05$) in the prevalence of respective risk factors between the three consumption groups (across number of risk factors).

[a]Calculation of total percentage also included individuals with 0 risk factors. Underlined p values remain significant after Bonferroni correction ($p < 0.05/6 = 0.008$). Two-sided Chi²-test applied.

Subsequently, we investigated in detail the distribution of individual risk factors in the consumption groups. There was a strong group difference regarding preadult cannabis exposure ($p = 4.59\mathrm{e}{-}93$, Table 1), with 100% of preadult polytoxicomanic individuals (irrespective of risk numbers) having consumed cannabis at early age. Among adult polytoxicomanic individuals, this number dropped to 91.7%, 87.5%, and 69.6% in the risk groups with ≥3, 2, or 1 risk factors, respectively. In comparison, within the non-polytoxicomanic group, the percentage of individuals with cannabis use in early life was lower (68.1%, 47.3%, 14.7%, respectively), yet still substantial. The prevalence of pre-adult problematic alcohol use followed a similar but less pronounced pattern. In addition, migration and physical abuse differed between consumption groups (Table 1). Overall, the most frequent risk factor was urbanicity (43.1%), followed by cannabis (38.3%) and physical abuse (16.5%) (Table 1).

Individuals in the consumption groups differed from each other with respect to age ($p = 6.26\mathrm{e}{-}62$), age at disease onset ($p = 5.87\mathrm{e}{-}38$), and premorbid intelligence (corrected for age and medication, $p = 0.002$), but not medication ($p = 0.38$; Table 2). Premorbid intelligence of preadult polytoxicomanic individuals was significantly lower than that of adult polytoxicomanic ($p = 0.01$) and non-polytoxicomanic ($p = 0.02$), but did not differ between the latter two groups ($p > 0.99$). A two-way ANOVA confirmed the main effects of environmental risk group and consumption group on age of onset without interaction between the two groups (environmental risks: $p = 8.71\mathrm{e}{-}08$, consumption: $p = 4.66\mathrm{e}{-}12$, risks×consumption: $p = 0.23$). Figure 2B depicts the substantial impact of polytoxicomanic behavior on age at disease onset. In the non-polytoxicomanic individuals, the age at disease onset step-wise decreases with the number of risk factors ($p = 1.73\mathrm{e}{-}08$). In preadult and adult polytoxicomanic individuals, an increasing number of risk factors had no appreciable further influence on the already early age at disease onset ($p = 0.89$ and $p = 0.30$, respectively).

Effects of accumulated preadult environmental risk on other behavioral outcomes

In view of these striking results, we explored the possibility that preadult environmental risk accumulation might be a potent predictor of any other behavioral outcome as well. Building on our previous findings of violent-aggressive behavior increasing with preadult environmental risk [16], we investigated its impact on autoaggressive behavior in form of suicidality. Indeed, with rising number of environmental risks, we also observed a surge in percentage of individuals with suicidal thoughts ($p = 0.012$, Cochran–Armitage test; OR = 1.5, 95% CI [1.1–2.2], extreme group comparison), suicidal plans ($p = 0.004$, Cochran–Armitage test; OR = 1.7, 95% CI [1.2–2.3], extreme group comparison) and suicide attempts (Fig. 2C; $p = 3.3\mathrm{e}{-}05$, Cochran–Armitage test; OR = 2.0, 95% CI [1.4–2.8], extreme group comparison). This surge,

Preadult polytoxicomania—strong environmental underpinnings and first genetic hints

Table 2 Sociodemographic and disease-related outcomes stratified by consumption group.

	Total Mean (SD)	Non-polytox	Adult	Preadult	*p*
Age (years)					
	39.59 (12.71)	41.98 (12.73)	34.00 (9.81)	28.86 (6.86)	**6.26e−62**
	$n = 1559$	$n = 1192$	$n = 213$	$n = 154$	
Age at disease onset (years)					
	25.95 (8.81)	27.21 (9.22)	22.60 (6.17)	20.82 (4.66)	**5.87e−38**
	$n = 1531$	$n = 1170$	$n = 210$	$n = 151$	
Chlorpromazine equivalents					
	679.25 (670.09)	669.81 (678.96)	740.58 (694.05)	669.71 (558.51)	0.38
	$n = 1513$	$n = 1161$	$n = 202$	$n = 150$	
Premorbid intelligence MWT-B-corrected					
	0.04 (1.00)	0.05 (1.04)	0.13 (0.96)	−0.16 (0.70)	**0.002**
	$n = 1440$	$n = 1101$	$n = 194$	$n = 145$	

MWT-B Mehrfachwahl–Wortschatz–Intelligenztest-B; Premobid intelligence: Standardized residuals corrected for Chlorpromazine equivalents and age. Sample sizes vary because of missing data. Bold values indicate significant differences between means of the three consumption groups. Underlined *p* values remain significant after Bonferroni correction ($p < 0.05/4 = 0.0125$). Two-sided Welch's ANOVA (age, age at disease onset, premorbid intelligence) or ANOVA (Chlorpromazine equivalents) applied.

however, appears to be explained only by individuals with additional heteroaggression (Fig. 2D).

As another behavioral readout, we assessed whether preadult risk accumulation can also predict severity of autistic features in adulthood (Fig. 2E). For this approach, we even included more risk factors, previously reported to play a role in autistic behavior, i.e., perinatal complications, early neurotrauma, season of birth, paternal age, and number of postnatal infections. Interestingly, we did not observe any association of autistic traits with any environmental risk factor, neither individually (all $p > 0.05$) nor in accumulation.

Genetic susceptibility to preadult polytoxicomania

In order to overcome the challenges associated with detecting genetic associations in relatively small, but deeply phenotyped, high-quality samples, we developed the novel multiple GWAS–PGAS approach to discover potential first associations of common genetic variants (SNPs) with preadult polytoxicomania. As depicted in Fig. 3A, B, this approach rests on multiple GWAS for polytoxicomania with minor variations in phenotype definitions. Supplementary Fig. 2 presents Manhattan plots for GWAS 1-6. The underlying working hypotheses of the workflow described in Fig. 3C, presume that (i) true genetic signals should be stable across (minor to moderate) changes in sample composition, (ii) true genetic signals are more likely to have neighbors in linkage disequilibrium which show a signal, too (but not entirely excluding that false do as well), and (iii) the here identified genetic associations with polytoxicomania should be independent of schizophrenia

diagnosis (although pleiotropic risk genes exist [38] but are a separate matter). Figure 4A, B depicts the overlap structure between different GWAS results at given *p* value threshold. Importantly, GWAS 1-4 (set1) have the highest number of shared SNPs among each other in the raw ($n = 3539$-red; Fig. 4A) as well as the clumped/LD-linked results ($n = 41$-red; Fig. 4B)—convincingly visualized by Jaccard index matrix (Supplementary Fig 3). Notably, clumping and usage of linkage information considerably condense the number of final polytoxicomania-associated SNPs, identifying 41 potentially relevant SNPs (at $p < 0.01$, with LD neighbors $p < 0.05$; graphically displayed as red dots in Manhattan plots, Supplementary Fig 2). Out of these, 28 were located in gene-coding regions (±10 kb, Supplementary Table 2). Interestingly, 15 of these genes (out of 20 with human tissue expression data available on Harmonizome [34]) are strongly expressed in brain and/or kidney (Supplementary Fig 4). In addition, gene-wide association results (MAGMAv1.07b) yielded 11 genes potentially associated with preadult polytoxicomanic behavior (Supplementary Table 3). We abstained from deeper interpretation of these genes at this stage because of the still required replication. Known associations, however, listed in Supplementary Tables 2 and 3, are promising.

Discussion

This study discovered a prominent association of polytoxicomania with early accumulation of environmental risk factors, comprising urbanicity, migration, sexual abuse, physical abuse and, as secondary risks, alcohol, and
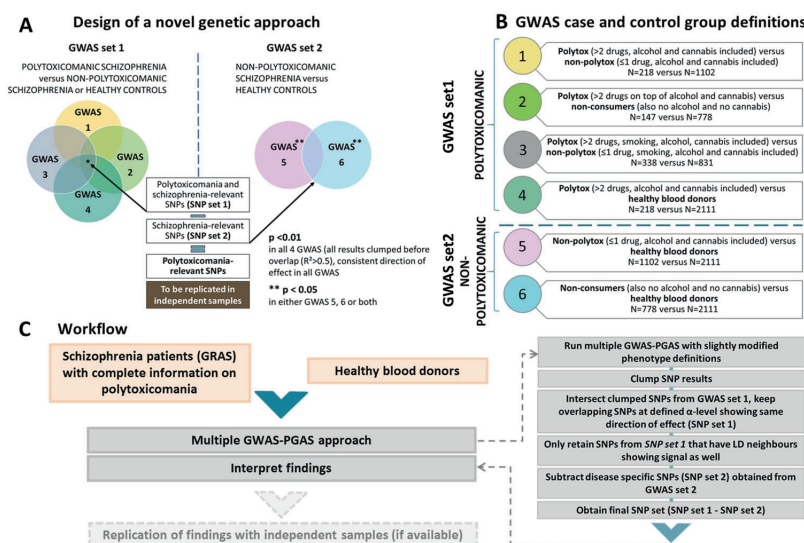
Fig. 3 Novel multiple GWAS–PGAS approach. A Overview of the analysis design. GWAS set 1 to obtain SNP set 1: 4 GWAS contrasting polytoxicomanic versus non-polytoxicomanic individuals (including healthy individuals) with slightly varied phenotype definitions (details in (**B**)) to identify SNPs that show consistent associations ($p < 0.01$) in all 4 GWAS. These SNPs are considered polytoxicomania and/or schizophrenia-associated. GWAS set 2 to obtain SNP set 2: SNPs associated exclusively with schizophrenia, but not polytoxicomania, resulting from GWAS 5 and/or 6 ($p < 0.05$) are subtracted from SNP set 1 (polytoxicomania and/or schizophrenia-associated), yielding the final set of polytoxicomania-relevant SNPs. **B** Diagram showing exact phenotype definitions and sample sizes per group for GWAS 1–6. **C** Detailed workflow of the novel GWAS–PGAS approach including clumping procedure to reduce number of SNPs in the final set.

cannabis. In particular, preadult polytoxicomania is >220 times more likely to develop in subjects exposed to ≥3 risks. In addition, polytoxicomania in later life occurs with higher probability after adolescent accumulation of negative environmental impact. Thus, our data show that multiple drug use has obviously remarkable roots in preadult risk factor buildup. In perfect agreement with previous reports (e.g., [39–41]), we find clear escalation in percentage of violent behavior with increasing numbers of drugs consumed. Strikingly, the number of accumulated risk factors appears to be more informative than the type of environmental risk factor. Nonetheless, our data strongly underline the well-known significance of cannabis and alcohol as gateway/starter drugs [29, 42–46].

In fact, all individuals with preadult polytoxicomania reported using cannabis. This confirms a tremendous association between cannabis and preadult polytoxicomania, even though not ultimately proving causality. A more causal perspective is perhaps offered by our data on polytoxicomania arising in adulthood. In adult polytoxicomanic individuals, the preadult risk factors temporally clearly precede the occurrence of polytoxicomania. Also in this group, cannabis is the by far most frequent preadult risk factor (occurring in 70–92% of individuals). Considering this extraordinary impact of cannabis, legalization and commercialization of its use will certainly increase not only incidence and prevalence of psychosis [47–53], but also of polytoxicomania.

Importantly, smoking as the sole risk factor did not increase the chance of developing polytoxicomania and did not influence our accumulation model further. Along these lines, heavy increase in tobacco consumption is highly frequently observed in alcoholics upon alcohol abstinence. This phenomenon is called "'Suchtverlagerung'" or shift in addictive behaviors and is not associated with generation of polytoxicomania (but causes other severe problems [54]), again emphasizing the "non-specificity" of nicotine consumption in this regard. Nevertheless, it cannot be entirely excluded that tobacco has a minor role as "co-gateway" drug together with cannabis (as cannabis use is tightly associated with smoking status).

Cannabis and alcohol are sometimes seen as potential consequences of early-life stress, like physical and/or sexual abuse, considered as some sort of self-treatment [55]. However, the VIF for all variables in our model was low (all VIF < 1.2), indicating that there was no considerable multicollinearity between the risk factor variables. This suggests an independent input of each variable to the model including independent contributions of cannabis/alcohol and stress-related variables such as physical or sexual abuse.

Preadult polytoxicomania—strong environmental underpinnings and first genetic hints

A

B
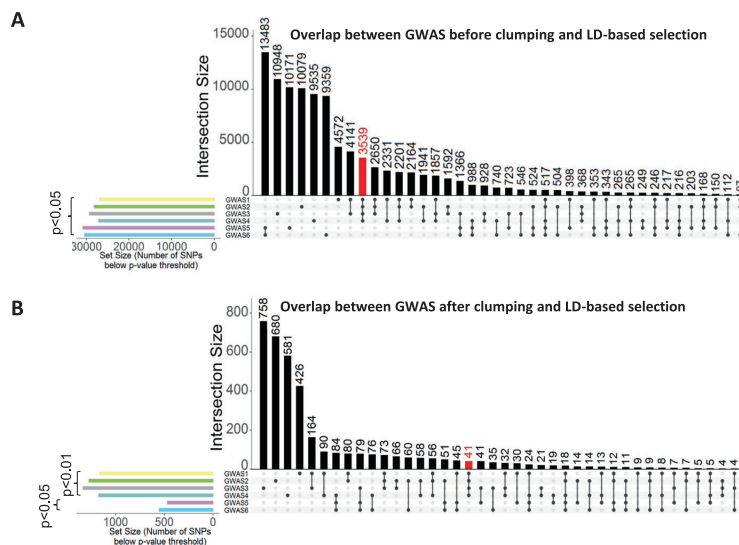
Fig. 4 Intersection of SNP results before and after clumping. A Intersection raw results before clumping of associated SNPs from all 6 GWAS. Black bars represent the number of intersecting SNPs below *p* value threshold 0.05. Dots indicate the respective GWAS for which the number of intersecting SNPs was calculated. Columns with single dots indicate SNPs unique to the corresponding GWAS. GWAS 1-4 and GWAS 5-6 show strong overlap within each other. Importantly, as indicated by the red bar, the largest intersection size when overlapping 4 GWAS is between GWAS 1-4 (polytoxicomania and/or schizophrenia GWAS). These SNPs show no association in GWAS 5-6. The novel approach applied to raw GWAS results would thus yield 3539 SNPs. Colored bars on the left indicate the number of associated SNPs per individual GWAS, i.e., the set size. **B** Intersections of associated SNPs from all 6 GWAS building on clumped SNP results and considering LD linkage neighbor signals. Black bars represent the number of intersecting SNPs below the given *p* value threshold on the left. Dots indicate the respective GWAS for which the number of intersecting SNPs was calculated. Columns with single dots indicate SNPs unique to the corresponding GWAS. Again, the intersection of SNPs associated in GWAS 1-4, but not GWAS 5-6, is larger than for any other combinations of 4 GWAS and yields now a strongly reduced set of 41 polytoxicomania-associated SNPs (red bar). Colored bars on the left indicate the number of associated SNPs per individual GWAS, i.e., the set size.

We show that suicidality, as a severe form of autoaggression, follows a similar stair-pattern, but only in individuals exhibiting heteroaggression as well. Based on all these results, one could speculate that any kind of behavioral traits might be shaped by preadult environmental risk exposure; nevertheless, we did not see any respective influence of the here determined risks on the severity of autistic phenotypes in adulthood. It seems that autistic features are predominantly genetically induced [56, 57]. However, impact of intrauterine damage, e.g., viral infections, on development of autism is well established [58] and, like other potential postnatal risk factors, not recorded here.

The present findings are derived from a large, deeply phenotyped sample of schizophrenic subjects with uniquely comprehensive information on multiple drug consumption, but their translation to the general population has still to ensue with some caution. Nevertheless, preadult polytoxicomania in our sample occurs way before onset of the disease, and may thus reflect general mechanisms of damage to the juvenile brain that predispose to multiple drug consumption rather than any direct association with mental illness. The view of essential generalizability

receives support by our studies on violent aggression, where we had the chance to include two general population samples that revealed the same stair-pattern of aggression development with risk accumulation as the 4 independent schizophrenia cohorts [16]. The earlier onset of mental illness in polytoxicomanic individuals shown here emphasizes another devastating role of multiple drug use on brain functions and on outcome in mental disease. Mechanistically, this phenomenon as well as the observed behavioral alterations are likely mediated by epigenetic changes that occur relatively non-specifically in response to accumulated risk factor exposure in early life. These epigenetic changes apparently increase, as others and we have reported previously, the propensity for later substance abuse, depression, violent aggression, and a range of other negative health outcomes [16, 59–61].

On top of the remarkable environmental impact on polytoxicomania, we provide first evidence of a genetic predisposition to this behavioral abnormality as extracted from our novel GWAS–PGAS approach. This novel approach was only possible based on the comprehensive and precise information on drug consumption in our

sample, which allowed the accurate classification of just mildly varying phenotypes for respective GWAS. We defined strict criteria for this GWAS–PGAS approach, which is potentially applicable to other genetic association studies as well. Our procedure is grounded on the working hypotheses that true genetic signals remain stable despite mild modifications in phenotype definition and are likely not isolated but in linkage disequilibrium with related signals, and that genetic associations with the target phenotype (here: polytoxicomania) are independent of any other disease diagnosis (here: schizophrenia). Diagnoses-overlapping, i.e., pleiotropic genes [38] were purposely excluded here. The mild variation of phenotype definitions allowed us to identify genetic associations that are more specific for polytoxicomania and not "contaminated" by associations stemming solely from single substance abuse.

We ultimately extracted an interesting set of markers as potential "bouquet of common genetic denominators" for juvenile polytoxicomania, many of them strongly expressed in brain and kidney. Unfortunately, no comparable sample of deeply phenotyped polytoxicomanic individuals is presently available for replication studies—despite intensive worldwide search—but would be crucial to have. Nevertheless, the nature of the obtained first genetic results seems encouraging.

Data availability

The data supporting the findings of this study are not publicly available because of strict obligation to human data protection laws. The contained information could lead to identification of subjects and compromise research participants' privacy and consent. Additional information and summary statistics are available on request from the corresponding author (HE).

Author contributions Concept and supervision of the study: HE Design: AAS & HE. Data acquisition/analysis/interpretation: AAS, VDG, JS, AR, MB and HE. Drafting manuscript: AAS & HE. Drafting display items: AAS & HE. All authors read and approved the final version of the manuscript.

Compliance with ethical standards

Conflict of interest The authors declare no competing interests.

Publisher's note Springer Nature remains neutral with regard to jurisdictional claims in published maps and institutional affiliations.

References

1. Toftdahl NG, Nordentoft M, Hjorthøj C. Prevalence of substance use disorders in psychiatric patients: a nationwide Danish population-based study. Soc Psychiatry Psychiatr Epidemiol. 2016;51:129–40.
2. Mueser KT, Yarnold PR, Rosenberg SD, Swett C, Miles KM, Hill D. Substance use disorder in hospitalized severely mentally ill psychiatric patients: Prevalence, correlates, and subgroups. Schizophr Bull. 2000;26:179–92.
3. Alaja R, Seppä K, Sillanaukee P, Tienari P, Huyse FJ, Herzog T, et al. Physical and mental comorbidity of substance use disorders in psychiatric consultations. Alcohol Clin Exp Res. 1998;22:1820–4.
4. Connor JP, Gullo MJ, White A, Kelly AB. Polysubstance use: diagnostic challenges, patterns of use and health. Curr Opin Psychiatry. 2014;27:269–75.
5. Hjorthøj C, Østergaard MLD, Benros ME, Toftdahl NG, Erlangsen A, Andersen JT, et al. Association between alcohol and substance use disorders and all-cause and cause-specific mortality in schizophrenia, bipolar disorder, and unipolar depression: a nationwide, prospective, register-based study. The Lancet. Psychiatry 2015;2:801–8.
6. Conway KP, Vullo GC, Nichter B, Wang J, Compton WM, Iannotti RJ, et al. Prevalence and patterns of polysubstance use in a nationally representative sample of 10th Graders in the United States. J Adolesc Heal. 2013;52:716–23.
7. Moss HB, Chen CM, Yi HY. Early adolescent patterns of alcohol, cigarettes, and marijuana polysubstance use and young adult substance use outcomes in a nationally representative sample. Drug Alcohol Depend. 2014;136:51–62.
8. White A, Chan GCK, Quek LH, Connor JP, Saunders JB, Baker P, et al. The topography of multiple drug use among adolescent Australians: findings from the national drug strategy household survey. Addict Behav. 2013;38:2068–73.
9. Bailey AJ, Farmer EJ, Finn PR. Patterns of polysubstance use and simultaneous co-use in high risk young adults. Drug Alcohol Depend. 2019;205:107656
10. Brière FN, Fallu JS, Descheneaux A, Janosz M. Predictors and consequences of simultaneous alcohol and cannabis use in adolescents. Addict Behav. 2011;36:785–8.
11. Collins RL, Ellickson PL, Bell RM. Simultaneous polydrug use among teens: prevalence and predictors. J Subst Abus. 1998;10:233–53.
12. Jongenelis M, Pettigrew S, Lawrence D, Rikkers W. Factors associated with poly drug use in adolescents. Prev Sci. 2019;20:695–704.
13. Stepniak B, Papiol S, Hammer C, Ramin A, Everts S, Hennig L, et al. Accumulated environmental risk determining age at schizophrenia onset: a deep phenotyping-based study. The Lancet. Psychiatry 2014;1:444–53.

14. Begemann M, Seidel J, Poustka L, Ehrenreich H. Accumulated environmental risk in young refugees—a prospective evaluation. EClinMed. 2020;22:100345.

15. Lederbogen F, Kirsch P, Haddad L, Streit F, Tost H, Schuch P, et al. City living and urban upbringing affect neural social stress processing in humans. Nature 2011;474:498–501.

16. Mitjans M, Seidel J, Begemann M, Bockhop F, Moya-Higueras J, Bansal V, et al. Violent aggression predicted by multiple pre-adult environmental hits. Mol Psychiatry. 2019;24:1549–64.

17. Evans GW, Li D, Whipple SS. Cumulative risk and child development. Psychol Bull. 2013;139:1342–96.

18. Adelmann PK. Social environmental factors and preteen health-related behaviors. J Adolesc Heal. 2005;36:36–47.

19. Racz SJ, Saha S, Trent M, Adger H, Bradshaw CP, Goldweber A, et al. Polysubstance use among minority adolescent males incarcerated for serious offenses. child youth care. Forum 2016;45: 205–20.

20. Sharma S, Mustanski B, Dick D, Bolland J, Kertes DA. Protective factors buffer life stress and behavioral health outcomes among high-risk youth. J Abnorm Child Psychol. 2019;47:1289–301.

21. Ribbe K, Friedrichs H, Begemann M, Grube S, Papiol S, Kästner A, et al. The cross-sectional GRAS sample: a comprehensive phenotypical data collection of schizophrenic patients. BMC Psychiatry. 2010;10:91.

22. Hancock DB, Guo Y, Reginsson GW, Gaddis NC, Lutz SM, Sherva R, et al. Genome-wide association study across European and African American ancestries identifies a SNP in DNMT3B contributing to nicotine dependence. Mol Psychiatry. 2018;23: 1911–9.

23. Gelernter J, Sherva R, Koesterer R, Almasy L, Zhao H, Kranzler HR, et al. Genome-wide association study of cocaine dependence and related traits: FAM53B identified as a risk gene. Mol Psychiatry. 2014;19:717–23.

24. Treutlein J, Cichon S, Ridinger M, Wodarz N, Soyka M, Zill P, et al. Genome-wide association study of alcohol dependence. Arch Gen Psychiatry. 2009;66(Jul):773–84.

25. Mallard TT, Ashenhurst JR, Harden KP, Fromme K. GABRA2, alcohol, and illicit drug use: an event-level model of genetic risk for polysubstance use. J Abnorm Psychol. 2018;127:190–201.

26. Sanchez-Roige S, Fontanillas P, Elson SL, Gray JC, De Wit H, MacKillop J, et al. Genome-wide association studies of impulsive personality traits (BIS-11 and UPPS-P) and drug experimentation in up to 22,861 adult research participants identify loci in the CACNA1I and CADM2 genes. J Neurosci. 2019;39:2562–72.

27. Zhang P-W, Ishiguro H, Ohtsuki T, Hess J, Carillo F, Walther D, et al. Human cannabinoid receptor 1: 5′ exons, candidate regulatory regions, polymorphisms, haplotypes and association with polysubstance abuse. Mol Psychiatry. 2004;9:916–31.

28. Waaktaar T, Kan KJ, Torgersen S. The genetic and environmental architecture of substance use development from early adolescence into young adulthood: a longitudinal twin study of comorbidity of alcohol, tobacco and illicit drug use. Addiction 2018;113:740–8.

29. Fergusson DM, Boden JM, Horwood LJ. Cannabis use and other illicit drug use: testing the cannabis gateway hypothesis. Addiction 2006;101:556–69.

30. Kandel D, Kandel E. The gateway hypothesis of substance abuse: developmental, biological and societal perspectives. Acta Paediatr Int J Paediatr. 2015;104:130–7.

31. Lehrl S. Mehrfachwahl-Wortschatz-Intelligenztest: MWT-B. Spitta; 1999.

32. Kästner A, Begemann M, Michel TM, Everts S, Stepniak B, Bach C, et al. Autism beyond diagnostic categories: characterization of autistic phenotypes in schizophrenia. BMC Psychiatry. 2015;15: 1–12.

33. Hammer C, Stepniak B, Schneider A, Papiol S, Tantra M, Begemann M, et al. Neuropsychiatric disease relevance of circulating anti-NMDA receptor autoantibodies depends on blood-brain barrier integrity. Mol Psychiatry. 2014;19:1143–9.

34. Rouillard AD, Gundersen GW, Fernandez NF, Wang Z, Monteiro CD, McDermott MG, et al. The harmonizome: a collection of processed datasets gathered to serve and mine knowledge about genes and proteins. Database (Oxf). 2016;2016:1–16.

35. Purcell S, Neale B, Todd-Brown K, Thomas L, Ferreira MAR, Bender D, et al. PLINK: a tool set for whole-genome association and population-based linkage analyses. Am J Hum Genet. 2007;81:559–75.

36. de Leeuw CA, Mooij JM, Heskes T, Posthuma D. MAGMA: generalized gene-set analysis of GWAS data. PLoS Comput Biol. 2015;11:1–19.

37. R Core Team. R: A Language and environment for statistical computing. Vienna, Austria: R Core Team; 2018.

38. Lee PH, Anttila V, Won H, Feng YCA, Rosenthal J, Zhu Z, et al. Genomic relationships, novel loci, and pleiotropic mechanisms across eight psychiatric disorders. Cell. 2019;179:1469.e11

39. Cuffel BJ, Shumway M, Chouljian TL, Macdonald T. A longitudinal study of substance use and community violence in schizophrenia. J Nerv Ment Dis. 1994;182:704–8.

40. Dornbusch SM, Lin IC, Munroe PT, Bianchi AJ. Adolescent polydrug use and violence in the United States. Int J Adolesc Med Health. 1999;11:197–219.

41. Beaudoin M, Potvin S, Giguère CE, Discepola SL, Dumais A. Persistent cannabis use as an independent risk factor for violent behaviors in patients with schizophrenia. npj Schizophr. 2020;6:1–8.

42. Olthuis JV, Darredeau C, Barrett SP. Substance use initiation: the role of simultaneous polysubstance use. Drug Alcohol Rev. 2013;32:67–71.

43. Secades-Villa R, Garcia-Rodríguez O, Jin CJ, Wang S, Blanco C. Probability and predictors of the cannabis gateway effect: a national study. Int J Drug Policy. 2015;26:135–42.

44. Fergusson DM, Horwood LJ. Does cannabis use encourage other forms of illicit drug use? Addiction. 2000;95:505–20.

45. Hall WD, Lynskey M. Is cannabis a gateway drug? Testing hypotheses about the relationship between cannabis use and the use of other illicit drugs. Drug Alcohol Rev. 2005;24:39–48.

46. Lynskey MT, Heath AC, Bucholz KK, Slutske WS, Madden PAF, Nelson EC, et al. Escalation of drug use in early-onset cannabis users vs co-twin controls. J Am Med Assoc. 2003;289:427–33.

47. Van OsJ, Bak M, Hanssen M, Bijl RV, De Graaf R, Verdoux H. Cannabis use and psychosis: a longitudinal population-based study. Am J Epidemiol. 2002;156:319–27.

48. Di Forti M, Morgan C, Dazzan P, Pariante C, Mondelli V, Marques TR, et al. High-potency cannabis and the risk of psychosis. Br J Psychiatry. 2009;195:488–91.

49. Semple DM, McIntosh AM, Lawrie SM. Cannabis as a risk factor for psychosis: systematic review. J Psychopharmacol. 2005;19:187–94.

50. Arseneault L, Cannon M, Poulton R, Murray R, Caspi A, Moffitt TE. Cannabis use in adolescence and risk for adult psychosis: Longitudinal prospective study. Br Med J. 2002;325:1212–3.

51. Murray RM, Hall W. Will legalization and commercialization of cannabis use increase the incidence and prevalence of psychosis? JAMA Psychiatry. 2020;77:777–8.

52. Gage SH, Hickman M, Zammit S. Association between cannabis and psychosis: epidemiologic evidence. Biol Psychiatry. 2016;79:549–56.

53. Fergusson DM, Poulton R, Smith PF, Boden JM. Cannabis and psychosis. Bmj 2006;332:172–5.

54. Hüttner E, Matthies U, Nikolova T, Ehrenreich H. A follow-up study on chromosomal aberrations in lymphocytes of alcoholics

during early, medium, and long-term abstinence. Alcohol Clin Exp Res. 1999;23:344–8.

55. Temple EC, Driver M, Brown RF. Cannabis use and anxiety: Is stress the missing piece of the puzzle? Front Psychiatry. 2014;5:1–13.

56. Bailey A, Le Couteur A, Gottesman I, Bolton P, Simonoff E, Yuzda E, et al. Autism as a strongly genetic disorder: evidence from a British twin study. Psychol Med. 1995;25:63–77.

57. Tick B, Bolton P, Happé F, Rutter M, Rijsdijk F. Heritability of autism spectrum disorders: a meta-analysis of twin studies. J Child Psychol Psychiatry Allied Discip. 2016;57:585–95.

58. Brown AS. Epidemiologic studies of exposure to prenatal infection and risk of schizophrenia and autism. Dev Neurobiol. 2012;72:1272–6.

59. Lewis CR, Olive MF. Early-life stress interactions with the epigenome: potential mechanisms driving vulnerability toward psychiatric illness. Behav Pharm. 2014;25:341–51.

60. Vaiserman AM. Epigenetic programming by early-life stress: evidence from human populations. Dev Dyn. 2015;244:254–65.

61. Bahari-Javan S, Varbanov H, Halder R, Benito E, Kaurani L, Burkhardt S, et al. HDAC1 links early life stress to schizophrenia-like phenotypes. Proc Natl Acad Sci. 2017;114:E4686–94.

SUPPLEMENTARY TABLES
Preadult polytoxicomania – strong environmental underpinnings and first genetic hints

Agnes A. Steixner-Kumar[1], Vinicius Daguano Gastaldi[1], Jan Seidel[1],
Albert Rosenberger[2], Martin Begemann[1,3], and Hannelore Ehrenreich[1]*

[1]Clinical Neuroscience, Max Planck Institute of Experimental Medicine, Göttingen, Germany
[2] Department of Genetic Epidemiology, University Medical Center,
Georg-August-University, Göttingen, Germany
[3]Department of Psychiatry and Psychotherapy, University Medical Center,
Georg-August-University, Göttingen, Germany

Running head: Origins of polytoxicomania

Key words: Multiple drug use, schizophrenia, environmental risk, cannabis, alcohol, genome-wide association study (GWAS), phenotype-based genetic association study (PGAS), suicidality, autism

*Correspondence:
Prof. Hannelore Ehrenreich, MD, DVM
Clinical Neuroscience
Max Planck Institute of Experimental Medicine
Hermann-Rein-Str.3
37075 Göttingen, GERMANY
Phone +49-551-3899628
Fax +49-551-3899670
E-Mail: **ehrenreich@em.mpg.de**

 Supplementary Table file contains:
 - Supplementary Tables1-3
Please note: **In addition to this file, a Supplementary Figures file is available containing:**
 - Supplementary Figures1-4

Supplementary Table1. Lifetime prevalence (%) of illicit drug use amongst non-polytoxicomanic and polytoxicomanic individuals.

Non-polytoxicomanic individuals (lifetime)

Frequency of lifetime use	(almost) daily	several times per week	1 per month to 1 per week	3-11 times per year	up to 2 times per year	never
Drug	% Individuals using a particular drug at given frequency					
Cocaine	0.08	0.08	0.17	0.08	3.67	95.91
Opioids	0.5	0.08	0.08	0	1.5	97.84
Hallucinogens	0	0	0.25	0	4.28	95.48
Ecstasy	0	0	0.08	0	2.31	97.6
Amphetamines	0.25	0.17	0.33	0	1.58	97.67
Prescription drugs	1.48	0.08	0.25	0.08	0.16	97.94
Inhalants	0.33	0	0.08	0	0.66	98.92

Polytoxicomanic individuals (lifetime)

Frequency of lifetime use	(almost) daily	several times per week	1 per month to 1 per week	3-11 times per year	up to 2 times per year	never
Drug	% Individuals using a particular drug at given frequency					
Cocaine	15.31	5.94	7.81	3.44	54.69	12.81
Opioids	17.87	1.25	2.82	0.31	32.29	45.45
Hallucinogens	2.79	2.23	6.7	3.63	66.76	17.88
Ecstasy	5.57	24.46	11.76	2.48	31.58	24.15
Amphetamines	22.67	14.67	11.67	2	33	16
Prescription drugs	11.78	0.82	1.1	1.37	9.86	75.07
Inhalants	1.19	0.59	0.59	0.59	24.63	72.4

Supplementary Table2. Top 41 polytoxicomania-associated SNPs

SNP	Chr	Position	A1>A2	Gene (±10kb)	Region	Annotation	Full name of gene	Previously reported GWAS associations (p<1x10^-5) with SNP or gene (psychiatric phenotypes only)
rs41270726	1	167633270	G>T	RCSD1	protein coding	intronic	RCSD Domain Containing 1	None
rs12038205	1	83897416	C>T	-	intergenic	-	-	None
rs1840328	2	165785586	A>G	SLC38A11	protein coding	intronic	Solute Carrier Family 38 Member 11	None
rs16849964	2	165802505	C>T	SLC38A11	protein coding	intronic	Solute Carrier Family 38 Member 11	
rs1115381■	2	234505285	T>C	-	intergenic	-	-	None
rs7592624	2	234602906	G>A	UGT1A complex region	protein coding	-	UDP Glucuronosyltransferase Family 1 Member A Complex Locus	None
rs3821165	2	36610069	G>A	CRIM1	protein coding	intronic	Cysteine Rich Transmembrane BMP Regulator 1	Irritability[1] (gene)
rs10490237	2	50377832	A>C	NRXN1	protein coding	intronic	Neurexin 1	Depressive affect subcluster and symptoms[1-3] (SNP, gene*), neuroticism[1,2,4](SNP, gene*), well-being[2] (SNP, gene*), alcohol dependence[5] (gene), initiation*/ever*/current/never/regular smoking[1,6-8] (gene), nicotine dependence symptoms[9] (gene), miserableness, fed-up and guilty feelings[1,10]* (gene), schizophrenia[11] (gene), temperament/novelty seeking[12] (gene)
rs10198285	2	61979566	A>G	-	intergenic	-	-	None
rs10496205	2	77493707	C>T	LRRTM4	protein coding	intronic	Leucine Rich Repeat Transmembrane Neuronal 4	ADHD[13] (gene), past/ever smoking, alcohol with meals* and ever cannabis*[2] (gene), cannabis use[14] (gene), number of sexual partners*[7] (gene), risky behaviors 1st PC*[7] (gene), schizophrenia[11,15,16] (gene), insomnia*[17] (gene)
rs9862216	3	147368416	G>A	-	intergenic	-	-	None

rs16852499	3	168326057	G>A	EGFEM1P	pseudo-gene	intronic	EGF Like And EMI Domain Containing 1, Pseudogene	Epilepsy[18] (gene), response to paliperidone in schizophrenia[19] (gene)
rs11131889■	4	179851965	T>C	-	intergenic	-	-	None
rs10027326	4	19056854	A>G	-	intergenic	-	-	None
rs2703898	4	38511326	G>A	RP11-83C7.2	lincRNA	intronic	-	None
rs10517941■	4	66694545	C>A	-	intergenic	-	-	None
rs13126941	4	7372806	C>T	SORCS2	protein coding	intronic	Sortilin Related VPS10 Domain Containing Receptor 2	Alcohol dependence* and withdrawal symptoms*[5,20] (gene), insomnia[1,21](gene), tense*[1] (gene), attention function in ADHD[22] (gene), depressive/manic episodes in bipolar disorder[23] (gene), neuroticism[24] (gene), anorexia nervosa[25] (gene), response to antidepressants[26] (gene), coffee consumption[27] (gene)
rs17284960	5	163623502	C>T	CTC-207P7.1	lincRNA	intronic	-	None
rs6926569	6	150375211	A>G	ULBP3	protein coding	-	UL16 Binding Protein 3	None
rs390661	6	95090661	C>T	-	intergenic	-	-	None
rs11764575	7	115611309	G>A	TFEC	protein coding	intronic	Transcription Factor EC	Chronotype/morningness*[17,28,29] (gene)
rs2286248	7	14216609	G>A	DGKB	protein coding	intronic	Diacylglycerol Kinase Beta	Alcohol dependence[5] (gene), Sensitivity*[1,10] (gene), morningness[17] (gene), major depression[30] (gene), nicotine dependence symptoms[9] (gene).
rs10279025	7	21247253	T>C	RN7SL542P	misc RNA	-	-	None
rs501344	8	103114573	G>A	NCALD	protein coding	intronic	Neurocalcin Delta	Sleep duration[1,17,31] (gene), major depression and alcohol dependence comorbidity[32] (gene), coffee consumption[33] (gene)
rs10098626■	8	34888914	G>A	-	intergenic	-	-	None
rs2169385	8	9206678	G>A	RP11-115J16.1	lincRNA	intronic	-	Neuroticism[4] (SNP)
rs4743569	9	105414408	A>G	LINC00587	lincRNA	intronic	-	None
rs2122582	9	107009131	T>C	-	intergenic	-	-	None

SNP	Chr	Position	A1>A2	Gene		Region	Gene name	Previously reported associations
rs7851907	9	9006519	C>G	PTPRD	protein coding	intronic	Protein Tyrosin Phosphatase Receptor Type D	Response to amphetamine[34] (gene), insomnia*[1,21] (gene), alcohol dependence*[5] (gene), baseline positive affect factor score*[34] (gene), chronotype/morningness/sleep duration*[1,2,29] (gene), depressive symptoms[2] (gene), well-being[2] (gene), ADHD and conduct disorder[35] (gene), smoking initiation*[6] (gene), opioid use cessation[36] (gene), restless leg syndrome[37] (gene), epilepsy remission after treatment[38] (gene), migraine[39] (gene)
rs11258725	10	5720424	T>A	FAM208B	protein coding	-	Transcription Activation Suppressor Family Member 3	None
rs7101264■	10	91293184	C>A	SLC16A12	protein coding	intronic	Solute Carrier Family 38 Member 10	None
rs35724134	11	116306907	C>A	-	intergenic	-	-	None
rs599905	11	128544891	A>G	RP11-744N12.3	antisense	intronic	-	None
rs10501240■	11	40695479	C>G	LRRC4C	protein coding	intronic	Leucine Rich Repeat Containing 4C	Risky behaviors 1st PC*[7] (gene), ever/regular smoker[6,7](gene), age at smoking initiation*[7] (gene), social support[1] (gene)
rs12284778	11	80829874	T>C	-	intergenic	-	-	None
rs11111457	12	103525945	G>T	RP11-328J6.1	antisense	intronic	-	None
rs1863879	12	105046250	G>A	CHST11	protein coding	intronic	Carbohydrate Sulfotransferase 12	Cannabis dependence[40] (gene), response to major depression treatment[41] (gene)
rs12316797	12	43160744	T>G	-	intergenic	-	-	None
rs8007030	14	102399354	T>A	PPP2R5C	protein coding	-	Protein Phosphatase 2 Regulatory Subunit B'Gamma	Insomnia[17] (gene), autism[42] (gene)
rs2241035	16	90108832	C>T	GAS8, URAHP	protein coding	intronic, 3' downstream	Growth Arrest Specific 8	Use of sun/UV protection*[1] (gene)
rs2267213■	22	33863218	G>A	LARGE	protein coding	intronic	LARGE Xylosyl- And Glucuronyltransferase 1	Alcohol dependence*[5] (gene), neuroticism[2] (gene), well-being[2] (gene)

Chr: Chromosome. A1: Major allele, A2: Minor allele. For all SNP-genes highlighted in green, human tissue expression is depicted in Supplementary Figure2. ■ indicates the 7 SNPs with p<0.001 in all GWAS from set 1. Previously reported associations passing genome-wide significance ($p < 5 \times 10^{-8}$) are marked with an asterisk. "Gene" or "SNP" in brackets indicate the origin of the reported association: previous association of one or more SNPs located in the respective gene (gene) or a direct association of the here reported SNP with the phenotype (SNP).

Supplementary Table3. Top polytoxicomania-associated genes (MAGMA gene-based analysis)

Gene	Chr	Start	Stop	# SNPs	Full name of gene	Previously reported GWAS associations (p<1x10^-5) (psychiatric phenotypes only)
CAD	2	27440258	27466660	2	Carbamoyl-Phosphate Synthetase 2, Aspartate Transcarbamylase, And Dihydroorotase	Alcohol intake* /drinks per week*/drinks per day[1,6,7]
ROCK1	18	18529701	18691812	4	Rho Associated Coiled-Coil Containing Protein Kinase 1	None
SLC30A3	2	27477440	27501093	1	Solute Carrier Family 30 Member 3	Positive affect[2], alcohol intake*/drinks per week*/drinks per day*
SLC5A6	2	27422455	27435175	2	Solute Carrier Family 5 Member 6	Alcohol intake*/weekly red wine intake/drinks per week*/drinks per day[1,6,7]
SMC2	9	106856213	106903700	15	Structural Maintenance Of Chromosomes 2	None
PLA2G2E	1	20246800	20250110	1	Phospholipase A2 Group IIE	None
FAM208B	10	5726801	5807742	14	Transcription Activation Suppressor Family Member 2	None
ACKR3	2	237469424	237491001	8	Atypical Chemokine Receptor 3	Age at onset of alcohol dependence[43]
OR51G1	11	4944604	4945569	4	Olfactory Receptor Family 51 Subfamily G Member 1 (Gene/Pseudogene)	None
KRTAP1-5	17	39182278	39183454	1	Keratin Associated Protein 1-5	None
LOC100133128	4	9400867	9405291	1	-	NA

Chr: Chromosome; # SNPs: Number of SNPs per gene included in analysis. Previously reported associations passing genome-wide significance (p<5x10^-8) are marked with an asterisk. NA: Locus not listed in GWAS atlas or GWAS catalogue.

1   Watanabe, K. *et al. Nat Genet* **51**, 1339-1348 (2019).
2   Baselmans, B. M. L. *et al. Nat Genet* **51**, 445-451 (2019).
3   Nagel, M. *et al. Nat Genet* **50**, 920-927 (2018).
4   Luciano, M. *et al. Nat Genet* **50**, 6-11 (2018).
5   Wang, J. C. *et al. Mol Psychiatry* **18**, 1218-1224 (2013).
6   Liu, M. *et al. Nat Genet* **51**, 237-244 (2019).
7   Karlsson Linner, R. *et al. Nat Genet* **51**, 245-257 (2019).
8   Kichaev, G. *et al. Am J Hum Genet* **104**, 65-75 (2019).
9   Gelernter, J. *et al. Biol Psychiatry* **77**, 493-503 (2015).
10   Nagel, M. *et al. Nat Commun* **9**, 905 (2018).
11   Pardinas, A. F. *et al. Nat Genet* **50**, 381-389 (2018).
12   Service, S. K. *et al. Transl Psychiatry* **2**, e116 (2012).
13   Middeldorp, C. M. *et al. J Am Acad Child Adolesc Psychiatry* **55**, 896-905 e896 (2016).
14   Pasman, J. A. *et al. Nat Neurosci* **21**, 1161-1170 (2018).
15   Goes, F. S. *et al. Am J Med Genet B Neuropsychiatr Genet* **168**, 649-659 (2015).
16   Ikeda, M. *et al. Schizophr Bull* **45**, 824-834 (2019).
17   Jansen, P. R. *et al. Nat Genet* **51**, 394-403 (2019).
18   International League Against Epilepsy Consortium on Complex Epilepsies. Electronic address, e.-a. u. e. a. *Lancet Neurol* **13**, 893-903 (2014).
19   Li, Q. *et al. Pharmacogenet Genomics* **27**, 7-18 (2017).
20   Smith, A. H. *et al. Alcohol Clin Exp Res* **42**, 2337-2348 (2018).
21   Lane, J. M. *et al. Nat Genet* **51**, 387-393 (2019).
22   Alemany, S. *et al. Am J Med Genet B Neuropsychiatr Genet* **168**, 459-470 (2015).
23   Fabbri, C. *et al. Prog Neuropsychopharmacol Biol Psychiatry* **65**, 17-24 (2016).
24   Okbay, A. *et al. Nat Genet* **48**, 624-633 (2016).
25   Duncan, L. *et al. Am J Psychiatry* **174**, 850-858 (2017).
26   Fabbri, C. *et al. Pharmacogenomics J* **18**, 413-421 (2018).
27   Jia, H. *et al. BMC Genet* **20**, 61 (2019).
28   Jones, S. E. *et al. PLoS Genet* **12**, e1006125 (2016).
29   Jones, S. E. *et al. Nat Commun* **10**, 343 (2019).
30   Hall, L. S. *et al. Transl Psychiatry* **8**, 9 (2018).
31   Dashti, H. S. *et al. Nat Commun* **10**, 1100 (2019).
32   Zhou, H. *et al. JAMA Psychiatry* **74**, 1234-1241 (2017).
33   Amin, N. *et al. Mol Psychiatry* **17**, 1116-1129 (2012).
34   Hart, A. B. *et al. PLoS One* **7**, e42646 (2012).
35   Anney, R. J. *et al. Am J Med Genet B Neuropsychiatr Genet* **147B**, 1369-1378 (2008).
36   Cox, J. W. *et al. J Clin Med* **9** (2020).
37   Schormair, B. *et al. Nat Genet* **40**, 946-948 (2008).
38   Speed, D. *et al. Hum Mol Genet* **23**, 247-258 (2014).
39   Anttila, V. *et al. Nat Genet* **45**, 912-917 (2013).
40   Agrawal, A. *et al. Addict Biol* **16**, 514-518 (2011).
41   Ji, Y. *et al. Br J Clin Pharmacol* **78**, 373-383 (2014).
42   Anney, R. *et al. Hum Mol Genet* **19**, 4072-4082 (2010).
43   Kapoor, M. *et al. Drug Alcohol Depend* **142**, 56-62 (2014).

SUPPLEMENTARY FIGURES

Preadult polytoxicomania – strong environmental underpinnings and first genetic hints

Agnes A. Steixner-Kumar[1], Vinicius Daguano Gastaldi[1], Jan Seidel[1],
Albert Rosenberger[2], Martin Begemann[1,3], and Hannelore Ehrenreich[1]*

[1]Clinical Neuroscience, Max Planck Institute of Experimental Medicine, Göttingen, Germany
[2] Department of Genetic Epidemiology, University Medical Center,
Georg-August-University, Göttingen, Germany
[3]Department of Psychiatry and Psychotherapy, University Medical Center,
Georg-August-University, Göttingen, Germany

Running head: Origins of polytoxicomania

Key words: Multiple drug use, schizophrenia, environmental risk, cannabis, alcohol, genome-wide association study (GWAS), phenotype-based genetic association study (PGAS), suicidality, autism

*Correspondence:
Prof. Hannelore Ehrenreich, MD, DVM
Clinical Neuroscience
Max Planck Institute of Experimental Medicine
Hermann-Rein-Str.3
37075 Göttingen, GERMANY
Phone +49-551-3899628
Fax +49-551-3899670
E-Mail: **ehrenreich@em.mpg.de**

This Supplementary Figure file contains:

> **Supplementary Figures1-4**
>
> *Please note*: **In addition to this file, a Supplementary Tables file is available, containing:**
> Supplementary Tables1-3 showing prevalence of illicit drug use and listing top SNP and gene (MAGMA) results.

Steixner-Kumar et al Supplementary Figure1
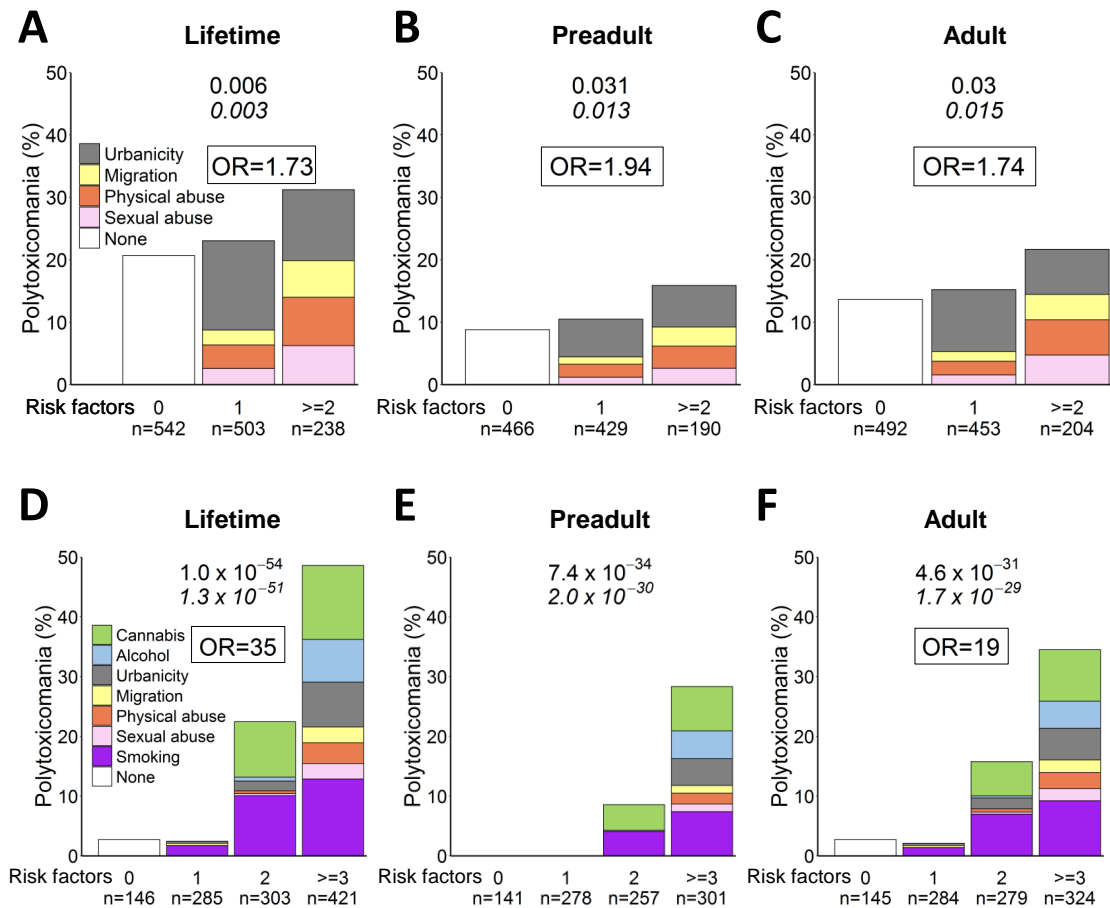
Supplementary Figure1: (A-C) Accumulation model of 4 risk factors (i.e. excluding cannabis and alcohol) as predictors of lifetime (A), preadult (B) and adult (C) polytoxicomania. **(D-F)** Accumulation model including smoking in an exploratory fashion (despite multicollinearity) as additional risk factor, i.e. 7 risk factor model, of lifetime (D), preadult (E) and postadult (F) polytoxicomania. Please note that statistics in D-F are just provided for orientation. These statistics should be interpreted with caution due to multicollinearity amongst risk factors (tight association of smoking and cannabis) and thus violation of independency assumptions. Therefore, also no OR was calculated for E (0 polytoxicomanic individuals in lowest risk group requiring permutation). Chi²-test p-values (two-sided) on top of graph, Cochran-Armitage test p-values (two-sided) underneath in italics. OR: Odds Ratio.

Steixner-Kumar et al Supplementary Figure2
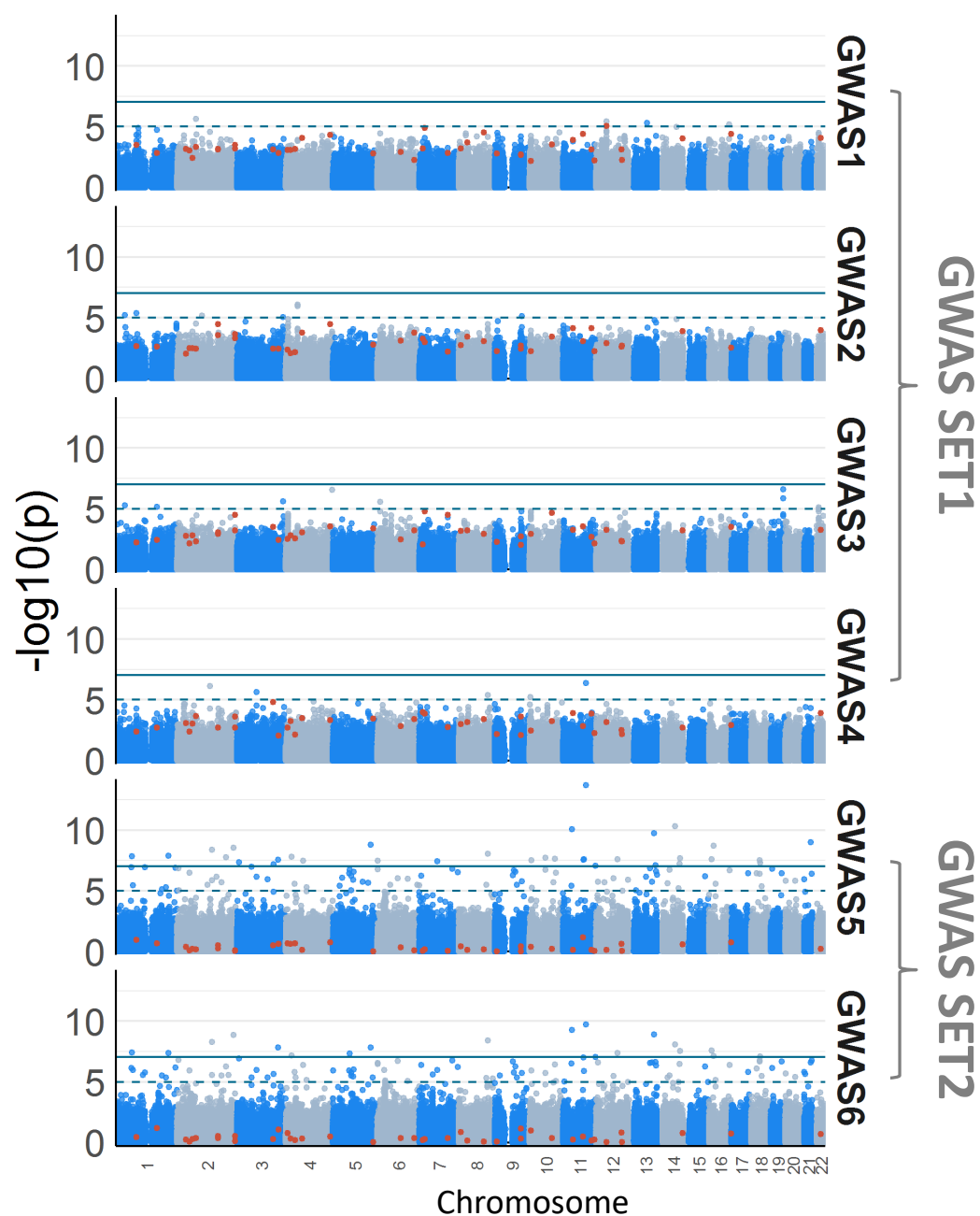
Supplementary Figure2:
Manhattan plots showing results from GWAS1-6. Final 41 top SNPs with p<0.01 in GWAS1-4 and p>0.05 in GWAS5-6 highlighted in red. Solid blue line indicates genome wide significance level (p<9.4x10^{-8} = 0.05/530,316). Dashed blue line indicates suggestive significance level (p<1x10^{-5}).

Steixner-Kumar et al Supplementary Figure3
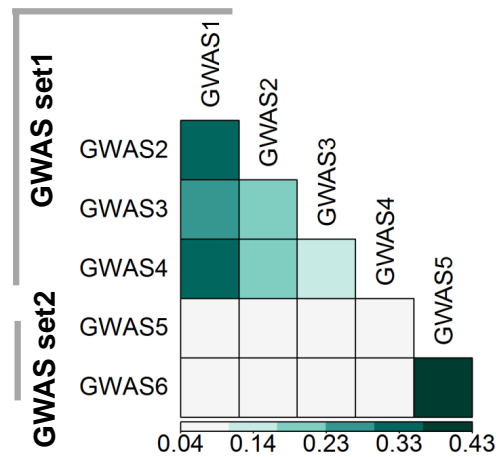
Supplementary Figure3:
Jaccard index matrix shows similarity between raw results (p<0.05)
from GWAS1-6. Note that GWAS1-4 (GWAS set1) form one similarity
cluster, whereas GWAS5-6 (GWAS set2) form another similarity cluster.

Steixner-Kumar et al Supplementary Figure4
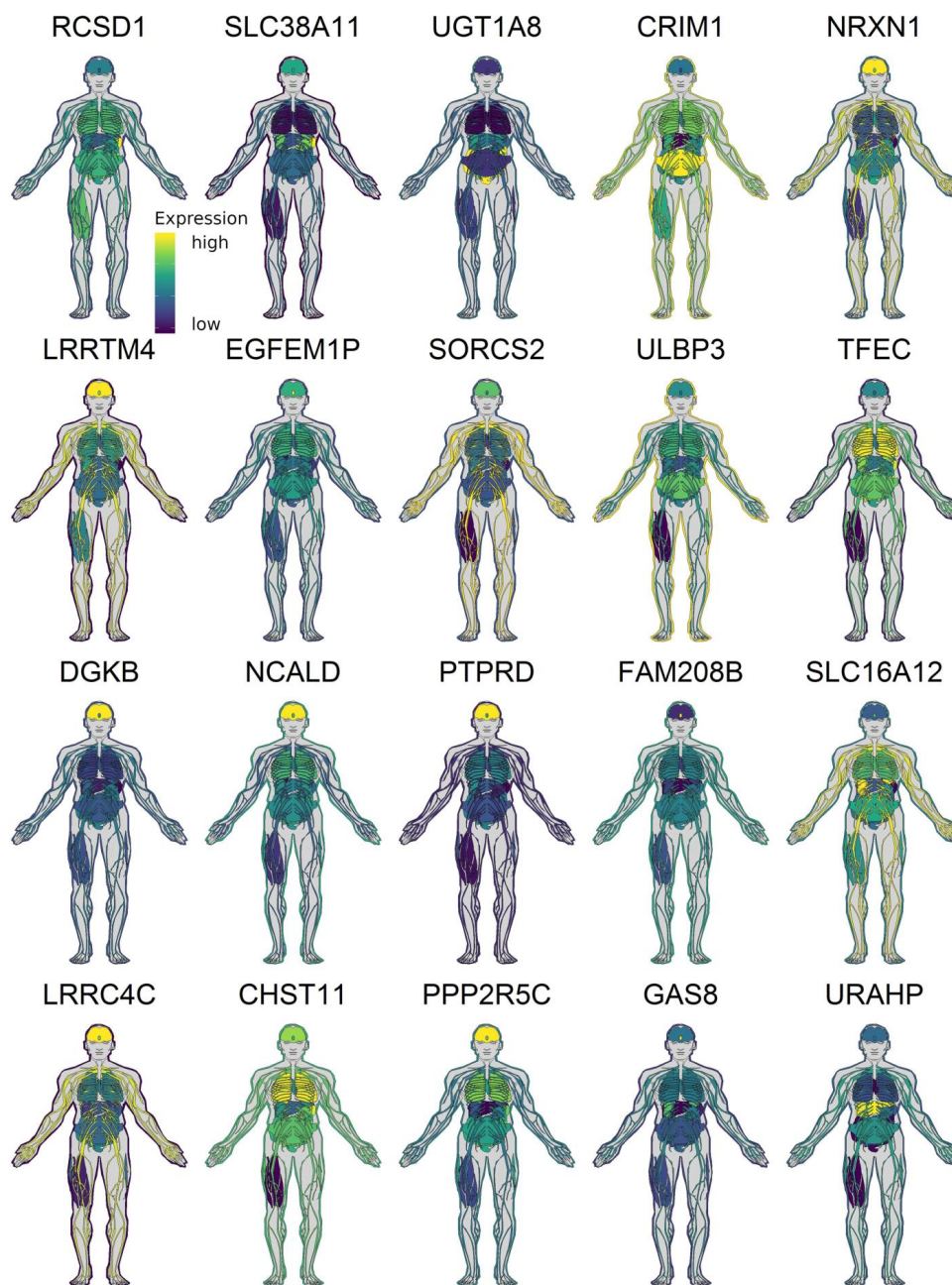
Supplementary Figure4:
Illustration of gene expression profiles. Human gene expression of the 20 genes in which top polytoxicomania-associated SNPs are located (expression data downloaded from Harmonizome). Genes correspond to the SNPs marked in green in Supplementary Table1.

4 Project II: Hippocampal neurons respond to brain activity with functional hypoxia

4.1 Overview of Project II

Hypoxia describes a condition under which cells or tissues are relatively deprived of oxygen, i.e., their oxygen demand exceeds the oxygen supply. Whereas the harmful effects hypoxia have often been studied in context of ischemia, cardiac arrest, apnea and cancer, more recently the crucial role of hypoxia in embryonic development, neurogenesis, angiogenesis and hematopoiesis has become apparent (Dunwoodie, 2009; Fagel et al., 2006; Parmar et al., 2007; Santilli et al., 2010; Semenza, 2001; Vieira et al., 2011; Zhu et al., 2005; Zhu et al., 2010). Thus, physiologically occurring hypoxia is by no means deleterious. In contrast, it is even necessary for the coordination of certain biological processes. For decades, hypoxia-regulated genes like EPO are known to have beneficial effects on brain function (Bond and Rex, 2014; Ehrenreich et al., 2007a; Ehrenreich et al., 2007b; Ghezzi and Brines, 2004; Iwai et al., 2010; Miskowiak et al., 2010; Miskowiak et al., 2015; Miskowiak et al., 2014a; Miskowiak et al., 2014b; Mitkovski et al., 2015; Sugawa et al., 2002). These findings stimulate the question to what extent physiological hypoxia is present in the healthy adult brain.

Functional magnetic resonance imaging (fMRI) exploits the phenomenon that oxygen levels in the cerebral blood vessels change dependent on brain activity. This so-called neuro-vascular coupling already demonstrates the tight link between neuronal oxygen demand and neuronal activation. However, previously it remained unknown if next to vascular oxygen changes also neuronal oxygen levels change upon neuronal activity.

Hence, the current project aimed to investigate if physiological hypoxia arises in response to brain activity. To this end, a refined (slightly modified from Kimura et al., 2015) transgenic reporter mouse line (CAG-CreERT2-ODD::R26R-tdTomato) was employed. This mouse line ubiquitously expresses a fusion protein of the ODD domain of Hif1α and tamoxifen-inducible Cre-recombinase (CreERT2). Upon hypoxia, the protein becomes stabilized as the ODD domain is not tagged for degradation. In the additional presence of tamoxifen, the Cre-recombinase can activate the expression of tdTomato, leading to a permanent red labelling of cells that underwent hypoxia. In order to validate the functionality of the construct, mice were first exposed to intermittent hypoxia of varying

intensity and duration (+number of tamoxifen injections). This showed a hypoxia intensity and duration-dependent tdTomato expression/number of red-labelled cells. Interestingly, the proportion of labelled cells differed substantially between cell types. It was highest in neurons and endothelial cells, followed by astrocytes, oligodendrocytes (only labelled outside of hippocampus) while labelling was completely absent in microglia. This phenomenon could be due to two possible reasons: Either ODD-stabilization mechanisms and/or responsivity to hypoxia differs between cell types or the construct is - contrary to expectation - not ubiquitously expressed and these differences merely reflects a technical artifact. In order to determine the reason for the observed cell-type heterogeneity with regard to hypoxia-labelling, we performed a scRNAseq experiment on hippocampal tissue from mice under normoxia or hypoxia (6% O_2 for 6 hours/day on 5 consecutive days). This experiment showed that construct mRNA (ODD and tdTomato) was present in all cell types at a comparable degree and that variation in construct expression levels did not correspond to the amount of tdTomato labelling observed in immunohistochemical quantifications. Accordingly, differences in hypoxia-labelling likely are caused by the variable responsivity to hypoxia of different cell types. Although the underlying mechanisms remain to be fully explored, a first insight was obtained by investigation of *Hexokinase2* (*Hk2*) expression across different cell types. Hk2 is an enzyme that catalyzes the first step of glycolysis and is centrally involved in metabolically regulating the switch from glycolysis to oxidative phosphorylation to cover cellular energy demands in low oxygen conditions (Warburg effect; Pedersen, 2007). The number of *Hk2*-expressing cells under hypoxia was inversely related to the proportion of tdTomato-labelled cells under hypoxia, e.g. the number of *Hk2+* cells was highest in microglia (already at baseline) and lowest in neurons and endothelial cells.

Light-sheet microscopy showed that labelled cells were dispersed across the entire brain. They were already present at normoxic conditions and significantly increased in number under hypoxia. To test the hypothesis that brain activation triggers physiological "functional" hypoxia in neurons, a complex running wheel (CRW) task was chosen to trigger motor-cognitive learning. This specially designed running wheel consists of irregularly inter-spaced bars (Mckenzie et al., 2014) and stimulates mice to acquire its pattern over time. Quantifications following immunohistochemical staining and light-sheet microscopy mapping revealed a step-wise increase in number of hypoxia-labelled cells from normoxia over CRW to hypoxia (6% O_2 for 6 hours/day on 5 consecutive days) in the hippocampal fields of CA1, CA3 and dentate gyrus at 4 and 24 weeks of age. Overall, the labelling was more abundant in female mice. In order to confirm the presence of functional hypoxia in the hippocampus after CRW on the transcriptomic level, a gene expression composite score was created. This score comprised the average expression of seven known hypoxia-regulated genes. Similarly to quantification results, the expression of these genes increased step-wise from normoxia over CRW to hypoxia (6 hours exposure to normoxia, CRW or 6% O_2).

This project provided insight into hypoxia as a physiologically arising condition that emerges in different cell types of the healthy adult mouse brain. Already at baseline, i.e.,

at normoxia, hypoxia-labelled cells were observed. Yet, under motor-cognitive challenge the number of labelled cells was significantly increased. This suggests that neuronal activity leads to transient hypoxia in strongly activated cells, which is probably a result of increased energy - and hence oxygen - demands of these cells. This phenomenon can be summarized under the term "functional hypoxia". The here reported findings might explain the previous reports of the beneficial effects of cognitive and physical challenges on brain function. Future studies will address the question further to what degree systemic hypoxia, e.g. during physical exercise, versus a more localized brain-specific hypoxia, e.g. during a demanding cognitive task, are comparable and how they possibly complement each other.

4.2   Original publication

Butt U.J.*, Steixner-Kumar A.A.*, Depp C.*, et al. (2021). Hippocampal neurons respond to brain activity with functional hypoxia.   Molecular Psychiatry, 1-18.
*equal contribution

Personal contribution

I was responsible for scRNAseq data alignment, quality control and analysis. I was also involved in interpretation of the results. Moreover, I assisted in statistical testing of quantification data, created the gene expression composite score and contributed to drafting figures, figure legends and the manuscript.

ARTICLE

Hippocampal neurons respond to brain activity with functional hypoxia

Umer Javed Butt [1] · Agnes A. Steixner-Kumar [1] · Constanze Depp [2] · Ting Sun[2,3] · Imam Hassouna[1] ·
Liane Wüstefeld[1] · Sahab Arinrad[1] · Matthias R. Zillmann[1] · Nadine Schopf[1] · Laura Fernandez Garcia-Agudo [1] ·
Leonie Mohrmann[1] · Ulli Bode[2] · Anja Ronnenberg[1] · Martin Hindermann[1] · Sandra Goebbels[2] · Stefan Bonn[3] ·
Dörthe M. Katschinski[4] · Kamilla W. Miskowiak[5] · Klaus-Armin Nave [2] · Hannelore Ehrenreich [1]

Abstract

Physical activity and cognitive challenge are established non-invasive methods to induce comprehensive brain activation and thereby improve global brain function including mood and emotional well-being in healthy subjects and in patients. However, the mechanisms underlying this experimental and clinical observation and broadly exploited therapeutic tool are still widely obscure. Here we show in the behaving brain that physiological (endogenous) hypoxia is likely a respective lead mechanism, regulating hippocampal plasticity via adaptive gene expression. A refined transgenic approach in mice, utilizing the oxygen-dependent degradation (ODD) domain of HIF-1α fused to CreERT2 recombinase, allows us to demonstrate hypoxic cells in the performing brain under normoxia and motor-cognitive challenge, and spatially map them by light-sheet microscopy, all in comparison to inspiratory hypoxia as strong positive control. We report that a complex motor-cognitive challenge causes hypoxia across essentially all brain areas, with hypoxic neurons particularly abundant in the hippocampus. These data suggest an intriguing model of neuroplasticity, in which a specific task-associated neuronal activity triggers mild hypoxia as a local neuron-specific as well as a brain-wide response, comprising indirectly activated neurons and non-neuronal cells.

These authors contributed equally: Umer Javed Butt, Agnes A. Steixner-Kumar, Constanze Depp

Supplementary information The online version of this article (https://doi.org/10.1038/s41380-020-00988-w) contains supplementary material, which is available to authorized users.

✉ Klaus-Armin Nave
nave@em.mpg.de

✉ Hannelore Ehrenreich
ehrenreich@em.mpg.de

1   Clinical Neuroscience, Max Planck Institute of Experimental Medicine, Göttingen, Germany

2   Department of Neurogenetics, Max Planck Institute of Experimental Medicine, Göttingen, Germany

3   Institute of Medical Systems Biology, Center for Molecular Neurobiology, University Clinic Hamburg-Eppendorf, Hamburg, Germany

4   Institute for Cardiovascular Physiology, University Medical Center Göttingen, Georg-August-University, Göttingen, Germany

5   Psychiatric Centre Copenhagen, University Hospital, Rigshospitalet, Copenhagen, Denmark

Introduction

Hypoxia is the term for reduced oxygen levels in cells or tissues, relative to their 'normal' content. In former times interpreted as principally pathological, for instance upon cardiac arrest, hypoxia is increasingly recognized as physiological driving force of early neurodevelopment including angiogenesis, hematopoiesis, and tissue regeneration. Known cellular environments experiencing hypoxia include developing embryos, stem cell niches, the renal papilla, inflammatory tissue, or the inner mass of tumours [1–10]. A specific transcriptional programme, induced by hypoxia, allows cells to adapt to lower oxygen levels and/or to limited metabolic support [11]. The transcription is partly independent of [10, 12] and partly controlled by hypoxia-inducible factors (HIF), binding to hypoxia-responsive elements to modulate expression of a myriad of genes, some of which are potent growth factors like vascular endothelial growth factor (VEGF) or erythropoietin (EPO) [10, 13–20].

On one hand, the tight association of neuronal activity with oxygen availability is the basis of functional magnetic

resonance imaging (fMRI), which works by detecting the level of oxygen in blood throughout the brain. Changes in oxygenation and hemodynamics generate a fast surrogate signal of brain activity based on structural and functional neurovascular coupling [21–23].

On the other hand, extensive physical activity as well as cognitive challenge lead to widespread brain activation, and are ultimately associated with improved global brain function including mood and emotional well-being in health and disease [24, 25]. Neurologists and psychiatrists encourage their patients to improve functions by practicing, following the old rule *'use-it-or-lose-it'*. For example, hippocampal volume increases following exercise in both healthy and schizophrenic subjects, and this plastic response correlates with improvement in test scores for short-term memory [26]. Despite these well-established observations, the underlying mechanisms have remained widely obscure.

In several clinical trials targeting different neuropsychiatric diseases, we showed over the last 2 decades that high-dose recombinant human EPO consistently improved cognition and reduced grey matter loss (e.g. [27–30]). Subsequently focusing on preclinical EPO studies for deeper mechanistic insight, we discovered that challenging cognitive tasks apparently induce transient neuronal hypoxia which triggers neuronal EPO expression. Endogenous EPO in turn enhances cognition via augmenting dendritic spine formation and increasing numbers of pyramidal neurons [31, 32]. In this context, we coined the term *'brain EPO circle'*, and reported an increase in hypoxia-labelled neurons after complex running wheel (CRW) exposure together with an amplified expression of EPO in pyramidal CA1 neurons [32].

Taking all this information together, we designed the present study, hypothesizing that for physiological postnatal and adult adaptation processes in the brain, hypoxia may be a crucial mediator of major general relevance. We show here that complex motor-cognitive activity leads to 'functional hypoxia' as a local, neuronal network-specific, as well as a brain-wide response, encompassing indirectly activated neurons and—to a lesser degree—non-neuronal cells. This activity-induced hypoxia regulates adaptive gene expression and fosters neuroplasticity.

Materials and methods

Important note: All experiments, including cell counting, were performed by investigators unaware of group assignment and treatments ('fully blinded').

Generation of CAG-CreERT2-ODD transgenic mice

The p-CAG vector, kindly provided by Hesham A. Sadek [33], was slightly modified (Fig. 1a). In brief, the vector contains the oxygen-dependent-degradation domain (ODD) of HIF-1α, fused with a tamoxifen-inducible cre-recombinase, driven by a ubiquitous CAG promoter. Under normoxic conditions, the ODD is hydroxylated by prolylhydroxylases, which tag HIF-1α upon binding of Von Hippel-Lindau (VHL) protein for proteasomal degradation. Hypoxic conditions lead to inactivation of these enzymes and thus stabilization of HIF-1α, allowing it to accumulate in the nucleus and activate transcription of its target genes. Analogously, under hypoxic conditions the ODD-cre-recombinase fusion construct is stabilized and—in the presence of tamoxifen—translocates to the nucleus to trigger tdTomato expression, which leads to permanent labelling of cells that were transiently exposed to hypoxia [33]. The vector was cloned and bacterial backbone (ampicillin sequence) removed by DraI and SpeI (New England Biolabs, MA, USA) restriction enzymes. The linearized vector for pro-nuclear microinjection was purified by QIAquick Gel Extraction kit (Qiagen, Venlo, Netherlands) and introduced into fertilized eggs for generation of CAG-CreERT2-ODD transgenic mice. Transgenic founder mice and the next generations were viable and breeding normally.

Mouse genotyping

Founder mice from the litters were screened by PCR amplification of genomic DNA for the transgene using following primer pair: forward 5′-GCTGAAGACACAG AAGCAAA-3′ and reverse 5′-GTGGGTAGGAGATG GAGATG-3′. Mice carrying the transgene were maintained on C57BL6/N (Charles River, MA, USA) background. F1 litters were bred to Rosa26R-tdTomato reporter mice [34]. For analysis of tdTomato transgene, primer1 5′-TCAATGGGCGGGGGTCGTT-3′, primer2 5′-CTCTGCTGCCTCCTGGCTTCT-3′ and primer3 5′-C GAGGCGGATCACAAGCAATA-3′ were used. CAG-CreERT2-ODD::R26R-tdTomato F2 litters were selected for histological analysis.

Experimental procedures

All experiments were approved by and conducted in accordance with the regulations of the local Animal Care and Use Committee (Niedersächsisches Landesamt für Verbraucherschutz und Lebensmittelsicherheit, LAVES). CAG-CreERT2-ODD::R26R-tdTomato mice were used at the age of 4 and 24 weeks in all experiments. Mice were single housed in standard plastic cages, starting 2–3 days before the respective experiments, and maintained in temperature-controlled environment (21 ± 2 °C) on 12 h light–dark cycle with food and water available *ad libitum*. Mice of each gender were randomly allocated to experimental and control groups.

Hippocampal neurons respond to brain activity with functional hypoxia
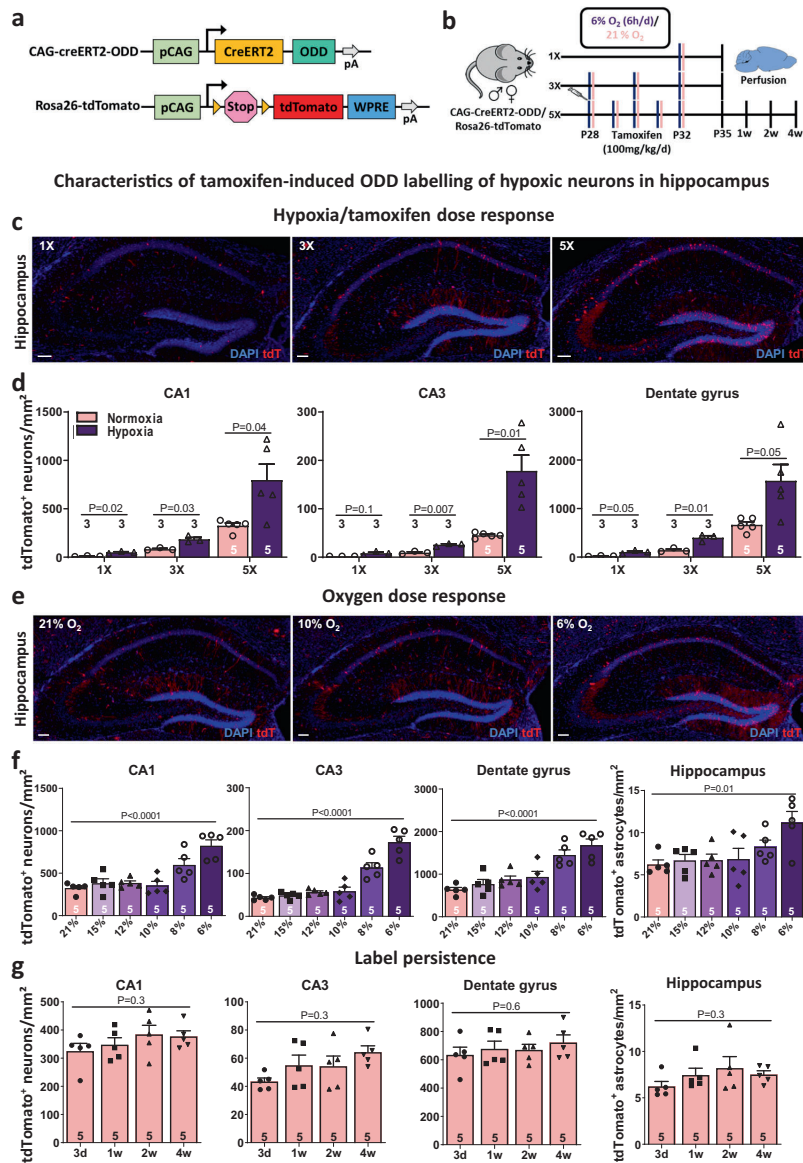
Fig. 1 Generation and characterization of CAG-CreERT2-ODD:: R26R-tdTomato mice as model to study hypoxic cells in the brain. a CAG-CreERT2-ODD and CAG-Rosa26R-tdTomato constructs. **b** Experimental outline for quantification of hypoxic cells in hippocampal regions CA1, CA3, and dentate gyrus under variable conditions, as displayed in (**c–g**). After the last day of treatment (P32), mice were sacrificed, perfused and brains harvested for histological analysis at the time points indicated. **c** Illustrative images of hippocampus from 1×, 3× and 5× hypoxia/tamoxifen-treated mice, showing tdTomato+ (red) hypoxic cells; DAPI (blue) as nuclear stain. **d** Quantitative results (based on counting of tdT+NeuN+ neurons) of the hypoxia/tamoxifen titration scheme, combining 1×, 3× or 5× placement of mice right after tamoxifen injection (100 mg/kg/d i.p.) for 6 h into a cage with hypoxia exposure (6%O_2) versus a cage with continued normoxia (21%O_2). **e** Illustrative images (5× tamoxifen), showing tdTomato+ (red) hypoxic cells and DAPI (blue) as nuclear stain and **f** quantification of the dose-response of hypoxic neurons (based on tdT+NeuN+ cells) and astrocytes (based on tdT+S100β+ cells) upon decreasing inspiratory O_2 concentration (5× tamoxifen; 21%O_2, 15%O_2, 12%O_2, 10%O_2, 8%O_2 and 6%O_2). **g** Tracking of tamoxifen-induced tdTomato+ hypoxic cells over the course of 4 weeks after treatment cessation under normoxic conditions (5× tamoxifen) reveals essentially label persistence; 2-tailed Welch's *t*-test and 1-way ANOVA were used for statistical analyses; error bars indicate SEM; scale bar represents 100 μm.

Tamoxifen injections

Tamoxifen stock solution was prepared by mixing 300 mg tamoxifen (Sigma, Darmstadt, Germany) in 30 ml of corn oil (Sigma) and stored at 4 °C; 100 mg/kg tamoxifen was injected intraperitoneally (i.p.) after preheating and sonication for 20 min. To control for non-induced expression of the transgene ('leakiness'), corn oil was injected.

Hypoxia exposure

A hypoxia chamber (60 cm × 38 cm × 20 cm) was designed in cooperation with Coy Laboratory Products (Michigan, USA). The hypoxia chamber is equipped with an oxygen sensor, oxygen controller and a ceiling fan for constant air circulation. In hypoxia experiments (Fig. 1b), animals were given a single dose of tamoxifen (100 mg/kg) before being placed in the hypoxia chamber for 6 h at 6%O_2. This procedure was repeated at identical time (10.30–16.30 h) for 5 consecutive days if not stated otherwise. O_2 was dropped from 21 to 6% over the course of 30 min, kept at 6% for 6 h and brought back up to 21% upon cessation of the experiment. Mice included in the normoxia group and oil-only control mice were handled identically but stayed at 21%O_2. For histological studies mice were perfused 3 days after the 5-day experiment (day 8) and brains dissected for further analysis. For single-cell RNAseq analysis, mice were sacrificed immediately after the last hypoxia/normoxia control session on day 5 without perfusion.

Running wheel experiment

CRW (TSE Systems, Bad Homburg, Germany) are characterized by randomized missing bars as previously described [35, 36] and running activity is computer-controlled via Phenomaster software (TSE Systems, Germany). Running-naïve mice, aged 4 or 24 weeks, were allowed to freely use CRW for 5 whole days. Tamoxifen injections were given daily during the light cycle, along with refill of fresh food and water. Non-running mice were excluded from the experiment (5/24 all together). Control mice were housed without CRW in standard cages. After day 5, CRW mice were returned to standard cages for 3 days before perfusion (day 8).

Tissue preparation and histology

Mice were anesthetized with Avertin (Tribromoethanol, Sigma-Aldrich, St Louis, MN, USA, 0.276 mg g^{-1}) and perfused with 0.9% saline and pre-chilled 4% paraformaldehyde (PFA; Sigma, Missouri, United States), followed by brain isolation. All tissues were post-fixed in 4% formaldehyde at 4 °C for 24 h and later cryoprotected in 30% sucrose prepared in phosphate buffer saline (PBS) for 48 h at 4 °C. Brains were further covered in cryoprotectant (O.C.T.^{TM} Tissue-Tek, Sakura, Netherlands) and kept until use at −80 °C. Whole mouse brains were cut into 30 μm thick coronal floating sections using a cryostat (Leica, Wetzlar, Germany) and stored in a cryoprotective solution (25% ethylene glycol and 25% glycerol in PBS) at 4 °C until further use.

Immunofluorescence staining

For immunofluorescence analysis, 5 sections (30 μm) from each mouse were washed and blocked for 1 h in 5% horse serum diluted in PBS with 0.5% Triton X-100 at room temperature (RT). Primary antibodies were diluted in 3% horse serum PBS/0.3% Triton X-100 and sections incubated for 48 h at 4 °C, followed by washing and incubation with respective secondary antibody for 2 h at RT. For nuclear counterstaining, 4′,6-diamidino-2-phenylindole (DAPI, Sigma, Missouri, United States) was used. The sections were then mounted on SuperFrostPlus Slides (Thermo Fisher, Germany) with Aqua-Polymount (Polysciences, Inc USA). For direct visualization of tdTomato, sections were only stained with DAPI and investigated by confocal microscope Leica TCS SP5-II. Primary antibodies used were anti-NeuN (MAB377, 1:1000, Mouse Millipore, Darmstadt, Germany), anti-IBA1 (234006, 1:1000, chicken; SYSY, Göttingen, Germany) and anti-Olig2 (AB9610, 1:1000, rabbit, Millipore), anti-alanyl aminopeptidase membrane (CD13)-AF647 (564352, rat, 1:200, 564352; BD Biosciences, San Jose, CA, USA), Lectin (DL-1174, 1:500, DyLight® 488 Lycopersicon Esculentum (Tomato), anti-S100β (287004/1-4, guinea pig, 1:500, SYSY). Secondary antibodies used were Alexa 488 anti-guinea pig (123588, 1:500, Invitrogen), Alexa 647 anti-chicken (121361, 1:500, Jackson ImmunoResearch, Cambridgeshire, UK), Alexa 647 anti-mouse (1757130), Alexa 647 anti-rabbit (1693297) and Alexa 647 anti-rat (A-21247, 1:500; Thermo Fisher).

Confocal imaging and quantification

For quantification of NeuN+tdTomato+ co-labelled cells, serial coronal sections from the dorsal part of hippocampus were taken (coordinates from Bregma: −1.34 to −2.54 mm posterior). Stained sections (30 μm) were imaged using a Leica confocal microscope TCS SP5 System equipped with a 20× objective (NA = 0.70). Neurons (NeuN+) from CA1, CA3 and DG were counted on both sides of hippocampus by Fiji software (https://imagej.net/Fiji). NeuN+tdTomato+ cells were considered as neurons having experienced hypoxia. Astrocytes (S100β+tdTomato+) and endothelial

cells (Lectin+tdTomato+) were counted bilaterally in whole hippocampus (5 sections per animal). For oligodendrocyte quantification, Olig2+tdTomato+ cells were counted in serial coronal sections of the rostral corpus callosum (both sides). Illustrative images were analyzed and processed with Imaris 9.1.0 (www.bitplane.com).

Light-sheet microscopy (LSM)

Whole mount tissue staining and clearing

To visualize tdTomato+ cells in the entire brain we performed LSM in combination with whole mount immune labelling and tissue clearing. Animals were deeply anesthetized and transcardially perfused using PBS and 4%PFA/PBS, respectively. Brains were removed, post-fixed in 4% PFA overnight and stored in PBS until further use. Brain hemispheres were processed for immune labelling and tissue clearing following a slightly modified iDISCO protocol [37]. Samples were dehydrated with a methanol/PBS series (50%, 80%, 100%, and $2 \times 100\%$, 1 h, RT) followed by overnight bleaching and permeabilization in a mixture of 5% H_2O_2/20% dimethyl sulfoxide (DMSO) in methanol at 4 °C. Samples were retrieved and washed further with methanol at 4 °C for 30 min and -20 °C for 3 h prior to incubation in 20% DMSO in methanol at RT for 2 h. Samples were then rehydrated using a descending methanol/PBS series (80%, 50%, PBS, 1 h each, RT) and further washed with in PBS/0.2% Triton X-100 for 2 h. The samples were then incubated overnight in 0.2% Triton X-100, 20% DMSO, and 0.3 M glycine in PBS at 37 °C and blocked using PBS containing 6% goat serum, 10% DMSO and 0.2% Triton X-100 for 2 days at 37 °C. Samples were retrieved, washed twice in PBS containing 0.2% Tween(r) 20 and 10 µg/ml heparin (PTwH) at RT for 1 h and incubated with primary antibody solution (anti-RFP; Rockland # 600-401-379; 1:250 in PTwH/5%DMSO/3% goat serum) for 14 days at 37 °C. After several washes during the day and an additional overnight wash in PTwH samples were incubated with secondary antibody solution (goat anti-rabbit Alexa555; Thermo Fisher Scientific # A-21428; 1:500 in PTwH/3% goat serum) for 7 days at 37 °C. Prior to clearing, the samples were again washed in PTwH (several solution changes during the day) followed by an additional overnight wash. Tissue was dehydrated using an ascending series of Methanol/PBS (20%, 40%, 60%, 80%, $2 \times 100\%$ 1 h, RT) followed by overnight incubation in a mixture of 33% dichloromethan (DCM) and 66% methanol at RT. Samples were further delipidated by incubation in 100% DCM for 40 min and transferred to pure ethyl cinnamate (Eci; Sigma-Aldrich #112372) as clearing agent. Tissues became transparent after 30 min in Eci and were stored at RT until imaging.

LSM and 3D analysis/visualization

LSM was performed using a LaVision Ultramicroscope II equipped with a 2× objective, corrected dipping cap and zoom body. Samples were mounted onto the sample holder with the medial surface of the brain hemisphere facing down in order to acquire sagittal images. The holder was placed into the imaging chamber filled with Eci. Images were acquired in mosaic acquisition mode with the following specifications: 5 µm sheet thickness; 20% sheet width; 2× zoom; 4×5 tiling; 4 µm z-step size; dual site sheet illumination; 50 ms camera exposure time; 1000px × 1600px field of view. Red fluorescence was recorded using 561 nm laser excitation (5–10%) and 585/40 emission filters. Images were loaded into Vision4D 3.0 (Arivis) and stitched using the tile sorter setup. Hippocampus and cortex regions of interests (ROIs) where manually annotated according to the sagittal Allen mouse brain atlas [38]. For this, hippocampus and cortex ROIs were traced manually in a few planes in 2D from which the 3D ROI was extrapolated automatically. Cortex and hippocampus annotations were then cropped with a medial cut-off of ~0.4 mm and a lateral cut-off of ~4.4 mm (corresponding to the lateral end of the hippocampal formation). Cortex ROIs spanned the dorsal parts of the cortex as defined by anatomical landmarks. Next, tdTomato+ cells per ROI were identified using the blob finder algorithm in Vision4D. Noise was removed by deleting objects with voxel sizes <10 from the object table. Objects were then critically reviewed, and any additional noise was manually removed from the dataset. The number of tdTomato+ cells per ROI was extracted from the object table and plotted using GraphPad (Prism). For visualization purposes, representative single planes of the 3D datasets displayed in inverted grayscale were extracted. To clearly visualize the distribution of tdTomato+ cells in the 3D hippocampus, the datasets were cropped along the respective hippocampus ROI, the grayscale 3D renderings were inverted, and a high resolution snapshot of the 3D ROIs was taken. Blobfinder identified objects were further displayed as simplified spheres using the centroid display mode of objects in Vision4D.

Single-cell RNA sequencing

Isolation and preparation of whole hippocampal cells

CAG-CreERT2-ODD::R26R-tdTomato mice, 4 weeks old, received tamoxifen (100 mg/kg/d) daily for 5 consecutive days before being exposed to either inspiratory hypoxia (6%O_2) or normoxia (21%O_2) for 6 h each. Mice were handled identically and sacrificed on day 5 immediately after the last hypoxia/normoxia session. Hippocampi were dissected in

Earle's Balanced Salt Solution (EBSS1) and later digested with a working solution of Papain/DNaseI prepared in EBSS1, according to the manufacturer's instructions (Worthington Biochemical Corp). All steps were carried out on ice except the Papain/DNaseI dissociation. The samples were then incubated at 37 °C for 40 min with constant shaking in water bath and switched to 5%CO_2 every 10 min. Papain/DNaseI was removed and samples were further diluted in 5 ml EBSS2. Dissociated tissues were manually triturated (avoid air bubbles), followed by centrifugation at 900 rpm for 10 min at 4 °C. Supernatant was discarded and the cell pellet gently resuspended in 200 μl of EBSS2 until a smooth and creamy suspension was obtained. Dissociated cells were washed frequently with DMEM/F12 (Sigma) without phenol-red containing 3% foetal bovine serum (FBS; Life Technologies) and centrifuged at 900 rpm for 10 min at 4 °C. Cell pellet was resuspended in 1 ml of DMEM/F12 and filtered through a 70 μm strainer cap (Corning) smoothly to harvest a clear cell suspension. Cell viability and yield was calculated by mixing an equal volume of acridine orange and propidium iodide and checked at the cell counter (Nexcelom Bioscience, MA, USA). Cell suspension (1 ml) was diluted with 3 ml PBS containing 0.04% BSA and centrifuged. Supernatant was removed and cell pellet resuspended in 400 μl PBS containing 0.04% BSA. Cells were fixed by adding 1.6 ml methanol dropwise and kept at −20 °C for 30 min and stored at −80 °C for further use.

Cell rehydration, single-cell library preparation and RNA sequencing (scRNA-seq)

The Methanol fixed cell suspensions were stored at −80 °C for less than 7 days before processing. For each sample, ~1.5 million cells were taken for rehydration and downstream scRNA-seq experiment. Cells were first placed on ice and equilibrated to 4 °C. After equilibration, cells were washed 2 times by 1 ml pre-chilled rehydration buffer (1.0% BSA, 0.5U/μl RNAse inhibitor in 1× Dulbecco's Phosphate-Buffered Saline, DPBS). Centrifugation was done at 3000 rcf for 10 min at 4 °C. Finally, cells were resuspended in pre-chilled 1× DPBS with 0.04% BSA and 0.5U/μl RNase inhibitor to achieve a concentration of 1000 cells/μl. Rehydrated cells were immediately used for the scRNA-seq using the 10× genomics chromium single-cell gene expression platform. Around 35,000 cells from each sample were loaded on 1 well of 10× Single Cell A chip, where each single cell was lysed and its transcriptome combined with a single barcoded gel bead in an oil droplet. Barcode cDNA libraries were then prepared using Chromium Single Cell 3′ Library and Gel-beads kit v2 according to the manufacturer's instructions. Library quality was checked using Agilent High Sensitivity DNA chip on Agilent 2100 Bioanalyzer. High quality libraries were

sequenced on Illumina HiSeq 4000 sequencer with an average depth of 200,000 reads per cell.

Alignment and initial processing of sequencing data

CellRanger v2.2.0 software was used to align sequence reads to the customized mouse mm10 reference genome to which the ODD and tdTomato sequences were added. A filtered gene expression matrix was generated by CellRanger and was afterwards loaded into Seurat for further analysis.

Single-cell sequencing data analysis

Additional quality control as well as sample integration, cell clustering and marker gene identification were done with R (v3.4.1) [39] using Seurat packages v2.3.0 (quality control, normalization) [40] and v3.0.0 (scaling, integration, clustering, differential expression) [41]. Genes that were detected in ≥3 cells and cells in which the number of detected genes ranged between 500 and 6000 (hypoxia samples) or 7500 (normoxia samples) respectively were retained for further analysis. In addition, cells that contained >20% mitochondrial genes were removed, resulting in a total number of 28,114 cells, expressing altogether 20,976 genes. After integration and clustering, another 2264 cells that were likely to be doublets upon examination of marker genes and/or predicted to be doublets by DoubletFinder [42] were excluded. This led to the final dataset containing 25,850 cells (normoxia: $n = 12,341$, hypoxia: $n = 13,509$) and 20,976 genes. This dataset was used for further analysis and graphical display. Gene expression levels were normalized via natural-log normalization of gene transcripts divided by total transcripts per cell and scaled by 10,000. Data integration of the 4 samples was done using the 20 first dimensions of CCA (canonical correlation analysis) and by calling the functions FindIntegrationAnchors() and IntegrateData(). After scaling of integrated data and dimension reduction through principal component analysis, uniform manifold approximation and projection (UMAP) dimension reduction was performed on the first 30 principal components. Subsequently, nearest neighbors were identified using the FindNeighbors() function and clusters were determined with FindClusters (resolution = 0.2). This initially revealed 21 cell clusters. After removal of doublet (sub)clusters (determined by co-expression of 2 main cell-type markers) and merging of clusters that were highly similar with regard to main marker expression, 16 different cell types were identified. Identification of cell types was based on differentially expressed genes (function FindAllMarkers(logfc.threshold = 0.5)) in each cluster and expression of known marker genes [43]. The FindMarkers() function was employed to determine differential expression

of *Vegfa* and *Hk2* between hypoxia and normoxia. A positive logFC indicates higher expression under hypoxia as compared to normoxia. Percentages of ODD, tdTomato or double-positive cells as well as *Hk2+* cells were determined by calculating the proportion of cells with non-zero expression in the respective genes. For all feature plots showing normalized expression levels, a minimal and maximal cut-off was set at 0.5 and 2, respectively.

Extraction of mRNA and real-time quantitative reverse transcription polymerase chain reaction (qPCR)

Juvenile female WT (C57BL/6N) P32 mice were sacrificed after 6 h of normoxia, hypoxia or CRW (during their active phase, i.e., lights-off) and hippocampi were dissected and directly frozen on dry ice. Total RNA was extracted from hippocampal tissue by using miRNeasy Mini Kit (Qiagen, Hilden, Germany). The cDNA was prepared using Super-Script® III Reverse Transcriptase (Thermo Fisher Scientific Life Technologies GmbH, Darmstadt, Germany), and 1 µg of RNA along with oligo (dT) and Random Hexamer Primer in a total volume of 20 µl. The qPCR was performed as described in detail earlier [31, 44]. For qPCR, 4 µl of 1:10 diluted cDNA were used as template with 5 µl of Power SYBR Green PCR Master Mix (Thermo Fisher Scientific Life Technologies) and 1 pmol of primers (in 1 µl H$_2$O).

For N-myc downstream-regulated gene 1 protein (*Ndrg1*), nitric oxide synthase 1 (*Nos1*), Ankyrin repeat domain-containing protein 37 (*Ankrd37*), HIG1 domain family member 1A (*Higd1a*), VEGF A (*Vegfa*), erythropoietin (*Epo*), enolase 2 (*Eno2*), beta-actin (*Actβ*) and hypoxanthine guanine phosphoribosyl transferase (*Hprt1*) the following primers were used:

Ndrg1 forward primer:
5′-CGAAGACCACCCTGCTCAAG-3′
Ndrg1 reverse primer:
5′-ATGCTGGCAGAAGGCATGTAT-3′
Nos1 forward primer: 5′-CATCAGGCACCCCAAGTT-3′
Nos1 reverse primer:
5′-CAGCAGCATGTTGGACACA-3′
Ankrd37 forward primer:
5′-AAACAGGTGCTGACCTCAACC-3′
Ankrd37 reverse primer:
5′-CAGTCCAGGCTTCCAACCTTT-3′
Higd1a forward primer:
5′-ACGATGAAGGTCAGGGGTCT-3′
Higd1a reverse primer:
5′-AGGCAACAATCGCTGCAAAG-3′
Vegfa forward primer:
5′-AGCACAGCAGATGTGAATGC-3′
Vegfa reverse primer:
5′-TTGACCCTTTCCCTTTCCTC-3′

Epo forward primer:
5′-AAGGTCCCAGACTGAGTGAAAATATTAC-3′
Epo reverse primer: 5′-GGACAGGCCTTGCCAAACT -3′
Eno2 forward primer:
5′-TGGAGTTTGGGGAGTGCTGGATG-3′
Eno2 reverse primer:
5′-AGGGCTGGGGAGAGGGTTAGAGG-3′
β-actin forward primer:
5′-CTTCCTCCCTGGAGAAGAGC-3′
β-actin reverse primer:
5′-ATGCCACAGGATTCCATACC-3′
Hprt1 forward primer:
5′-GCTTGCTGGTGAAAAGGACCTCTCGAAG-3′
Hprt1 reverse primer:
5′-CCCTGAAGTACTCATTATAGTCAAGGGCAT-3′

The qPCR reactions (3 technical replicates) were run on LightCycler® 480 System (Roche, Mannheim, Germany). Fold difference in mRNA expression was calculated by the ΔΔCt method and normalized to *Hprt1* and *β*-actin.

Statistical analyses

Data obtained for all quantifications were analyzed by GraphPad Prism 7 (GraphPad Software, Inc. San Diego, CA, USA). Statistical significance between multiple groups was calculated by 1-way or 2-way analysis of variance (ANOVA). Welch's *t*-test was performed to compare two groups. Jonckheere-Terpstra trend test was applied to identify stepwise increases in data. General and cell-type-specific differences in numbers of *Hk2+* cells were assessed via Chi-square tests (unadjusted *P* values reported). Differential expression (scRNA-seq) was evaluated by Wilcoxon rank sum test (Bonferroni-corrected *P* values reported, if not declared otherwise). A *P* value < 0.05 was considered statistically significant. Bar graphs show means and error bars represent standard error of mean (SEM). Sample sizes were selected based on previous work in order to allow sufficient statistical power to detect differences with a minimum number of animals (RRR principle). Datasets were routinely screened for statistical outliers using Grubb's test and outliers were excluded if indicated ($P < 0.05$).

For intercorrelation analyses and calculation of the gene composite score, following the reported standard operating procedure [44, 45], gene expression was Z-standardized. Intercorrelation between qPCR-genes was plotted using R-package 'corrplot'. Cronbach's alpha was used as measure of internal consistency and $α > 0.6$ considered acceptable. For calculation of the composite score, Z-standardized single gene expression values were averaged across all 7 genes.

Results and discussion

Transgenic approach to permanent labelling of hypoxic brain cells

To test our hypothesis that neuronal activity leads to 'functional hypoxia', we employed a transgenic mouse line (CAG-CreERT2-ODD::R26R-tdTomato) that allows permanent reporter labelling of cells that undergo hypoxia by expression of a fusion protein. This fusion protein is comprised of the ODD domain of HIF-1α and a tamoxifen-inducible CreERT2, driven by a ubiquitous CAG promoter (slightly modified from Kimura et al. [33]) (Fig. 1a). Using this transgenic approach, we first defined our 'gold standard' of a prominent positive control by comparing mice exposed to intermittent inspiratory hypoxia ($6\%O_2$ for 6 h daily, applied over 5 days) with mice under inspiratory normoxia ($21\%O_2$) that were handled identically, including the five tamoxifen injections as indicated (Fig. 1b).

Characterization of the model: hypoxia/tamoxifen and oxygen dose-response curves (inspiratory hypoxia) as well as persistence of labelling

Based on this 'gold standard' (tamoxifen injection, followed by $6\%O_2$ for 6 h daily, applied over 5 days), we determined the numbers of tdTomato+ cells (mainly neurons—see below) in cornu ammonis hippocampi, namely in CA1, which is a well-defined, highly cognition-relevant, and at the same time established hypoxia-vulnerable brain region (Sommer's sector) [46–49], and in CA3, as well as in the dentate gyrus (DG) [50, 51]. As deducible from the scheme in Fig. 1b, in pilot experiments, hypoxia days/tamoxifen injections (100 mg/kg/day) had first been experimentally 'titrated' by applying 1×, 3× or 5× hypoxia ($6\%O_2$ for 6 h daily, each preceded by a tamoxifen injection) and compared to respective normoxia days/tamoxifen injections. This led to a clear dose-response of the number of tdTomato+ cells to hypoxia/tamoxifen and our final decision to stay with 5× hypoxia/tamoxifen as our 'gold standard' in the following experiments (Fig. 1c, d).

We also explored in initial tests the influence of the degree of inspiratory hypoxia on the number of tdTomato+ neurons and obtained an 'oxygen dose-response curve' that started to rise appreciably only at $8\%O_2$, and made us select the $6\%O_2$ for our subsequent experiments (Fig. 1e, f).

Using pimonidazole as an immediate hypoxia marker for further confirming hypoxia mapping [4] allowed us at least to identify few scattered tdTomato+ cells that showed double-labelling, very similar to what was presented in a recent paper on heart [33]. Unfortunately, the temporal dynamics of tdTomato labelling (visible earliest ~6–8 h after hypoxia exposure) and pimonidazole which can be maximally applied for 90 min before the staining becomes increasingly unspecific, do not permit more extensive co-labelling (Supplementary Fig. 1).

Finally, we analyzed in preparatory work tdTomato labelling at various time points (3 days to 4 weeks) after completed exposure to the standard schedule of 5× tamoxifen injections under inspiratory normoxia ($21\%O_2$), which showed essentially persistence of labelling over up to 4 weeks (Fig. 1g). In all these experiments, characterizing our transgenic model, 4-week-old male and female mice were equally distributed across experimental groups.

Light-sheet microscopy discloses a distinct increase in labelled cells from baseline cage activity to inspiratory hypoxia

We next applied light-sheet microscopy (LSM) to obtain a 3-dimensional (3D) overview of tdTomato+ (ODD) labelling in whole brain (Fig. 2a–c) [37, 52]. Because of the slightly stronger response of female mice to the hypoxia stimulus (see below), we opted for females at the age of 4–5 weeks. Comparative 3D visualization of hypoxic cells revealed a striking, regionally distinct distribution pattern across the entire brain. Similar to our histological quantification (Fig. 1c, d), the amount of labelled cells all over the brain increased markedly from mice with just baseline cage activity to animals exposed to our defined 'gold standard' of inspiratory hypoxia ($6\%O_2$ for 6 h daily, applied over 5 days) (Fig. 2a–c). To control for non-induced expression of the transgene ('leakiness' of tdTomato labelling), corn oil ('no tamoxifen') was injected, which led to an only small percentage of labelled cells (quantified for normoxia in LSM, Fig. 2c; same depiction upon hypoxia, as screened by histology). We note that the olfactory bulb, the lead sensory organ of mice, showed an extraordinarily strong tdTomato+ labelling upon tamoxifen across conditions, offering in this species an 'internal control of functional hypoxia' (Fig. 2a-c and Supplementary Video I).

Hypoxic cells in cortex and hippocampus are predominantly neurons

We next explored the immunohistochemical nature of hypoxia signal-positive cells in cortex and hippocampus (representative illustrating images upon our defined 'gold standard' of inspiratory hypoxia given in Fig. 3a–e). Comparing normoxia (just baseline cage activity) with exogenous/inspiratory hypoxia (and later with endogenous/activity-related hypoxia; see below) revealed essentially quantitative, no noticeable qualitative differences between conditions. In other words, the cell types labelled under normoxia and exogenous hypoxia (as well as later under CRW performance as endogenous/activity-related hypoxia;
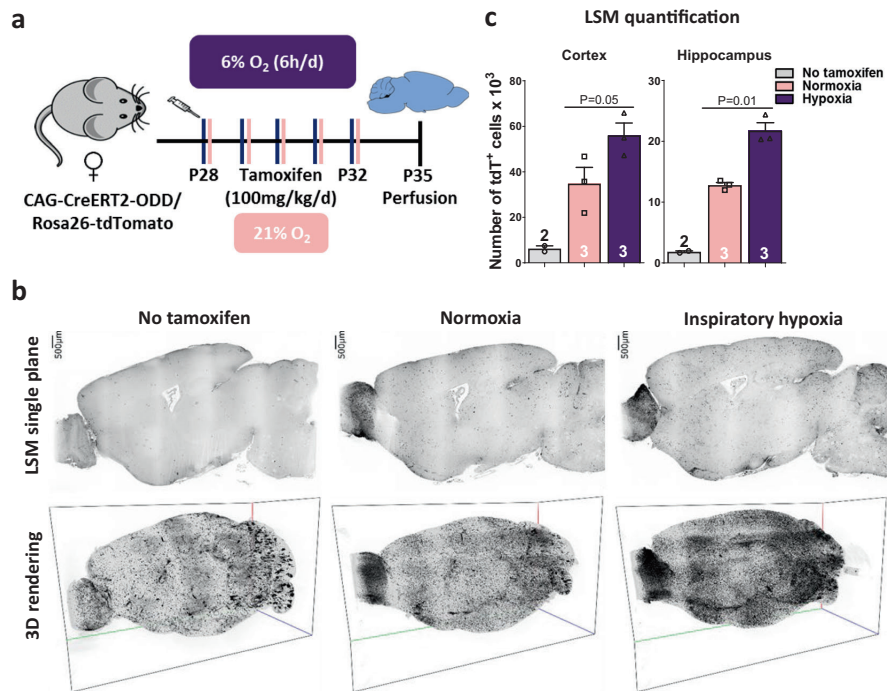
Fig. 2 Light-sheet microscopy (LSM) allows spatial mapping of hypoxic cells in whole brain using CAG-CreERT2-ODD::R26R reporter mice. a Experimental outline. **b** Light-sheet microscopy (LSM) 2D sagittal planes and maximal intensity projection 3D renderings of tdTomato+ cells in the entire brain hemispheres; images shown in inverted grey scale; scale in 3D images given by bounding box: x axis (green) 10 mm, y axis (red) 6.2 mm, z axis (blue) 4.2 mm. **c** Quantification of tdTomato+ cells in 3D hippocampus and cortex; 2-tailed Welch's t-test; error bars indicate SEM.

see below for quantifications), and their overall distribution were widely corresponding. Remarkably, the overwhelming fraction of tdTomato+ cells were neurons, followed by endothelial cells, whereas labelled astrocytes (mainly protoplasmic), oligodendrocytes and pericytes were much scarcer and displayed some regional differences. Rare, labelled oligodendrocytes, for instance, appeared mainly in white matter areas, whereas no labelled oligodendrocytes were found in the hippocampus. Surprisingly, microglia were never tdTomato+ labelled.

Single-cell transcriptomes show comparable expression of ODD and tdTomato in hippocampal cell lineages under normoxia or hypoxia

To exclude a merely technical problem as underlying cause of these surprising cellular differences in labelling, we determined whether the ODD-CreERT2 transgene, harbouring a ubiquitously active (CAG) promotor, is indeed equally expressed in all cell types. For this, we employed single-cell transcriptome analysis of whole hippocampus as a most sophisticated and comprehensive approach.

This approach confirmed comparable expression of both transgenes (ODD, tdTomato) in all hippocampal cell types under normoxia as well as upon our defined 'gold standard' of inspiratory hypoxia (Fig. 4a–c, Supplementary Fig. 2). As an example, we verified *Vegfa* as a prototypical hypoxia-inducible gene, upregulated in many cell types under hypoxia (for bulk comparison normoxia-hypoxia: $P = 8.96e-22$) and particularly highly expressed in OPC and astrocytes (avg_logFC>0.25, $p_{unadj} < 0.05$; Supplementary Fig. 3a, b).

Hexokinase2 expression is inversely related to the amount of tdTomato+ cells in each cell type

Searching for a first explanation of the apparent 'hypoxia tolerance' of microglia (never tdTomato+ labelled in any gender or treatment condition), we made an unexpected discovery. The expression of hexokinase2 (*Hk2*; catalyzing the first step of glycolysis) under hypoxia was found inversely related to the amount of tdTomato+ cells in each cell type (Fig. 4d). Cell types with a high percentage of *Hk2*+ cells under hypoxia showed a lower number of
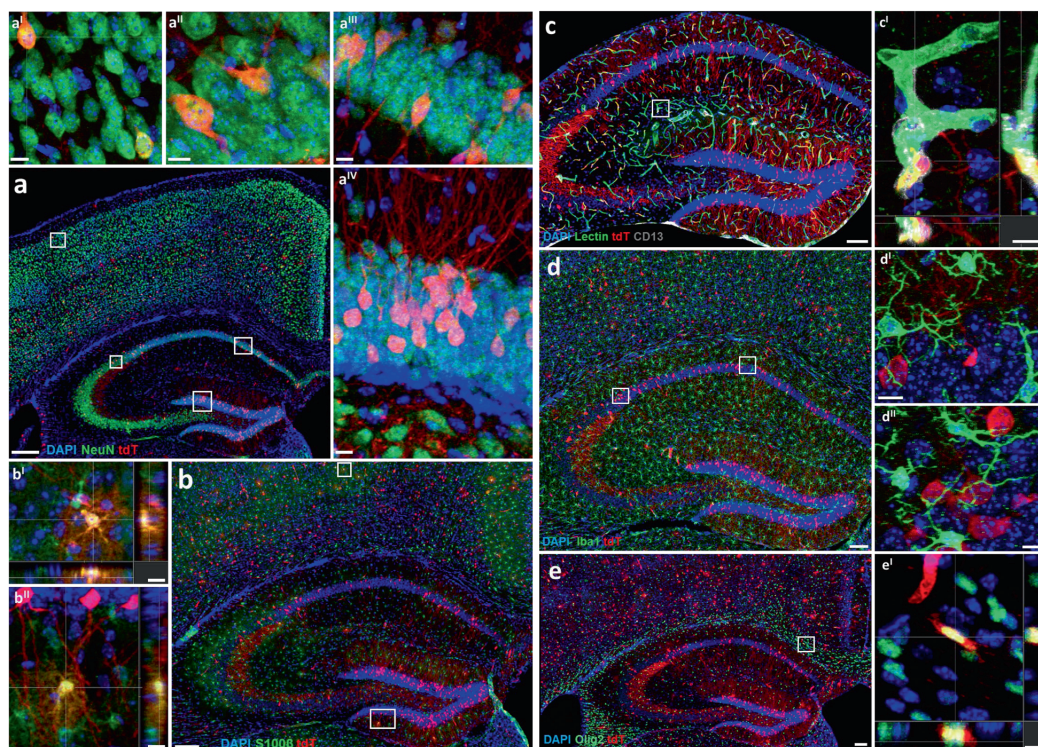
Fig. 3 Confocal images illustrate the predominance of neurons among hypoxic cells in hippocampus and cortex of CAG-CreERT2-ODD::R26R-tdTomato mice. Shown are representative images obtained upon our defined 'gold standard' of inspiratory hypoxia. *Note that normoxia and CRW (endogenous/activity-related 'functional hypoxia') revealed quantitative, no noticeable qualitative differences of labelled cell types.* **a** High density of tdTomato+ (tdT$^+$, red) neurons shown by co-labelling with the neuronal marker NeuN$^+$ (green). Magnified confocal images of tdT$^+$NeuN$^+$ neurons depict cortex (a^I), hippocampal CA2 (a^{II}), CA1 (a^{III}), and dentate gyrus, DG (a^{IV}). **b** S100β-stained astrocytes (green) show less frequent co-immunostaining with tdTomato. (b^I) and (b^{II}) display protoplasmic astrocytes from cortex and DG with orthogonal views. **c** Overview of hippocampal endothelial cells (lectin+, green) and pericytes (CD13+, grey), some co-immunostained with tdTomato; (c^I) zoom-in image of co-labelled cells. **d** Images of microglia staining (Iba1, green). (d^I) and (d^{II}) represent magnified images from CA1 and CA2, documenting lack of co-localization of Iba1 with tdTomato. **e** Olig2 staining (green) reveals sparse double labelling with tdTomato as illustrated in (e^I) depicting cells from the corpus callosum. Scale bars represent 200 μm in overview and 10 μm in zoom-in images.

tdTomato+ cells. Accordingly, microglia showed the most prominent expression compared to all other cell types under normoxic and hypoxic conditions (normoxia, $P = 6.02e-7$, logFC $= 0.07$; hypoxia, $P = 6.85e-15$, logFC $= 0.29$). Oligodendrocytes also exhibited high *Hk2* expression under hypoxia in the hippocampus. In line with this, no labelled oligodendrocytes appeared within the hippocampus, but predominantly (yet rarely) in white matter tracts (see also below). Hk2 is a glycolytic enzyme, well-recognized from tumour biology to promote cell survival by hypoxia resistance [53, 54]. Under inspiratory hypoxia, increased numbers of *Hk2*+ cells were identified among almost all cell types ($P < 0.05$ compared to the respective cell-type-specific normoxia numbers) (Fig. 4c, d). Even though highly interesting, Hk2 may not be the only explanation for the

observed differences between cell types. Notably, however, we did not observe on mRNA level any indicative expression patterns under normoxia or hypoxia of prolyl-hydroxylases, VHL gene or factor inhibiting hypoxia-inducible factor 1 that could potentially explain differences in tdTomato labelling due to different activity of the ODD degradation pathway in different cell types.

Nonetheless, the absence of tdTomato labelling in microglia is a highly intriguing finding. In some agreement with studies on brain tumours [55], we see in our scRNA-seq data that microglia clearly respond with an upregulation of hypoxia-related transcripts, yet it remains unclear why no ODD stabilization takes place. This could be partially explained by the high Hk2 expression, protecting microglia indirectly from a strong decrease in oxygen levels which
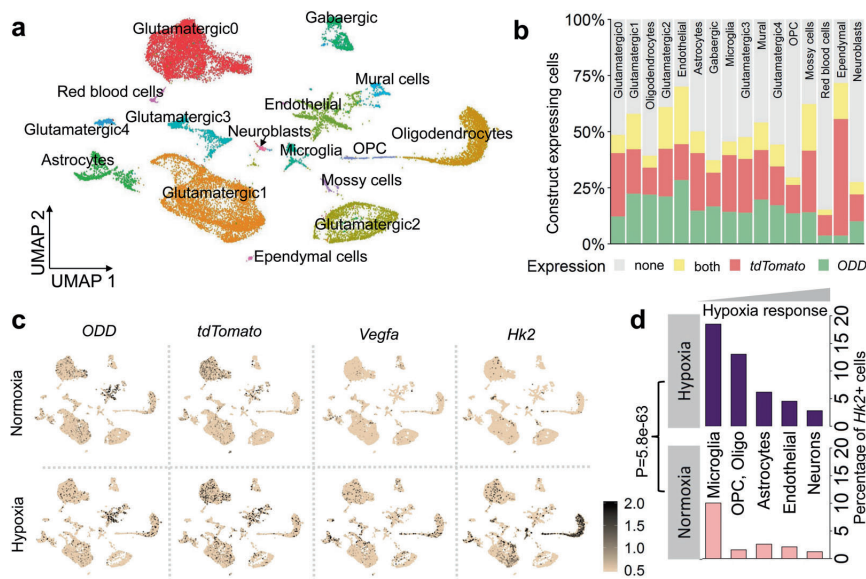
Fig. 4 Single-cell transcriptome analysis shows overall construct expression and indicates a role for hexokinase2 in the differential cellular hypoxia response. a Unbiased clustering of hippocampal cells from mice under normoxia ($n = 2$) or hypoxia ($n = 2$), represented in UMAP space, reveals 16 distinct cell populations across conditions. OPC: oligodendrocyte precursor cells. **b** ODD and tdTomato mRNAs are present in all cell types at comparable levels; percentage of cells shown where either ODD, tdTomato, both transcripts together, or none were detected (normalized expression >0). **c** Expression plots of ODD, tdTomato, and of 2 hypoxia-regulated genes, *Vegfa* and *Hk2*. Constructs ODD and tdTomato are expressed at similar levels in all cell types. *Hk2*+ cells were ordered by expression level (highly expressing cells plotted on top by setting FeaturePlot (order = T)) to prevent masking of relatively rare *Hk2*+ cells. **d** Percentage of detectable *Hk2* expressing cells increases to a varying degree in all cell types (borderline in endothelial cells under hypoxia). Microglia reveal the highest number of *Hk2* expressing cells under normoxia and a considerable increase under hypoxia; a strong increase under hypoxia is also observed in OPC and oligodendrocytes. For easier visualization, the cluster of ependymal cells, which was located far away from all other clusters, was shifted upwards on the UMAP2 axis (**a**, **c**). Chi-square test presented.

would be required for ODD stabilization. Alternatively, a different level of oxygen-dependence of microglia ('set-point'), a divergent activity of the HIF-1α degradation pathway or cell-type-related molecular features preventing ODD-stabilization could be relevant in this context. Possibilities range e.g. from different abundance of prolyl-hydroxylases or VHL protein, deviating availability of iron, ascorbate, tricarboxylic acid cycle intermediates, or levels of radical oxygen species (some only shown in vitro to be relevant) [56]. Moreover, less tight coupling of microglial and vascular oxygen levels (possibly related to distance from capillaries) may affect ODD-stabilization in microglia. All these speculations will have to be experimentally addressed in the future.

Number of tdTomato+ neurons upon motor-cognitive challenge suggests 'functional hypoxia'

Based on the characterization of our model and its validation by intermittent exogenous/inspiratory hypoxia, we next approached our hypothesis that neuronal activity leads to 'functional hypoxia'. For this purpose, we selected a multifaceted, demanding learning task for mice, i.e., running on complex wheels [35, 36]. CRW performance requires hippocampal involvement, but also activation of the motor circuits, somatosensory or visual cortex, and recruitment of the prefrontal-corticostriatal path [57–59]. Randomized missing bars, requiring continuous step-length adaptation and bilateral coordination characterize CRW task is entirely dependent on voluntary mouse activity and constitutes a marked cognitive challenge that stimulates complicated pattern recognition, intricate motor learning, and respective coordination. We thus compared mice, running on complex wheels, employed to induce our postulated, activity-related, 'functional endogenous hypoxia' ('CRW'; under inspiratory normoxia; $21\%O_2$), with mice upon spontaneous cage activity (unchallenged 'normoxia' controls; $21\%O_2$) and mice exposed to our 'gold standard' of a prominent positive control ('hypoxia'; $6\%O_2$ for 6 h daily) - all conditions applied over 5 days. Animals of all groups were handled identically, including tamoxifen injections as indicated

(Fig. 5a–c). In this series of experiments, we included also gender and age comparison. Hence, we determined tdTomato+ (ODD labelled) neurons upon normoxia (basal activity), cognitive challenge (CRW) or inspiratory hypoxia (6%O_2), in males and females separately, as well as in 2 different age groups (4 and 24 weeks, Fig. 5c), focusing again on CA1, CA3 and DG as our regions of interest. Altogether, a characteristic stair pattern from normoxia over CRW to hypoxia became obvious (Jonckheere–Terpstra trend test for both genders and time points significant), with female mice showing slightly higher amounts of tdTomato+ cells (for CA1: interaction treatment × gender: 4 weeks: $P_{interaction} = 0.048$, 24 weeks $P_{interaction} = 0.018$; for CA3: $P_{interaction} = 0.08$ and

b Normoxia, CRW, Hypoxia — DAPI tdT

c ODD-tdTomato labelling upon normoxia (basal activity), motor-cognitive challenge (CRW) and inspiratory hypoxia

d Hippocampus (4w) — tdTomato+ astrocytes/mm²; Males & females; DAPI tdT S100β

e Hippocampus (4w) — tdTomato+ endothelial cells/mm²; Females; DAPI tdT Lectin

f Corpus callosum (4w) — tdTomato+ oligodendrocytes/mm²; Females; DAPI tdT Olig2

◀ **Fig. 5 Number of tdTomato+ neurons in hippocampus after motor-cognitive challenge (CRW) versus inspiratory hypoxia support the concept of 'functional hypoxia'. a** Experimental outline. **b** Representative images of the hippocampus upon all 3 conditions. **c** Comparative quantification of labelled pyramidal neurons (tdT+NeuN+) in CA1, CA3 and DG of 4 and 24 week-old CAG-CreERT2-ODD::R26R-tdTomato mice of both genders upon spontaneous home cage activity (normoxia), CRW performance and inspiratory hypoxia ('gold standard'). (**d + d′**) The low numbers of hypoxic astrocytes (tdT+S100β+) in whole hippocampus of both genders display a stair pattern similar to neurons with increase upon CRW and inspiratory hypoxia in 4 week-old mice. (**e + e′**) Quantification of hypoxic endothelial cells (tdT+Lectin+) under normoxia, CRW and hypoxia in whole hippocampus of 4-week-old female mice does not yield significant differences between conditions. (**f + f′**) Quantification of hypoxic oligodendrocytes (tdT+Olig2+) in corpus callosum under normoxia, CRW and hypoxia in 4-week-old female mice shows a strong tendency of increases under both CRW and hypoxia. White arrows in d′, e′ and f′ illustrate quantified double-positive cells; two-tailed Welch's test for two-group comparison between normoxia and CRW (P value non-italicized). Jonckheere–Terpstra trend test (with 20,000 permutations in d–f) for comparing all three groups (P value in italics); error bars indicate SEM.

$P_{interaction} = 0.0001$; for DG: $P_{interaction} = 0.1$ and $P_{interaction} = 0.09$, respectively). Interestingly, this is in line with previous reports on gender differences in response to hypoxia [60–62], reflecting e.g. sex steroidal or oestrous cycle influence, perhaps in combination with a gender-diverse ventilatory response or stress perception during single housing. Of note in this context, even cultured male neurons, being more resistant under normoxia, are more vulnerable under strong hypoxia than female neurons and, interestingly, the male vulnerability pattern is acquired in cells from neonatally testosterone-primed females [63]. Age did not seem to play an appreciable role in the 2 groups (4 and 24 weeks) examined.

To provide a representative impression of the magnitude of the hypoxia response, we quantified in CA1 the percentage of hypoxic, i.e., tdTomato+ neurons among all neurons. These comprised in 4-week-old males $3.70 \pm 0.35\%$ upon normoxia, $4.85 \pm 0.26\%$ upon CRW and $8.02 \pm 1.37\%$ upon hypoxia. In 4-week-old females, fractions amounted to $3.13 \pm 0.33\%$, $5.44 \pm 0.46\%$ and $11.2 \pm 0.78\%$, respectively. In 24-week-old males they reached $2.51 \pm 0.16\%$, $4.43 \pm 0.35\%$ and $5.66 \pm 0.41\%$, and in 24-week-old females $4.34 \pm 0.54\%$, $6.37 \pm 0.75\%$ and $9.28 \pm 0.63\%$ (all trend test P values <0.01). Importantly, CRW performance as pronounced motor-cognitive challenge, enhanced number of tdTomato+ neurons over normoxia throughout, strengthening our hypothesis that neuronal activity leads to 'functional hypoxia', i.e. activity-induced endogenous hypoxia.

Interestingly, also quantification of tdTomato+ astrocytes in whole hippocampus revealed a characteristic stair pattern from normoxia over CRW to hypoxia (Fig. 5d). The percentage of hypoxic astrocytes, i.e. tdTomato+ of all

astrocytes, encompassed under normoxia $0.90 \pm 0.06\%$, CRW $1.30 \pm 0.17\%$ and hypoxia $1.49 \pm 0.14\%$ (trend test $P = 0.004$). In contrast, no significant differences in the number of hypoxic endothelial cells in whole hippocampus were observed between the three conditions (Fig. 5e), with percentages amounting to $7.98 \pm 0.91\%$ for normoxia, $9.11 \pm 1.34\%$ for CRW and $7.77 \pm 0.86\%$ for hypoxia (trend test $P = 0.61$). Overall, we cannot exclude additional region-specific differences (on top of hippocampus), since we did not systematically quantify other brain regions (except for whole cortex in LSM, see below). To provide an extra overview, coronal brain sections illustrate overall brain tdTomato labelling following normoxia versus CRW (Supplementary Fig. 4a, b).

Since in whole hippocampus, there were no hypoxia-labelled tdTomato+ oligodendrocytes found (in perfect accordance with the high *Hk2* expression of these cells, compare Fig. 4d), we had to move to corpus callosum for representative quantifications. There we saw a comparably strong tendency of an increase in hypoxic (tdTomato+) oligodendrocytes upon both, CRW and hypoxia (Fig. 5f). Percentages were as follows: $0.53 \pm 0.11\%$ for normoxia, $1.26 \pm 0.14\%$ for CRW and $1.91 \pm 0.06\%$ for hypoxia (trend test $P = 0.002$). These cell-type-specific findings—in addition to neurons—are highly interesting but will have to be investigated in more depth in future work, employing e.g. different reporter systems and challenges.

We next planned to demonstrate by cFos labelling that induced neuronal activity leads to 'functional hypoxia', searching for double-labelling by cFos and tdTomato+ of those neurons that have been activated during CRW. However, the ODD-tdTomato labelling occurs much too late, i.e., when cFos expression has already disappeared; thus, double-labelling cannot be detected due to the different cFos/ODD-tdTomato kinetics [32]. For instance, at 4 h after CRW start, there is plenty of cFos labelling (e.g. cFos+ neurons/mm² in CA1: non-runner controls, 40 ± 20.83, versus CRW, 150 ± 24.36; $P = 0.01$), however, essentially no ODD-tdTomato labelling visible yet.

Hippocampal mRNA expression of hypoxia-regulated genes after 6 h of CRW supports 'functional hypoxia'

CRW exposure enhanced the number of tdTomato+ (ODD labelled) neurons over normoxia throughout, supporting that neuronal activity induces 'functional hypoxia'. Interestingly, intensive treadmill exercise has been reported earlier to increase expression of HIF-1α and its downstream transcript targets [64]. Nevertheless, we next measured hypoxia-regulated gene expression as an additional way of verifying that motor-cognitive challenge causes cellular/neuronal hypoxia. For this, we extracted mRNA from
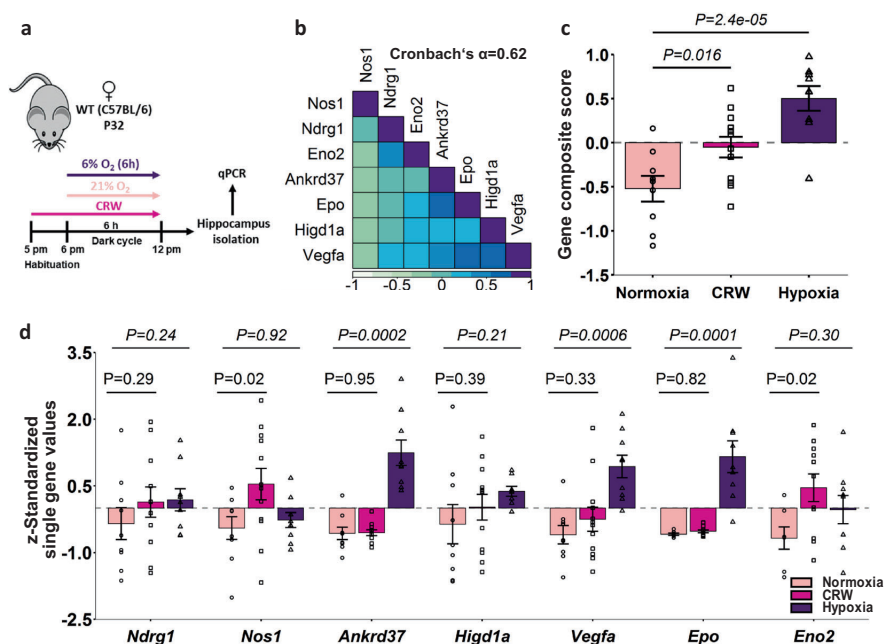
Fig. 6 Selected hypoxia-regulated genes' mRNA expression in hippocampus after 6 h of motor-cognitive challenge versus inspiratory hypoxia support 'functional hypoxia'. a Experimental outline for hippocampal mRNA expression analyses by qPCR. **b** Intercorrelation pattern and Cronbach's alpha of selected hypoxia-regulated genes. **c** Composite gene score shows clear stepwise increase from normoxia over CRW to hypoxia. **d** Z-transformed qPCR results show comparative expression stair patterns (normalized to *Hprt1* and *β*-actin) of all selected single genes, namely *Ndrg1, Nos1, Ankrd37, Higd1a, Vegfa, Epo*, and *Eno2*; *t*-test with pooled standard deviation for two-group comparison between normoxia and CRW (*P* value non-italicized); Jonckheere–Terpstra trend test (20,000 permutations in (**d**)) for comparing all three groups (*P* value in italics); error bars indicate SEM.

hippocampus of mice, exposed for 6 h in a highly standardized fashion to either normoxia, hypoxia or CRW (Fig. 6a–d). As target genes, we selected *Ndrg1, Nos1, Ankrd37, Higd1a, Vegfa, Epo* and *Eno2*, all confirmed by our scRNA-seq of whole hippocampus or by respective literature [32, 65] to be hypoxia-regulated in neurons and other cell types. We determined mRNA of *Epo* as a very potent hypoxia-inducible gene, which had escaped scRNA-seq analysis due to its very low expression, a known dropout effect of this methodology. For *Epo*, we know from our previous work using in situ hybridization, that CRW induces its expression in pyramidal neurons, however, peaking at 9 h [32].

For most of these selected genes, we see a similar picture as with ODD-tdTomato quantifications, with stepwise increase in hippocampal mRNA expression from normoxia over CRW to hypoxia (Fig. 6d). Although gene expression changes under CRW appear to be slight and are often not nominally significant, the consistently obtained pattern (trend test significant or gene expression CRW/hypoxia>normoxia) at a single defined time point (6 h) is still remarkable, considering variable individual gene

expression dynamics and the fact that we exposed mice to only 6 h of CRW, a relatively mild stimulus when compared to 6%O$_2$ for 6 h, as used in our positive control. Nevertheless, since we aimed at proving with our selected transcripts and the obtained data that CRW performance indeed causes cellular/neuronal hypoxia, resembling the inspiratory hypoxia configuration, we performed intercorrelation analyses. Based hereon, we calculated a novel composite score of gene expression, following our previously described standard operating procedure [44, 45]. The internal consistency of the mRNA expression data is reflected by a Cronbach's alpha of >0.6, allowing us to calculate the transcript composite scores for normoxia, CRW and hypoxia, respectively, which turned out to be clearly significant (Fig. 6b–d).

LSM mapping of tdTomato+ cells upon normoxia versus motor-cognitive challenge indicates 'functional hypoxia' in the behaving brain

Having substantiated by transcript analyses that motor-cognitive challenge causes endogenous hypoxia, we
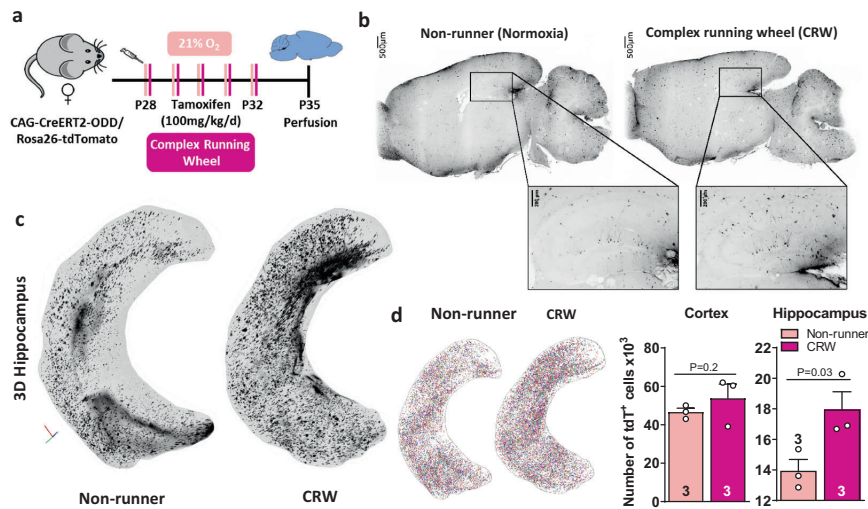
Fig. 7 LSM mapping of tdTomato+ cell distribution upon motor-cognitive challenge indicates 'functional hypoxia' in the behaving brain. a Experimental outline. **b** LSM 2D sagittal planes of tdTomato+ cells; images in inverted grey scale; magnified views of hippocampal area. **c** Dorsal view of 3D hippocampi. Hippocampi cropped from LSM hemisphere dataset and visualized as 3D maximal intensity projection; orientation given in left corner. **d** Quantification of tdTomato+ cells in hippocampus and cortex; left images display 3D renderings shown in (**d**) with tdTomato+ cells represented as random-coloured blobs; 1-tailed Welch's *t*-test, error bars indicate SEM.

conducted a second round of LSM analyses. We directly compared female non-runner mice (normoxia) with mice exposed to CRW (Fig. 7a–d). Display in 3D and quantification of tdTomato+ cells in hippocampus revealed a marked increase upon CRW, again strongly supporting our 'functional hypoxia' hypothesis (Fig. 7a–d; Supplementary Video II). Strikingly, however, upon performing a particular task (here: CRW) requiring an activation of defined groups of neurons, one might perhaps expect more region-specific activation. The fact that whole hippocampus (and not just *cornu ammonis*) showed an increase in tdTomato+ cells, and that even the cortex displayed a respective tendency, seems less puzzling in light of recent reports that demonstrate a global/brain-wide neuronal activation during certain tasks and behaviours in mice [66] and zebrafish [67]. Moreover, even normal wheel running leads to increased brain activation (measured by cFos expression) in the majority of 25 investigated brain regions [68]. Thus, the focused 'functional hypoxia' in hippocampal regions upon CRW that we see is embedded in a global/brain-wide neuronal activation. Of note, some degree of overreporting by the used reporter system, caused e.g. by tamoxifen-induced cellular stress [69], cannot be entirely ruled out. While overall, this does not invalidate the above conclusions, future studies might want to co-administer vitamin E with tamoxifen in order to reduce any potential undesired cellular stress.

Working model of activity-induced hypoxia as a driver of neuroplasticity

The present data suggest a novel working model in which energy-consuming neuronal activity induces hypoxia with its well-known transcriptional programme that—via HIF stabilization—includes metabolic adaptations and the expression of potent growth factors like EPO and VEGF [10, 13–16]. According to this model, activity-induced physiological hypoxia hereby acts as a critical driver of neuroplasticity, engaging e.g. brain-expressed EPO [32]. Notably, recent work even widened our understanding of the hypoxia response, highlighting hundreds of genes expressed under low oxygen, yet most unrelated to HIF [10, 12]. This suggests that the entire hypoxia response is only in part detectable with our ODD reporter that depends on HIF stabilization. The mechanism is even more complex, as HIF-1α stabilization can also be stimulated e.g. by the PI3K-Akt-mTOR pathway [70], suggesting that HIF-1α dependent gene regulation is kept in a cell-type-specific physiological window. Thus, also CreERT2-ODD dependent activation of the reporter gene may be cell type-specifically co-regulated at the cellular level, partly explaining response differences between cell types, as discussed above and exemplified particularly by microglia that appear nearly unresponsive to hypoxia.

Therefore, all data presented in this manuscript have to be understood in this greater context. We are also aware that

functional hypoxia due to specific neuronal network activity, as induced here by CRW, might with our reporter system not equally be detectable in all theoretically involved brain regions (hippocampus versus motor cortex), since HIF may not be the exclusive mediator of the entire hypoxia response. In fact, we see with our reporter a brain-wide 'general' neuronal hypoxia answer to tasks such as complex motor-cognitive learning, on top of stimulated specific areas like the hippocampal cornu ammonis (demonstrated in Video II). This response includes the participation of indirectly activated neurons and of non-neuronal cells in adjusting the brain to specific activity-induced challenges. CRW being a strong motor-cognitive test, we do expect both components (general and specific) to be involved. In addition, 'systemic reactions' *('out of breath')*, evoked by physical exercise, may add globally to this particular hypoxia response. Future experiments will further tackle these thought-provoking, still open questions and help disentangle the relative contributions of general versus specific components.

To conclude, our 'functional hypoxia model' integrates not only the specific activity-induced hypoxia, as described here for the hippocampus, but may also help understanding previously unexplained observations. These range from the 'hypoxia vulnerability' of brain areas highly relevant for cognition, as the CA1 region of the hippocampus (Sommer's Sector) [46–49], or the observed HIF-1α expression upon exercise in activity-involved brain areas [64], to the beneficial effects of HIF stabilizers on cognitive performance [16]. Moreover, our model suggests a general response to specific activity-induced neuronal challenges, such as complex motor-cognitive tasks, which includes indirectly activated neurons and non-neuronal cells. The widespread 'functional hypoxia' arising from increasing energy demands may explain the advantageous effects of physical and cognitive challenges on brain dimensions and global brain function. A picture of hypoxia-induced adaptive neuroplasticity in the postnatal/adult brain is emerging that could also provide the ground for exploring the beneficial therapeutic role of hypoxia in pathological states.

Data availability

Raw and processed scRNA-seq data are publicly available on GEO via accession code GSE162079.

Code availability

Analysis scripts for scRNA-seq analysis are available at https://github.com/AgnesSteixner/Butt_et_al_ODD_hypoxia

Compliance with ethical standards

References

1. Kaelin WG, Ratcliffe PJ. Oxygen sensing by metazoans: the central role of the HIF hydroxylase pathway. Mol Cell. 2008;30: 393–402.
2. Ratcliffe PJ. Oxygen sensing and hypoxia signalling pathways in animals: the implications of physiology for cancer. J Physiol. 2013;591:2027–42.
3. Semenza GL. Targeting HIF-1 for cancer therapy. Nat Rev Cancer. 2003;3:721–32.
4. Kullmann JA, Trivedi N, Howell D, Laumonnerie C, Nguyen V, Banerjee SS, et al. Oxygen tension and the VHL-Hif1alpha pathway determine onset of neuronal polarization and cerebellar germinal zone exit. Neuron. 2020;106:607–623 e605.
5. Ivashkiv LB. The hypoxia–lactate axis tempers inflammation. Nat Rev Immunol. 2020;20:85–86.
6. Huang X, Trinh T, Aljoufi A, Broxmeyer HE. Hypoxia signaling pathway in stem cell regulation: good and evil. Curr Stem Cell Rep. 2018;4:149–57.

7. Morikawa T, Takubo K. Hypoxia regulates the hematopoietic stem cell niche. Pflug Arch. 2016;468:13–22.

8. Taylor CT, Colgan SP. Regulation of immunity and inflammation by hypoxia in immunological niches. Nat Rev Immunol. 2017;17:774–85.

9. Baik AH, Jain IH. Turning the oxygen dial: balancing the highs and lows. Trends Cell Biol. 2020;30:516–36.

10. Lee P, Chandel NS, Simon MC. Cellular adaptation to hypoxia through hypoxia inducible factors and beyond. Nat Rev Mol Cell Biol. 2020;21:268–83.

11. Yuen TJ, Silbereis JC, Griveau A, Chang SM, Daneman R, Fancy SP, et al. Oligodendrocyte-encoded HIF function couples post-natal myelination and white matter angiogenesis. Cell. 2014;158: 383–96.

12. Jain IH, Calvo SE, Markhard AL, Skinner OS, To TL, Ast T, et al. Genetic screen for cell fitness in high or low oxygen highlights mitochondrial and lipid metabolism. Cell. 2020;181:716–727 e711.

13. Kaelin WG. Proline hydroxylation and gene expression. Annu Rev Biochem. 2005;74:115–28.

14. Kenneth NS, Rocha S. Regulation of gene expression by hypoxia. Biochemical J. 2008;414:19–29.

15. Marti HH. Erythropoietin and the hypoxic brain. J Exp Biol. 2004;207:3233–42.

16. Adamcio B, Sperling S, Hagemeyer N, Walkinshaw G, Ehren-reich H. Hypoxia inducible factor stabilization leads to lasting improvement of hippocampal memory in healthy mice. Beha-vioural Brain Res. 2010;208:80–84.

17. Brines M, Cerami A. Emerging biological roles for erythropoietin in the nervous system. Nat Rev Neurosci. 2005;6:484–94.

18. Suresh S, Rajvanshi PK, Noguchi CT. The many facets of ery-thropoietin physiologic and metabolic response. Front Physiol. 2020;10:1534.

19. Schuler B, Vogel J, Grenacher B, Jacobs RA, Arras M, Gassmann M. Acute and chronic elevation of erythropoietin in the brain improves exercise performance in mice without inducing ery-thropoiesis. FASEB J. 2012;26:3884–90.

20. Jelkmann W. Erythropoietin: structure, control of production, and function. Physiological Rev. 1992;72:449–89.

21. Logothetis NK, Pfeuffer J. On the nature of the BOLD fMRI contrast mechanism. Magn Reson Imaging. 2004;22:1517–31.

22. Hillman EMC. Coupling mechanism and significance of the BOLD signal: a status report. Annu Rev Neurosci. 2014;37: 161–81.

23. Raichle ME. Behind the scenes of functional brain imaging: a historical and physiological perspective. Proc Natl Acad Sci USA. 1998;95:765–72.

24. Erickson KI, Hillman CH, Kramer AF. Physical activity, brain, and cognition. Curr Opin Behav Sci. 2015;4:27–32.

25. Kramer AF, Erickson KI. Capitalizing on cortical plasticity: influence of physical activity on cognition and brain function. Trends Cogn Sci. 2007;11:342–8.

26. Pajonk FG, Wobrock T, Gruber O, Scherk H, Berner D, Kaizl I, et al. Hippocampal plasticity in response to exercise in schizo-phrenia. Arch Gen Psychiatry. 2010;67:133–43.

27. Ehrenreich H, Fischer B, Norra C, Schellenberger F, Stender N, Stiefel M, et al. Exploring recombinant human erythropoietin in chronic progressive multiple sclerosis. Brain. 2007;130:2577–88.

28. Ehrenreich H, Hinze-Selch D, Stawicki S, Aust C, Knolle-Veentjer S, Wilms S, et al. Improvement of cognitive functions in chronic schizophrenic patients by recombinant human ery-thropoietin. Mol Psychiatry. 2007;12:206–20.

29. Miskowiak KW, Vinberg M, Christensen EM, Bukh JD, Harmer CJ, Ehrenreich H, et al. Recombinant human erythropoietin for treating treatment-resistant depression: a double-blind, randomized, placebo-controlled phase 2 trial. Neuropsycho-pharmacology. 2014;39:1399–408.

30. Miskowiak KW, Vinberg M, Macoveanu J, Ehrenreich H, Koster N, Inkster B, et al. Effects of erythropoietin on hippocampal volume and memory in mood disorders. Biol Psychiatry. 2015;78:270–7.

31. Hassouna I, Ott C, Wüstefeld L, Offen N, Neher RA, Mitkovski M, et al. Revisiting adult neurogenesis and the role of ery-thropoietin for neuronal and oligodendroglial differentiation in the hippocampus. Mol Psychiatry. 2016;21:1752–67.

32. Wakhloo D, Scharkowski F, Curto Y, Butt UJ, Bansal V, Steixner-Kumar AA, et al. Functional hypoxia drives neuroplas-ticity and neurogenesis via brain erythropoietin. Nat Commun. 2020;11:1–12.

33. Kimura W, Xiao F, Canseco DC, Muralidhar S, Thet S, Zhang HM, et al. Hypoxia fate mapping identifies cycling cardiomyo-cytes in the adult heart. Nature. 2015;523:226–30.

34. Madisen L, Zwingman TA, Sunkin SM, Oh SW, Zariwala HA, Gu H, et al. A robust and high-throughput Cre reporting and char-acterization system for the whole mouse brain. Nat Neurosci. 2010;13:133.

35. Liebetanz D, Merkler D. Effects of commissural de- and remye-lination on motor skill behaviour in the cuprizone mouse model of multiple sclerosis. Exp Neurol. 2006;202:217–24.

36. McKenzie IA, Ohayon D, Li H, Paes de Faria J, Emery B, Tohyama K, et al. Motor skill learning requires active central myelination. Science. 2014;346:318–22.

37. Liebmann T, Renier N, Bettayeb K, Greengard P, Tessier-Lavigne M, Flajolet M. Three-dimensional study of Alzheimer's disease hallmarks using the iDISCO clearing method. Cell Rep. 2016;16: 1138–52.

38. Lein ES, Hawrylycz MJ, Ao N, Ayres M, Bensinger A, Bernard A, et al. Genome-wide atlas of gene expression in the adult mouse brain. Nature. 2006;445:168–76.

39. Team RC. R: a language and environment for statistical com-puting. Vienna: R Foundation for Statistical Computing; 2018.

40. Butler A, Hoffman P, Smibert P, Papalexi E, Satija R. Integrating single-cell transcriptomic data across different conditions, tech-nologies, and species. Nat Biotechnol. 2018;36:411–20.

41. Stuart T, Butler A, Hoffman P, Hafemeister C, Papalexi E, Mauck WM III, et al. Comprehensive Integration of single-cell data. Cell. 2019;177:1888–1902.e1821.

42. McGinnis CS, Murrow LM, Gartner ZJ. DoubletFinder: doublet detection in single-cell RNA sequencing data using artificial nearest neighbors. Cell Syst. 2019;8:329–337 e324.

43. Zeisel A, Muñoz-Manchado AB, Codeluppi S, Lönnerberg P, La Manno G, Juréus A, et al. Cell types in the mouse cortex and hippocampus revealed by single-cell RNA-seq. Science. 2015;347:1138.

44. Dere E, Dahm L, Lu D, Hammerschmidt K, Ju A, Tantra M, et al. Heterozygous AMBRA1 deficiency in mice: a genetic trait with autism-like behavior restricted to the female gender. Front Behav Neurosci. 2014;8:181.

45. Ribbe K, Friedrichs H, Begemann M, Grube S, Papiol S, Kästner A, et al. The cross-sectional GRAS sample: A comprehensive phenotypical data collection of schizophrenic patients. BMC Psychiatry. 2010;10:91.

46. Penny JE, Kukums JR, Tyrer JH, Eadie MJ. Selective vulner-ability of the hippocampus to hypoxia: cytophotometric studies of enzyme activity in single neurones. Proc Aust Assoc Neurol. 1974;11:177–81.

47. Ng T, Graham DI, Adams JH, Ford I. Changes in the hippocampus and the cerebellum resulting from hypoxic insults: frequency and distribution. Acta Neuropathol. 1989;78: 438–43.

48. Schmidt-Kastner R. Genomic approach to selective vulnerability of the hippocampus in brain ischemia–hypoxia. Neuroscience. 2015;309:259–79.

49. Sommer W. Erkrankung des Ammonshorns als aetiologisches Moment der Epilepsie. Arch Psychiatr Nervenkr. 1880;10: 631–75.

50. Chatzi C, Schnell E, Westbrook GL. Localized hypoxia within the subgranular zone determines the early survival of newborn hippocampal granule cells. Elife. 2015;4:e08722.

51. Mazumdar J, O'brien WT, Johnson RS, LaManna JC, Chavez JC, Klein PS, et al. O2 regulates stem cells through Wnt/β-catenin signalling. Nat Cell Biol. 2010;12:1007–13.

52. Power RM, Huisken J. A guide to light-sheet fluorescence microscopy for multiscale imaging. Nat Methods. 2017;14: 360–73.

53. Mathupala SP, Rempel A, Pedersen PL. Glucose catabolism in cancer cells: Identification and characterization of a marked activation response of the type ii hexokinase gene to hypoxic conditions. J Biol Chem. 2001;276:43407–12.

54. Wolf A, Agnihotri S, Micallef J, Mukherjee J, Sabha N, Cairns R, et al. Hexokinase 2 is a key mediator of aerobic glycolysis and promotes tumor growth in human glioblastoma multiforme. J Exp Med. 2011;208:313–26.

55. Brandenburg S, Müller A, Turkowski K, Radev YT, Rot S, Schmidt C, et al. Resident microglia rather than peripheral macrophages promote vascularization in brain tumors and are source of alternative pro-angiogenic factors. Acta Neuropathol. 2016;131:365–78.

56. Pan Y, Mansfield KD, Bertozzi CC, Rudenko V, Chan DA, Giaccia AJ, et al. Multiple factors affecting cellular redox status and energy metabolism modulate hypoxia-inducible factor prolyl hydroxylase activity in vivo and in vitro. Mol Cell Biol. 2007;27:912–25.

57. Guo Y, Wang Z, Prathap S, Holschneider DP. Recruitment of prefrontal-striatal circuit in response to skilled motor challenge. Neuroreport. 2017;28:1187–94.

58. Fabel K, Wolf SA, Ehninger D, Babu H, Leal-Galicia P, Kempermann G. Additive effects of physical exercise and environmental enrichment on adult hippocampal neurogenesis in mice. Front Neurosci. 2009;3:50.

59. Kobilo T, Liu QR, Gandhi K, Mughal M, Shaham Y, van Praag H. Running is the neurogenic and neurotrophic stimulus in environmental enrichment. Learn Mem. 2011;18:605–9.

60. Cuffe JS, Walton SL, Singh RR, Spiers JG, Bielefeldt-Ohmann H, Wilkinson L, et al. Mid- to late term hypoxia in the mouse alters placental morphology, glucocorticoid regulatory pathways and nutrient transporters in a sex-specific manner. J Physiol. 2014;592:3127–41.

61. Lan WC, Priestley M, Mayoral SR, Tian L, Shamloo M, Penn AA. Sex-specific cognitive deficits and regional brain volume loss in mice exposed to chronic, sublethal hypoxia. Pediatr Res. 2011;70:15–20.

62. Soliz J, Thomsen JJ, Soulage C, Lundby C, Gassmann M. Sex-dependent regulation of hypoxic ventilation in mice and humans is mediated by erythropoietin. Am J Physiol Regul Integr Comp Physiol. 2009;296:R1837–46.

63. Heyer A, Hasselblatt M, von Ahsen N, Häfner H, Sirén A-L, Ehrenreich H. In vitro gender differences in neuronal survival on hypoxia and in 17β-estradiol-mediated neuroprotection. J Cereb Blood Flow Metab. 2005;25:427–30.

64. Halliday MR, Abeydeera D, Lundquist AJ, Petzinger GM, Jakowec MW. Intensive treadmill exercise increases expression of hypoxia-inducible factor 1alpha and its downstream transcript targets: a potential role in neuroplasticity. Neuroreport. 2019;30:619–27.

65. Jögi A, Vallon-Christersson J, Holmquist L, Axelson H, Borg Å, Påhlman S. Human neuroblastoma cells exposed to hypoxia: induction of genes associated with growth, survival, and aggressive behavior. Exp Cell Res. 2004;295:469–87.

66. Steinmetz NA, Zatka-Haas P, Carandini M, Harris KD. Distributed coding of choice, action and engagement across the mouse brain. Nature. 2019;576:266–73.

67. Marques JC, Li M, Schaak D, Robson DN, Li JM. Internal state dynamics shape brainwide activity and foraging behaviour. Nature. 2020;577:239–43.

68. Rhodes JS, Garland T Jr, Gammie SC. Patterns of brain activity associated with variation in voluntary wheel-running behavior. Behav Neurosci. 2003;117:1243.

69. Denk F, Ramer LM, Erskine EL, Nassar MA, Bogdanov Y, Signore M, et al. Tamoxifen induces cellular stress in the nervous system by inhibiting cholesterol synthesis. Acta Neuropathol Commun. 2015;3:74.

70. Joshi S, Singh AR, Durden DL. MDM2 regulates hypoxic hypoxia-inducible factor 1alpha stability in an E3 ligase, proteasome, and PTEN-phosphatidylinositol 3-kinase-AKT-dependent manner. J Biol Chem. 2014;289:22785–97.

SUPPLEMENTARY INFORMATION

Hippocampal neurons respond to brain activity with functional hypoxia

Umer Javed Butt[1§], Agnes A. Steixner-Kumar[1§], Constanze Depp[2§], Ting Sun[2,3],
Imam Hassouna[1], Liane Wüstefeld[1], Sahab Arinrad[1], Matthias R. Zillmann[1], Nadine Schopf[1], Laura Fernandez Garcia-Agudo[1],
Leonie Mohrmann[1], Ulli Bode[2], Anja Ronnenberg[1], Martin Hindermann[1], Sandra Goebbels[2], Stefan Bonn[3], Dörthe M. Katschinski[4],
Kamilla W. Miskowiak[5], Klaus-Armin Nave[2*], and Hannelore Ehrenreich[1*]

[§]*Shared first authorship*

[1]Clinical Neuroscience and [2]Department of Neurogenetics, Max Planck Institute of Experimental Medicine, Göttingen, Germany
[3]Institute of Medical Systems Biology, Center for Molecular Neurobiology,
University Clinic Hamburg-Eppendorf, Hamburg, Germany
[4]Institute for Cardiovascular Physiology, University Medical Center Göttingen,
Georg-August-University, Göttingen, Germany
[5]Psychiatric Centre Copenhagen, University Hospital, Rigshospitalet, Copenhagen, Denmark

*Correspondence:
Prof. Hannelore Ehrenreich, MD, DVM
Clinical Neuroscience, Max Planck Institute of Experimental Medicine
Hermann-Rein-Str.3, 37075 Göttingen, GERMANY
Phone +49-551-3899615; Fax +49-551-3899670
E-Mail: **ehrenreich@em.mpg.de**
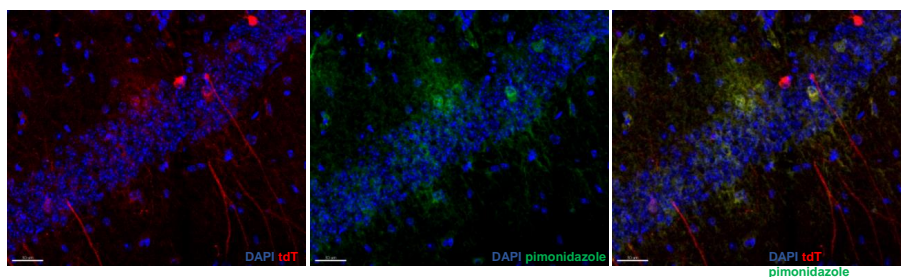
Prof. Klaus-Armin Nave, PhD
Neurogenetics, Max Planck Institute of Experimental Medicine
Hermann-Rein-Str.3, 37075 Göttingen, GERMANY
Phone: +49-551-3899754; Fax: +49-551-3899758
E-Mail: **nave@em.mpg.de**
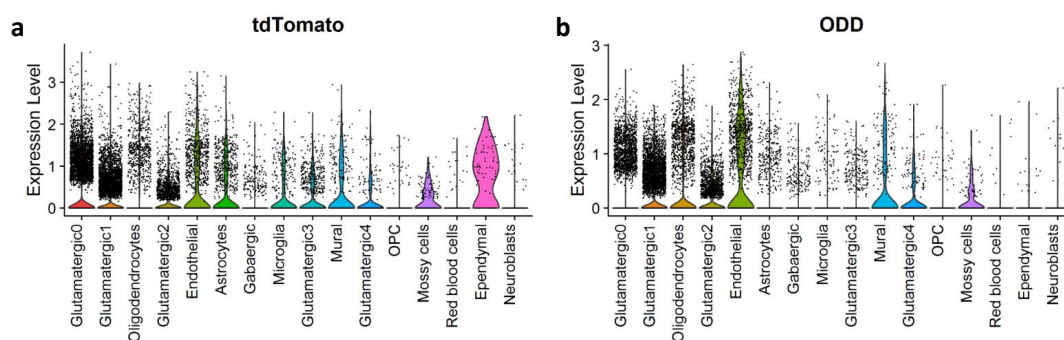
Butt et al Supplementary Figure 1

Supplementary Figure 1: Pimonidazole staining confirms functional hypoxia in tdTomato+ cells. Co-labelling of tdTomato and pimonidazole (*Sato et al 2011*) shows the presence of hypoxia in a subset of tdTomato+ cells (compare *Kimura et al 2015*). Pimonidazole was administered 16 hours after 1X tamoxifen injection (100mg/kg i.p.) and CRW start, and mice were sacrificed 90 minutes after pimonidazole administration. Scale bar represents 30 μm.

References:

Sato, Y., Endo, H., Okuyama, H., Takeda, T., Iwahashi, H., Imagawa, A., et al. Cellular hypoxia of pancreatic β-cells due to high levels of oxygen consumption for insulin secretion in vitro. *Journal of Biological Chemistry* **286**, 12524-12532 (2011).

Kimura W, Xiao F, Canseco DC, Muralidhar S, Thet S, Zhang HM et al. Hypoxia fate mapping identifies cycling cardiomyocytes in the adult heart. *Nature* 2015; **523**(7559): 226-230.

Butt et al Supplementary Figure 2

Supplementary Figure 2: Normalized expression levels of (a) tdTomato and (b) ODD in respective cell clusters. No differences in mean expression of either tdTomato or ODD ($p > 0.2$, Wilcoxon test, 2-tailed) were observed between microglia and neurons, i.e. the least (microglia) and the most pronounced (neurons, comprising glutamatergic0-4, gabaergic and mossy cell clusters) hypoxia-labelled cell types.

Butt et al Supplementary Figure 3a
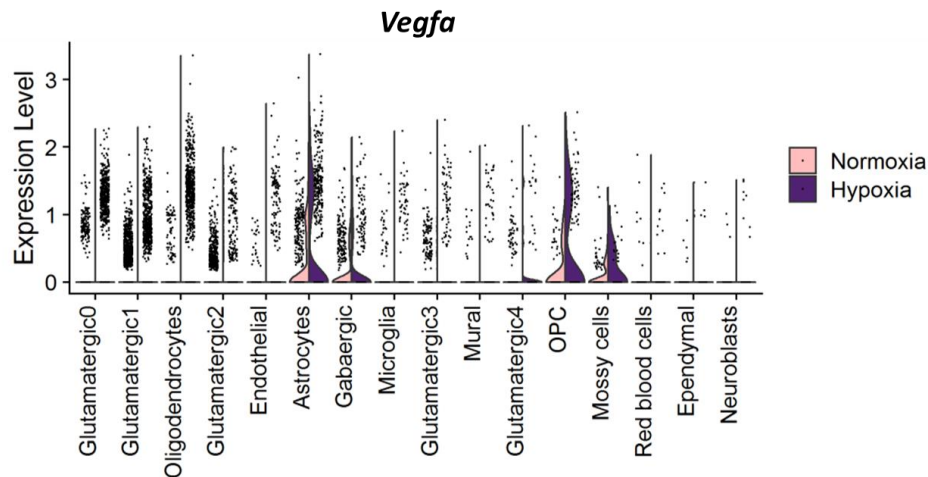
Supplementary Figure 3a: Violin plots showing expression of *Vegfa* under normoxia and hypoxia in all hippocampal cell populations. *Vegfa* was highest expressed in OPC and astrocytes (avg_logFC>0.25, p_{unadj}<0.05) when compared to all other cell types.

Butt et al Supplementary Figure 3b

Cluster	p_val	avg_logFC	Hypoxia proportion	Normoxia proportion	p_val_adj
Glutamatergic0	1.06E-32	0.221406	0.118	0.044	2.0E-28
Glutamatergic1	6.28E-04	0.169033	0.173	0.163	1.0E+00
Oligodendrocytes	4.84E-20	0.468132	0.228	0.092	9.2E-16
Glutamatergic2	1.27E-01	0.205379	0.222	0.225	1.0E+00
Endothelial	3.62E-03	0.211827	0.101	0.057	1.0E+00
Astrocytes	1.68E-05	0.470057	0.374	0.35	3.2E-01
Gabaergic	8.91E-01	0.154432	0.258	0.293	1.0E+00
Microglia	6.40E-01	0.09817	0.153	0.188	1.0E+00
Glutamatergic3	3.30E-03	0.313916	0.225	0.171	1.0E+00
Mural cells	2.00E-01	0.049427	0.129	0.203	1.0E+00
Glutamatergic4	4.94E-01	0.317821	0.25	0.246	1.0E+00
OPC	6.77E-03	0.531906	0.389	0.293	1.0E+00
Mossy cells	4.25E-02	0.141386	0.417	0.293	1.0E+00
Red blood cells	6.89E-01	-0.05511	0.108	0.129	1.0E+00
Ependymal cells	1.92E-01	0.255091	0.174	0.086	1.0E+00
Neuroblasts	4.49E-01	0.141355	0.116	0.075	1.0E+00

Supplementary Figure 3b: Differential expression testing for *Vegfa* (as shown in Figure 3a) under hypoxia versus normoxia in all cell types (Wilcoxon test, 2-tailed); **avg_logFC**: positive log fold-change values indicate upregulation under hypoxia, negative values downregulation under hypoxia. **Hypoxia proportion**: Proportion of cells expressing *Vegfa* under hypoxia; **Normoxia proportion**: Proportion of cells expressing *Vegfa* under normoxia. P_val_adj: Bonferroni adjusted p-value (adjusted for all genes in data set).
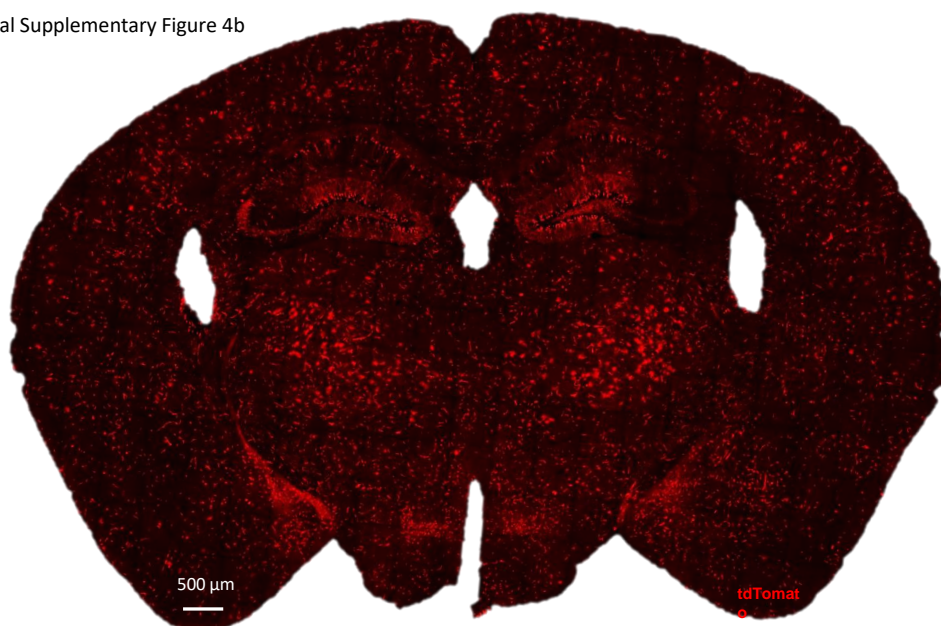
Butt et al Supplementary Figure 4a

Supplementary Figure 4a: Representative coronal brain section of a CAG-CreERT2-ODD::R26R-tdTomato mouse shows brain-wide distribution of scattered tdTomato+ cells under normoxia (5X tamoxifen injections).

Butt et al Supplementary Figure 4b

Supplementary Figure 4b: Representative coronal brain section of a CAG-CreERT2-ODD::R26R-tdTomato mouse shows globally enhanced numbers and intensity of tdTomato+ cells after exposure to CRW (5 consecutive nights, 5X tamoxifen injections). The widely distributed tdTomato labelling indicates brain-wide response to motor-cognitive challenge.

5 Project III: Brain erythropoietin, neurodifferentiation and the neuron-microglia cross-talk in the adult hippocampus

5.1 Overview of Project III

EPO and EPOR are highly expressed during embryonic development - a phase of extensive neuro- and angiogenesis - and remain expressed at lower levels throughout adulthood (Liu et al., 1997). Administration of rhEPO has frequently been shown to exert beneficial effects on cognitive function and neuroregeneration (Ehrenreich et al., 2007a; Ehrenreich et al., 2007b; Miskowiak et al., 2010; Miskowiak et al., 2015; Miskowiak et al., 2014a; Miskowiak et al., 2014b; Mitkovski et al., 2015). In 2016, Hassouna et al. showed that EPO administration over 3 weeks leads to a ∼20% increase in neurons within the CA1 without altered proliferation or decrease in apoptosis. As mentioned above, endogenously EPO expression is induced under hypoxia by HIF1α, which can occur in the brain in response to neuronal activity, as shown in Project II. Moreover, it was previously shown that EPO enhances long-term potentiation (Adamcio et al., 2008). However, the precise mechanisms how (endogenous or administered) EPO fosters neurodifferentiation and neuroplasticity remained obscure.

Consequently, the current project aimed to further investigate the EPO-induced effects on neurodifferentiation and neuroplasticity. To this end, two experimental paradigms were used: One paradigm, in which rhEPO is injected intraperitoneally, and another that utilizes inspiratory (ambient lowered O_2 levels) and functional hypoxia (CRW task) to induce EPO expression endogenously. While our lab previously observed the ∼20% increase in neurons within the CA1, the identity and origin of these cells remained unclear. Thus, in Wakhloo et al. (2020) a tamoxifen-inducible NexCreERT2 tdTomato reporter mouse line was used to label all existing cells before start of EPO administration. Afterwards, mice were treated with rhEPO for three weeks (+1 week of break) and labelled, i.e., pre-existing, and unlabelled, i.e., newly formed, neurons were quantified. This showed that the previously observed numerical increase in CA1 neurons was largely attributable to a substantial increase in newly formed neurons. In order to better understand the temporal dynamics of this process, single-cell RNA-seq analysis was performed six hours

after a single EPO injection. This analysis revealed that the number of immature neurons in the CA1 was already increased at this early time point. Amongst other markers, these cells were characterized by expression of immature neuron markers *T-Box Brain Transcription Factor 1 (Tbr1)* and *TLE Family Member 4, Transcriptional Corepressor (Tle4)*. The numerical increase in neurons expressing these genes was confirmed with immunohistochemical staining 24 hours after a single EPO injection. Furthermore, pseudotime analysis confirmed the immature identity of these cells and an increase in immature neurons could be substantiated by a decreased pseudotime in the EPO- as compared to the placebo-treated group. Interestingly, in a consecutive study (Fernandez Garcia-Agudo et al, under review), we could show that these initially immature cells under stimulation with EPO progress over the course of three weeks towards maturity. Accordingly, after one week of rhEPO treatment the number of TBR1+ cells does not differ anymore as these cells have matured and now express markers of intermediate maturity such as *Zinc Finger And BTB Domain Containing 20 (Zbtb20)*. Additonal EPO-effects included an increase in synaptic spine density and improved CRW performance (both mediated via neuronally expressed EPOR). Interestingly, there was a reciprocal relationship between EPO and motor-cognitive challenge: While rhEPO administration boosted motor-cognitive performance, motor-cognitive challenge in turn lead to increased EPO and EPOR expression in pyramidal neurons of the hippocampus, again supporting the concept of "functional hypoxia".

In Fernandez Garcia-Agudo et al (under review), we could show that CRW, as inducer of functional hypoxia, as well as inspiratory hypoxia (three weeks, 12% O_2 hypoxia) leads to a decrease in microglial cells in the pyramidal layer of CA1. A similar reduction was observed after administration of rhEPO over three weeks. This reduction was most likely due to an short-lived initial increase of microglial apoptosis (24 hours after rhEPO treatment) as shown by caspase-3 staining and a subsequent prolonged phase of reduced proliferation demonstrated by a decrease number of Ki67+ cells. Overall, protein turnover in microglia was reduced after rhEPO as measured by incorporation of labelled ^{15}N-leucine and microglia displayed an increased perimeter/area ratio pointing to a less activated phenotype. At the same time, microglial contacts with pyramidal neurons were reduced. In context of our previous findings delineating EPO effects on neurons, these results appeared particularly intriguing and opened the question whether EPO does not only affect each cell type individually but also alters the cross-talk between neurons and microglia. To address this question, first the expression of *colony stimulating factor 1 receptor (Csf1r)* and its known ligands *colony stimulating factor 1 (Csf1)* and *interleukin 34 (Il34)* was assessed. CSF1R signalling is known to be crucial for microglial maintenance and survival (Elmore et al., 2014). Strikingly, in the hippocampus the mRNA expression of CSF1R-ligand *Il34* was significantly reduced after 3 weeks of EPO treatment (qPCR) as well as 5 days of hypoxia exposure (6 hours/day, 6% O_2, scRNA-seq). At the same time, CSF1R was upregulated (on protein and mRNA level), probably representing a compensatory response to the reduction in *Il34*. Moreover, after microglia-specific knock-out of EPOR, the previously discovered increase in pyramidal neurons was abolished (results included

in revision).

Collectively, these findings provide deeper understanding of brain-EPO effects and give insight into how neuronal and microglial responses to EPO together orchestrate EPO-mediated brain adaptation that ultimately results in improved cognitive performance.

5.2 Original publications

Wakhloo, D.*, Scharkowski, F.*, Curto, Y.*, Butt U.J., Bansal, V., Steixner-Kumar, A.A. et al. (2020). Functional hypoxia drives neuroplasticity and neurogenesis via brain erythropoietin. Nature Communications, 11(1), 1-12.

Fernandez Garcia-Agudo, L.*, Steixner-Kumar A.A.*, Curto, Y.* et al. Brain erythropoietin fine-tunes a counterbalance between neurodifferentiation and microglia in the adult hippocampus. Under Review.

*equal contribution

Personal contribution

In Wakhloo et al. (2020) I contributed to scRNAseq analyses and performed the trajectory analysis. I helped drafting figure legends, figure items and wrote parts of the manuscript. In Fernandez Garcia-Agudo et al. (under review) I conducted all scRNAseq analyses, assisted in data interpretation and provided figures, figure legends and manuscript text for the respective parts.

Brain erythropoietin fine-tunes a counterbalance between neurodifferentiation and microglia in the adult hippocampus

Laura Fernandez Garcia-Agudo[1][§], Agnes A. Steixner-Kumar[1][§], Yasmina Curto[1][§],
Imam Hassouna[1], Nadine Schopf[1], Sebastian Jähne[2], Umer Javed Butt[1], Katharina Grewe[2],
Martin S. Weber[3], Kim Green[4], Silvio Rizzoli[2], Juan Nacher[5], Klaus-Armin Nave[6]*,
and Hannelore Ehrenreich[1]*

[§]*Shared first authorship*

[1]Clinical Neuroscience, Max Planck Institute of Experimental Medicine, Göttingen, Germany
[2]Department of Neuro- and Sensory Physiology, University Medical Center Göttingen, Germany
[3]Institute of Neuropathology and Department of Neurology, UMG, Göttingen, Germany
[4]Department of Neurobiology and Behavior, Institute for Memory Impairments and Neurological Disorders, University of California, Irvine, CA, USA
[5]Neurobiology Unit, Program in Neurosciences and Interdisciplinary Research Structure for Biotechnology and Biomedicine (BIOTECMED), Universitat de València, Burjassot, Spain
[6]Department of Neurogenetics, Max Planck Institute of Experimental Medicine, Göttingen, Germany

Running title: Neuron – microglia balance under EPO

Key words: Hypoxia, recombinant human EPO, neurogenesis, CSF1R, IL-34, PLX5622, microglia activity, apoptosis, proliferation

Word counts: Abstract 150 words; Text Body: 3823

*Correspondence:
Prof. Hannelore Ehrenreich, MD, DVM
Clinical Neuroscience
Max Planck Institute of Experimental Medicine
Hermann-Rein-Str.3, 37075 Göttingen, GERMANY
Phone +49-551-3899615; Fax +49-551-3899670
E-Mail: **ehrenreich@em.mpg.de**

Prof. Klaus-Armin Nave, PhD
Neurogenetics
Max Planck Institute of Experimental Medicine
Hermann-Rein-Str.3, 37075 Göttingen, GERMANY
Phone: +49-551-3899754; Fax: +49-551-3899758
E-Mail: **nave@em.mpg.de**

ABSTRACT

In postnatal cornu ammonis hippocampi, erythropoietin (EPO) expression drives the differentiation of new neurons, independent of DNA synthesis, and increases dendritic spine density. This substantial brain hardware upgrade is part of a regulatory cycle: During motor-cognitive challenge, neurons experience 'functional' hypoxia, triggering neuronal EPO production, which in turn promotes improved performance *(EPO brain doping).* Here, we show an unexpected involvement of resident microglia. During EPO upregulation and stimulated neurodifferentiation, either by functional or inspiratory hypoxia, we noted that microglia numbers decrease. Treating mice with recombinant human (rh)EPO or exposure to hypoxia recapitulates these changes and reveals that neuronally expressed IL-34 and microglial CSF1R are involved. Surprisingly, EPO affects microglia in phases, initially by stimulating apoptosis, later by reducing proliferation, and overall dampens microglia activity and metabolism, as proven by genetic targeting of microglial EPO receptor. We suggest that during accelerating neuronal differentiation, EPO acts as regulator of the CSF1R-dependent microglia.

INTRODUCTION

Erythropoietin (EPO) is a hypoxia-inducible growth factor, expressed in brain (Brines and Cerami, 2005; Digicaylioglu et al., 1995; Jelkmann, 1992; Marti et al., 1996; Siren et al., 2009; Suresh et al., 2019). In numerous clinical trials and 'back-translational' rodent studies for deeper mechanistic insight, recombinant human (rh)EPO treatment consistently improved cognitive performance, including executive functions, many facets of learning, memory, attention, and processing speed. At the same time, it reduced brain matter loss (Adamcio et al., 2008; Ehrenreich et al., 2007a; Ehrenreich et al., 2007b; El-Kordi et al., 2009; Miskowiak et al., 2014; Miskowiak et al., 2015; Siren et al., 2006; Wustenberg et al., 2011). Searching for underlying mechanisms, we discovered that 3-week rhEPO treatment of mice leads to ~20% increase in the number of pyramidal neurons and oligodendrocytes in cornu ammonis (CA) hippocampi in absence of altered cell proliferation or apoptosis (Hassouna et al., 2016; Wakhloo et al., 2020). An equivalent ~20% of neurons showed elevated *de-novo* protein production. In EPO-treated NG2-CreERT2 mice, we directly confirmed enhanced differentiation of pre-existing oligodendrocyte precursors without elevated DNA synthesis (Hassouna et al., 2016). Regarding neuronal lineages, the picture is much more complex, with EPO apparently driving fast differentiation of diverse, non-dividing, local neuronal precursors (Hassouna et al., 2016; Wakhloo et al., 2020), similar to its established role in the hematopoietic system (Brown and Ceredig, 2019; Dessypris et al., 1988; Grover et al., 2014; Krantz, 1991). Exposure to motor-cognitive challenge, namely complex running wheels (CRW) (Liebetanz and Merkler, 2006), leads to endogenous hypoxia in pyramidal neurons, augmenting expression of EPO and EPO receptor (EPOR) (Butt et al., *Mol Psychiatry*, in press; Wakhloo et al., 2020). These in turn prompt via auto/paracrine signaling the emergence of newly generated CA neurons, enhance dendritic spine densities, and improve performance *(EPO brain doping)*. Single cell RNA sequencing (scRNA-seq) in CA1, only 6h after one intraperitoneal rhEPO injection, revealed rapid increase in newly differentiating neurons. Exposure to either moderate inspiratory hypoxia ($12\%O_2$) or to CRW ('functional hypoxia') imitated the formation of new pyramidal neurons seen under rhEPO, and inspiratory hypoxia combined with CRW even acted synergistically. All these effects depend on pyramidal neuronal expression of the EPOR gene (Wakhloo et al., 2020). Thus, a novel model of neuroplasticity emerged in which neuronal networks, challenged by motor-cognitive tasks, drift into 'functional hypoxia', which in

turn triggers neuronal EPO expression. This regulatory brain EPO cycle causes lasting neuroplastic adaptation, which we coined 'brain hardware upgrade'. Importantly, these EPO-mediated adaptation processes likely also involve other brain cell types that express and/or bind EPO, at least in disease models (Brines and Cerami, 2005; Ott et al., 2015; Sargin et al., 2010; Siren et al., 2009).

In the physiological context of challenge-induced neuroplasticity, the contribution of microglia is of particular interest, but still entirely unexplored. In fact, microglia have crucial roles in neurotrophic support, neuro- and synaptogenesis including synaptic and axonal pruning or removal of dying neurons, and are constantly responding to neuronal signals by extending and withdrawing their processes from around synapses (Kierdorf and Prinz, 2017; Werneburg et al., 2017). Thereby, they shape developmental and postnatal neuronal circuits, the latter in an activity-dependent manner. Interestingly, recent work reports that microglia respond to neuronal activation by suppressing neuronal activity in the sense of a microglia-driven negative feedback mechanism. This mechanism operates similarly to inhibitory neurons, protects the brain from excessive activation, and depends on microglia sensing and catabolizing extracellular ATP that is released upon neuronal activation by neurons and astrocytes (Badimon et al., 2020).

The way, however, in which microglia co-regulate adult neurogenesis and particularly adult neurodifferentiation in various states of neuronal activation, and outside the classical neurogenesis niches, is still poorly understood (Butovsky and Weiner, 2018). The present study has been designed to explore in healthy mice how microglia behave in the context of EPO-mediated ample brain hardware upgrade in hippocampal CA1. Surprisingly, we show that EPO decreases microglia numbers, first by inducing apoptosis, followed by inhibiting proliferation. In parallel, EPO dampens microglia activity and metabolism. This effective EPO containment of microglia in CA1 involves the colony-stimulating factor 1 receptor (CSF1R) system and enables undisturbed neuronal differentiation.

4

RESULTS AND DISCUSSION

Inspiratory as well as functional hypoxia induce endogenous EPO expression in brain and diminish microglia numbers in CA1

We first determined by qPCR the EPO expression in CA1 after 6h of strong inspiratory hypoxia (positive control; 6%O_2) and compared it to 6h of functional hypoxia, employing our CRW paradigm of motor-cognitive challenge (Wakhloo et al., 2020). Under both conditions, EPO mRNA expression increased compared to normoxia baseline (Figure1A-B). Endogenous EPO induction in brain by functional and inspiratory hypoxia promotes adult hippocampal neurodifferentiation in CA1, similar to exogenously applied rhEPO (Hassouna et al., 2016; Wakhloo et al., 2020). We wondered how this would reflect on the microglial population dynamics, which in this context has remained unexplored. To elucidate the physiological effect of endogenous brain EPO on microglia, we exposed WT mice, starting at P28, to 3 weeks of CRW versus permanent moderate inspiratory hypoxia (12%O_2; Figure1C). In both conditions, IBA1+ microglia in CA1 pyramidal layer were reduced immediately after these 3 weeks (P49), compared to normoxia control mice (Figure1D). Importantly, this reduction was comparable to that obtained after treating WT mice with rhEPO (5000 IU/kg i.p. every other day for 3 weeks) versus placebo injections (Figure1E). Here, the amount of rhEPO reaching the brain in healthy rodents with an intact blood-brain-barrier is similar to the endogenously induced brain EPO (Ehrenreich et al., 2004). The decrease of microglia numbers in CA1 simultaneously with increased neurodifferentiation upon EPO (Hassouna et al., 2016; Wakhloo et al., 2020), validated rhEPO treatment as highly standardizable and convenient model procedure for the present study.

Effect of rhEPO on microglia numbers and activity depends on microglial EPOR

We next asked how long the reduction of microglia numbers seen on P49, i.e. immediately after cessation of rhEPO treatment, would last. To answer this question and, at the same time, to use a permanent cell label in addition to IBA1 staining, we treated CX$_3$CR1CreERT2:tdTomato mice for 3 weeks with rhEPO according to our schedule. Notably, already 1 week later (P55), microglia numbers (all consistently tdTomato+IBA1+) were no longer different from placebo treated mice (Figure1F), pointing to a tight and time-limited regulation of microglia under EPO with fast repopulation thereafter. Since all tdTomato+ cells were also IBA1+, the possibility of

5

microglia losing their identity or transdifferentiating to other cell types upon EPO could be discarded.

We thus explored other reasons behind the decreased microglia numbers under rhEPO. On P49, caspase-3 staining revealed no enhanced apoptosis, whereas Ki67 was significantly diminished (Figure1G), pointing to a reduced cell cycle/proliferation of microglia after 3 weeks of rhEPO. Application of EdU for 1 week, starting immediately after rhEPO treatment cessation (P49), disclosed a trend for more proliferating microglia compared to placebo at P55 (Figure1H). This certainly contributes to the quick recovery of microglia numbers (Figure1F).

Microglial morphology is notorious for accurately reflecting the activation status of these cells (Sierra et al., 2016). Parameters of microglia process complexity (Figure1I) did not show differences between rhEPO and placebo groups. However, analysis of the microglia cell body revealed an increased perimeter/area ratio, consistent with a less active phenotype (Peskin et al., 2010) upon rhEPO treatment (Figure1J). The decreased number of contacts with Thy1-YFP+ pyramidal neurons further supports the reduced activity of microglia after 3 weeks of rhEPO (Figure1K), as does an abridged metabolic turnover, measured by ^{15}N-leucine incorporation into IBA1+ cells using NanoSIMS (Figure1L). This is in contrast to the increased ^{15}N-leucine incorporation in NeuN+ neurons upon rhEPO (Hassouna et al., 2016). Hence, in parallel to the rhEPO-stimulated neurodifferentiation in CA1, resulting in a substantial number of new functional pyramidal neurons with their expectedly enhanced protein turnover (Hassouna et al., 2016; Wakhloo et al., 2020), microglia are decreased in number, metabolism and activity. To investigate whether the rhEPO effects on microglia depend on microglial EPOR, we selectively erased the EPOR in microglia by generating CX$_3$CR1CreERT2:EPOR-KO mice. After tamoxifen-induced deletion and subsequent rhEPO treatment following our 3-week schedule, we found neither reduction of microglia numbers nor changes in cell body size (Figure1M-N). This supports direct effects of EPO on microglia that disappear after microglial EPOR elimination.

Counterbalance between microglia and newly generated neurons upon EPO

We previously reported EPO to powerfully drive neurodifferentiation, leading to increased numbers of immature or mature neurons, depending on the time point studied (Hassouna et al., 2016; Wakhloo et al., 2020). Since microglia are dampened by EPO, but reportedly crucial for proper neuronal development and differentiation

(Hattori et al., 2020; Nandi et al., 2012), we wondered whether, when and how EPO would provide a physiological counterbalance between neuronal and microglial populations in the neurodifferentiation process. Treating mice for only 1 week with rhEPO or placebo resulted in reduced microglia numbers (Figure2A-B). Notably, at this early time point, caspase-3 or Ki67 were unaltered (Figure2C), however, microglia activity was already reduced (Figure2D). How was the observed microglia reduction achieved and could this indicate protection of ongoing neurodifferentiation? We first quantified mature CTIP2+ and immature TBR1+ neurons at the 1-week time point, as both are increased in the CA1 pyramidal layer upon rhEPO, the former after 3 weeks, the latter at 24h (Hassouna et al., 2016; Wakhloo et al., 2020). No differences were seen at 1 week of rhEPO treatment in either population, suggesting that this time point was too early to find mature neurons increased, and too late to see still the initial TBR1 wave of precursors (Figure2E). We thus hypothesized that after 1 week of rhEPO treatment, newly differentiating neurons would be in an intermediate stage, having further progressed along the maturation path (pseudotime trajectory (Wakhloo et al., 2020)), obtained by scRNA-seq of CA1 at 6h after a single rhEPO injection (Figure2F-G). Whereas TBR1 marks an early immature stage (Figure2H), we focused on a population of intermediately mature neurons in the pseudotime trajectory (Wakhloo et al., 2020), and selected *Zbtb20* as marker, highly specific for maturing pyramidal neurons of CA1 (Nielsen et al., 2010; Nielsen et al., 2014; Xie et al., 2010) (p=2.31e-63, Figure2I). Indeed, immunohistochemical quantification showed an increased number of ZBTB20+ cells in CA1 pyramidal layer after 1 week of rhEPO (Figure2J), confirming the ongoing wave of stimulated neurodifferentiation.

To elucidate the mechanisms that could have led to the observed reduction of IBA1+ cells after 1 week of rhEPO, we next quantified microglia at 24 h after a single rhEPO or placebo injection (Figure2K). At this early time point, no difference in IBA1+ cells yet appeared but, surprisingly, the number of caspase-3+ microglia was elevated in rhEPO treated mice (Figure2L). As EPO is usually associated with a strong anti-apoptotic role (Krantz, 1991; Siren et al., 2001) and has pro-apoptotic effects only in unphysiologically high doses, at least in neurons (Ehrenreich et al., 2005), we wondered whether such unexpected consequence of rhEPO would similarly be detectable in primary microglia in culture. Indeed, also pure microglia cultures revealed a rapid pro-apoptotic function of rhEPO in this cell type, reflected by increased caspase-3 expression after only 6h (Figure2M). At the 24h time point, the enhanced

caspase-3 expression in culture had already disappeared (not shown). This suggests that EPO *in vivo* as well as *in vitro* quickly and just transiently induces apoptosis of microglia. This temporary apoptosis within the microglia population, prompted by EPO, is in perfect agreement with a recent report showing that microglia self-renewal is maintained by coupled proliferation and apoptosis, resulting in a stable microglia number (Askew et al., 2017). Thus, apoptosis is a physiological regulatory instrument in this cell type next to controlled proliferation, and with our data, we unify these effects for the first time to one particular factor, namely EPO, which mediates these regulating mechanisms in a phasic fashion. Together with our previous (Hassouna et al., 2016; Wakhloo et al., 2020) and present studies on neurodifferentiation, collectively, these data suggest a delicate counterbalance, orchestrated by EPO, between neuronal differentiation and microglial numbers and activity.

Endogenous and exogenous EPO affects microglial proliferation via CSF1R

We next hypothesized that EPO might interfere with CSF1R that is crucial for microglial proliferation and survival (Elmore et al., 2014). Thus, we depleted brains of microglia by feeding WT mice for 10 days the CSF1R inhibitor PLX5622. Immediately after inhibitor withdrawal, when fast microglia repopulation takes place (Dagher et al., 2015), we started our usual 3-week rhEPO treatment, and simultaneously added EdU to the drinking water for the first week. Since we were interested in observing how the neuronal population would respond to this challenge of the neuron-microglia counterbalance, we allowed 1 week of break after rhEPO treatment cessation (Figure3A-B), imitating the experimental paradigm that had led to an increase in CTIP2+ neurons of the CA1 pyramidal layer (Hassouna et al., 2016). Expectedly, we found no changes anymore in the overall IBA1+ cell numbers at this time point (Figure3C, compare Figure1F). However, the EdU+ microglia, marking proliferation during the first week of repopulation, were decreased upon rhEPO by around 50% (Figure3C). We replicated our previous finding of rhEPO increasing CTIP2+ neuron numbers (Hassouna et al., 2016) (Figure3D) but, surprisingly, this increase was similarly observed in PLX5622 treated mice, independent of rhEPO. This indicated that in absence of microglia, the neuronal differentiation advances to reach a ceiling effect, not amplified further by addition of rhEPO. As shown earlier (Hassouna et al., 2016), the proliferation of cells in the pyramidal layer was again slightly reduced upon rhEPO. However, no such changes were observed after PLX5622 treatment (Figure3D),

perhaps reflecting increased neuronal proliferation under CSF1R inhibition (Elmore et al., 2018). In summary, these findings underline again the counterbalance between microglia and neurons, with rhEPO treatment as well as CSF1R inhibition transiently reducing numbers of proliferating microglia, paralleled by augmented CA1 pyramidal neuron numbers (Figure3C-E).

For deeper mechanistic insight, we processed hippocampi of rhEPO or placebo treated mice (Figure 3F-G) in order to measure the expression of CSF1R and its ligands, CSF1 and IL-34. Flow cytometry revealed upregulation of CSF1R expression in CD11b+CD45lo cells upon rhEPO, while EPOR remained unchanged (Figure3H). The mRNA levels confirmed the trend of increased *Csf1r* expression, while *Csf1* expression was unaffected. Most importantly, the neuronally expressed ligand *Il34* (Easley-Neal et al., 2019a) was significantly downregulated after rhEPO (Figure3I). This may suggest that the decrease of *Il34*, as part of a cross talk between neurons and microglia, adds to reducing microglia numbers during EPO-mediated neurodifferentiation.

We now wondered whether similar alterations in the CSF1R axis would be detectable in conditions of hypoxia-induced brain EPO, as demonstrated above (Figure1A-D). To address this question, we employed our hypoxia scRNA-seq data set, obtained from whole hippocampus after 5 days of daily exposure to 6%O_2 for 6 hours each (Butt et al., *Mol Psychiatry*, in press) (Figure4A), to explore the expression of *Csf1r* and its ligands *Csf1* and *Il34*. In whole hippocampus, we observed despite their relatively scarce average expression a mild increase in *Csf1r* (logFC=0.16) and a mild decrease of *Il34* (logFC=-0.12), whereas *Csf1* was practically unchanged, i.e. log-fold change was close to zero (logFC=0.04), indicating basically unchanged levels of *Csf1* even though statistically significant (Figure4B-C). A more detailed look at specific cell populations known to primarily express the respective genes, revealed under hypoxia a marked increase in *Csf1r* expression in microglia (Figure 4D), a negligible increase of *Csf1* in glial cells (Figure4E), and a mild decrease of *Il34* in glutamatergic neurons (Figure4F), consistent with our findings by qPCR and FACS following rhEPO treatment.

Among the CSF1R ligands, IL-34 is mainly produced by neurons and responsible for microglia maintenance in grey matter regions, as opposed to CSF1, which is mostly expressed by glia and responsible for maintenance of microglia in white matter regions

(Easley-Neal et al., 2019b). The observed decrease in *Il34* expression shown here, probably contributes to the counterbalance between neurodifferentiation/numbers of maturing neurons and numbers/activity of microglia under EPO. In fact, glutamatergic neuronal production of *Il34* diminishes after endogenous as well as exogenous EPO, likely to keep the microglia population reduced and less active, while increased neuronal differentiation/maturation proceeds under this growth factor. This explanation is in perfect agreement with the observation that microglia numbers decrease in CA1 after administration of an IL-34 blocking antibody (Obst et al., 2020). The upregulation of *Csf1r* in turn might well be a compensatory homeostatic feedback mechanism in response to decreased *Il34* expression. Together, these data once more imply a role for the CSF1R system in EPO-mediated effects on microglia and neurogenesis.

Working model of a delicate counterbalance between neurodifferentiation and microglia in the adult hippocampal CA1 revealed by EPO

During embryonic development, microglia were reported to assist the accurate differentiation of CTIP2+ and TBR1+ neurons, and these neuronal subpopulations are dependent on CSF1R signaling for survival (Hattori et al., 2020; Nandi et al., 2012). According to Hattori and coworkers, 'sanctuarization' from microglia in the midembryonic cortical plate is required for neurons to appropriately fine-tune the expression of molecules needed for proper differentiation, thus securing the establishment of functional cortical circuits (Hattori et al., 2020). Also in disease models and brain injury studies, decreased microglia proliferation, activity or motility upon rhEPO treatment has been described, together with improved neuronal proliferation or survival. In fact, rhEPO treatment in these conditions even prevented neurodegeneration, brain atrophy and cognitive decline (Mitkovski et al., 2015; Sargin et al., 2009; Siren et al., 2006; Wang et al., 2017; Zhang et al., 2019).

In contrast, such neurodifferentiation-microglia counterbalance in healthy postnatal and adult CA1 (or anywhere else outside the classical neurogenesis areas) has never been reported nor illuminated to understand its physiological significance and underpinnings. Just in the dentate gyrus, the number of microglia was found inversely correlated with the number of proliferating progenitor cells in the granule cell layer upon running (Gebara et al., 2013; Kohman et al., 2012). Therefore, the present work focused on the healthy adult hippocampal CA1 and the role of endogenous and exogenous EPO in coordinating conduct of different cell types to achieve proper brain

hardware upgrade as prerequisite for improved performance. As conclusion from the present study, a novel working model arises, in which the importance of a fine-tuned counterbalance between effective neurodifferentiation and microglia activity in CA1 during normal adulthood is discovered by studying EPO effects. This working model includes CSF1R and its neuronal ligand IL-34 in the way how tight regulation of microglia contributes to adult neurogenesis and in particular to adult neurodifferentiation.

MATERIALS AND METHODS

All experiments were approved by the local Animal Care and Use Committee (Niedersächsisches Landesamt für Verbraucherschutz und Lebensmittelsicherheit) and conducted in accordance with the German Animal Protection Law. In all experiments, investigators were unaware of group assignment or treatment condition ('fully blinded').

Mice

$CX_3CR1CreERT2$ mice were crossed to R26R-tdTomato reporter mice for genetic labeling of microglia ($CX_3CR1CreERT2$:tdTomato) or to EPOR-floxed (Wakhloo et al., 2020) animals to generate conditional EPOR deletion ($CX_3CR1CreERT2$:EPOR-KO). CreERT2 activity was induced with tamoxifen [10mg/ml intraperitoneal (i.p.) injections over 5 consecutive days, from postnatal day 23 (P23) until P27]. Juvenile wildtype (WT) C57BL/6N or Thy1-YFPH mice were treated as indicated in the figures. All mice used in this work were of male gender, except where indicated otherwise, and maintained on a 12h light-dark cycle at 20-22°C, with food and water *ad libitum*.

Treatments

For inspiratory hypoxia experiments, mice were put into custom-designed hypoxia chambers (Coy Laboratory Products, Grass Lake, MI, USA) at $6\%O_2$ for 6h/day, either once on P32 (female mice), or on 5 consecutive days from P28 to P32. Other groups were exposed to $12\%O_2$ for 3 weeks from P28 to P49, starting with gradual reduction of $3\%O_2$ per day for 3 days. **Complex running wheels** (CRW (Wakhloo et al., 2020); TSE Systems, Bad Homburg, Germany) for voluntary running were placed into normoxia cages for 6h on P32 (female mice), or for 3 weeks from P28 to P49. **Recombinant human (rh) EPO** (5000IU/kg body weight; NeoRecormon, Roche, Welwyn Garden City, UK) or placebo (PL; solvent control solution) were applied via i.p. injections (0.01ml/g) either once or every other day for 1 or 3 weeks as indicated in treatment schemes. **For nanoscale secondary ion mass spectrometry (NanoSIMS)**, mice obtained food pellets containing 1.025% L-leucine-^{15}N stable isotope (Sigma-Aldrich, St Louis, MN, USA) for 3 weeks between P28 and P49 (in parallel with EPO/PL injections). **PLX5622** (1200 ppm in AIN-76A standard chow, Research Diets, New Brunswick, NJ, USA) or control food (AIN-76A standard chow), kindly provided by Plexxikon, were given for 10 days (P21-P30). **EdU** (0.2 mg/ml, Thermo Fisher Scientific, Waltham, MA, USA) was applied via drinking water in light-protected flasks and exchanged on alternate days for the period indicated in schemes.

Quantitative RT-PCR

Mice were anesthetized by i.p. injection of Avertin (tribromoethanol, Sigma-Aldrich) and perfused via left cardiac ventricle with Ringer's solution. RNA of one whole hippocampus per mouse was extracted using miRNeasy Mini Kit (217004, Qiagen, Hilden, Germany) following the manufacturer´s instructions; cDNA was synthesized using SuperScript III (18080044, Thermo Fisher Scientific); RT-qPCR was performed with Power SYBR Green PCR Master Mix (4367660, Thermo Fisher Scientific). Fold changes in gene expression were calculated with the ΔΔCt method using *Hprt1* as housekeeper.

The following primer pairs were used: for *Epo*, forward 5'-CATCTGCGACAGTCGAGTTCTG-3' and reverse 5'-CACAACCCATCGTGACATTTTC-3'; for *Csf1r*, forward 5'-GCAGTACCACCATCCACTTGTA-3' and reverse 5'-GTGAGACACTG TCCTTCAGTGC-3'; for *Csf1*, forward 5'-CCACATGATTGGGAATGGACAC-3' and reverse 5'-GATCATCCAGCTGTTCCTGGTCTA-3'; for *Il34*, forward 5'-CTTTGGGAAACGAGAAT TTGGAGA-3' and reverse 5'-GCAATCCTGTAGTTGATGGGGAAG-3'; and for *Hprt1*, forward 5'-GCTTGCTGGTGAAAAGGACCTCTCGAAG-3' and reverse 5'-CCCTGAAGTACTCATT ATAGTCAAGGGCAT-3'.

Immunohistochemistry

Mice were anesthetized by i.p. injection of Avertin and perfused via left cardiac ventricle with Ringer's solution followed by 4% formaldehyde. The dissected brains were postfixed overnight in 4% formaldehyde and frozen at -80°C after cryoprotection with 30% sucrose. Coronal sections of 30µm thickness were obtained with cryostat Leica CM1950 (Leica Microsystems, Wetzlar, Germany) and stored at -20°C in 25% ethylene glycol and 25% glycerol in PBS. Following blocking and permeabilization with 5% normal horse serum (NHS) in 0.3% Triton X-100 in PBS (PBST) for 1h at room temperature (RT), primary antibodies IBA1 (chicken, 1:1000, 234006; Synaptic Systems, Göttingen, Germany), IBA1 (rabbit, 1:1000, ab178846; Abcam, Cambridge, UK), Ki67 (rabbit, 1:1000, NCL-Ki67p; Novocastra, Newcastle Upon Tyne, UK), caspase-3 (goat, 1:250, sc1225; Santa Cruz Biotechnologies, Heidelberg, Germany), CTIP2 (guinea pig, 1:1000, 325005; Synaptic Systems), TBR1 (rabbit, 1:500, ab183032; Abcam) and ZBTB20 (rabbit, 1:500, 362003; Synaptic Systems) were incubated in 5%NHS with 0.3%PBST over 2-3 nights at 4°C. Secondary antibodies donkey anti-chicken Alexa-Fluor-488 (703546155; Jackson ImmunoResearch, Cambridgeshire, UK), donkey anti-chicken Alexa-Fluor-647 (1:500, 703605155; Jackson ImmunoResearch), goat anti-rabbit Alexa-Fluor-555 (1:500, A21428; Invitrogen by Thermo Fisher Scientific), donkey anti-guinea pig Cy5 (1:500, 706175148; Jackson ImmunoResearch) donkey anti-guinea pig Alexa-Fluor-488 (1:500, 706545148; Jackson ImmunoResearch), donkey anti-rabbit Alexa-Fluor-594 (1:500, D-301-C-ABS2; R&D Systems, Wiesbaden, Germany), donkey anti-goat Alexa-Fluor-633 (1:500,

A21082; Invitrogen) and donkey anti-rabbit Alexa-Fluor-488 (1:500, A21206; Invitrogen) were incubated in 3%NHS with 0.3%PBST for 2h at RT. EdU detection was done with Click-IT EdU Alexa-Fluor-647 Imaging kit (C10340; Invitrogen). Cell nuclei were stained with DAPI (1:5000; Millipore-Sigma, Burlington, MA, USA).

NanoSIMS

After immunohistochemistry of the sections, CA1 hippocampal regions were dissected and embedded in LR-White-Resin (AGR1281; Agar Scientific, Wetzlar, Germany) and accelerator mixture (AGR1283; Agar Scientific) following a dehydration protocol as described previously (Saka et al., 2014). Sections were further cut into 200nm thick sections with an EM-UC6 Ultramicrotome (Leica Microsystems) and placed on silicon wafers (Siegert Wafer GmbH, Aachen, Germany). Epifluorescent imaging of IBA1 with a Nikon Ti-E inverted microscope and 100x objective (NA 1.59) was followed by scanning with a Cs^+ primary ion beam in a nanoscale secondary ion mass spectrometry (NanoSIMS 50L) instrument (Cameca, Gennevilliers Cedex, France). Samples were eroded and ionized at 60pA for 3min, and the measurements were carried out at 2.5pA with a dwell time per pixel of 4000ms. From the resulting secondary ions, $^{12}C^{14}N^-$ and $^{12}C^{15}N^-$ were detected and measured, and are referred to as ^{14}N and ^{15}N, respectively, in this work. The mass resolving power was tuned to enable optimal separation of $^{12}C^{15}N^-$ from $^{13}C^{14}N$. For each measurement, 3 planes of 40x40μm (256x256 pixels) were recorded in a total of 4 animals/group, drift-corrected, and summed for analysis using OpenMIMS-plugin (NRIMS) for ImageJ. The resulting NanoSIMS images were then aligned to corresponding fluorescent images in Adobe-Photoshop. IBA1-positive signals were selected and corresponding NanoSIMS regions quantified in Matlab (Mathworks, Ismaning, Germany) using a custom written plugin. IBA1-positive regions were normalized to negative ones and compared between conditions in GraphPad Prism8.

Pure microglia culture

Brains from P0-P1 WT mice were freed from meninges before digestion with trypsin/EDTA 0.05% for 10min at 37°C. Enzymatic reaction was stopped by adding microglia medium (10% horse serum and 0.5%penicillin/streptomycin in DMEM; all from Invitrogen) supplemented with 400IU/brain of DNaseI (Worthington Biochemical, Lakewood, NJ, USA). After mechanical trituration, cells were centrifuged (10min, 150g) and added to 10ml pre-warmed microglia medium into poly-D-lysine (PDL)-coated (50μg/ml) 75cm^2 cell-culture flask. Cells were incubated at 37°C and 5%CO_2 for 10-14 days. Pure microglia were harvested by manual shaking of flask and seeded in astrocyte-conditioned medium (ACM) at densities of 20,000 cells/well on PDL-coated 12mm diameter glass-coverslips. ACM was obtained from mixed glial cultures grown in microglia medium for 5-7 days. After 24 h, cells were stimulated with 0.3 or 3IU/ml EPO or equivalent volume of solvent solution (placebo) for 6h or 24h.

Immunocytochemistry

Mixed glial cultures were fixed with 2%acrolein and 3%formaldehyde in PBS, followed by permeabilization and blocking with 5%NHS in 0.1%PBST for 1h at RT. Primary antibodies IBA1 (chicken, 1:1000, 234006; Synaptic Systems) and caspase-3 (goat, 1:500, sc1225; Santa Cruz Biotechnologies) were incubated with 1%NHS and 3%BSA in 0.05%PBST overnight at 4°C. As secondary antibodies, donkey anti-chicken Alexa-Fluor-488 (703546155; Jackson ImmunoResearch) and donkey anti-goat Alexa-Fluor-633 (1:500, A21082; Invitrogen) were used in 1%NHS and 3%BSA in 0.05%PBST for 1h at RT. Cell nuclei were counterstained with DAPI (1:5000, Millipore-Sigma).

Imaging and analysis

For analysis of IBA1, CX$_3$CR1CreERT2:tdTomato, caspase-3, Ki67, EdU and CTIP2 a Nikon Ti2 Eclipse (Nikon, Tokyo, Japan) epifluorescent microscope with 40x objective (NA0.6) was used. Confocal imaging of IBA1, CTIP2, TBR1 and ZBTB20 was done with Leica TCS-SP5 inverted system equipped with 20x objective (NA0.7), or 40x objective (NA1.25) for morphological analysis of IBA1+ microglia. Image analysis and manual quantifications were done with Fiji or Imaris v9.1.0 software (Oxford-Instruments, Abingdon, UK) in 3-7 sections/animal (-1.34 to -2.54mm posterior from Bregma) and in hippocampal regions indicated in figure schemes. For morphological analysis of microglia, the following parameters were obtained with Imaris: filament dendrite length (sum, shown as "Process length (sum)"), filament full branch level (shown as "Full branch level"), and filament number of dendrite terminal points (shown as "Process terminal points"). Perimeter/area ratio was measured in Fiji by outlining the microglial cell body. A maximum of 20cells/animal were analyzed. For analysis of IBA1 contacts to dendritic spines, a Leica TCS-SPE system with a 63x objective (NA1.4) was used. The number of IBA1+ contacts on principal apical dendrites of Thy1-YFP+ pyramidal neurons was quantified in average of 17 segments/animal of 50µm each using Fiji. The segments were randomly selected from the CA1 radiatum layer. Pure microglia cultures were analyzed by imaging 3 different regions of interest (ROIs) in 3 biological replicates of 2050x2050µm (7400x7400pixels) each.

Flow Cytometry

Mice were anesthetized (i.p. Avertin) and perfused via left cardiac ventricle with Ringer's solution. One whole hippocampus per mouse was mechanically dissociated via dounce homogenization in 15mM HEPES, 0.5%glucose and 1000IU DNaseI (Worthington Biochemical) in HBSS. After washing, cells were stained with Hoechst3352 (1:500; Thermo Fisher Scientific) and Zombie NIR (1:100, 423105; BioLegend, San Diego, CA, USA). Blocking of Fc-receptors was done with CD16/32 antibody (rat, 1:100, 14016185; Thermo Fisher

Scientific) in fluorescence-activated cell sorting (FACS) buffer (2% FCS, 0.01M EDTA pH8.0 and 0.01% NaN$_3$ in PBS). Primary antibodies CD11b Alexa-Fluor-488 (rat, 1:100, 53011282; eBioscience by Thermo Fisher Scientific) and CD45 PerCP-Cy5.5 (rat, 1:100, 103132; BioLegend) in FACS buffer were used in extracellular staining for microglia identification. After fixation and permeabilization with commercially available solutions (775775, Invitrogen), intracellular staining with CSF1R PE (rat, 1:100, 135505; BioLegend), EPOR (rabbit, 1:250, SA7378; Synaptic Systems) and donkey anti-rabbit Alexa-Fluor-594 (1:250, A21207; Invitrogen) was done in 0.1%saponin, 1%BSA and 5%NHS in PBS. Fluorescent minus one controls were processed in parallel. Filtered samples were acquired on BD-LSR-Fortessa (BD-Biosciences, San Jose, CA, USA) and data was analyzed in FlowJo software (BD Biosciences).

Single cell RNA sequencing

Single cell RNA sequencing (scRNA-seq) data was obtained and processed as described in detail earlier [GSE144444 (Wakhloo et al., 2020) and GSE162079 (Butt et al., *Mol Psychiatry*, in press)]. In order to identify neuronal genes characteristic of an intermediate stage of maturity, differential expression testing was performed by contrasting cells with a pseudotime within or outside the range of 3-25. Top 30 candidate genes (sorted by p-value) were initially screened for expression patterns that indicated temporal upregulation during maturation and matched literature reports. The best candidate was selected for immunohistochemistry.

Statistics

Data is shown as mean±standard error of the mean (SEM). Statistical analyses were performed with GraphPad Prism5 or R4.0.0. Student's unpaired two- or one-tailed *t* test were performed in normally distributed data and two-tailed Mann-Whitney *U* test in non-parametric data. Differential expression analysis (scRNA-seq, whole hippocampus) was performed using the FindMarkers() function in Seurat-3.1.5 (Stuart et al., 2019) (two-tailed correlation-adjusted Mann-Whitney *U* test). Reported p-values were adjusted for total number of genes (n=18976) expressed in the dataset. Differential expression-testing used to identify intermediate neuronal markers on pseudotime trajectory (scRNA-seq, CA1) was performed in Monocle-2.16.0 (Qiu et al., 2017), using the function differentialGeneTest(), and false-discovery rate adjusted p-values were reported.

References

Adamcio, B., Sargin, D., Stradomska, A., Medrihan, L., Gertler, C., Theis, F., Zhang, M., Muller, M., Hassouna, I., Hannke, K.*, et al.* (2008). Erythropoietin enhances hippocampal long-term potentiation and memory. BMC Biol *6*, 37.

Askew, K., Li, K., Olmos-Alonso, A., Garcia-Moreno, F., Liang, Y., Richardson, P., Tipton, T., Chapman, M.A., Riecken, K., Beccari, S.*, et al.* (2017). Coupled Proliferation and Apoptosis Maintain the Rapid Turnover of Microglia in the Adult Brain. Cell Rep *18*, 391-405.

Badimon, A., Strasburger, H.J., Ayata, P., Chen, X., Nair, A., Ikegami, A., Hwang, P., Chan, A.T., Graves, S.M., Uweru, J.O.*, et al.* (2020). Negative feedback control of neuronal activity by microglia. Nature *586*, 417-423.

Brines, M., and Cerami, A. (2005). Emerging biological roles for erythropoietin in the nervous system. Nat Rev Neurosci *6*, 484-494.

Brown, G., and Ceredig, R. (2019). Modeling the Hematopoietic Landscape. Frontiers in cell and developmental biology *7*, 104-104.

Butovsky, O., and Weiner, H.L. (2018). Microglial signatures and their role in health and disease. Nat Rev Neurosci *19*, 622-635.

Butt, U.J., Steixner-Kumar, A.A., Depp, C., Sun, T., Hassouna, I., Wustefeld, L., Arinrad, S., Zillmann, M.R., Schopf, N., Fernandez Garcia-Agudo, L.*, et al.* (*Mol Psychiatry*, in press). Functional hypoxia as primarily neuronal response to brain activity.

Dagher, N.N., Najafi, A.R., Kayala, K.M., Elmore, M.R., White, T.E., Medeiros, R., West, B.L., and Green, K.N. (2015). Colony-stimulating factor 1 receptor inhibition prevents microglial plaque association and improves cognition in 3xTg-AD mice. J Neuroinflammation *12*, 139.

Dessypris, E., Graber, S., Krantz, S., and Stone, W. (1988). Effects of recombinant erythropoietin on the concentration and cycling status of human marrow hematopoietic progenitor cells in vivo. Blood *72*, 2060-2062.

Digicaylioglu, M., Bichet, S., Marti, H.H., Wenger, R.H., Rivas, L.A., Bauer, C., and Gassmann, M. (1995). Localization of specific erythropoietin binding sites in defined areas of the mouse brain. Proc Natl Acad Sci U S A *92*, 3717-3720.

Easley-Neal, C., Foreman, O., Sharma, N., Zarrin, A.A., and Weimer, R.M. (2019a). CSF1R Ligands IL-34 and CSF1 Are Differentially Required for Microglia Development and Maintenance in White and Gray Matter Brain Regions. Front Immunol *10*, 2199.

Easley-Neal, C., Foreman, O., Sharma, N., Zarrin, A.A., and Weimer, R.M. (2019b). CSF1R Ligands IL-34 and CSF1 Are Differentially Required for Microglia Development and Maintenance in White and Gray Matter Brain Regions. Frontiers in immunology *10*, 2199-2199.

Ehrenreich, H., Degner, D., Meller, J., Brines, M., Behe, M., Hasselblatt, M., Woldt, H., Falkai, P., Knerlich, F., Jacob, S.*, et al.* (2004). Erythropoietin: a candidate compound for neuroprotection in schizophrenia. Mol Psychiatry *9*, 42-54.

Ehrenreich, H., Fischer, B., Norra, C., Schellenberger, F., Stender, N., Stiefel, M., Siren, A.L., Paulus, W., Nave, K.A., Gold, R.*, et al.* (2007a). Exploring recombinant human erythropoietin in chronic progressive multiple sclerosis. Brain *130*, 2577-2588.

Ehrenreich, H., Hasselblatt, M., Knerlich, F., von Ahsen, N., Jacob, S., Sperling, S., Woldt, H., Vehmeyer, K., Nave, K.A., and Siren, A.L. (2005). A hematopoietic growth factor, thrombopoietin, has a proapoptotic role in the brain. Proc Natl Acad Sci U S A *102*, 862-867.

Ehrenreich, H., Hinze-Selch, D., Stawicki, S., Aust, C., Knolle-Veentjer, S., Wilms, S., Heinz, G., Erdag, S., Jahn, H., Degner, D.*, et al.* (2007b). Improvement of cognitive functions in chronic schizophrenic patients by recombinant human erythropoietin. Mol Psychiatry *12*, 206-220.

El-Kordi, A., Radyushkin, K., and Ehrenreich, H. (2009). Erythropoietin improves operant conditioning and stability of cognitive performance in mice. BMC Biol *7*, 37.

Elmore, M.R., Najafi, A.R., Koike, M.A., Dagher, N.N., Spangenberg, E.E., Rice, R.A., Kitazawa, M., Matusow, B., Nguyen, H., West, B.L.*, et al.* (2014). Colony-stimulating factor 1 receptor signaling is necessary for microglia viability, unmasking a microglia progenitor cell in the adult brain. Neuron *82*, 380-397.

Elmore, M.R.P., Hohsfield, L.A., Kramar, E.A., Soreq, L., Lee, R.J., Pham, S.T., Najafi, A.R., Spangenberg, E.E., Wood, M.A., West, B.L.*, et al.* (2018). Replacement of microglia in the aged brain reverses cognitive, synaptic, and neuronal deficits in mice. Aging Cell *17*, e12832.

Gebara, E., Sultan, S., Kocher-Braissant, J., and Toni, N. (2013). Adult hippocampal neurogenesis inversely correlates with microglia in conditions of voluntary running and aging. Frontiers in Neuroscience *7*.

Grover, A., Mancini, E., Moore, S., Mead, A.J., Atkinson, D., Rasmussen, K.D., O'Carroll, D., Jacobsen, S.E.W., and Nerlov, C. (2014). Erythropoietin guides multipotent hematopoietic progenitor cells toward an erythroid fate. The Journal of experimental medicine *211*, 181-188.

Hassouna, I., Ott, C., Wustefeld, L., Offen, N., Neher, R.A., Mitkovski, M., Winkler, D., Sperling, S., Fries, L., Goebbels, S.*, et al.* (2016). Revisiting adult neurogenesis and the role of erythropoietin for neuronal and oligodendroglial differentiation in the hippocampus. Mol Psychiatry *21*, 1752-1767.

Hattori, Y., Naito, Y., Tsugawa, Y., Nonaka, S., Wake, H., Nagasawa, T., Kawaguchi, A., and Miyata, T. (2020). Transient microglial absence assists postmigratory cortical neurons in proper differentiation. Nat Commun *11*, 1631.

Jelkmann, W. (1992). Erythropoietin: structure, control of production, and function. Physiological reviews *72*, 449-489.

Kierdorf, K., and Prinz, M. (2017). Microglia in steady state. The Journal of Clinical Investigation *127*, 3201-3209.

Kohman, R.A., DeYoung, E.K., Bhattacharya, T.K., Peterson, L.N., and Rhodes, J.S. (2012). Wheel running attenuates microglia proliferation and increases expression of a proneurogenic phenotype in the hippocampus of aged mice. Brain Behav Immun *26*, 803-810.

Krantz, S.B. (1991). Erythropoietin. Blood *77*, 419-434.

Liebetanz, D., and Merkler, D. (2006). Effects of commissural de- and remyelination on motor skill behaviour in the cuprizone mouse model of multiple sclerosis. Exp Neurol *202*, 217-224.

Marti, H.H., Wenger, R.H., Rivas, L.A., Straumann, U., Digicaylioglu, M., Henn, V., Yonekawa, Y., Bauer, C., and Gassmann, M. (1996). Erythropoietin gene expression in human, monkey and murine brain. Eur J Neurosci *8*, 666-676.

Miskowiak, K.W., Ehrenreich, H., Christensen, E.M., Kessing, L.V., and Vinberg, M. (2014). Recombinant human erythropoietin to target cognitive dysfunction in bipolar disorder: a double-blind, randomized, placebo-controlled phase 2 trial. J Clin Psychiatry *75*, 1347-1355.

Miskowiak, K.W., Vinberg, M., Macoveanu, J., Ehrenreich, H., Koster, N., Inkster, B., Paulson, O.B., Kessing, L.V., Skimminge, A., and Siebner, H.R. (2015). Effects of Erythropoietin on Hippocampal Volume and Memory in Mood Disorders. Biol Psychiatry *78*, 270-277.

Mitkovski, M., Dahm, L., Heinrich, R., Monnheimer, M., Gerhart, S., Stegmuller, J., Hanisch, U.K., Nave, K.A., and Ehrenreich, H. (2015). Erythropoietin dampens injury-induced microglial motility. J Cereb Blood Flow Metab *35*, 1233-1236.

Nandi, S., Gokhan, S., Dai, X.M., Wei, S., Enikolopov, G., Lin, H., Mehler, M.F., and Stanley, E.R. (2012). The CSF-1 receptor ligands IL-34 and CSF-1 exhibit distinct developmental brain expression patterns and regulate neural progenitor cell maintenance and maturation. Dev Biol *367*, 100-113.

Nielsen, J.V., Blom, J.B., Noraberg, J., and Jensen, N.A. (2010). Zbtb20-induced CA1 pyramidal neuron development and area enlargement in the cerebral midline cortex of mice. Cereb Cortex *20*, 1904-1914.

Nielsen, J.V., Thomassen, M., Mollgard, K., Noraberg, J., and Jensen, N.A. (2014). Zbtb20 defines a hippocampal neuronal identity through direct repression of genes that control projection neuron development in the isocortex. Cereb Cortex *24*, 1216-1229.

Obst, J., Simon, E., Martin-Estebane, M., Pipi, E., Barkwill, L.M., Gonzalez-Rivera, I., Buchanan, F., Prescott, A.R., Faust, D., Fox, S.*, et al.* (2020). Inhibition of IL-34 Unveils Tissue-Selectivity and Is Sufficient to Reduce Microglial Proliferation in a Model of Chronic Neurodegeneration. Front Immunol *11*, 579000.

Ott, C., Martens, H., Hassouna, I., Oliveira, B., Erck, C., Zafeiriou, M.P., Peteri, U.K., Hesse, D., Gerhart, S., Altas, B.*, et al.* (2015). Widespread Expression of Erythropoietin Receptor in Brain and Its Induction by Injury. Mol Med *21*, 803-815.

Peskin, A.P., Dima, A.A., Chalfoun, J., and Elliott, J.T. (2010). Predicting Segmentation Accuracy for Biological Cell Images. Paper presented at: Advances in Visual Computing (Berlin, Heidelberg: Springer Berlin Heidelberg).

Qiu, X., Mao, Q., Tang, Y., Wang, L., Chawla, R., Pliner, H.A., and Trapnell, C. (2017). Reversed graph embedding resolves complex single-cell trajectories. Nature methods *14*, 979.

Saka, S.K., Vogts, A., Kröhnert, K., Hillion, F., Rizzoli, S.O., and Wessels, J.T. (2014). Correlated optical and isotopic nanoscopy. Nature Communications *5*, 3664.

Sargin, D., Friedrichs, H., El-Kordi, A., and Ehrenreich, H. (2010). Erythropoietin as neuroprotective and neuroregenerative treatment strategy: comprehensive overview of 12 years of preclinical and clinical research. Best Pract Res Clin Anaesthesiol *24*, 573-594.

Sargin, D., Hassouna, I., Sperling, S., Siren, A.L., and Ehrenreich, H. (2009). Uncoupling of neurodegeneration and gliosis in a murine model of juvenile cortical lesion. Glia *57*, 693-702.

Sierra, A., de Castro, F., del Río-Hortega, J., Rafael Iglesias-Rozas, J., Garrosa, M., and Kettenmann, H. (2016). The "Big-Bang" for modern glial biology: Translation and comments on Pío del Río-Hortega 1919 series of papers on microglia. Glia *64*, 1801-1840.

Siren, A.L., Fasshauer, T., Bartels, C., and Ehrenreich, H. (2009). Therapeutic potential of erythropoietin and its structural or functional variants in the nervous system. Neurotherapeutics *6*, 108-127.

Siren, A.L., Fratelli, M., Brines, M., Goemans, C., Casagrande, S., Lewczuk, P., Keenan, S., Gleiter, C., Pasquali, C., Capobianco, A.*, et al.* (2001). Erythropoietin prevents neuronal apoptosis after cerebral ischemia and metabolic stress. Proc Natl Acad Sci U S A *98*, 4044-4049.

Siren, A.L., Radyushkin, K., Boretius, S., Kammer, D., Riechers, C.C., Natt, O., Sargin, D., Watanabe, T., Sperling, S., Michaelis, T.*, et al.* (2006). Global brain atrophy after unilateral parietal lesion and its prevention by erythropoietin. Brain *129*, 480-489.

Stuart, T., Butler, A., Hoffman, P., Hafemeister, C., Papalexi, E., Mauck, W.M., 3rd, Hao, Y., Stoeckius, M., Smibert, P., and Satija, R. (2019). Comprehensive Integration of Single-Cell Data. Cell *177*, 1888-1902 e1821.

Suresh, S., Rajvanshi, P.K., and Noguchi, C.T. (2019). The Many Facets of Erythropoietin Physiologic and Metabolic Response. Front Physiol *10*, 1534.

Wakhloo, D., Scharkowski, F., Curto, Y., Javed Butt, U., Bansal, V., Steixner-Kumar, A.A., Wustefeld, L., Rajput, A., Arinrad, S., Zillmann, M.R.*, et al.* (2020). Functional hypoxia drives neuroplasticity and neurogenesis via brain erythropoietin. Nat Commun *11*, 1313.

Wang, R., Li, J., Duan, Y., Tao, Z., Zhao, H., and Luo, Y. (2017). Effects of Erythropoietin on Gliogenesis during Cerebral Ischemic/Reperfusion Recovery in Adult Mice. Aging Dis *8*, 410-419.

Werneburg, S., Feinberg, P.A., Johnson, K.M., and Schafer, D.P. (2017). A microglia-cytokine axis to modulate synaptic connectivity and function. Current opinion in neurobiology *47*, 138-145.

Wustenberg, T., Begemann, M., Bartels, C., Gefeller, O., Stawicki, S., Hinze-Selch, D., Mohr, A., Falkai, P., Aldenhoff, J.B., Knauth, M.*, et al.* (2011). Recombinant human erythropoietin delays loss of gray matter in chronic schizophrenia. Mol Psychiatry *16*, 26-36, 21.

Xie, Z., Ma, X., Ji, W., Zhou, G., Lu, Y., Xiang, Z., Wang, Y.X., Zhang, L., Hu, Y., Ding, Y.Q.*, et al.* (2010). Zbtb20 is essential for the specification of CA1 field identity in the developing hippocampus. Proceedings of the National Academy of Sciences *107*, 6510-6515.

Zhang, S.J., Wang, R.L., Zhao, H.P., Tao, Z., Li, J.C., Ju, F., Han, Z.P., Ma, Q.F., Liu, P., Ma, S.B.*, et al.* (2019). MEPO promotes neurogenesis and angiogenesis but suppresses gliogenesis in mice with acute ischemic stroke. Eur J Pharmacol *849*, 1-10.

Acknowledgements

Author contributions

Concept, design and supervision of the study: HE

Data acquisition/analysis/interpretation:

LFGA, AASK, YC, IH, SJ, UJB, NS, KaG, MSW, SR, JN, KG, KAN, and HE

Drafting manuscript: LFGA, AASK, YC, together with HE

Drafting display items: LFGA, AASK, YC, together with HE

All authors read and approved the final version of the manuscript.

Competing interest statement

The authors declare no competing financial or other interests.

Code availability

Analysis scripts are accessible on GitHub:

https://github.com/AgnesSteixner/Fernandez_Garcia-Agudo_et_al_EPO_microglia.

FIGURE LEGENDS

Figure 1: Inspiratory and functional hypoxia induce brain EPO expression and diminish microglia numbers – imitation by rhEPO and dependence on EPOR. **(A)** Treatment scheme and hippocampal area of analysis for **(B)** *EPO* mRNA expression (normalized to *Hprt1*) in P32 WT C57BL/6 mice, exposed for 6h to normoxia (21%O_2; N), functional hypoxia upon complex running wheel performance (CRW), or inspiratory hypoxia (6%O_2; H). **(C)** Scheme for normoxia, CRW or inspiratory hypoxia (12%O_2) exposure extended to 3 weeks and area of IBA1 quantification, given in **(D).** **(E)** IBA1 quantification after 3 weeks of rhEPO or placebo (PL) treatment. **(F)** Quantification of tdTomato+IBA1+ cells 1 week after cessation of rhEPO versus placebo (PL) treatment of CX$_3$CR1CreERT2:tdTomato mice. **(G)** Quantification of caspase-3+ and Ki67+ microglia in mice of (E). **(H)** Scheme for administration of EdU for 1 week after rhEPO or placebo treatment cessation and area/quantification of IBA1+EdU+ cells. **(I)** Morphological analysis of microglia processes in mice of (E). **(J)** Morphological analysis of microglia cell bodies in mice of (E). **(K)** Density of IBA1$^+$ contacts on apical dendrites of Thy1-YFP+ pyramidal neurons after 3 weeks of rhEPO or placebo treatment and illustration thereof. **(L)** NanoSIMS experiment after ^{15}N-leucine enriched food, provided for the same 3-week duration as rhEPO or placebo; representative images and calculated ^{15}N/^{14}N ratio in IBA1+ cells as a measure of ^{15}N-leucine incorporation (normalized to IBA1- areas); area of analysis shown in (A). **(M)** IBA1 quantification in CX$_3$CR1CreERT2:EPOR-KO mice after 3 weeks of rhEPO or placebo treatment and **(N)** morphological analysis of microglia cell bodies. All graphs show mean±SEM with n numbers in bars and unpaired two-tailed *t* tests, except for (L), where a two-tailed Mann-Whitney *U* test was performed. Analyses were conducted in the area shown in (C), except otherwise indicated.

Figure 2: Counterbalance between microglia and newly generated neurons upon EPO. (A) Scheme for 1 week of rhEPO or placebo (PL) treatment in P28 WT C57BL/6 mice and hippocampal area of analysis for **(B)** IBA1 as well as **(C)** quantifications of caspase-3+ and Ki67+ microglia. **(D)** Morphological analysis of microglia cell bodies. **(E)** Representative illustrating images and quantifications of cells with neuronal markers CTIP2 and TBR1. **(F)** Single cell RNA sequencing (scRNA-seq) analysis after 6h of a single rhEPO or placebo injection. **(G)** Pseudotime trajectory of glutamatergic cells of CA1 (Wakhloo et al., 2020). **(H)** *Tbr1* expression along the pseudotime

trajectory/neuronal maturation stages (Wakhloo et al., 2020); expression indicated as log10(normalized expression+0.1). **(I)** Selection of a population of neurons with intermediate maturity and identification of *Zbtb20* as marker, transiently increased during maturation, i.e. highly expressed in this population. **(J)** Quantification and representative illustrating image of ZBTB20 in mice from (A). **(K)** Scheme for 24h of rhEPO or placebo treatment. **(L)** Quantification of IBA1+ and caspase-3+ microglia. **(M)** Percentage of IBA1+caspase-3+ cells in pure microglia cultures after 6h of rhEPO or placebo addition. All graphs show mean±SEM with n numbers in bars and unpaired *t* tests (two-tailed, one-tailed in (D)); scRNA-seq data from 3 mice/group; *in vitro* data represent 3 measurements from 3 biological replicates.

Figure 3: Endogenous and exogenous EPO affects microglial proliferation via CSF1R. (A) Treatment scheme for the CSF1R inhibition experiment starting in P21 WT C57BL/6 mice with 10 days of control food (CF) or PLX5622 (PLX), followed by 3 weeks of rhEPO or placebo (PL); EdU applied from P30 to P36. **(B)** Hippocampal area of analysis. **(C)** Quantifications of all IBA1+ and proliferating IBA1+EdU+ microglia. **(D)** Quantifications of all CTIP2+ and proliferating CTIP2+EdU+ neurons. **(E)** Representative images from animals treated with PLX5622 and rhEPO or placebo. **(F)** Scheme for 3 weeks of rhEPO or placebo treatment. **(G)** Area of analysis for **(H)** flow cytometry analysis of median fluorescent intensity (MFI) of CSF1R and EPOR in nucleated, single, viable microglial cells (Hoechst+ZombieNIR-CD11b+CD45lo shown in ellipse-shaped gate) and **(I)** mRNA expression of *Csf1r*, *Csf1* and *Il34* (normalized to *Hprt1*). All graphs show mean±SEM with n numbers in bars or graph; all unpaired two-tailed *t* tests.

Figure 4: Expression of *Csf1r* and its ligands *Csf1* and *Il34* under hypoxia (scRNA-seq). (A) Acquisition scheme of the scRNA-seq data set (Butt et al., *Mol Psychiatry*, in press) following normoxia or hypoxia ($6\%O_2$, 6h/day, 5 days) treatment, and hippocampal area of analysis. **(B)** UMAP embedding of cell populations of the hippocampus. **(C)** Expression of *Csf1r*, *Csf1* and *Il34* in whole hippocampus. **(D)** Expression of *Csf1r* in microglia. **(E)** Expression of *Csf1* in glial cells (including microglia, OPC, oligodendrocytes, ependymal cells and astrocytes). **(F)** Expression of *Il34* in glutamatergic neurons. Bonferroni-corrected p-values of correlation-adjusted two-tailed Mann-Whitney *U* tests reported in (C-F); scRNA-seq data based on 2 mice/group.
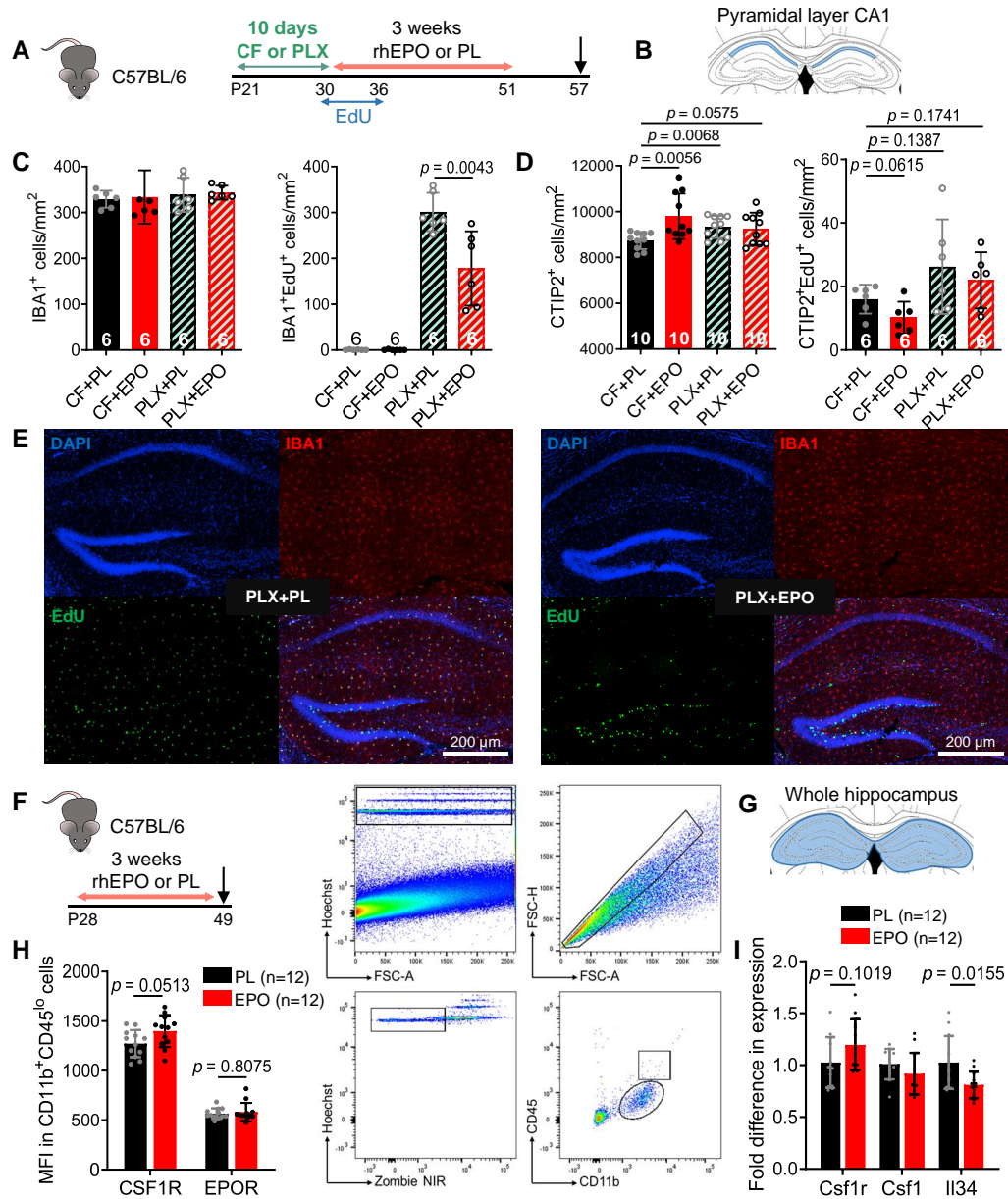
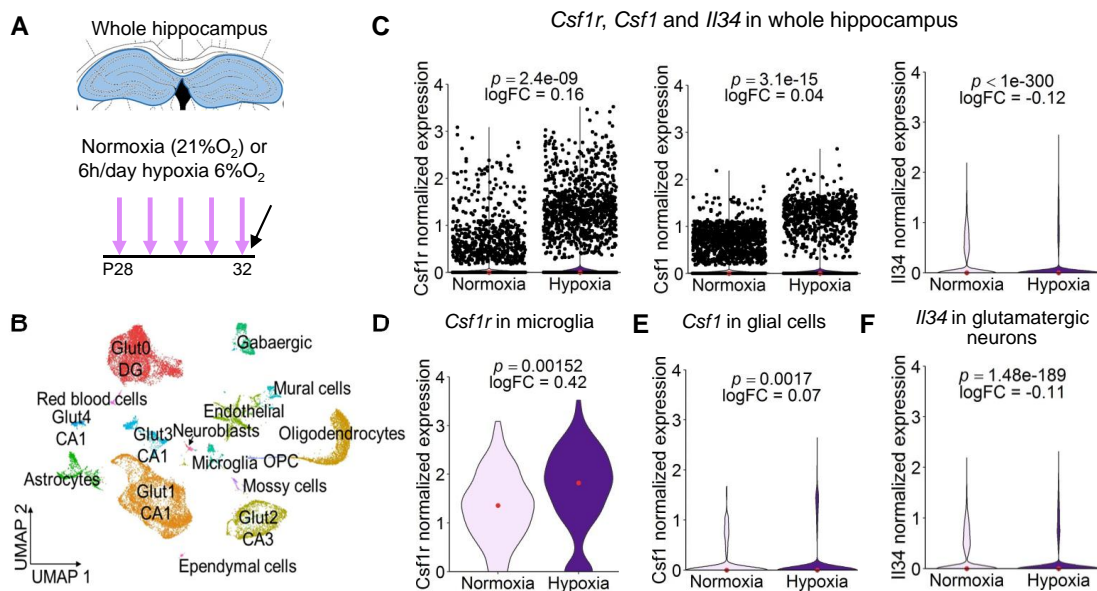Fernandez Garcia-Agudo et al Figure 1
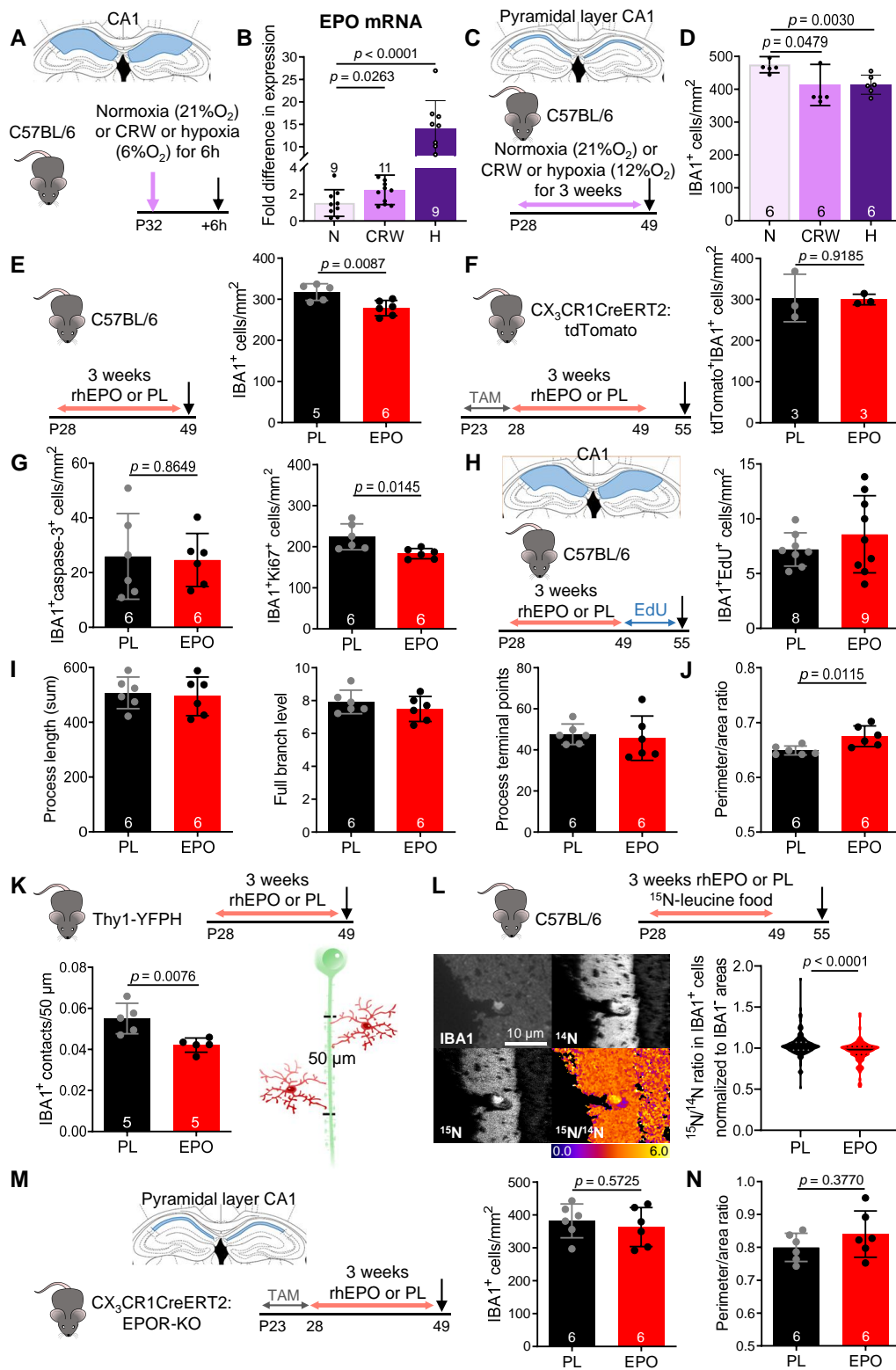
Fernandez Garcia-Agudo et al Figure 2

Fernandez Garcia-Agudo et al Figure 3

Fernandez Garcia-Agudo et al Figure 4

A Whole hippocampus

Normoxia (21%O_2) or
6h/day hypoxia 6%O_2

P28   32

B

Glut0 DG
Gabaergic
Mural cells
Red blood cells
Glut4 CA1
Endothelial
Glut3 Neuroblasts
Oligodendrocytes
Microglia OPC
Astrocytes
Glut1 CA1
Mossy cells
Glut2 CA3
Ependymal cells
UMAP 2
UMAP 1

C *Csf1r*, *Csf1* and *Il34* in whole hippocampus

$p = 2.4e\text{-}09$
logFC = 0.16
Csf1r normalized expression
Normoxia   Hypoxia

$p = 3.1e\text{-}15$
logFC = 0.04
Csf1 normalized expression
Normoxia   Hypoxia

$p < 1e\text{-}300$
logFC = -0.12
Il34 normalized expression
Normoxia   Hypoxia

D *Csf1r* in microglia

$p = 0.00152$
logFC = 0.42
Csf1r normalized expression
Normoxia   Hypoxia

E *Csf1* in glial cells

$p = 0.0017$
logFC = 0.07
Csf1 normalized expression
Normoxia   Hypoxia

F *Il34* in glutamatergic neurons

$p = 1.48e\text{-}189$
logFC = -0.11
Il34 normalized expression
Normoxia   Hypoxia

ARTICLE

Check for updates

Functional hypoxia drives neuroplasticity and neurogenesis via brain erythropoietin

Debia Wakhloo [1,11], Franziska Scharkowski [1,11], Yasmina Curto [1,2,11], Umer Javed Butt[1], Vikas Bansal [1,3], Agnes A. Steixner-Kumar [1], Liane Wüstefeld[1], Ashish Rajput [3], Sahab Arinrad [1], Matthias R. Zillmann [1], Anna Seelbach [1], Imam Hassouna[1], Katharina Schneider[1], Abdul Qadir Ibrahim [3], Hauke B. Werner [4], Henrik Martens [5], Kamilla Miskowiak [6], Sonja M. Wojcik[7], Stefan Bonn[3,8], Juan Nacher[2,9,10], Klaus-Armin Nave [4,8✉] & Hannelore Ehrenreich [1,8✉]

Erythropoietin (EPO), named after its role in hematopoiesis, is also expressed in mammalian brain. In clinical settings, recombinant EPO treatment has revealed a remarkable improvement of cognition, but underlying mechanisms have remained obscure. Here, we show with a novel line of reporter mice that cognitive challenge induces local/endogenous hypoxia in hippocampal pyramidal neurons, hence enhancing expression of EPO and EPO receptor (EPOR). High-dose EPO administration, amplifying auto/paracrine EPO/EPOR signaling, prompts the emergence of new CA1 neurons and enhanced dendritic spine densities. Single-cell sequencing reveals rapid increase in newly differentiating neurons. Importantly, improved performance on complex running wheels after EPO is imitated by exposure to mild exogenous/inspiratory hypoxia. All these effects depend on neuronal expression of the *Epor* gene. This suggests a model of neuroplasticity in form of a fundamental regulatory circle, in which neuronal networks—challenged by cognitive tasks—drift into transient hypoxia, thereby triggering neuronal EPO/EPOR expression.

[1] Clinical Neuroscience, Max Planck Institute of Experimental Medicine, Göttingen, Germany. [2] Neurobiology Unit, Program in Neurosciences and Interdisciplinary Research Structure for Biotechnology and Biomedicine (BIOTECMED), Universitat de València, Burjassot, Spain. [3] Institute of Medical Systems Biology, Center for Molecular Neurobiology, University Clinic Hamburg-Eppendorf, Hamburg, Germany. [4] Department of Neurogenetics, Max Planck Institute of Experimental Medicine, Göttingen, Germany. [5] Synaptic Systems GmbH, Göttingen, Germany. [6] Copenhagen Affective Disorder Research Centre, Psychiatric Centre Copenhagen, Copenhagen University Hospital, Rigshospitalet, Copenhagen, Denmark. [7] Department of Molecular Neurobiology, Max Planck Institute of Experimental Medicine, Göttingen, Germany. [8] DFG Research Center for Nanoscale Microscopy and Molecular Physiology of the Brain (CNMPB), Göttingen, Germany. [9] CIBERSAM: Spanish National Network for Research in Mental Health, Valencia, Spain. [10] Fundación Investigación Hospital Clínico de Valencia, INCLIVA, Valencia, Spain. [11] These authors contributed equally: Debia Wakhloo, Franziska Scharkowski, Yasmina Curto. ✉email: nave@em.mpg.de; ehrenreich@em.mpg.de

Erythropoietin (EPO) is a hypoxia-inducible growth factor in mammalian kidney, named after its role in hematopoiesis[1,2]. Unexpectedly, both EPO and its receptor (EPOR) were later detected in the brain, where they are upregulated by injury conditions. High-dose recombinant human (rh) EPO, a drug in clinical use for anemic patients, exerts neuroprotective and neuroregenerative effects that are independent of the hematocrit, which is mechanistically unexplained[3–8]. Moreover, rhEPO improves cognitive function and reduces gray matter loss in a range of neuropsychiatric conditions[9–13]. Even in healthy mice, rhEPO treatment improves cognition, which is associated with enhanced hippocampal long-term potentiation[14–16]. Surprisingly, rhEPO increases the number of mature hippocampal pyramidal neurons without underlying effect on cell proliferation or cell death[17]. This effect is mediated in neurons mainly by JAK-STAT, PI3K/AKT/PKB, Ras-MEK, and ERK1/2, as well as NF-κB; pathways widely comparable to the hematopoietic system[18–20]. This raises the question whether the expression of EPO and its receptor serves a physiological function in the nervous system, and what could be the triggering factors of EPO expression under physiological conditions.

Results

Generation of pyramidal neurons in adult mice and amplification by rhEPO.
First, we developed a method to directly label and quantify newly generated neurons in the hippocampal cornu ammonis (CA) field of adult mice. This was possible by permanently labeling all mature pyramidal neurons present at P27 using a tamoxifen-inducible reporter gene in *NexCreERT2::R26R-tdT* mice (Fig. 1a, b)[21]. Thus, all neurons differentiating and maturing after termination of the tamoxifen-induced Cre recombination lack tdTomato, but can be positively identified by Ctip2, a specific marker of pyramidal neurons, thereby revealing adult 'neurogenesis' independent of DNA synthesis.

Immediately after tamoxifen induction, at P28, the number of such unlabeled (tdTomato[−], Ctip2^{+}) pyramidal neurons, quantified for control purposes, was <3% of all Ctip2^{+} cells. When rhEPO treatment was initiated at P28 as described[17], and mice were analyzed at P55, we found a considerable number of newly differentiated (tdTomato[−]/Ctip^{+}) neurons in CA1, without evidence by 5-Ethynyl-2′-deoxyuridine (EdU) incorporation of proliferating precursors, as we reported previously[17]. Upon rhEPO treatment, the number of pyramidal cells was higher compared to placebo, but even untreated mice revealed a remarkable increase in new neurons (Fig. 1c).

Strikingly, when we applied the same rhEPO treatment to older mice (age 3 months), we detected a comparable effect on pyramidal neuron numbers (Fig. 1d). Thus, there is a substantial generation of pyramidal neurons from pre-existing (non-proliferating) precursors also in adulthood, suggesting a previously overlooked aspect of adult neurogenesis, discovered by serendipity in rhEPO-treated mice.

EPO increases dendritic spine density.
Using *Thy1-EYFP* transgenic mice[22], we noted that EPO treatment also enhanced the dendritic spine density in pyramidal neurons at both P55 and 4 months (Fig. 1e–i). The analysis of spine morphology (Fig. 1j–l) showed an increase in stubby immature spines and a trend toward more mature mushroom spines[23]. Reflecting the increased pyramidal neuron number, we also noted a higher density of Map2 immunoreactive primary dendrites in the stratum radiatum (Fig. 1m–o).

Immediate differentiation response of neuronal precursors to rhEPO.
We employed single-cell transcriptome analysis (scRNA-

seq) to explore the immediate response of cells in CA1 to rhEPO, detectable 6 h after a single intraperitoneal (i.p.) injection of 5000U rhEPO/kg (Fig. 2, Supplementary Figs. 1–3, Source Data File). This revealed alterations in the cell cluster composition as defined by gene expression profiles[24], with more cells in the immature glutamatergic differentiation cluster after rhEPO (Fig. 2a–d). Markers that characterize this cluster include doublecortin (*Dcx*), transducin-like enhancer family member4 (*Tle4*), T-box brain1 (*Tbr1*), rhabdomyosarcoma 2-associated transcript (*Rmst*), SRY-Box5 (*Sox5*), DNA-binding protein SATB1 (*Satb1*), ELAV-like neuron-specific RNA-binding protein4 (*Elavl4*), fucosyltransferase9 (*Fut9*), CUGBP Elav-like family member4 (*Celf4*), and heparan sulfate-glucosamine 3-sulfotransferase4 (*Hs3st4*). For two of them, *Tle4* and *Tbr1*, in situ validation of protein expression by immunohistochemistry (IHC), predominantly in Ctip^{+} neurons (confirmed by double labeling) at P29, i.e., 24 h after a single injection of EPO/placebo, exemplifies the distinct EPO effect (Fig. 2e). Note that Tbr1^{+} neurons upon EPO are rapidly and strongly detected in CA1 at P29, but only rarely anymore at P55. Tbr1^{+} cells in dentate gyrus serve as positive control for both time points (Supplementary Fig. 3e). Other neuronal clusters and non-neuronal cell types were not obviously different between treatment groups at 6 h (Supplementary Fig. 3b).

In order to further investigate the EPO-induced effects on cell differentiation, we performed a trajectory (pseudotime) analysis on cells in the immature glutamatergic cluster and its neighboring cluster, mature glutamatergic1, in *Monocle2*[25]; Fig. 2f; list of differentially expressed genes between these two clusters given in Source Data File). The analysis confirmed the immature identity of cells in the immature glutamatergic cluster, reflected by a homogeneously low pseudotime of almost all cells in this cluster, which was significantly lower as compared to cells in the mature glutamatergic1 cluster (Fig. 2g). After post hoc exploratory removal of immature cells with high pseudotime (>15, $n = 10$), the increase in immature cells upon EPO still remained significant ($p = 0.039$; Fisher's exact test, one sided). Even if the immature cells with high pseudotime (>15) were reassigned to the mature glutamatergic cluster, a significance level of $p = 0.041$ was obtained. Importantly, we observed a generally lower pseudotime upon EPO, independent of cluster assignment, further supporting our observation of an increase in immature cells and excluding a mere 'clustering artifact' (Fig. 2h). Also, reclustering in *Monocle2* of cells from the two clusters revealed a robust detection of the immature cluster across methods (*Seurat* and *Monocle2*; Supplementary Fig. 3a) and a robustly increased number of immature cells upon EPO as compared to placebo treatment, independent of the analysis platform ($p = 0.0008$). For further validation of the immature identity of these cells see Supplementary Fig. 3c, d.

Together, these data provide supportive evidence of an immediate effect of EPO on pre-existing precursors to instantaneously initiate neuronal differentiation, thereby rapidly increasing the numbers of cells in the immature glutamatergic differentiating cluster. Expectedly, EPO and EPOR were not detected by scRNA-seq due to their very low expression level, a known drop-out effect in scRNA-seq data.

Elevated expression of EPO and EPOR by pyramidal neurons upon CRW.
Searching for the physiological significance of these responses, we explored whether EPO and EPOR are endogenously expressed by pyramidal neurons. Using a highly sensitive in situ hybridization (ISH) method, capable of detecting even single mRNA molecules, we identified both EPO and EPOR transcripts in pyramidal neurons of the hippocampal CA1 region (Fig. 3a–d). The overall mRNA abundance in the hippocampus
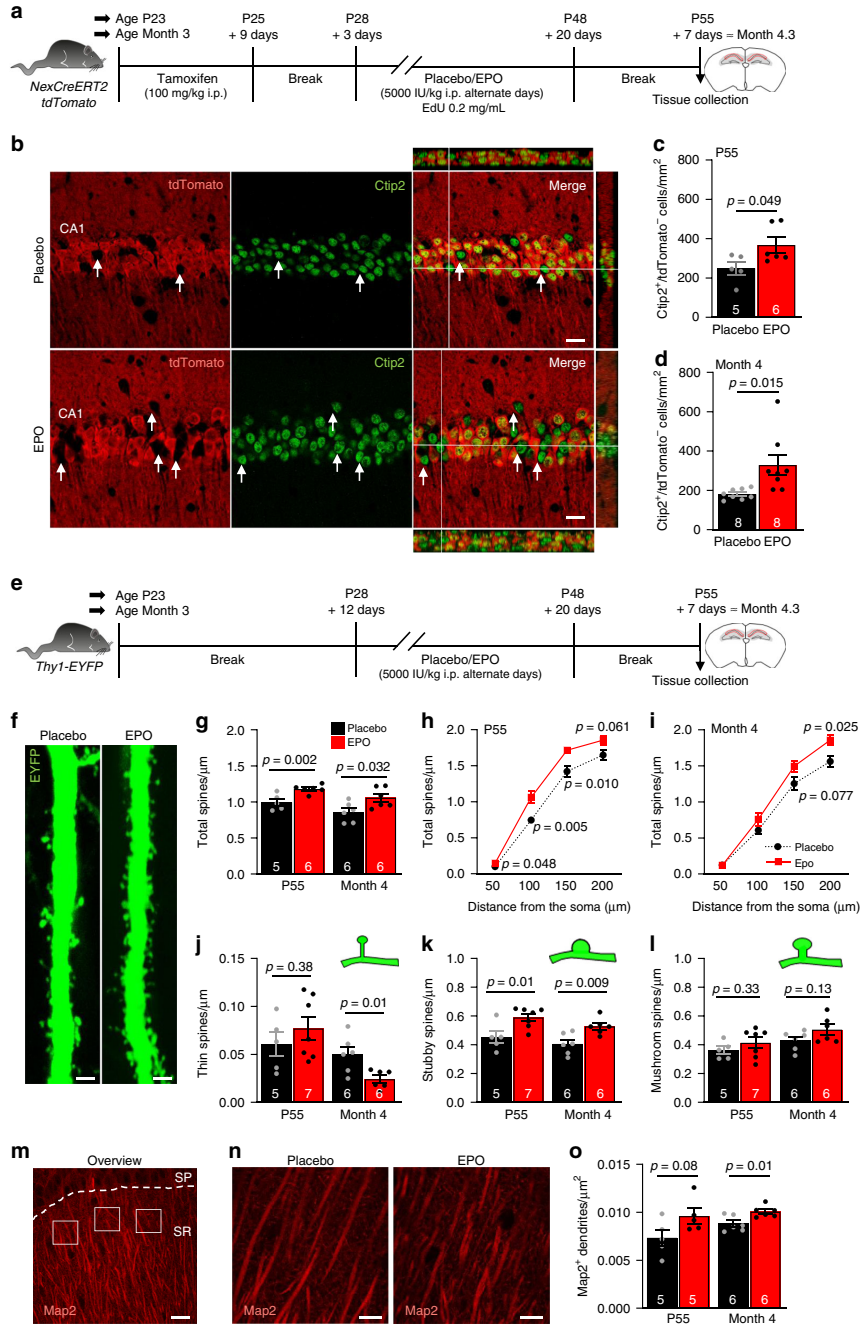
was higher than in cortex and other brain regions. Interestingly, when mice were placed into cages with complex running wheels (CRW)[26], a cognitive challenge that stimulates intricate motor learning and coordination, only 5–9 h of running in the dark phase were sufficient to upregulate the expression of EPO and EPOR transcripts in pyramidal neurons (Fig. 3a–d).

Permanent labeling of hypoxic neurons in CA1 by CRW exposure. We therefore wondered which mechanism would lead to the swift upregulation of EPO in pyramidal neurons upon cognitive challenge. In the kidney, it is hypoxia and hypoxia-inducible factors (Hif), which are well known to induce EPO expression[1,2,7,27]. We therefore hypothesized that cognitive

Fig. 1 EPO increases number of pyramidal neurons and spine density in the CA1 region of the hippocampus. a Experimental design to determine the effect of EPO on neuron numbers: two cohorts of *NexCreERT2::tdTomato* mice (starting at age P23 or month 3) were administered tamoxifen (at P23: 5× i.p.; at month 3: 10× i.p.), followed by placebo or EPO (5000IU/kg; 11× i.p.) on alternate days for 3 weeks. **b** Representative images of tdTomato (red) and Ctip2 (green; excitatory neuronal marker) staining in CA1 of placebo or EPO-treated mice. White arrows indicate newly generated neurons. **c, d** Quantification of newly generated neurons (Ctip2$^+$/tdTomato$^-$) in CA1 of P55 **c** and ~4-month-old mice **d** treated with placebo or EPO. Data from $n = 5/8$ (placebo; 1c/d) and $n = 6/8$ (EPO; 1c/d) mice. **e** Experimental design to determine the effect of EPO on dendritic spine number and morphology: *Thy1-EYFP* mice (starting at age P28 or month 3) were treated with placebo or EPO (11× i.p.) on alternate days, for 3 weeks. **f** Representative images of EYFP (green) expression in principal apical dendrites in CA1 of placebo or EPO mice. **g–i** For P55 and ~4-month-old mice, total number of spines (per µm) are given as bar graphs **g** and, additionally, as line graphs **h–i** presenting their distance from the soma. Data from $n = 5/6$ (placebo; P55/4 months) and $n = 6$ (EPO) mice (6 cells/mouse analyzed). **j–l** Based on the morphology (illustrated as green insets), the number of thin **j**, stubby **k**, and mushroom **l** spines (per µm) were sub-quantified. **m** Representative image of the quantification method employed for determining the number of dendrites using dendritic marker Map2 (red) in CA1 stratum radiatum (SR); stratum pyramidale (SP). White boxes denote areas of measurements. **n** Representative images of Map2 (red) staining in ~4-month-old mice treated with placebo or EPO. **o** Quantification of Map2$^+$ dendrites in P55 and 4-month-old mice treated with placebo or EPO. Data from $n = 5/6$ (placebo; P55/4 months) and $n = 5/6$ (EPO; P55/4 months) mice. Within bars, mouse n numbers indicated; mean ± SEM presented; two-tailed Student's t-test; scale bars: **b** 50 µm; **f** 10 µm; **m** 20 µm; and **n** 10 µm. Source data underlying graphs **c, d, g–l,** and **o** are provided as a Source Data File.

challenge, such as learning of complex motor tasks, is associated with neuronal activity that requires more oxygen than present in the normal steady state. This could induce a mild (transient) endogenous hypoxia as a potential signal underlying upregulated expression of EPO in highly active pyramidal neurons. To test this hypothesis, we asked whether 'functional hypoxia' can be detected in the brain after cognitive challenge, such as complex wheel running. To this end, we created a novel transgenic mouse for the ubiquitous expression of a chimeric fusion protein between the tamoxifen-inducible CreERT2 recombinase and the oxygen-dependent degradation (ODD) domain of Hif-1α[28]. In mice bearing this *CreERT2-ODD* transgene, driven by the CAG promoter, 'fate mapping' and identification of (transiently) hypoxic cells is possible with the tdTomato reporter (*CAG-CreERT2-ODD::R26R-tdTomato*). Indeed, exposing these mice after tamoxifen injection to CRW over one night, we determined a distinctly increased number of 'ODD-labeled' pyramidal neurons in the CA1 region when compared to non-runners. This indicates that a new challenging task has led to more (transiently) hypoxic neurons, which became permanently labeled. Parallel quantification of cFos expression as neuronal activity marker[29] revealed a tendency of increased cFos labeling upon CRW (Fig. 3e–h), but no double labeling with ODD-tdTomato. The latter likely occurs too late in a respective cell, i.e., when its immediate early gene (cFos) expression has already disappeared. In contrast, after only 4 h of CRW, cFos labeling was obvious, but no ODD-tdTomato labeling yet detected (cFos$^+$ cells: non-runners 40.1 ± 20.8, $n = 3$; CRW 143.3 ± 24.4, $n = 7$; $p = 0.034$, mean ± SEM). Additional confirmation of hypoxic cell labeling by ODD-tdTomato was obtained using pimonidazole, resulting in findings similar to a previous report on heart[28] (Supplementary Fig. 4).

EPO treatment strongly increases motor learning and endurance. To further address the potential of rhEPO to lastingly improve cognitive performance, we treated juvenile mice with our protocol that results in ~20% more pyramidal neurons (starting at P28, i.p. injection of rhEPO/placebo every other day for 3 weeks, followed by a 1-week break). Afterward, the running-naive mice were transferred to cages containing CRW. During the initial learning phase, a rise in performance was observed, clearly dissociating EPO from placebo-treated mice after just a few hours, followed by enhanced endurance over the whole night.

Deletion of neuronal EPOR attenuates EPO-/hypoxia-induced motor learning. Theoretically, the EPO-induced increase in

hematocrit could account for this enhanced performance. To rule this out and to explore whether pyramidal EPOR is mediating this effect, we deleted the *Epor* gene from pyramidal neurons (*NexCre::EpoRfl/fl*; Supplementary Fig. 5). More details on the generation of this conditional *Epor* allele, its recombination with different Cre-lines, and a comprehensive phenotype analysis will be described elsewhere (manuscript in preparation). As delineated in Fig. 4a–c, the remarkable rise in performance of wild-type (WT) mice following EPO treatment reported above was well replicated, whereas EPOR-cKO mice failed to show any noticeable effect of EPO treatment on CRW performance (i.e., complex motor learning and endurance). Placebo-treated EPOR-cKO did not appreciably differ from WT mice (Fig. 4c, inset). The behavioral phenotype of EPOR-cKO mice strongly suggested that also neuronal complexity, i.e., dendritic spine density of pyramidal neurons, would be affected by EPOR deletion. Indeed, Golgi staining revealed that lack of EPOR in pyramidal neurons prevented the EPO-induced increase in dendritic spines (Fig. 4d, e).

Mild inspiratory hypoxia acts synergistically with cognitive challenge. Since learning to run on CRW leads to endogenous ('functional') hypoxia in pyramidal neurons, as demonstrated by ODD labeling, and since pyramidal EPO and EPOR mRNAs are upregulated by functional hypoxia, we wondered whether CRW exposure for several weeks would (similar to rhEPO treatment) also lead to more pyramidal neurons. Moreover, would a sustained exposure of mice to a mild exogenous (inspiratory) hypoxia (12% O_2), when coinciding with running activity, result in similar or even synergistic effects, i.e., better learning performance and more neurons in the stratum pyramidale? In the respective large-scale, multi-arm experiment over 3 weeks, we indeed detected improved motor learning and endurance on the CRW of mice under mild hypoxia when compared to normoxia (Fig. 4f–k). To unequivocally demonstrate that the neuronal EPO/EPOR system is responsible for the observed effects, we employed again our mice with targeted deletion of the *Epor* gene in pyramidal neurons. In fact, lack of EPOR in pyramidal neurons resulted in a distinct reduction of the learning curve slope over time, both under normoxic and hypoxic conditions, when compared to the respective WT controls. Also, non-running EPOR-cKO mice have already less pyramidal neurons independent of hypoxia (normoxia: 7834.07 ± 223.18 in cKO versus 9377.48 ± 864.48 in WT; hypoxia: 8431.51 ± 320.40 in cKO versus 10730.78 ± 497.00 in WT; overall genotype effect $p = 0.0012$) and fail to show the increase in pyramidal neurons found in WT mice upon running with or without hypoxia (Fig. 4f–k).

ARTICLE

a

b

c

d

e

f

g

h
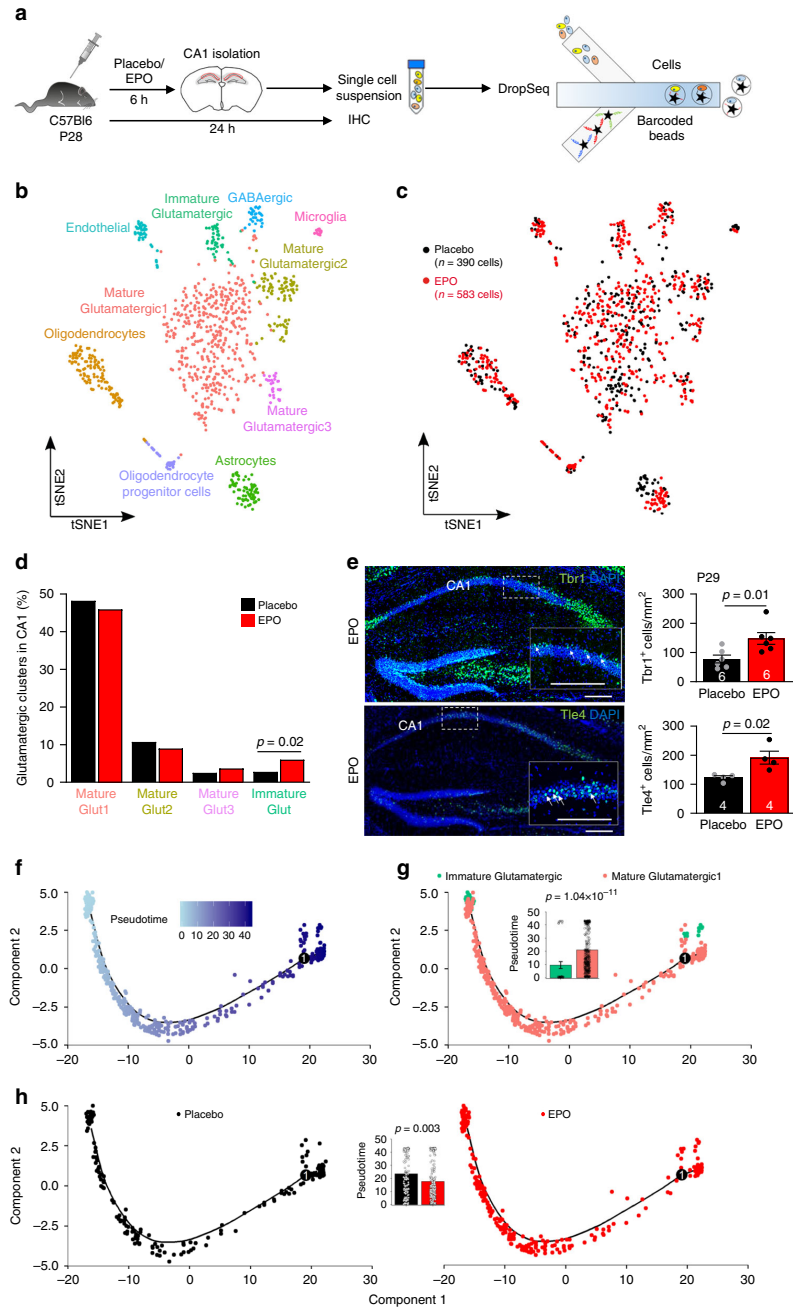
Expression of cFos marks newly differentiated neurons. Under both normoxic and hypoxic conditions, we counted more recently differentiated (EdU negative) pyramidal neurons in runners than in non-runners in the hippocampal CA1 field. We thus wondered whether the newly differentiated pyramidal neurons, generated in mice placed into CRW cages, are functional. To address this question, we challenged animals for 3 weeks in CRW (with or without mild inspiratory hypoxia) but moved them first back to regular cages for 1 week, in analogy to the rhEPO treatment scheme. Then, we re-exposed the mice to CRW for only 4 h at the beginning of their dark phase. Immediately thereafter, they were sacrificed and brains processed for IHC. As readout of neuronal activity and functional integration, cFos expression[29] was used again and found to be enhanced following hypoxia, and in

Fig. 2 Transcriptome analysis (scRNA-seq) demonstrates an immediate increase in neurodifferentiation upon EPO application. a Experimental design of WT C57Bl6 mice ($n = 3$ per group), treated at P28 with a single i.p. injection of placebo or EPO (5000 IU/kg), followed by isolation of the CA1 region after 6 h and processing for DropSeq analysis (processing of biological replicates performed separately, followed by pooling for graphical presentation and final analysis), as well as after 24 h for immunohistochemistry (figure created by Debia Wakhloo). **b** Visualization of hippocampal CA1 cell clusters using t-distributed stochastic neighbor embedding (tSNE). Each color represents a cluster of specific cells, characterized by a defined gene expression profile. **c** Individual cells derived from either EPO (red) or placebo (black)-treated mice are denoted. **d** Percentage of cells in the respective glutamatergic clusters per treatment condition (EPO: $n = 583$, placebo: $n = 390$); two-tailed Fisher's exact test. **e** Representative images and quantification of Tbr1 and Tle4 staining (immature neuronal markers) in CA1 of mice at P29, i.e., 24 h after a single injection of EPO. Within bars, mouse n numbers indicated; mean ± SEM presented; two-tailed student's t-test. **f** Trajectory analysis in *Monocle2* of cells in the 'Mature Glutamatergic1' and the 'Immature Glutamatergic' cluster colored by pseudotime (the darker the more mature). **g** Trajectory colored by cell identity. Bar graph indicates average pseudotime of the respective clusters; mean ± SEM; two-tailed Mann–Whitney U test. **h** Trajectory colored and split by placebo (black; left) versus EPO treatment (red; right). Bar graph shows average pseudotime of cells in the respective treatment groups; two-tailed Mann–Whitney U test; mean ± SEM; see also Supplementary Figs. 1–3. Source data underlying graph **e** are provided as a Source Data File.

particular after running. Unexpectedly, cFos was mainly detected in the recently differentiated neurons, whereas the fraction of pre-existing neurons expressing cFos was small (Fig. 4l–p).

Discussion

Taken together (Fig. 5), we have discovered that EPO - experimentally and clinically shown to improve cognition[9–17] - stimulates a previously unrecognized mechanism of cellular neuroplasticity. Specifically, rhEPO (when peripherally administered) enters the brain, where it mimics the effects of endogenous neuronal EPO/EPOR signaling, stimulating dendritic spine formation on mature cells, and the differentiation of new pyramidal neurons from pre-existing (non-proliferating) precursors, the identity of which is currently unknown.

The EPO-responsive cells undergoing adult neurogenesis likely have no defining single genetic marker, suitable for CreER-based lineage tracing (unlike the EPO-responsive OPC[17]). Not even direct transdifferentiation of endothelial and astroglial cells or dedifferentiation of neurons can be completely excluded at this point. Jak2-Stat5 signaling, however, a pathway important for neuronal EPOR effects[18,20], is known in various tissues to induce terminal differentiation, not dedifferentiation.

We hypothesize that the entire precursor cell lineage that is ready to differentiate toward pyramidal neurons in adult mice remains 'in flow'. Similar to adaptive metabolic pathways, in which the 'flux' of metabolites matters more than the different steady-state concentrations, also in the proposed neuronal lineage progression, the EPO-responsive progenitor cells may never constitute abundant clusters in a cross-sectional steady-state analysis. This is remarkably similar to the effects of EPO on multiple precursors at different stages in the hematopoietic system[1,30–32].

Pyramidal neurons, when challenged by novel tasks, undergo mild hypoxia, as detected here by 'ODD labeling', using hypoxia reporter mice. This activity-induced 'functional hypoxia' stimulates endogenous EPO expression by pyramidal neurons. In parallel, we find also EPOR expression enhanced, caused either directly by hypoxia[33] or by EPO in an auto/paracrine manner[34]. When EPOR expression is deleted from pyramidal neurons, the endogenous EPO/EPOR system can no longer contribute to adaptive increase in performance.

Contrary to popular viewpoints that hypoxia is detrimental, recent reviews also consider beneficial effects and protection against cognitive dysfunction[35,36]. Our data using CRW indicate that hypoxia can act as driving force of long-lasting cellular neuroplasticity, complementing synaptic plasticity. Neuronally produced EPO/EPOR likely constitutes an auto/paracrine mechanism, possibly in concert with other hypoxia-inducible genes, like vascular endothelial growth factor, which has previously also been reported to enhance cognition[37]. We suggest a

model of an intrinsic EPO/EPOR-mediated mechanism of cellular neuroplasticity (Fig. 5), in form of a fundamental regulatory circle, which can explain the remarkable procognitive effects of rhEPO, consistently found in humans and rodents, health and disease[9,10,12,14–16,38].

A recent study documented EPO mRNA in different neural cell types in the embryonic brain (mouse organogenesis cell atlas— MOCA[39]). The extraordinarily low expression of EPO and EPOR in the adult brain may explain why this system has previously not been rigorously studied. So far, we have focused on the hippocampal CA1 region, where we had obtained first evidence of substantially increased neuron numbers after rhEPO treatment[17]. CA1 is involved in temporal pattern association and different facets of memory formation and consolidation[40]. Future studies will have to address EPO/EPOR functions in other CNS regions, including cortical areas known to be also engaged in CRW learning[41], as well as neuron–glial interactions.

'Adult neurogenesis' from pre-existing precursors without proliferation extends the concept and pivotal work from many groups who discovered adult neurogenesis in distinct brain regions based on the selective labeling of proliferating cells in S-phase[42–48]. More complex than oligodendrogenesis from pre-existing precursors[49], multiple neuronal progenitors may be relevant for maintaining neuron numbers in steady state, for adjustment to demand, and for rapid regenerative processes. The genetic approach of EPOR deletion in pyramidal neurons, together with the discovery of 'functional hypoxia' in the behaving brain, allowed us to propose a novel working model (Fig. 5). This model may add to our present concepts of neuroplasticity and adult neurogenesis.

Methods

Experimental models and mouse genetics. All experiments were approved by and conducted in accordance with the regulations of the local Animal Care and Use Committee (Niedersächsisches Landesamt für Verbraucherschutz und Lebensmittelsicherheit, LAVES). WT C57BL/6N (Charles River), *NexCreERT2*[21], *R26R-tdTomato*[50], *Thy1-YFPH* (Jackson Laboratory, 003782), *CAGCreERT2-ODD*[28], *NexCre*[51], and EPOR-floxed (EPOR^{fl/fl}) mice were used for the experiments. Juvenile (P23) and adult (3 months old) mice were used in this study. For genetic labeling of projection neurons, *NexCreERT2* mice were bred with *Rosa26 floxed-stop tdTomato* (*R26R-tdTomato*) reporter mice to generate *NexCreERT2:R26R-tdTomato* mice. For labeling cells undergoing hypoxia, *CAGCreERT2-ODD* mice were employed[28]. Briefly, a fusion protein consisting of the ODD domain of Hif-1α and a ubiquitous *CAGCreERT2* is expressed upon tamoxifen induction. *CAGCreERT2-ODD* were bred with *R26R-tdTom*ato to generate *CAGCreERT2-ODD:tdTomato* reporter mice. Upon tamoxifen induction, cells are irreversibly labeled with tdTomato containing stabilized Hif-1α. *NexCre::Epor^{fl/fl}* mice were generated to specifically delete *Epor* in projection neurons. For the generation of *Epor^{fl/fl}* mice, embryonic stem cells (ES) harboring an engineered allele (*Epor[tm1a(KOMP)Wtsi]*) of the *Epor* gene were acquired from the Knockout Mouse Project (KOMP, University of California, Davis CA 95618, USA). ES cells were microinjected into blastocysts derived from C57BL/6N mice and the embryos were transferred to pseudopregnant foster mothers, yielding chimeric males. For ES clone *EPD0316_5_A03*, germline transmission was achieved upon breeding with

ARTICLE
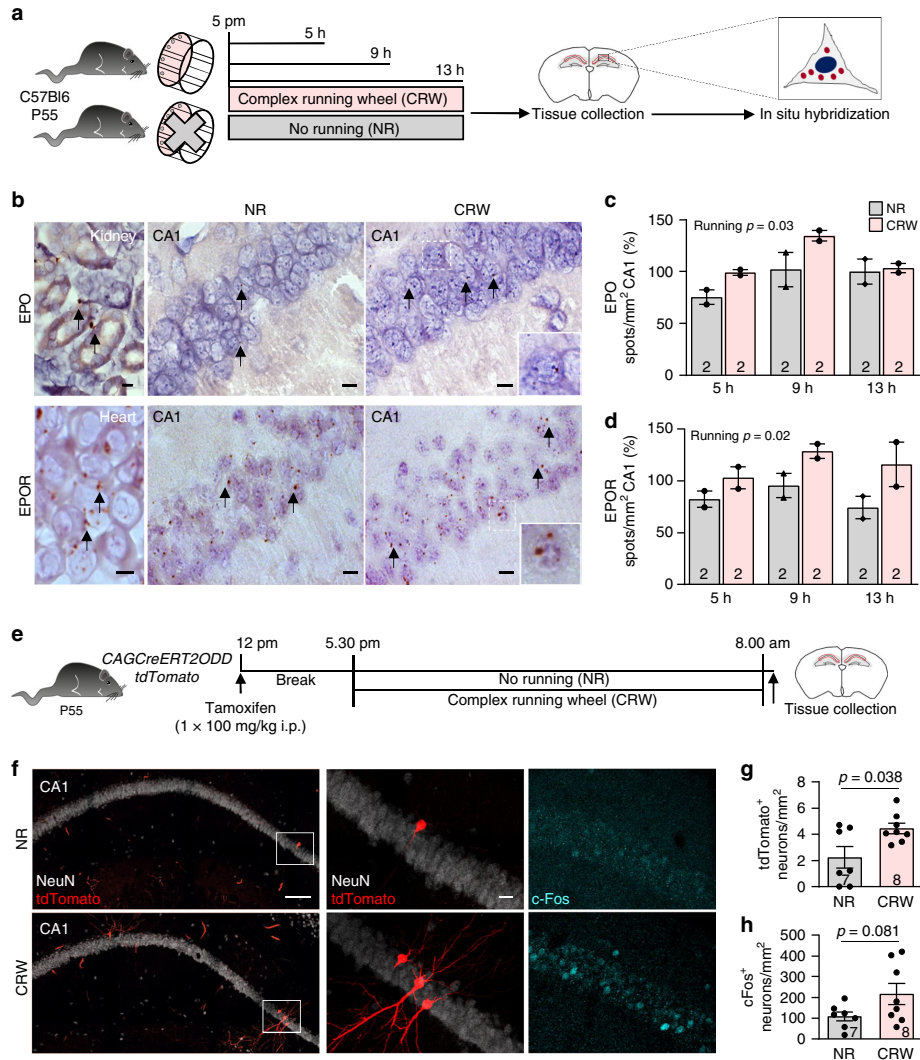
Fig. 3 Expression of the EPO/EPOR system in pyramidal neurons shown by ISH and its upregulation by functional hypoxia. a Experimental design of WT C57Bl6 mice exposed to no running (NR) or voluntary running on CRW at P55 for 5, 9, or 13 h. ISH was performed on CA1 regions (figure created by Debia Wakhloo). **b** Representative ISH images of CA1 regions of non-runners (NR) and runners (CRW), demonstrating EPO and EPOR mRNA expression in pyramidal neurons (brown spots). As positive controls for EPO/EPOR mRNA expression, sections of kidney (P55) and heart (E14.5) from WT C57Bl6 mice are presented. **c, d** Quantification of total number of EPO or EPOR mRNA spots in CA1 of non-runners (NR) and runners (CRW), shown at 5, 9, and 13 h; mean and range shown; two-way ANOVA; n numbers indicated within bars; scale bars in **b**: 10 μm; for heart 5 μm. **e** Experimental design to determine the effect of running on the induction of functional hypoxia in the CA1 region. *CAGCreERT2-ODD::tdTomato* mice were administered tamoxifen at P55 of age and exposed to either no running (NR) or overnight voluntary CRW. **f** Representative images of neuronal marker NeuN (white), tdTomato (red; labeling hypoxia), and cFos (cyan) in non-runner (NR) and runner mice (CRW); scale bars 100 μm (left); 10 μm for magnifications. **g, h** Quantification of hypoxic neurons (tdTomato+) and active neurons (cFos+) in CA1 after CRW versus NR overnight (12 h); mean ± SEM; two-tailed Student's t-test; data from $n = 7$ (non-runners, NR) and $n = 8$ (CRW) mice. Source data underlying graphs **c**, **d**, **g**, and **h** are provided as a Source Data File.

C57BL/6N females, generating mice harboring the *Epor*[tm1a(KOMP)Wtsi] allele (termed *Epor*[lacZ-neo]). The lacZ-neo cassette was excised in vivo upon interbreeding with mice expressing FLIP recombinase (*129S4/SvJaeSor-Gt(ROSA)26Sor*[tm1(FLP1)Dym/J]; backcrossed into C57BL/6N), yielding mice carrying the *Epor*[tm1c(KOMP)Wtsi] allele (termed *Epor*[flox]). To recombine the *Epor* gene specifically in projection neurons, exons 3–6 were excised in vivo upon appropriate interbreedings of *Epor*[tm1c(KOMP)Wtsi] mice with mice expressing Cre recombinase under control of

the *Nex1/Neurod6* promoter[51], generating mice carrying the *Epor*[tm1d(KOMP)Wtsi] allele (*NexCre::Epor*^{fl/fl} mice).

All mice were housed in a temperature controlled environment (21 ± 2 °C) on a 12 h light–dark cycle with food and water available ad libitum. Male mice of the same age were used for the experiments, unless stated otherwise. All animals were genotyped before the start of each experiment. Detailed PCR protocols are available on request.
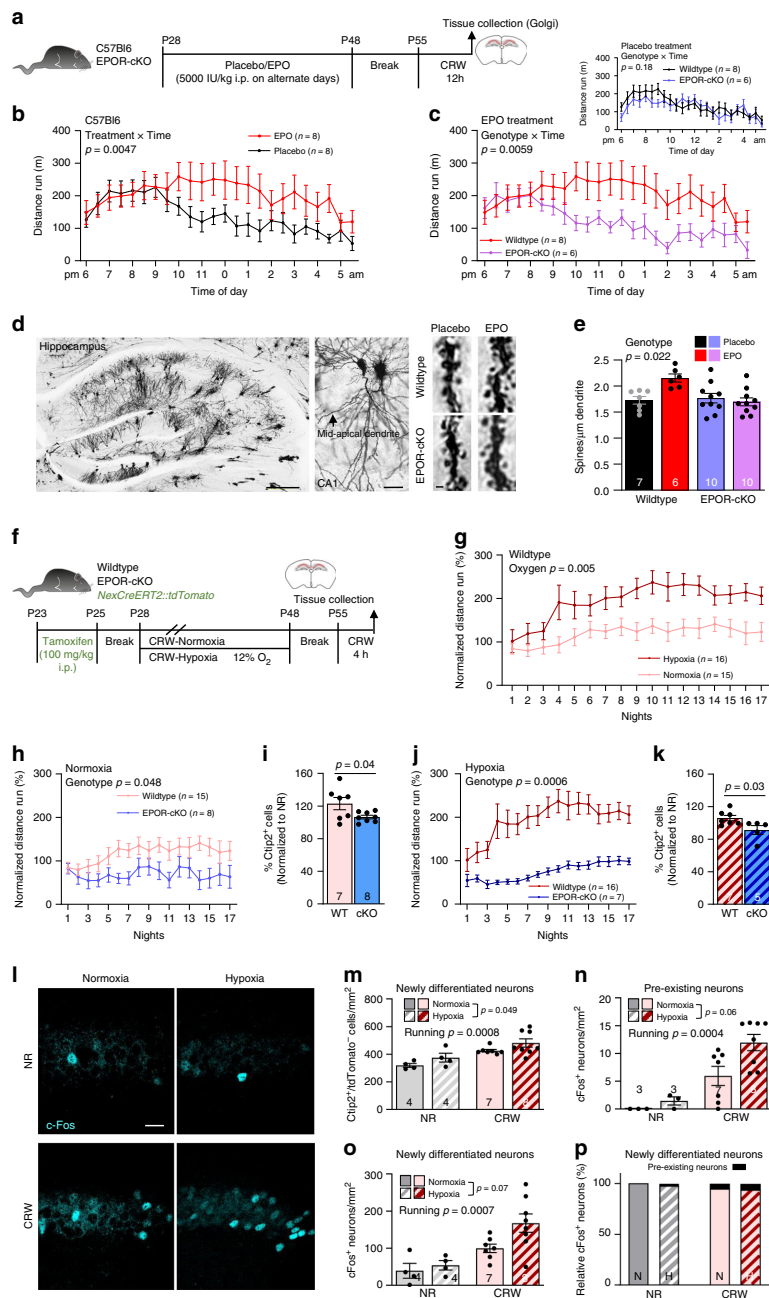
Mouse treatment. *Tamoxifen:* Tamoxifen solution (10 mg/ml) was freshly prepared by dissolving tamoxifen freebase (Sigma) in corn oil (Sigma) at room temperature (RT) for 45 min. Postnatal CreERT2 activity in *NexCreERT2* mice was induced by a total of five i.p. injection of 100 mg/kg tamoxifen over the course of 3 days in juvenile mice. For CreERT2 induction in adult *NexCreERT2* mice, a total of ten i.p. injections of 100 mg/kg tamoxifen were administered over the course of ten consecutive days. For the desired induction of CreERT2 in *CAGCreERT2-ODD* mice, a single i.p. injection of 100 mg/kg tamoxifen was sufficient.

EPO: Male mice were i.p. injected with 5000IU/kg rhEPO (NeoRecormon, Roche) or placebo (solvent solution, 0.01 ml/g). At 48 h after the last tamoxifen injection, EPO/placebo treatment was initiated in P28 or 3-month-old *NexCreERT2*, *Thy1-YFPH* and also in P28 old WT and *NexCre::EPOR^{fl/fl}* mice, and carried out every other day for 3 weeks. For DropSeq analysis, EPO was administered once followed by tissue collection 6 h later. Additionally, for labeling of proliferating cells, *NexCreERT2* mice obtained EdU (0.2 mg/ml; ThermoFisher) via drinking water (exchanged on all alternate days).

Fig. 4 Targeted deletion of EPOR in pyramidal neurons attenuates EPO/hypoxia-induced motor learning. a Experimental design. **b** Total distance run by placebo (black) and EPO (red) treated WT mice. **c** Total distance run by WT (red) and EPOR-cKO mice (purple) following EPO; insert shows for comparison total distance run by WT (black) and EPOR-cKO mice (blue) upon placebo. **d** Representative images of hippocampal section processed with GolgiStain^{TM}Kit (scale bar: 100 µm), CA1 pyramidal neurons (scale bar: 20 µm), and mid-apical dendrites (scale bar: 1 µm). **e** Quantification of dendritic spines in WT and EPOR-cKO mice treated with placebo or EPO. **f** Experimental design. WT and EPOR-cKO mice were exposed to NR or CRW under normoxia (21% O_2) or inspiratory hypoxia (12% O_2), starting at P28 for 3 weeks. After 1 week of break, CRW mice were again exposed to voluntary CRW for 4 h (cFos activation) before being sacrificed at P55 (results in **g**–**k**); *NexCreERT2::tdTomato* mice were injected with tamoxifen (5× i.p.—starting at P23) and exposed to same experimental paradigm (results in **l**–**p**). **g** CRW curves over 17 nights (normalized to mean distance over first three nights) of WT mice exposed to continuous inspiratory normoxia versus hypoxia. **h**–**k** Effect of EPOR deletion in pyramidal neurons: **h** CRW curves of WT and EPOR-cKO mice exposed to normoxia and **i** quantification of their Ctip2+ cells in CA1 (normalized to NR controls). **j** CRW curves of WT and EPOR-cKO mice exposed to inspiratory hypoxia, and **k** quantification of their Ctip2+ cells in CA1 (normalized to NR controls). **l** Representative images of cFos+ neurons (cyan) in NR and CRW mice exposed to normoxia or hypoxia (scale bar: 25 µm). **m** Quantification of newly formed neurons (Ctip2+/tdTomato−) in NR and CRW mice exposed to normoxia or hypoxia. **n**, **o** Quantification of active neurons classified as pre-existing neurons (cFos+/Ctip2+/tdTomato+) or as newly formed neurons (cFos+/Ctip2+/tdTomato−) in CA1 of mice quantified in **m**. **p** Presentation of the small percentage of pre-existing neurons among cFos+ neurons. Data given as mean ± SEM; two-tailed Student's *t*-test (i & k) or two-way ANOVA; mouse *n* numbers in panels. Source data of graphs **b**, **c**, **e**, **g**–**k**, and **m**–**p** provided as Source Data File.

Hypoxia: The hypoxia chamber was designed in cooperation with Coy Laboratory Products Inc. (Grass Lake, MI, USA) with the dimensions 164 cm × 121 cm × 112 cm. The system includes an air filtration system consisting of carbolime and activated charcoal. The oxygen and carbon dioxide levels were constantly detected and controlled via online monitoring. A gradual reduction of 3% oxygen per day resulted in 12% oxygen level in 3 days and was maintained until the end of the experiment. During the course of the experiment, mice were treated with EdU via drinking water as described above.

Complex running wheels (CRW). Post weaning, mice were single-housed and tamoxifen treatment was initiated for *NexCreERT2::tdTomato* mice (described above). *NexCreERT2::tdTomato* and *NexCre::EpoR$^{fl/fl}$* were divided into four groups and monitored for 17 days. Groups included (1) normoxic room conditions (at 21% O_2) in standard cages, (2) normoxic conditions with voluntary running on CRW, (3) hypoxic conditions (hypoxia chamber to 12% O_2) in standard cages, and (4) hypoxic conditions with voluntary running on CRW. CRW (TSE Systems, Bad Homburg, Germany) is characterized by randomized missing bars as previously described[26,41]. The testing period of 17 days was followed by 1 week of normal conditions for all groups (no running, normoxia). The mice that were previously running (in normoxic or hypoxic conditions) were finally exposed again to CRW for 4 h (as cFos inducing challenge) before being sacrificed (Fig. 4f). For ISH experiments, male WT mice (P55) were exposed to 5, 9, or 13 h of CRW (Fig. 3a). For the experiment involving *CAGCreERT2-ODD::tdTomato* mice, animals were exposed to overnight complex wheel running (Fig. 3e). Running was voluntary at all times with ad libitum access to food and water. Control mice (no running) were housed in standard cages. Mice were sacrificed, perfused, and brains collected as described below. Running was tracked automatically via Phenomaster software (TSE Systems, Germany) for the whole day. Since mice are mainly night-active (dark phase), the total distance run between 6 p.m. and 6 a.m. was summarized for every individual animal. The total distance run on each night was normalized to the average distance of each animal run in the first 3 nights (data expressed as % performance in relation to the first 3 nights). For the experiments involving EPO treatment, mice were treated with EPO (5000IU/kg, 11 i.p. injections on alternate days for 3 weeks), followed by 1-week break. They were then exposed to 12 h of CRW overnight (Fig. 4a–c). Data for this experiment are expressed as distance run summarized for every 30 min.

Immunohistochemistry (IHC). Mice were anesthetized and perfused transcardially with 4% cold formaldehyde. Dissected brains were post fixed in 4% formaldehyde at 4 °C and equilibrated in 30% sucrose dissolved in phosphate-buffered saline (PBS) at 4 °C overnight. Brains were then embedded in cryoprotectant (O.C.T.^{TM} Tissue-Tek, Sakura) and stored at −80 °C. Whole mouse brains were cut into 30 µm thick coronal sections (coordinates from bregma: −1.34 to −2.54 mm posterior) using a cryostat (Leica) and stored in a cryoprotective solution (25% ethylene glycol and 25% glycerol in PBS) at −20 °C until further use. For analysis of dendritic spines and Map2 dendrites, the right hemisphere, destined to the neuronal structural analysis, was cut in 100 µm coronal sections with a vibratome (Leica VT 1000E, Leica), collected in three subseries and stored at 4 °C in PB 0.1 M with sodium azide (0.05%).

For IHC, sections were permeabilized in PBS containing 0.3% Triton X-100 and blocked in 5% horse serum for 1 h at RT. Brain sections were incubated with primary antibodies in blocking solution overnight at 4 °C, followed by 2 h incubation of appropriate fluorophore-conjugated secondary antibodies in blocking solution containing 3% horse serum (or 5% normal donkey serum) and counterstained with 4′,6-diamidino-2-phenylindole (DAPI). The sections were then mounted on SuperFrostPlus Slides (ThermoFisher) with Aqua-Poly/mount (Polysciences, Inc). Primary antibodies used were: anti-Ctip2 (1:500; Guinea pig polyclonal; SYSY 325005), anti-Map2 (1:1000; mouse monoclonal; Sigma M9942), anti-Tbr1 (1:200; rabbit monoclonal; Abcam ab183032), anti-Tle4 (1:200; rabbit polyclonal; Abcam ab64833), anti-NeuN (1:500; mouse monoclonal; Millipore MAB377), and anti-cFos (1:1000; rabbit polyclonal; SYSY 226003). Secondary antibodies were: Alexa488 anti-Guinea pig (1:500; Jackson Immuno Research 706-548-148) and Alexa635 anti-mouse (1:400; ThermoFisher A31575). Depending on the need for a triple or a quadruple staining, Alexa405 anti-rabbit (1:1000; Abcam 175652) or Alexa647 anti-rabbit (1:500; ThermoFisher A31573) were used. Following IHC, sections were stained for EdU using Click-iT^{TM} EdU Alexa Fluor^{TM} 647 Imaging kit (ThermoFisher E10415), according to the manufacturer's instructions.

Golgi-Cox staining. Mice were anesthetized and decapitated. The brain was removed, shortly rinsed in PBS, and processed with the ND Rapid GolgiStain^{TM} Kit (FDNeuroTechnologies, PK401) according to the manufacturer's instructions. After impregnation, the brains were embedded in 2% Agar Agar in PBS and cut in 100 µm coronal sections with a vibratome (Leica, VT 1000 S) and placed on gelatin-coated glass slides (FDNeuroTechnologies, PO101). The slices were stained and dehydrated as described in the kit protocol. Slices were mounted with Perimount (ThermoFisher).

Imaging and analysis. *Pyramidal neurons:* Imaging was performed using the Andor Eclipse TiE microscope system (Nikon, Tokyo, Japan) with a 40× objective (Plan Apo λ 40×, NA = 0.95) to image the hippocampal layers. Ctip2+ cells among total neuron numbers were manually counted. Ctip2+ and tdTomato− cells were characterized as newly generated neurons. Quantifications are expressed as number of newly generated neurons divided by the total area of CA1 stratum pyramidale (mm²). For Ctip2 staining, a total of 16 hippocampi with 8 sections per animal were used. Quadruple (tdTomato, Ctip2, cFos, and EdU) staining was acquired with a TCS SP5-II System (Leica) equipped with a 20× objective (NA = 0.70). For total Ctip2+ counts, six hippocampi with three sections per animal were used. Quantifications for CRW mice were expressed as percentage of Ctip2+ cells normalized to their respective non-running controls. Whole hippocampi were imaged and analyzed by Fiji software. Neurons showing positive immunoreactivity for cFos were identified and quantified manually. These neurons were further subcategorized into pre-existing (cFos+, tdTomato+, Ctip2+) or newly generated (cFos+, tdTomato−, Ctip2+) neurons. Again, quantifications are indicated as cFos+ cells divided by the total area of the CA1 stratum pyramidale (mm²). For cFos staining, a total of eight hippocampi with four sections per animal were used. For quantification of hypoxic neurons, whole hippocampus sections of *CAG-CreERT2-ODD::tdTomato* mice were imaged. The tdTomato+ cells were characterized as neurons undergoing hypoxia and manually quantified. Quantifications are expressed as number of hypoxic neurons divided by the total area of CA1 stratum pyramidale (mm²). A total of ten hippocampi with five sections per animal were used. The cFos+ cells were also analyzed as described above. For Map2+ dendritic density analysis, the stratum radiatum of the CA1 region was imaged using a laser scanning confocal microscope (Leica TCS SPE). Per animal, three dorsal hippocampal slices were selected starting at bregma −1.58 mm. Confocal z-stacks (0.38 µm intervals) of whole sections were taken using a 63× objective (NA = 1.40). Per hippocampus, three images were captured, and four fields of the dimension 36.67 µm × 36.67 µm were analyzed in each image (total 36 fields per animal). Images were processed using Fiji software and Map2+ principal apical dendrites were manually quantified. The quantifications are expressed as number of Map2+ dendrites divided by the area of each image (1344.7 µm²).

Dendritic spines: Images were captured using a 63× oil immersion objective (NA = 1.40) and a 3.5× additional digital zoom to investigate the first 200 µm of the principal apical dendrite in segments of 50 µm. Confocal z-stacks (0.38 µm
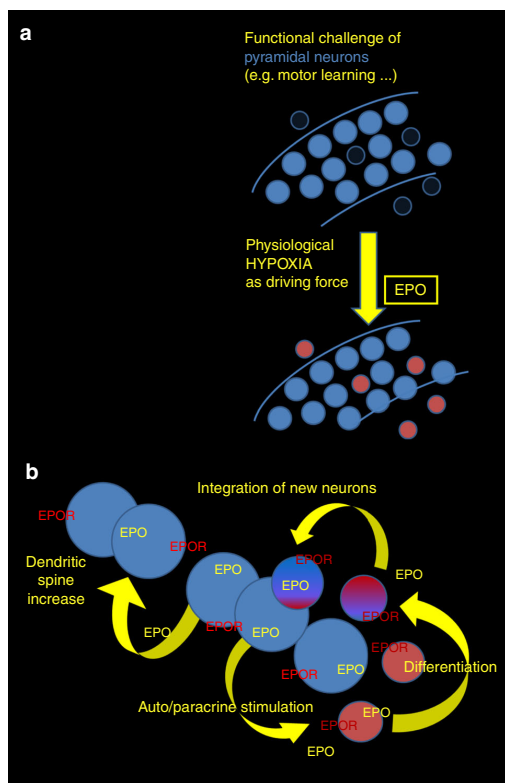
Fig. 5 Comprehensive working model of EPO function in the brain. Panels illustrate the suggested cellular mechanisms and effects of EPO/EPOR in CA1 (hypotheses and respective figure created by Hannelore Ehrenreich). **a** Functional challenge of pyramidal neurons (blue) via, e.g., learning of new complex tasks provokes physiological hypoxia in the involved neurons. Hypoxia in turn induces neuronal production/release of EPO, which initiates differentiation of diverse non-proliferating precursors (red) with currently unknown identity to neurons. **b** Neuronal EPO binds in an auto/paracrine manner to EPOR on pyramidal neurons (blue), leading to an increase in dendritic spines. EPO simultaneously binds to EPOR on likely diverse neighboring cells (red), ready to differentiate into neurons on demand. Together, these integrative steps may explain the consistently found improvement of cognitive function under rhEPO treatment and, even more importantly, delineate physiological mechanisms, accomplishing lasting adaptation to challenge via the brain EPO system.

intervals) of whole sections were performed. Dendrites included in the study were at least 200 μm in length. Per animal, six such dendrites of six different *Thy1-YFPH* expressing pyramidal neurons were randomly selected from the CA1 region. The stitching plugin in Fiji software (2.0.0) was used to reconstruct three-dimensional images of the apical dendrites. The spines were further sub-categorized as proximal (0–50 μm), medial (50–100 μm), medial-distal (100–150 μm), and distal (150–200 μm) segments of the dendrite, depending on their distance from the soma. The total density of spines was also analyzed. Based on their morphology[23,52], the spines were manually divided into (1) stubby, i.e., length of the protrusion was <1 μm and no neck is observed; (2) mushroom, when a clear head-like structure could be observed (maximum diameter of the head was at least 1.5 times the average length of the neck) and the total length of the protrusion was <1.5 μm; and (3) thin, i.e., the length of the protrusion was >1.5 μm or the length was between 1 and 1.5 μm and a clear head-like structure could not be distinguished.

For dendritic spine quantification using the Golgi–Cox method: Images were acquired using the Nikon Ti2 using a 100× objective (NA = 1.45). Stretches of mid-apical dendrites in CA1 pyramidal neurons were recorded with a *z*-stack size of

0.3 μm. Per animal, ten dendrites of ten different cells were quantified for the number of spines (calculated as spines per μm dendrite).

RNAscope in-situ hybridization (ISH): RNAscope® 2.5 HD Brown Reagent Kit (CatNo.322300), Advanced Cell Diagnostics (ACD), Hayward, CA, USA was used for the detection of EPO and EPOR mRNA. ISH was performed according to the manufacturer's instructions. Briefly, coronal cryosections of 15 μm thickness were mounted on SuperFrostPlus Slides, dried, and stored at −80 °C. Sections were then pretreated by dropwise addition of hydrogen peroxide and incubated for 10 min at RT. Slides were immersed in boiling target retrieval buffer for 15 min, followed by incubation with protease plus for 30 min at 40 °C. Sections were then hybridized with the corresponding target probe Mm-Epo-01 (CatNo.444941) or Mm-Epor (CatNo.412351) for 2 h at 40 °C, followed by a series of amplification and washing steps. Chromogenic signal detection was performed with 3,3′-diaminobenzidine (DAB) incubation for 20 min at RT. Sections were counterstained with 50% Mayer's hemalum (Merck) and mounted with EcoMount (BioCare Medical). Brown punctate dots in the CA1 were counted in a total of 12 hippocampi with 6 sections per animal using a light microscope (Olympus BX-50, Tokyo, Japan) equipped with a 100× oil immersion objective (NA = 1.35) and normalized to the area of the respective region (mm²). Sagittal 15 μm sections from kidney (P55) and heart (E11.5) of WT mice were used as positive controls for EPO and EPOR, respectively. According to manufacturer's instructions, each dot represents a single molecule of mRNA in these sections. The quantification is normalized and presented as percentage of the mean dot number of groups and time points [% value = (number/mm²)/(mean dot number/mm²) × 100].

Drop sequencing. *Tissue dissociation:* Juvenile male WT mice (P28; three mice/group to allow biological replication) were injected i.p. with placebo or EPO and sacrificed after 6 h. The hippocampi were dissected and sliced into 600 μm sections using McIlwain Tissue chopper (Cavey Laboratory Engineering Co. Ltd). The CA1 region was digested with a working solution of Papain/DNaseI in Earle's Balanced Salt Solution, according to manufacturer's instructions (Worthington Biochemical Corp). The samples were then incubated at 37 °C for 40 min with constant agitation before gentle manual trituration. The samples were centrifuged for 10 min at 200 × g at 4 °C. After discarding the Papain/DNaseI supernatant, cells were resuspended in 1 mL of sterile DMEM/F12 (Sigma) without phenol-red containing 3% fetal bovine serum (FBS; Life Technologies) and the suspension was passed through a 40 μm strainer cap (Corning) to yield a uniform single-cell suspension.

Single-cell barcoding and library preparation: Barcoded single cells, or STAMPs (single-cell transcriptomes attached to microparticles), and cDNA libraries were generated following the protocol[53]. Briefly, single-cell suspensions (100 cells/μl), droplet generation oil (Bio-Rad), and barcoded microparticles (ChemGenes; 120 beads/μl) were co-flowed through a FlowJEM aquapel-treated DropSeq microfluidic device (FlowJEM) and droplets were generated for 15 min. Captured RNA on the bead surface was recovered by washing the beads in saline-sodium citrate buffer and perflurooctanol solutions, and then reverse transcribed using Maxima H minus reverse transcriptase kit (ThermoFisher). Excess primer on the surface of the bead uncaptured by an RNA molecule was digested using Exonucleases I kit (ThermoFisher). A cDNA amplification PCR was performed using 10 μM SMART PCR primer and 2X Kapa HiFi HotStart ReadyMix (Kapa Biosystems) with 5000 beads per tube, and amplified for nine PCR cycles. The resulting samples were purified using AMPureXP beads (Beckman Coulter) and the quality and concentration of the cDNA was assessed using High-sensitivity DNA bioanalyzer (Agilent Technologies). Library sizes were adjusted using the Nextera Amplicon Tagmentase enzyme and DNA was amplified for 14 cycles using 10 μM New-P5-SMART PCR hybrid oligo, 10 μM Nextera Index, and the Nextera PCR mix (Nextera XT DNA Library Preparation kit; Illumina). Tagmented libraries were again purified (AMPureXP), quality controlled (high-sensitivity DNA Bioanalyzer), quantified (Qubit dsDNA HS assay kit; Life Technologies), and sequenced (Illumina Hi-seq 2500). All assays mentioned above have been performed according to manufacturer's protocol.

Single-cell RNA-seq processing: Unique molecular identifier (UMI) gene counts for each group (placebo or EPO) was imported into R (v3.4.1). *Seurat* (v2.3.0) function within the R environment was used for filtering, normalization, canonical correlation analyses (CCA), unsupervised clustering, visualization, and differential expression analyses.

Filtering and data normalization: Cells with minimum and maximum of 1000 and 8000 genes expressed (≥1 count), respectively, and the genes that were expressed in at least three cells were retained. Cells with >40% of counts on mitochondrial genes were excluded (Supplementary Fig. 1). After filtering, there were 14,061 genes in 390 cells from placebo and 14,971 genes in 583 cells from EPO group.

Gene UMI counts for each cell were normalized via natural-log normalization of gene UMI counts divided by total UMI counts per cell and scaled by 10,000. After normalization, scaled expression (*z*-scores for each gene) for downstream analyses was calculated.

Canonical correlation analysis: Integration of scRNA-seq data from the two groups (placebo and EPO) was performed using CCA. Top 1000 highly variable genes from each group were used to calculate canonical correlation vectors (reduced dimension) and subsequently, first 20 vectors were aligned using dynamic time warping.

ARTICLE

Clustering, visualization, and differential expression: Clustering was performed using "*FindClusters*" function with default parameters with resolution set to 1 and first 20 CCA aligned dimensions were used in the construction of the shared-nearest neighbor graph and to generate two-dimensional embeddings for data visualization using *t*SNE. Based on the visualization the glutamatergic cluster 0 and 1 were merged manually to represent a single cluster. The percentages of 'immature glutamatergic cells' for each mouse were: placebo 1.6%, 2.3%, and 4.3%; EPO 3.7%, 6.8%, and 7.0%. We used the "*FindAllMarkers*" function with default parameters and tested genes with a detected threshold of minimum of 25% of cells in either of the two clusters. Genes with an adjusted $p < 0.01$ were considered to be differentially expressed (for a list of cluster markers see Source Data File). A heatmap showing the top ten marker genes, i.e., differentially expressed genes per cluster is provided in the Supplementary Fig. 2.

Cell trajectory (pseudotime) analysis: Trajectory analysis of cells from the 'Immature Glutamatergic' and 'Mature Glutamatergic1' clusters ($n = 502$) was performed in *Monocle*2[25]. The trajectory was constructed according to the documentation of *Monocle*2. Prior to cell ordering, reclustering was performed to confirm robust detection of the immature cluster across methods, which revealed three clusters (one cluster largely corresponding to *Seurat*'s 'Immature Glutamatergic' cluster and two corresponding to *Seurat*'s 'Mature Glutamatergic1' cluster; Supplementary Fig. 3a). Subsequently, dimension reduction using the 'DDRTree' method was performed. Differentially expressed genes ($q < 0.01$) between the three clusters obtained by reclustering in *Monocle*2 were used as input for pseudotemporal ordering.

Quantification and statistical analysis. All statistical analysis was performed using GraphPad Prism 5. For comparisons across multiple groups, a two-way analysis of variance (ANOVA) was used. For comparisons across two groups, an unpaired Student's *t*-test was performed. A $p < 0.05$ is considered statistically significant. Variance was similar between compared groups for their respective experiments. All values represent mean ± SEM (standard error of the mean). All analysis and quantification were performed in a double-blinded fashion.

Reporting summary. Further information on research design is available in the Nature Research Reporting Summary linked to this article.

Data availability
The data that support this study are available from the corresponding authors upon reasonable request. A Source Data File is provided. Raw and processed scRNA-seq data are available via the GEO with accession code GSE144444.

Code availability
Analysis scripts are accessible from github: https://github.com/AgnesSteixner/EPO_Wakhloo_et_al_NATCOMM.

References
1. Krantz, S. B. Erythropoietin. *Blood* **77**, 419–434 (1991).
2. Jelkmann, W. Regulation of erythropoietin production. *J. Physiol.* **589**, 1251–1258 (2011).
3. Digicaylioglu, M. et al. Localization of specific erythropoietin binding sites in defined areas of the mouse brain. *Proc. Natl Acad. Sci. USA* **92**, 3717–3720 (1995).
4. Marti, H. H. et al. Erythropoietin gene expression in human, monkey and murine brain. *Eur. J. Neurosci.* **8**, 666–676 (1996).
5. Shingo, T., Sorokan, S. T., Shimazaki, T. & Weiss, S. Erythropoietin regulates the in vitro and in vivo production of neuronal progenitors by mammalian forebrain neural stem cells. *J. Neurosci.* **21**, 9733–9743 (2001).
6. Brines, M. & Cerami, A. Emerging biological roles for erythropoietin in the nervous system. *Nat. Rev. Neurosci.* **6**, 484 (2005).
7. Sirén, A.-L., Faßhauer, T., Bartels, C. & Ehrenreich, H. Therapeutic potential of erythropoietin and its structural or functional variants in the nervous system. *Neurotherapeutics* **6**, 108–127 (2009).
8. Schuler, B. et al. Acute and chronic elevation of erythropoietin in the brain improves exercise performance in mice without inducing erythropoiesis. *FASEB J.* **26**, 3884–3890 (2012).
9. Ehrenreich, H. et al. Exploring recombinant human erythropoietin in chronic progressive multiple sclerosis. *Brain* **130**, 2577–2588 (2007).
10. Ehrenreich, H. et al. Improvement of cognitive functions in chronic schizophrenic patients by recombinant human erythropoietin. *Mol. Psychiatry* **12**, 206 (2007).
11. Wüstenberg, T. et al. EPO treatment preserves gray matter in discrete brain regions of chronic schizophrenic patients: indication of areas with most progressive neurodegeneration inherent to the disease process. *Mol. Psychiatry* **16**, 1 (2011).
12. Miskowiak, K. W. et al. Recombinant human erythropoietin for treating treatment-resistant depression: a double-blind, randomized, placebo-controlled phase 2 trial. *Neuropsychopharmacology* **39**, 1399 (2014).
13. Miskowiak, K. W. et al. Effects of erythropoietin on hippocampal volume and memory in mood disorders. *Biol. Psychiatry* **78**, 270–277 (2015).
14. Adamcio, B. et al. Erythropoietin enhances hippocampal long-term potentiation and memory. *BMC Biol.* **6**, 37 (2008).
15. El-Kordi, A., Radyushkin, K. & Ehrenreich, H. Erythropoietin improves operant conditioning and stability of cognitive performance in mice. *BMC Biol.* **7**, 37 (2009).
16. Sargin, D. et al. Expression of constitutively active erythropoietin receptor in pyramidal neurons of cortex and hippocampus boosts higher cognitive functions in mice. *BMC Biol.* **9**, 27 (2011).
17. Hassouna, I. et al. Revisiting adult neurogenesis and the role of erythropoietin for neuronal and oligodendroglial differentiation in the hippocampus. *Mol. Psychiatry* **21**, 1752 (2016).
18. Sirén, A.-L. et al. Erythropoietin prevents neuronal apoptosis after cerebral ischemia and metabolic stress. *Proc. Natl Acad. Sci. USA* **98**, 4044–4049 (2001).
19. Digicaylioglu, M. & Lipton, S. A. Erythropoietin-mediated neuroprotection involves cross-talk between Jak2 and NF-κB signalling cascades. *Nature* **412**, 641 (2001).
20. Byts, N. et al. Essential role for Stat5 in the neurotrophic but not in the neuroprotective effect of erythropoietin. *Cell Death Differ.* **15**, 783 (2008).
21. Agarwal, A. et al. In vivo imaging and noninvasive ablation of pyramidal neurons in adult NEX-CreERT2 mice. *Cereb. Cortex* **22**, 1473–1486 (2011).
22. Feng, G. et al. Imaging neuronal subsets in transgenic mice expressing multiple spectral variants of GFP. *Neuron* **28**, 41–51 (2000).
23. Kasai, H., Fukuda, M., Watanabe, S., Hayashi-Takagi, A. & Noguchi, J. Structural dynamics of dendritic spines in memory and cognition. *Trends Neurosci.* **33**, 121–129 (2010).
24. Wu, Y. E., Pan, L., Zuo, Y., Li, X. & Hong, W. Detecting activated cell populations using single-cell RNA-seq. *Neuron* **96**, 313–329. e316 (2017).
25. Qiu, X. et al. Reversed graph embedding resolves complex single-cell trajectories. *Nat. Methods* **14**, 979 (2017).
26. Liebetanz, D. et al. A highly sensitive automated complex running wheel test to detect latent motor deficits in the mouse MPTP model of Parkinson's disease. *Exp. Neurol.* **205**, 207–213 (2007).
27. Kietzmann, T., Mennerich, D. & Dimova, E. Y. Hypoxia-inducible factors (HIFs) and phosphorylation: impact on stability, localization, and transactivity. *Front. Cell Dev. Biol.* **4**, 11 (2016).
28. Kimura, W. et al. Hypoxia fate mapping identifies cycling cardiomyocytes in the adult heart. *Nature* **523**, 226 (2015).
29. Morgan, J. I., Cohen, D. R., Hempstead, J. L. & Curran, T. Mapping patterns of c-fos expression in the central nervous system after seizure. *Science* **237**, 192–197 (1987).
30. Dessypris, E., Graber, S. E., Krantz, S. B. & Stone, W. J. Effects of recombinant erythropoietin on the concentration and cycling status of human marrow hematopoietic progenitor cells in vivo. *Blood* **72**, 2060–2062 (1988).
31. Grover, A. et al. Erythropoietin guides multipotent hematopoietic progenitor cells toward an erythroid fate. *J. Exp. Med.* **211**, 181–188 (2014).
32. Brown, G. & Ceredig, R. Modelling the hematopoietic landscape. *Front. Cell Dev. Biol.* **7**, 104 (2019).
33. Manalo, D. J. et al. Transcriptional regulation of vascular endothelial cell responses to hypoxia by HIF-1. *Blood* **105**, 659–669 (2005).
34. Zhao, W., Kitidis, C., Fleming, M. D., Lodish, H. F. & Ghaffari, S. Erythropoietin stimulates phosphorylation and activation of GATA-1 via the PI3-kinase/AKT signaling pathway. *Blood* **107**, 907–915 (2006).
35. Zhang, K., Zhu, L. & Fan, M. Oxygen, a key factor regulating cell behavior during neurogenesis and cerebral diseases. *Front. Mol. Neurosci.* **4**, 5 (2011).
36. Dale, E., Ben Mabrouk, F. & Mitchell, G. Unexpected benefits of intermittent hypoxia: enhanced respiratory and nonrespiratory motor function. *Physiology* **29**, 39–48 (2014).
37. Cao, L. et al. VEGF links hippocampal activity with neurogenesis, learning and memory. *Nat. Genet.* **36**, 827 (2004).
38. Miskowiak, K., O'Sullivan, U. & Harmer, C. J. Erythropoietin enhances hippocampal response during memory retrieval in humans. *J. Neurosci.* **27**, 2788–2792 (2007).
39. Cao, J. et al. The single-cell transcriptional landscape of mammalian organogenesis. *Nature* **566**, 496 (2019).
40. Kesner, R. P., Lee, I. & Gilbert, P. A behavioral assessment of hippocampal function based on a subregional analysis. *Rev. Neurosci.* **15**, 333–352 (2004).
41. McKenzie, I. A. et al. Motor skill learning requires active central myelination. *Science* **346**, 318–322 (2014).

ARTICLE

42. Altman, J. & Das, G. D. Autoradiographic and histological evidence of postnatal hippocampal neurogenesis in rats. *J. Comp. Neurol.* **124**, 319–335 (1965).

43. Kaplan, M. S. & Hinds, J. W. Neurogenesis in the adult rat: electron microscopic analysis of light radioautographs. *Science* **197**, 1092–1094 (1977).

44. Rakic, P. Adult neurogenesis in mammals: an identity crisis. *J. Neurosci.* **22**, 614–618 (2002).

45. Doetsch, F. The glial identity of neural stem cells. *Nat. Neurosci.* **6**, 1127 (2003).

46. Gould, E. How widespread is adult neurogenesis in mammals? *Nat. Rev. Neurosci.* **8**, 481 (2007).

47. Sanai, N. et al. Corridors of migrating neurons in the human brain and their decline during infancy. *Nature* **478**, 382 (2011).

48. Aimone, J. B. et al. Regulation and function of adult neurogenesis: from genes to cognition. *Physiol. Rev.* **94**, 991–1026 (2014).

49. Hughes, E. G., Kang, S. H., Fukaya, M. & Bergles, D. E. Oligodendrocyte progenitors balance growth with self-repulsion to achieve homeostasis in the adult brain. *Nat. Neurosci.* **16**, 668 (2013).

50. Muzumdar, M. D., Tasic, B., Miyamichi, K., Li, L. & Luo, L. A global double-fluorescent Cre reporter mouse. *Genesis* **45**, 593–605 (2007).

51. Goebbels, S. et al. Genetic targeting of principal neurons in neocortex and hippocampus of NEX-Cre mice. *Genesis* **44**, 611–621 (2006).

52. Guirado, R. et al. The dendritic spines of interneurons are dynamic structures influenced by PSA-NCAM expression. *Cereb. Cortex* **24**, 3014–3024 (2013).

53. Macosko, E. Z. et al. Highly parallel genome-wide expression profiling of individual cells using nanoliter droplets. *Cell* **161**, 1202–1214 (2015).

Author contributions

Concept, study design, and supervision: H.E., together with K.-A.N. and J.N. Experimental design and Interpretation: H.E., together with D.W. and F.S. Data acquisition and analysis: D.W., F.S., Y.C., U.J.B., V.B., A.A.S.-K., L.W., A.R., S.A., A.S., I.H., K.S., A.Q.I., M.Z., H.W., H.M., K.M., S.M.W., S.B., K.-A.N., J.N., and H.E. Drafting manuscript: H.E., together with D.W. and F.S. Drafting display items: H.E. together with D.W., F.S., and Y.C. All authors read and approved the final version of the manuscript.

Competing interests

H.E. has submitted/holds user patents for EPO in stroke, schizophrenia, and M.S. Henrik Martens is an employee of Synaptic Systems GmbH. Apart from that, the authors declare no competing interests.

Additional information

Supplementary information is available for this paper at https://doi.org/10.1038/s41467-020-15041-1.

Correspondence and requests for materials should be addressed to K.-A.N. or H.E.

Peer review information *Nature Communications* thanks the anonymous reviewers for their contribution to the peer review of this work. Peer reviewer reports are available.

Reprints and permission information is available at http://www.nature.com/reprints

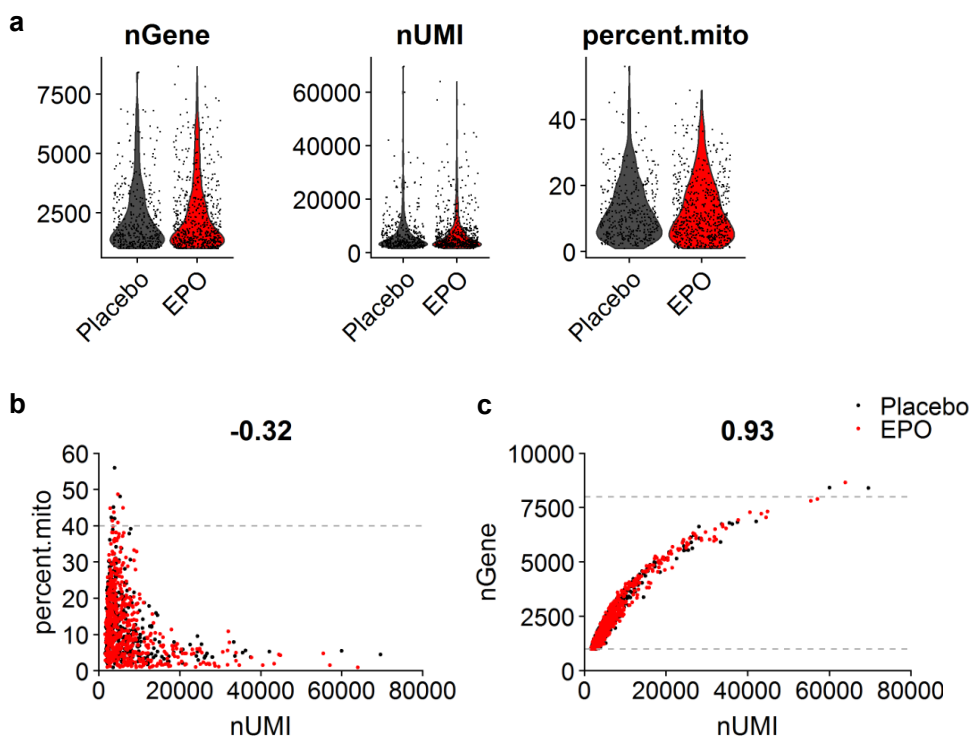**Publisher's note** Springer Nature remains neutral with regard to jurisdictional claims in published maps and institutional affiliations.

SUPPLEMENTARY INFORMATION

Functional hypoxia drives neuroplasticity and neurogenesis via brain erythropoietin
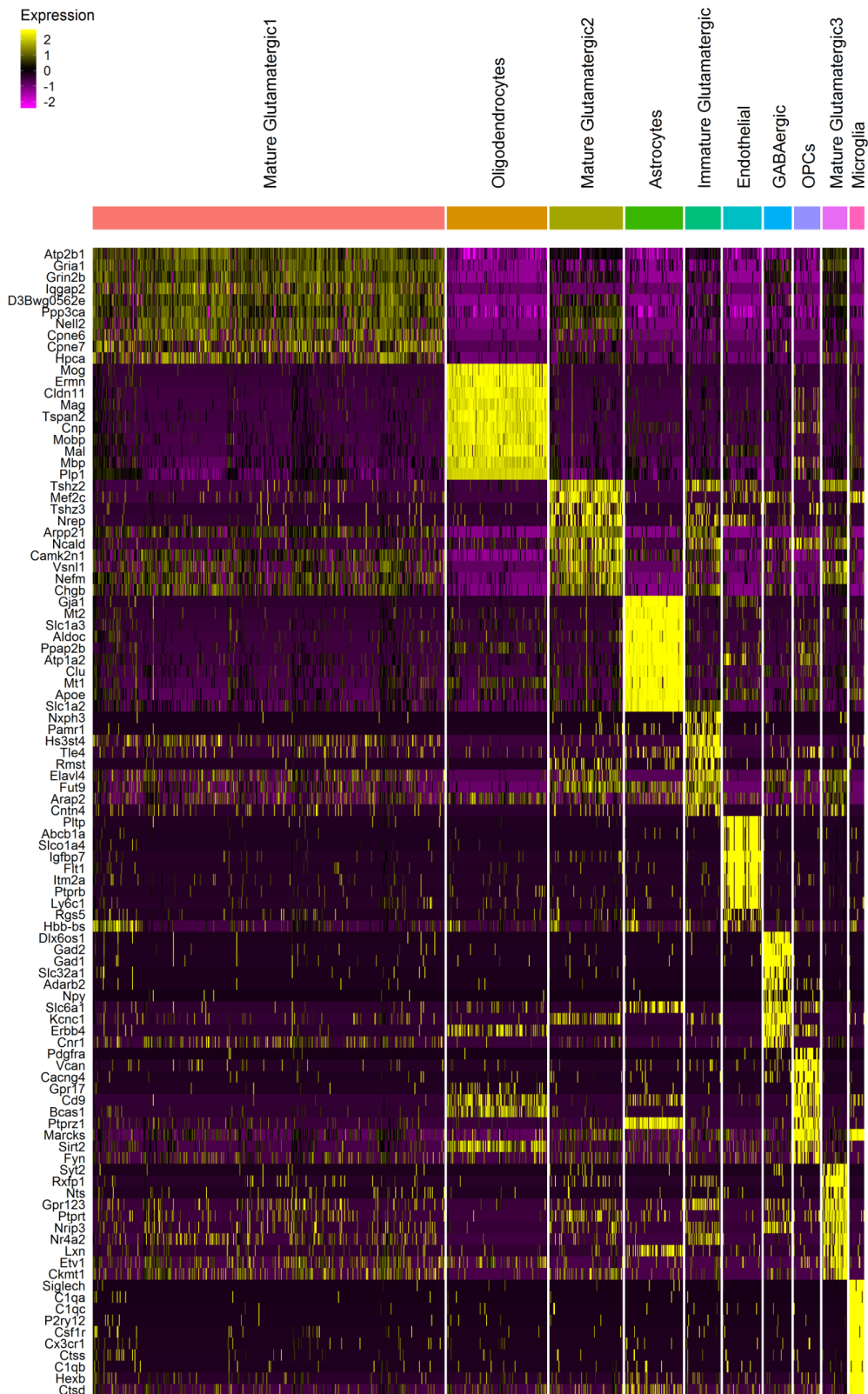
Wakhloo et al

Wakhloo et al Supplementary Figure 1

***Supplementary Figure 1:* DropSeq quality control information**

Quality control information on pre-filtered (genes expressed in ≥3 cells, cells expressing ≥1000 genes) raw data from 6 male mice (P28). **(a)** Placebo and EPO treated groups are widely comparable with regard to major quality control readouts: number of genes detected (nGene), number of UMIs detected (nUMI) and percentage of mitochondrial genes expressed. **(b)** Correlation of percentage of mitochondrial genes expressed (percent.mito) and number of UMIs detected (nUMI), colored by treatment group. Cells above the dashed grey line were discarded before downstream analysis. **(c)** Correlation between number of genes (nGene) and number of UMIs detected (nUMI), colored by treatment group. Cells outside the upper and lower dashed grey lines were discarded before downstream analysis.

Wakhloo et al Supplementary Figure 2

Supplementary Figure 2: **Heatmap of top 10 marker genes (ordered by average log fold-change) per cluster.**

Wakhloo et al Supplementary Figure 3

a

b

Legend
Oligo: Oligodendrocytes
Astro: Astrocytes
Endo: Endothelial cells
GABA: GABAergic neurons
Micro: Microglia
OPCs: Oligodendrocyte percursor cells

c

	Tbr1	Dcx	Tle4	Any	Triple+	Tbr1+Dcx	Tbr1+Tle4	Tle4+Dcx
				% positive cells				
Immature (pseudotime >15)	60	30	100	100	20	20	60	30
Immature (pseudotime < 15)	33.3	33.3	69.4	88.9	8.3	13.9	25	16.7
Mature	9.6	8.6	18.6	30.7	0.7	1.8	3.3	1.8

d
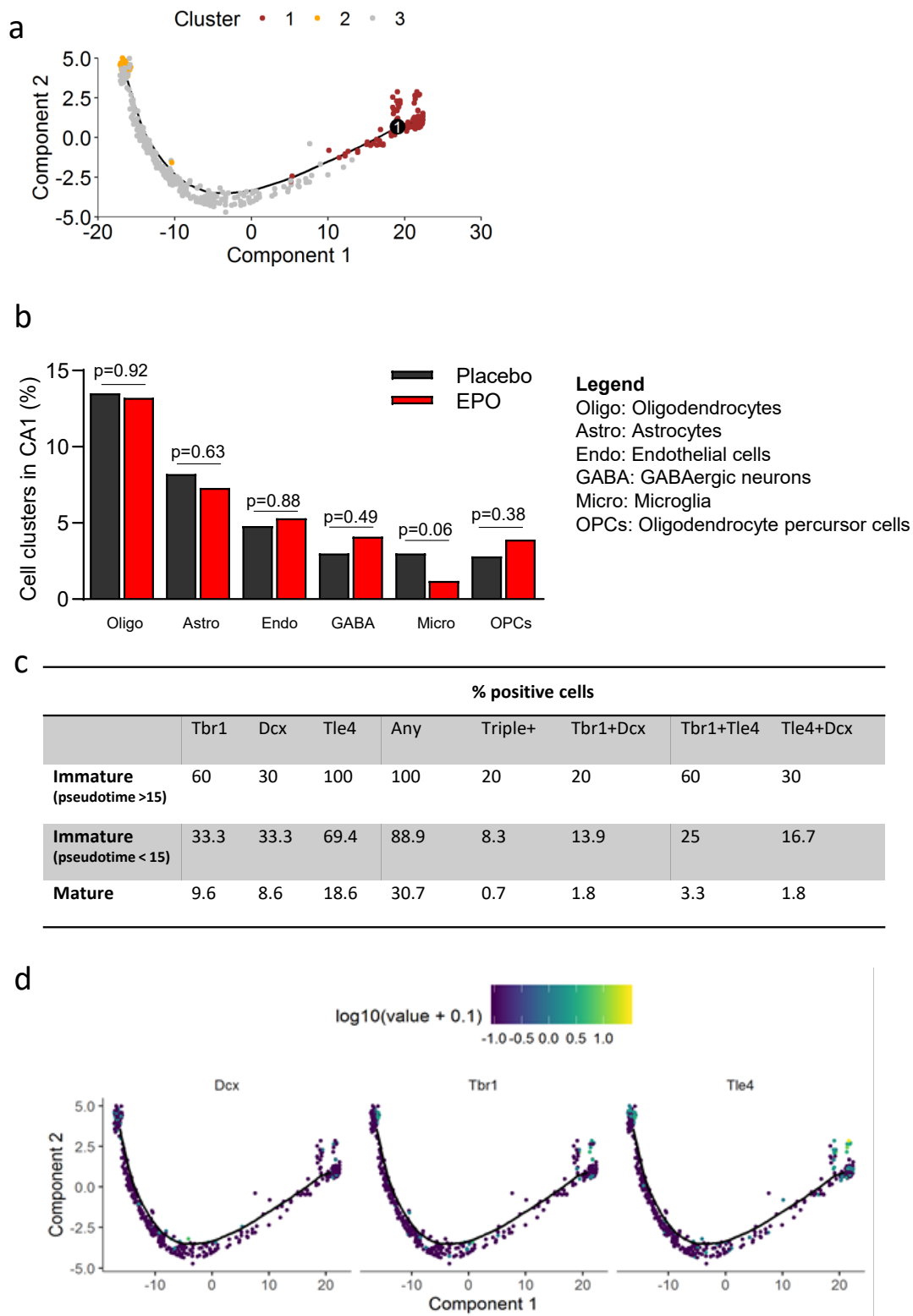
Wakhloo et al Supplementary Figure 3, continued

e
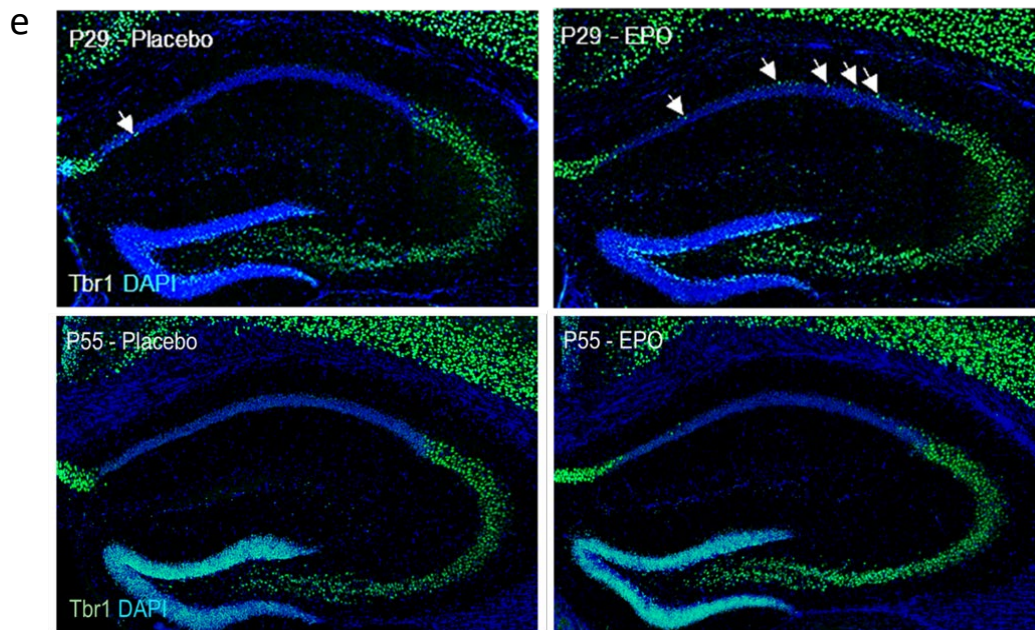
Supplementary Figure 3: **(a) Characterization of the immature glutamatergic cluster by trajectory analysis.** Trajectory colored by clusters as identified by *Monocle2*. Cluster 2 (yellow) widely corresponds to the 'Immature Glutamatergic' cluster defined by Seurat. Clusters 1 (brown) and 3 (grey) largely correspond to the 'Mature Glutamatergic1' cluster (Figure 2g). **(b) Percentage of cells in the respective non-glutamatergic cell clusters** per treatment condition (EPO: n=583, placebo: n=390); 2-tailed Fisher's exact test. **(c) Percentage of cells expressing immature cluster markers.** The table-figure shows the percentage of cells included in the trajectory analysis (split by pseudotime, i.e. high vs. low, and cluster identity) that are positive for 3 characteristic markers taken as examples of the immature cluster. Percentage of cells expressing each marker (and their different combinations) within 3 cell groups, i.e. immature with high pseudotime, immature with low pseudotime and mature cells, are provided. Note that marker expression of immature cells with high pseudotime resembles more closely that of immature cells with low pseudotime than that of mature cells, suggesting an immature identity of these cells despite of their high pseudotime. In particular, Dcx - a well-established marker of immature neurons - is detected in 30% of immature neurons with pseudotime >15 and 33% of immature neurons with pseudotime <15, but only in 8.6% of mature neurons, providing additional support for the immature identity of cells. **(d) Immature cluster marker expression along the trajectory.** Expression of 3 selected prominent markers of the immature cluster along the trajectory, showing that the population of immature neurons with pseudotime >15 clearly expresses these 3 markers highly similar to the remaining immature neurons. **(e) Tbr1 expression in the hippocampus.** IHC staining for Tbr1 at P29 and P55 shows that in CA1, Tbr1 upon EPO is strongly detected at P29 but rarely at P55. Tbr1+ cells in dentate gyrus serve as positive control for both time-points.

109

Wakhloo et al Supplementary Figure 4
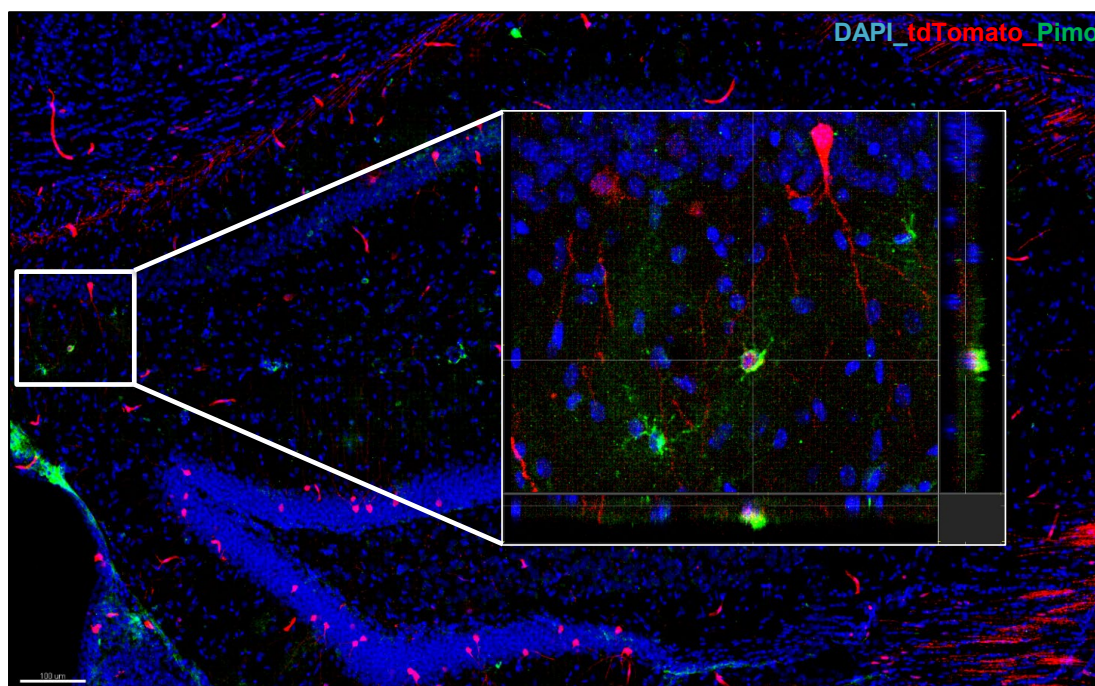
Supplementary Figure 4: **Validation of hypoxia by pimonidazole staining**

Hypoxic cells were validated with pimonidazole staining (according to *Sato et al 2011*) in CAG-CreERT2-ODD::R26R-tdTomato mice. Mice received a single tamoxifen injection (100mg/kg body weight), followed after 16 hours by pimonidazole administration, and were sacrificed 90min later. Double-labeled hypoxic cells occur typically dispersed (compare *Kimura et al 2015*). Scale bar represents 100µm in the overview image.

Pimonidazole (Hypoxyprobe-1 Mab1) from NPI (Belmont, MA USA) is used to detect hypoxia in cells and tissue. Pimonidazole (60mg/kg body weight) solution is injected intravenously (tail vein) and staining performed according to manufacturer's instructions.

Wakhloo et al Supplementary Figure 5

P1 Sense — P3 Antisense — P2 Antisense
FRT — loxP — FRT loxP — loxP
LacZ — neo — Exon3-6
Eucomm original modified allele
P1-P3: 296bp P1-P2: >5000bp

P1 Sense — P2 Antisense — P4 Antisense
Exon3-6
FRT recombined/Floxed allele P1-P2: 759bp

P1 Sense — P4 Antisense
LoxP recombined, P1-P4: 203bp

P1 Sense — P2 Antisense — P4 Antisense
Exon3-6
Wildtyp allele P1-P2: 541bp
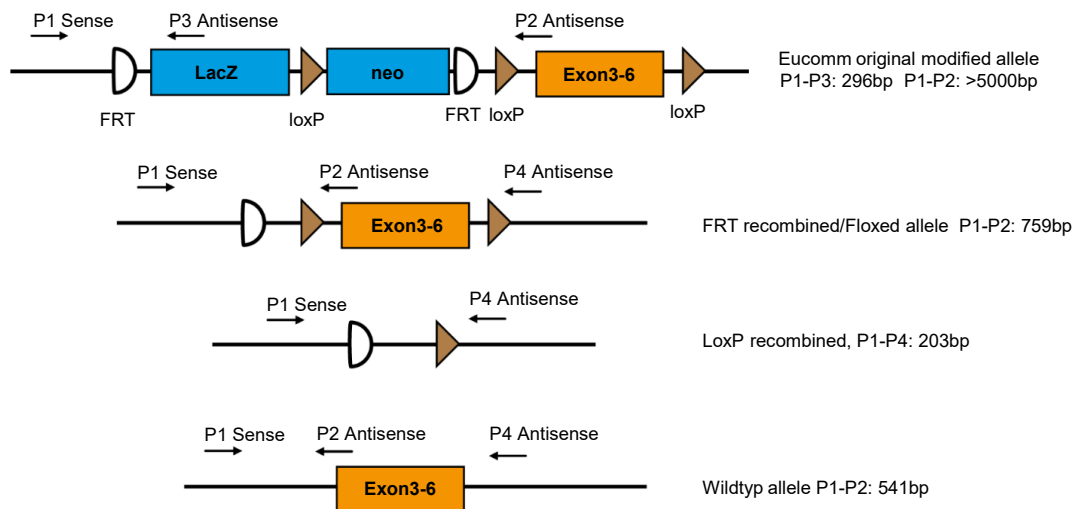
P1: 29825 5'-GTCCTCAGGACTGGGTGGC-3'
P2: 29826 5'-CATCGATGTCGCTCCCAT-3'
P3: 15048 5'-CAACGGGTTCTTCTGTTAGTCC-3'
P4: 32002 5'-GAGCTCAGACCATAACTTCG-3'
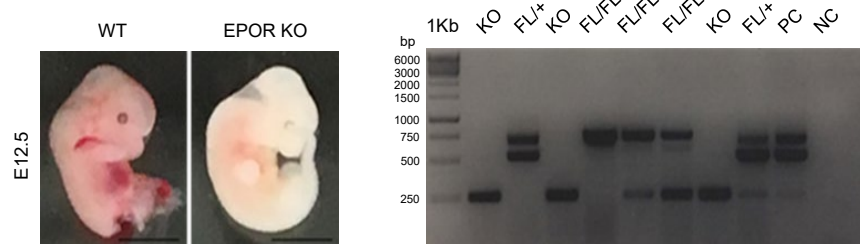
Supplementary Figure 5: **Description of pyramidal neuronal EPOR KO**

To generate the specific conditional EPOR KO in pyramidal neurons (NexCre::EPORflox/flox), we had to first validate whether the generated EPOR KO mice are indeed functional knockouts. Therefore cross breeding of the female EPORflox/flox mice with male mice homozygous for the Cre-recombinase gene (under control of the ubiquitous adenovirus EIIA-promoter), was used to obtain deleter mice. EIIA-regulated Cre-recombinase was expressed in pre-implantation embryos leading to site specific deletion of LoxP flanked (fl) sequence in all tissues including germ cells. Interbreeding of first generation progenies resulted in efficient germline transmission of the deletion to subsequent generations. The presence of deleted alleles was determined by PCR-based genotyping using specific primers for EPOR (listed below) and also further confirmed using EIIA-cre primers. We were able to observe a global EPOR KO at E12.5, validating functionality of generated EPOR KO mice. P1-4 (primer 1-4); E12.5 (embryonic day 12.5); PC (positive control); NC (negative control).

Supplementary References

Sato, Y., Endo, H., Okuyama, H., Takeda, T., Iwahashi, H., Imagawa, A., Yamagata, K., Shimomura, I. & Inoue, M. Cellular hypoxia of pancreatic β-cells due to high levels of oxygen consumption for insulin secretion in vitro. *Journal of Biological Chemistry* **286**, 12524-12532 (2011).

Kimura, W., Xiao, F., Canseco, D. C., Muralidhar, S., Thet, S., Zhang, H. M., Abderrahman, Y., Chen, R., Garcia, J. A., Shelton, J. M., Richardson, J., Abderrahman, A., Aroumougame, A., Liang, H., Xing, C., Lu, Z., Zhang, C. & Sadek, H. Hypoxia fate mapping identifies cycling cardiomyocytes in the adult heart. *Nature* **523**, 226 (2015).

6 Summary and conclusion

The landscape of neuropsychiatric diseases is vast and heterogeneous. Its complexity lies in the fact that delineation of health and disease borders is often difficult and co-morbidities are frequent. Furthermore, it proves challenging to establish reliable inter-disease borders in view of the very variable presentation of disease phenotypes across affected individuals. Treatments for many of these diseases are of limited effectiveness and often associated with unwanted side-effects (Agid et al., 2011; Conley and Buchanan, 1997; Lieberman et al., 1993). Hence, the idea that endogenous bodily systems can be stimulated to achieve a shift from a disease towards a healthy state appears even more attractive. The brain hypoxia/EPO-system presents such an endogenous target for potential treatment as shown previously (Ehrenreich et al., 2004; Ehrenreich et al., 2007a).

The current thesis project aimed to first provide a better characterization of patients affected by a frequent and deleterious comorbidity of psychiatric disease, namely poly-toxicomania, regarding their exposure to environmental risk factors in early life as well as possible genetic risk factors associated with this condition (Project I). The second part of the thesis explored the effects of hypoxia and EPO on the brain to better understand its mode of action and prepare the grounds for potential future treatment strategies. Here, the main focus was to track hypoxia in the healthy adult brain with the use of a reporter mouse line. In this context, the response to motor-cognitive challenge as inducer of func-tional hypoxia was of particular interest (Project II). Additionally, this thesis work tried to further elucidate the influence of hypoxia and EPO on neurodifferentiation, microglia and the neuron-microglia balance (Project III).

In the frame of Project I, we could show that the preadult accumulation of environ-mental risk factors is strongly associated with polytoxicomania. The presented data re-vealed the considerable impact of accumulated risk factor exposure on psychiatric out-comes. Our findings are in accordance with previous studies illustrating the far-reaching effects of environmental risk accumulation in early life, e.g. on violent aggression (Mit-jans et al., 2019) and age at schizophrenia onset (Stepniak et al., 2014). Since our sample consisted of schizophrenia/schizoaffective patients, our findings do not allow direct con-clusions about other disease groups or the general population. Yet, the generalizability of findings on risk accumulation and violent aggression to various independent cohorts of healthy and diseased individuals suggests that the effects observed on polytoxicoma-nia might also not be exclusive to the cohort of schizophrenia patients. Applicability to a wider population appears plausible, especially because the same set of risk factors was investigated in both studies. In our study, cannabis as a "secondary risk factor" and known gateway drug (Fergusson and Horwood, 2000; Fergusson et al., 2006a; Hall

and Lynskey, 2005; Kandel and Kandel, 2015; Lynskey et al., 2003; Olthuis et al., 2013; Secades-Villa et al., 2015) proved to be an exceptionally prominent predictor of (preadult) polytoxicomania. This finding underlines the critical importance socio-political decisions regarding broader availability of cannabis, e.g. through legalization and commercialization, may have for the prevalence of polytoxicomania and other debilitating psychiatric disease conditions such as psychosis (Arseneault et al., 2002; Di Forti et al., 2009; Fergusson et al., 2006a; Murray and Hall, 2020; Semple et al., 2005; Van Os et al., 2002). Notably, cigarette smoking was not directly associated with polytoxicomania, but probably exerts its function as co-gateway drug by lowering the barrier to use other "harder" drugs such as cannabis. In addition to environmental effects, we reported the first genetic association signals with preadult polytoxicomania. These associations were identified with the use of a newly developed GWAS-PGAS approach that fully utilizes the potential of relative small, but extensively phenotyped samples. Whereas these first genetic associations are exciting and several of the identified variants have previously been associated with related phenotypes, e.g. alcohol dependence, cannabis use, risky behaviors, these results await replication in a - hopefully at some point available - independent cohort. Irrespective of this, it needs to be emphasized that environmental factors present a by magnitudes stronger determinant of polytoxicomanic behavior than the here investigated common genetic variants.

Project II was designed to obtain a better understanding of hypoxia as a physiological condition in the brain. To this end, a tamoxifen-inducible hypoxia-reporter mouse line was utilized to permanently label cells that underwent hypoxia. Interestingly, already at baseline, i.e., inspiratory normoxia and normal home-cage activity of mice, dispersed hypoxic cells were observed across the brain. The density of labelled cells was particularly high in the olfactory bulb - a region that is expected to have generally high neuronal activity in rodents due to its sensory importance. Under inspiratory hypoxia, the number of labelled cells was markedly increased in the hippocampus and to a somewhat lesser degree in the cortex. In addition to these regional differences, the amount of hypoxia-labelling varied between cell types: The highest fraction of labelled cells was observed among neurons and endothelial cells, whereas labelling of other cells types was less abundant (e.g. astrocytes, oligodendrocytes) or even absent (microglia). Notably, the observed cell type differences could not be explained by variable abundance of construct RNA in the different cell types. Expression data suggested Hk2 as a possible mediator of this variable hypoxia responsivity across cell types. This enzyme might confer relative resistance to hypoxia by promoting a metabolic shift from oxydative phoshorylation to glycolysis (Wolf et al., 2011; Yasuda et al., 2004). Another central finding of this project was that motor-cognitive challenge (CRW) leads to an increase in the number of hypoxic cells in the hippocampus. This phenomenon was termed "functional hypoxia" as it reflects the physiological occurrence of cellular hypoxia upon intense neuronal activation and probably acts as a trigger for processes of neuroplasticity. This phenomenon is in line with previous observations of a rise in Hif1α and its target genes after intensive exercise (Halliday et al., 2019). More generally, functional hypoxia likely induces cellular adaptation in

a range of neuronal and non-neuronal cell types, e.g. astrocytes and oligodendrocytes, in response to brain activity to facilitate the process of learning. This discovery is highly intriguing as it shows that besides its relevance in neurogenic niches of the brain, hypoxia is also a common condition in mature cells throughout the brain and presumably mediates cellular changes necessary for learning. This finding contributes to the understanding of the mechanisms behind previously observed beneficial effects of hypoxia, cognitive challenge and physical exercise on cognitive performance (Gheysen et al., 2018; Hillman et al., 2008; Pajonk et al., 2010; Wang et al., 2020).

In order to gain additional insight into the underlying mechanisms, a detailed investigation of neuronal response to hypoxia and specifically EPO, as one of the key hypoxia-induced genes, was conducted within Project III. Here, we studied EPO effects on cognitive performance as well as on neuronal characteristics and neurodifferentiation. Moreover, we demonstrated effects of EPO and hypoxia on microglia and how these are linked to processes of neurodifferentiation. In young adult (P55) and older (4 months old) mice, 3-week rhEPO treatment led to a marked increase in newly differentiated neurons in CA1. Strikingly, already six hours after a single EPO injection, an increase of immature neurons was observed in the CA1 using scRNA-seq, both numerically and in form of a decreased pseudotime in EPO-treated neurons. This population of very young immature neurons was characterized by the expression of various immature neuron markers, including *doublecortin* (*Dcx*), *Tbr1* and *Tle4*. Under the influence of EPO, these neurons continued to mature. After one week of EPO treatment they were characterized by the expression of *Zbtb20*, a marker of intermediate maturity and of great importance for the differentiation of CA1 neurons (Nielsen et al., 2014; Nielsen et al., 2010; Xie et al., 2010), while losing expression of early markers such as *Tbr1* to eventually express Ctip2 (also known as *Bcl11b - BAF Chromatin Remodeling Complex Subunit BCL11B*) at maturity around two weeks later (Figure 2).

While EPO as well as endogenous functional hypoxia (CRW) certainly substantially affect neurons, these stimuli simultaneously modify microglial number and behavior. We could show that these microglial changes are "paving the way" for the boost in neurodifferentiation that occurs upon EPO administration and functional hypoxia. The initial, rapid numeric reduction of microglia through apoptosis is followed by a decreased proliferation activity that helps to maintain lowered microglial numbers. At the same time, microglia exhibit a less-activated phenotype and establish less contacts with neurons as compared to placebo treatment. These changes appear to allow and support enhanced neuronal differentiation under EPO. Microglial CSF1R-signalling as central survival signal for microglia (Elmore et al., 2014) via its neuronally expressed ligand IL34 presented as a likely mechanism mediating the cross-talk between neurons and microglia in this situation. While *Il34* expression was reduced under EPO and inspiratory hypoxia (thereby weakening the survival signal for microglia), a - presumably compensatory - upregulation of *Csf1r* was observed. Accordingly, newly differentiating neurons constrain their stimulating signal to microglia in order to ensure their own undisturbed differentiation. Our findings are well in line with previous reports of microglial adaptation to exercise
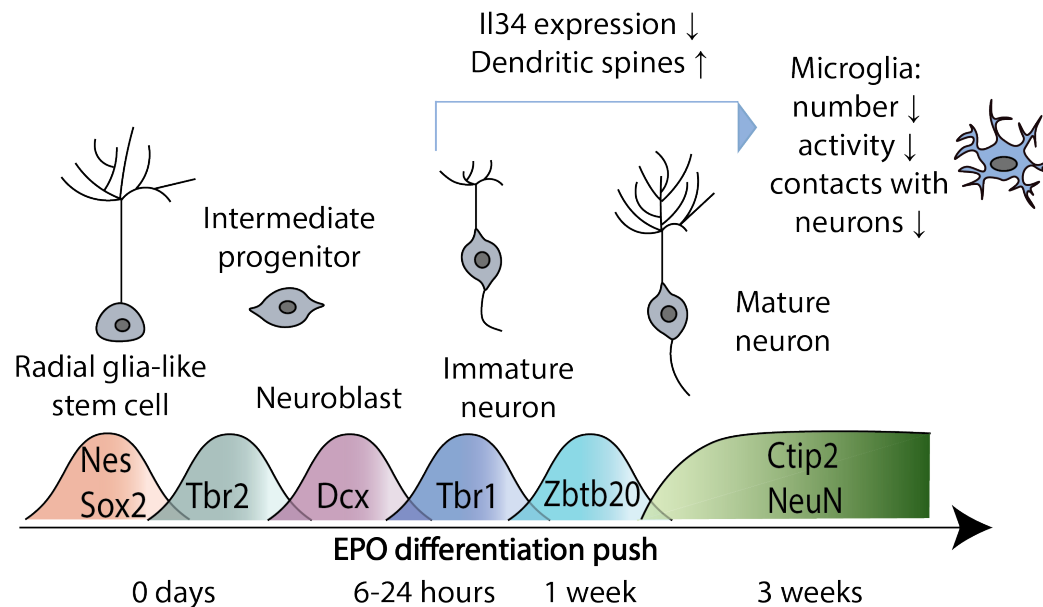
FIGURE 2: **Neuronal differentiation in the hippocampus under EPO.** Under influence of endogenously expressed (hypoxia) or administered EPO, early progenitors are activated and differentiate into immature neurons expressing initially DCX, followed by TBR1 and ZBTB20 before reaching maturity, marked by expression of CTIP2 and NEUN. Simultaneously to increased neuronal differentiation and dendritic spine increase, microglial numbers and activation as well as their established contacts with neurons are decreased, likely partially mediated by a reduction in IL34 expression of immature and mature neurons.

that lead to their decreased activation and proliferation in the hippocampus (Kohman et al., 2012), while supporting adult neural precursor activation (Vukovic et al., 2012). These reports can now be interpreted as microglial response to physiological endogenous hypoxia that was triggered by exercise. This perspective allows to acknowledge mild to moderate hypoxia (endogenously or exogenously induced) as a facilitator of neuroplasticity, neuronal differentiation and the consequently necessary adaptive changes in microglia.

In conclusion, this thesis work started from the detailed study of polytoxicomania as a clinical phenotype that is often observed in schizophrenic and other psychiatric patients and progressed to the experimental investigation of hypoxia and EPO as important endogenous players in brain function and plasticity with great therapeutic potential for neuropsychiatric and neurodegenerative diseases. Findings suggest that development of polytoxicomania is strongly influenced by the accumulation of environmental risk factors in early life. In comparison, the here identified first genetic associations were considerably weaker. Furthermore we could show that hypoxia occurs under physiological conditions (normoxia baseline and upon motor-cognitive challenge) in various cell

types across the brain. This functional hypoxia stimulates, similarly to direct EPO administration, processes of neuronal differentiation in the CA1 by orchestrating the fine balance between neurons and microglia. Both, EPO and hypoxia, thus present powerful instruments that can potentially be applied in various disease conditions as therapeutic measures that exploit endogenous physiological mechanisms to foster cognitive function and regeneration in the brain.

Bibliography

Adamcio, B., Sargin, D., Stradomska, A., Medrihan, L., Gertler, C., Theis, F., . . . Ehrenreich, H. (2008). Erythropoietin enhances hippocampal long-term potentiation and memory. *BMC Biology*, *6*(1), 37.

Adelmann, P. K. (2005). Social environmental factors and preteen health-related behaviors. *Journal of Adolescent Health*, *36*(1), 36–47.

Agid, O., Shapira, B., Zislin, J., Ritsner, M., Hanin, B., Murad, H., . . . Lerer, B. (1999). Environment and vulnerability to major psychiatric illness: A case control study of early parental loss in major depression, bipolar disorder and schizophrenia. *Molecular Psychiatry*, *4*(2), 163–172.

Agid, O., Arenovich, T., Sajeev, G., Zipursky, R. B., Kapur, S., Foussias, G., & Remington, G. (2011). An algorithm-based approach to first-episode schizophrenia: response rates over 3 prospective antipsychotic trials with a retrospective data analysis. *The Journal of clinical psychiatry*, *72*(11), 1439–1444.

Agrawal, A., Chou, Y. L., Carey, C. E., Baranger, D. A., Zhang, B., Sherva, R., . . . Nelson, E. C. (2018). Genome-wide association study identifies a novel locus for cannabis dependence. *Molecular Psychiatry*, *23*(5), 1293–1302.

Agrawal, A., Lynskey, M. T., Hinrichs, A., Grucza, R., Saccone, S. F., Krueger, R., . . . Bierut, L. J. (2011). A genome-wide association study of DSM-IV: Cannabis dependence. *Addiction Biology*, *16*(3), 514–518.

Alaja, R., Seppä, K., Sillanaukee, P., Tienari, P., Huyse, F. J., Herzog, T., . . . Lobo, A. (1998). Physical and mental comorbidity of substance use disorders in psychiatric consultations. *Alcoholism: Clinical and Experimental Research*, *22*(8), 1820–1824.

Arseneault, L., Cannon, M., Poulton, R., Murray, R., Caspi, A., & Moffitt, T. E. (2002). Cannabis use in adolescence and risk for adult psychosis: Longitudinal prospective study. *British Medical Journal*, *325*(7374), 1212–1213.

Bailey, A. J., Farmer, E. J., & Finn, P. R. (2019). Patterns of polysubstance use and simultaneous co-use in high risk young adults. *Drug and Alcohol Dependence*, *205*, 107656.

Begemann, M., Seidel, J., Poustka, L., & Ehrenreich, H. (2020). Accumulated environmental risk in young refugees – A prospective evaluation. *EClinicalMedicine*, *22*, 100345.

Bernaudin, M., Marti, H. H., Roussel, S., Divoux, D., Nouvelot, A., MacKenzie, E. T., & Petit, E. (1999). A potential role for erythropoietin in focal permanent cerebral ischemia in mice. *Journal of Cerebral Blood Flow and Metabolism*, *19*(6), 643–651.

Bernaudin, M., Bellail, A., Marti, H. H., Yvon, A., Vivien, D., Duchatelle, I., . . . Petit, E. (2000). Neurons and astrocytes express EPO mRNA: Oxygen-sensing mechanisms that involve the redox-state of the brain. *Glia*, *30*(3), 271–278.

Bierut, L. J., Madden, P. A. F., Breslau, N, Johnson, E. O., Hatsukami, D, Pomerleau, O. F., . . . Ballinger, D. G. (2007). Association study for nicotine dependence. *Human Molecular Genetics*, *16*(1), 24–35.

Bond, W. S., & Rex, T. S. (2014). Evidence that erythropoietin modulates neuroinflammation through differential action on neurons, astrocytes, and microglia. *Frontiers in Immunology*, *5*, 1–8.

Brines, M., & Cerami, A. (2005). Emerging biological roles for erythropoietin in the nervous system. *Nature Reviews Neuroscience*, *6*(6), 484–494.

Chatzi, C., Schnell, E., & Westbrook, G. L. (2015). Localized hypoxia within the subgranular zone determines the early survival of newborn hippocampal granule cells. *eLife*, *4*, 1–18.

Chen, Z. Y., Asavaritikrai, P., Prchal, J. T., & Noguchi, C. T. (2007). Endogenous erythropoietin signaling is required for normal neural progenitor cell proliferation. *Journal of Biological Chemistry*, *282*(35), 25875–25883.

Cheng, Z., Zhou, H., Sherva, R., Farrer, L. A., Kranzler, H. R., & Gelernter, J. (2018). Genome-wide Association Study Identifies a Regulatory Variant of RGMA Associated With Opioid Dependence in European Americans. *Biological Psychiatry*, *84*(10), 762–770.

Chong, Z. Z., Kang, J.-Q., & Maiese, K. (2003). Erythropoietin fosters both intrinsic and extrinsic neuronal protection through modulation of microglia, Akt1, Bad, and caspase-mediated pathways. *British Journal of Pharmacology*, *138*(6), 1107–1118.

Clarke, T. K., Adams, M. J., Davies, G., Howard, D. M., Hall, L. S., Padmanabhan, S., . . . McIntosh, A. M. (2017). Genome-wide association study of alcohol consumption and genetic overlap with other health-related traits in UK biobank (N=112117). *Molecular Psychiatry*, *22*(10), 1376–1384.

Collins, R. L., Ellickson, P. L., & Bell, R. M. (1998). Simultaneous polydrug use among teens: Prevalence and predictors. *Journal of Substance Abuse*, *10*(3), 233–253.

Conley, R. R., & Buchanan, R. W. (1997). Evaluation of Treatment-Resistant Schizophrenia. *Schizophrenia Bulletin*, *23*(4), 663–674.

Connor, J. P., Gullo, M. J., White, A., & Kelly, A. B. (2014). Polysubstance use: Diagnostic challenges, patterns of use and health. *Current Opinion in Psychiatry*, *27*(4), 269–275.

Constanthin, P. E., Contestabile, A., Petrenko, V., Quairiaux, C., Salmon, P., Hüppi, P. S., & Kiss, J. Z. (2020). Endogenous erythropoietin signaling regulates migration and laminar positioning of upper-layer neurons in the developing neocortex. *Development*, *147*(19), dev190249.

Conway, K. P., Vullo, G. C., Nichter, B., Wang, J., Compton, W. M., Iannotti, R. J., & Simons-Morton, B. (2013). Prevalence and patterns of polysubstance use in a nationally representative sample of 10th Graders in the United States. *Journal of Adolescent Health*, *52*(6), 716–723.

Dammak, M. (2013). Treatment-resistant schizophrenia: prevalence and risk factors. In *Mental disorders-theoretical and empirical perspectives*. IntechOpen.

Dengler, V. L., Galbraith, M. D., & Espinosa, J. M. (2014). Transcriptional regulation by hypoxia inducible factors. *Critical Reviews in Biochemistry and Molecular Biology*, *49*(1), 1–15.

Di Forti, M., Morgan, C., Dazzan, P., Pariante, C., Mondelli, V., Marques, T. R., ... Murray, R. M. (2009). High-potency cannabis and the risk of psychosis. *British Journal of Psychiatry*, *195*(6), 488–491.

Digicaylioglu, M., Bichet, S., Marti, H. H., Wenger, R. H., Rivas, L. A., Bauer, C., & Gassmann, M. (1995). Localization of specific erythropoietin binding sites in defined areas of the mouse brain. *Proceedings of the National Academy of Sciences of the United States of America*, *92*(9), 3717–3720.

Doyle, K. P., Simon, R. P., & Stenzel-Poore, M. P. (2008). Mechanisms of ischemic brain damage. *Neuropharmacology*, *55*(3), 310–318.

Dunwoodie, S. L. (2009). The Role of Hypoxia in Development of the Mammalian Embryo. *Developmental Cell*, *17*(6), 755–773.

Ehrenreich, H., Degner, D., Meller, J., Brines, M., Béhé, M., Hasselblatt, M., ... Sirén, A. L. (2004). Erythropoietin: A candidate compound for neuroprotection in schizophrenia. *Molecular Psychiatry*, *9*(1), 42–54.

Ehrenreich, H, Hinze-Selch, D., Stawicki, S, Aust, C, Knolle-Veentjer, S., Wilms, S, ... Krampe, H. (2007a). Improvement of cognitive functions in chronic schizophrenic patients by recombinant human erythropoietin. *Molecular Psychiatry*, *12*(2), 206–220.

Ehrenreich, H., Fischer, B., Norra, C., Schellenberger, F., Stender, N., Stiefel, M., ... Bartels, C. (2007b). Exploring recombinant human erythropoietin in chronic progressive multiple sclerosis. *Brain*, *130*(10), 2577–2588.

Elmore, M. R., Najafi, A. R., Koike, M. A., Dagher, N. N., Spangenberg, E. E., Rice, R. A., ... Green, K. N. (2014). Colony-stimulating factor 1 receptor signaling is necessary for microglia viability, unmasking a microglia progenitor cell in the adult brain. *Neuron*, *82*(2), 380–397.

Evans, G. W., Li, D., & Whipple, S. S. (2013). Cumulative risk and child development. *Psychological Bulletin*, *139*(6), 1342–1396.

Fagel, D. M., Ganat, Y., Silbereis, J., Ebbitt, T., Stewart, W., Zhang, H., ... Vaccarino, F. M. (2006). Cortical neurogenesis enhanced by chronic perinatal hypoxia. *Experimental Neurology*, *199*(1), 77–91.

Fergusson, D. M., & Horwood, L. J. (2000). Does cannabis use encourage other forms of illicit drug use? *Addiction*, *95*(4), 505–520.

Fergusson, D. M., Poulton, R., Smith, P. F., & Boden, J. M. (2006a). Cannabis and psychosis. *Bmj*, *332*(7534), 172–175.

Fergusson, D. M., Boden, J. M., & Horwood, L. J. (2006b). Cannabis use and other illicit drug use: Testing the cannabis gateway hypothesis. *Addiction*, *101*(4), 556–569.

Furberg, H., Kim, Y., Dackor, J., Boerwinkle, E., Franceschini, N., Ardissino, D., ... Sullivan, P. F. (2010). Genome-wide meta-analyses identify multiple loci associated with smoking behavior. *Nature Genetics*, *42*(5), 441–447.

Gelernter, J, Sherva, R, Koesterer, R, Almasy, L, Zhao, H., Kranzler, H. R., & Farrer, L. (2014). Genome-wide association study of cocaine dependence and related traits: FAM53B identified as a risk gene. *Molecular Psychiatry*, *19*(6), 717–723.

Gheysen, F., Poppe, L., DeSmet, A., Swinnen, S., Cardon, G., De Bourdeaudhuij, I., … Fias, W. (2018). Physical activity to improve cognition in older adults: Can physical activity programs enriched with cognitive challenges enhance the effects? A systematic review and meta-analysis. *International Journal of Behavioral Nutrition and Physical Activity*, *15*(1), 1–13.

Ghezzi, P., & Brines, M. (2004). Erythropoietin as an antiapoptotic, tissue-protective cytokine. *Cell Death and Differentiation*, *11*(1), 37–44.

Gorgias, N., Maidatsi, P., Tsolaki, M., Alvanou, A., Kiriazis, G., Kaidoglou, K., & Giala, M. (1996). Hypoxic pretreatment protects against neuronal damage of the rat hippocampus induced by severe hypoxia. *Brain Research*, *714*(1-2), 215–225.

Hall, W. D., & Lynskey, M. (2005). Is cannabis a gateway drug? Testing hypotheses about the relationship between cannabis use and the use of other illicit drugs. *Drug and Alcohol Review*, *24*(1), 39–48.

Halliday, M. R., Abeydeera, D., Lundquist, A. J., Petzinger, G. M., & Jakowec, M. W. (2019). Intensive treadmill exercise increases expression of hypoxia-inducible factor 1α and its downstream transcript targets: A potential role in neuroplasticity. *NeuroReport*, *30*(9), 619–627.

Hancock, D. B., Guo, Y, Reginsson, G. W., Gaddis, N. C., Lutz, S. M., Sherva, R., … Johnson, E. O. (2018). Genome-wide association study across European and African American ancestries identifies a SNP in DNMT3B contributing to nicotine dependence. *Molecular Psychiatry*, *23*(9), 1911–1919.

Hasselblatt, M., Ehrenreich, H., & Sirén, A. L. (2006). The brain erythropoietin system and its potential for therapeutic exploitation in brain disease. *Journal of Neurosurgical Anesthesiology*, *18*(2), 132–138.

Hassouna, I, Ott, C, Wüstefeld, L, Offen, N, Neher, R. A., Mitkovski, M, … Ehrenreich, H. (2016). Revisiting adult neurogenesis and the role of erythropoietin for neuronal and oligodendroglial differentiation in the hippocampus. *Molecular Psychiatry*, *21*(12), 1752–1767.

Hawkins, J. D., Catalano, R. F., & Miller, J. Y. (1992). Risk and protective factors for alcohol and other drug problems in adolescence and early adulthood: Implications for substance abuse prevention. *Psychological Bulletin*, *112*(1), 64–105.

Hellewell, S. C., Yan, E. B., Alwis, D. S., Bye, N., & Morganti-Kossmann, M. C. (2013). Erythropoietin improves motor and cognitive deficit, axonal pathology, and neuroinflammation in a combined model of diffuse traumatic brain injury and hypoxia, in association with upregulation of the erythropoietin receptor. *Journal of Neuroinflammation*, *10*, 1–21.

Hillman, C. H., Erickson, K. I., & Kramer, A. F. (2008). Be smart, exercise your heart: exercise effects on brain and cognition. *Nature Reviews Neuroscience*, *9*(1), 58–65.

Hjorthøj, C., Østergaard, M. L. D., Benros, M. E., Toftdahl, N. G., Erlangsen, A., Andersen, J. T., & Nordentoft, M. (2015). Association between alcohol and substance use disorders and all-cause and cause-specific mortality in schizophrenia, bipolar disorder, and unipolar depression: A nationwide, prospective, register-based study. *The Lancet Psychiatry*, *2*(9), 801–808.

Iwai, M., Stetler, R. A., Xing, J., Hu, X., Gao, Y., Zhang, W., . . . Cao, G. (2010). Enhanced oligodendrogenesis and recovery of neurological function by erythropoietin after neonatal hypoxic/ischemic brain injury. *Stroke*, *41*(5), 1032–1037.

Jongenelis, M., Pettigrew, S., Lawrence, D., & Rikkers, W. (2019). Factors Associated with Poly Drug Use in Adolescents. *Prevention Science*, *20*(5), 695–704.

Juul, S. E., Anderson, D. K., Li, Y., & Christensen, R. D. (1998). Erythropoietin and Erythropoietin Receptor in the Developing Human Central Nervous System. *Pediatric Research*, *43*(1), 40–49.

Kandel, D., & Kandel, E. (2015). The Gateway Hypothesis of substance abuse: Developmental, biological and societal perspectives. *Acta Paediatrica, International Journal of Paediatrics*, *104*(2), 130–137.

Kapoor, M., Wang, J.-c., Wetherill, L., Le, N., Bertelsen, S., Hinrichs, A. L., . . . Goate, A. (2014). Genome-wide survival analysis of age at onset of alcohol dependence in extended high-risk COGA families. *Drug and alcohol dependence*, *142*, 56–62.

Kessler, R. C., Davis, C. G., & Kendler, K. S. (1997). Childhood adversity and adult psychiatric disorder in the US National Comorbidity Survey. *Psychological Medicine*, *27*(5), 1101–1119.

Kessler, R. C., Berglund, P., Demler, O., Jin, R., Merikangas, K. R., & Walters, E. E. (2005). Lifetime prevalence and age-of-onset distributions of DSM-IV disorders in the national comorbidity survey replication. *Archives of General Psychiatry*, *62*(6), 593–602.

Khalid, K., Frei, J., Aboouf, M. A., Koester-Hegmann, C., Gassmann, M., Fritschy, J.-M., & Schneider Gasser, E. M. (2021). Erythropoietin Stimulates GABAergic Maturation in the Mouse Hippocampus. *eneuro*, *8*(1), ENEURO.0006–21.2021.

Kiernan, E. A., Smith, S. M., Mitchell, G. S., & Watters, J. J. (2016). Mechanisms of microglial activation in models of inflammation and hypoxia: Implications for chronic intermittent hypoxia. *Journal of Physiology*, *594*(6), 1563–1577.

Kiernan, E. A., Wang, T., Vanderplow, A. M., Cherukuri, S., Cahill, M. E., & Watters, J. J. (2019). Neonatal Intermittent Hypoxia Induces Lasting Sex-Specific Augmentation of Rat Microglial Cytokine Expression. *Frontiers in Immunology*, *10*, 1–17.

Kimura, W., Xiao, F., Canseco, D. C., Muralidhar, S., Thet, S., Zhang, H. M., . . . Sadek, H. A. (2015). Hypoxia fate mapping identifies cycling cardiomyocytes in the adult heart. *Nature*, *523*(7559), 226–230.

Kohman, R. A., DeYoung, E. K., Bhattacharya, T. K., Peterson, L. N., & Rhodes, J. S. (2012). Wheel running attenuates microglia proliferation and increases expression of a proneurogenic phenotype in the hippocampus of aged mice. *Brain, Behavior, and Immunity*, *26*(5), 803–810.

Kreisel, T., Wolf, B., Keshet, E., & Licht, T. (2019). Unique role for dentate gyrus microglia in neuroblast survival and in VEGF-induced activation. *GLIA*, *67*(4), 594–618.

Lederbogen, F., Kirsch, P., Haddad, L., Streit, F., Tost, H., Schuch, P., ... Meyer-Lindenberg, A. (2011). City living and urban upbringing affect neural social stress processing in humans. *Nature*, *474*(7352), 498–501.

Lee, P. H., Anttila, V., Won, H., Feng, Y.-C. A., Rosenthal, J., Zhu, Z., ... Smoller, J. W. (2019). Genomic Relationships, Novel Loci, and Pleiotropic Mechanisms across Eight Psychiatric Disorders. *Cell*, *179*(7), 1469–1482.e11.

Lee, S. M., Hong Nga, N. T., Park, M. H., Kim, K. S., Cho, K. J., Moon, D. C., ... Hong, J. T. (2004). EPO receptor-mediated ERK kinase and NF-κB activation in erythropoietin-promoted differentiation of astrocytes. *Biochemical and Biophysical Research Communications*, *320*(4), 1087–1095.

LeTendre, M. L., & Reed, M. B. (2017). The Effect of Adverse Childhood Experience on Clinical Diagnosis of a Substance Use Disorder: Results of a Nationally Representative Study. *Substance Use \& Misuse*, *52*(6), 689–697.

Lieberman, J., Jody, D., Geisler, S., Alvir, J., Loebel, A., Szymanski, S., ... Borenstein, M. (1993). Time Course and Biologic Correlates of Treatment Response in First-Episode Schizophrenia. *Archives of General Psychiatry*, *50*(5), 369–376.

Liu, C., Shen, K., Liu, Z., & Noguchi, C. T. (1997). Regulated human erythropoietin receptor expression in mouse brain. *Journal of Biological Chemistry*, *272*(51), 32395–32400.

Lynskey, M. T., Heath, A. C., Bucholz, K. K., Slutske, W. S., Madden, P. A., Nelson, E. C., ... Martin, N. G. (2003). Escalation of drug use in early-onset cannabis users vs co-twin controls. *Journal of the American Medical Association*, *289*(4), 427–433.

Mallard, T. T., Ashenhurst, J. R., Harden, K. P., & Fromme, K. (2018). GABRA2, alcohol, and illicit drug use: An event-level model of genetic risk for polysubstance use. *Journal of Abnormal Psychology*, *127*(2), 190–201.

Marti, H. H., Wenger, R. H., Rivas, L. A., Straumann, U., Oigicaylioglu, M., Volker, H., ... Gassmann, M. (1996). Erythropoietin gene expression in human, monkey and murine brain. *European Journal of Neuroscience*, *8*(4), 666–676.

Mateika, J. H., El-Chami, M., Shaheen, D., & Ivers, B. (2015). Intermittent hypoxia: A low-risk research tool with therapeutic value in humans. *Journal of Applied Physiology*, *118*(5), 520–532.

McCutcheon, R. A., Krystal, J. H., & Howes, O. D. (2020). Dopamine and glutamate in schizophrenia: biology, symptoms and treatment. *World Psychiatry*, *19*(1), 15–33.

McGrath, J., Saha, S., Welham, J., El Saadi, O., MacCauley, C., & Chant, D. (2004). A systematic review of the incidence of schizophrenia: The distribution of rates and the influence of sex, urbanicity, migrant status and methodology. *BMC Medicine*, *2*, 1–22.

McGrath, J., Saha, S., Chant, D., & Welham, J. (2008). Schizophrenia: A Concise Overview of Incidence, Prevalence, and Mortality. *Epidemiologic Reviews*, *30*(1), 67–76.

Mckenzie, I. A., Ohayon, D., Li, H., Faria, J. P. D., Emery, B., Tohyama, K., & Richardson, W. D. (2014). Motor skill learning requires active central myelination. *346*(6207), 318–323.

McRae, A., Gilland, E., Bona, E., & Hagberg, H. (1995). Microglia activation after neonatal hypoxic-ischemia. *Developmental Brain Research*, *84*(2), 245–252.

Miskowiak, K. W., Vinberg, M., Harmer, C. J., Ehrenreich, H., Knudsen, G. M., Macoveanu, J., . . . Kessing, L. V. (2010). Effects of erythropoietin on depressive symptoms and neurocognitive deficits in depression and bipolar disorder. *Trials*, *11*, 1–10.

Miskowiak, K. W., Vinberg, M., Macoveanu, J., Ehrenreich, H., Køster, N., Inkster, B., . . . Siebner, H. R. (2015). Effects of Erythropoietin on Hippocampal Volume and Memory in Mood Disorders. *Biological Psychiatry*, *78*(4), 270–277.

Miskowiak, K. W., Vinberg, M., Christensen, E. M., Bukh, J. D., Harmer, C. J., Ehrenreich, H., & Kessing, L. V. (2014a). Recombinant human erythropoietin for treating treatment-resistant depression: A double-blind, randomized, placebo-controlled phase 2 trial. *Neuropsychopharmacology*, *39*(6), 1399–1408.

Miskowiak, K. W., Ehrenreich, H., Christensen, E. M., Kessing, L. V., & Vinberg, M. (2014b). Recombinant human erythropoietin to target cognitive dysfunction in bipolar disorder: a double-blind, randomized, placebo-controlled phase 2 trial. *The Journal of clinical psychiatry*, *75*(12), 1347–1355.

Mitjans, M., Seidel, J., Begemann, M., Bockhop, F., Moya-Higueras, J., Bansal, V., . . . Ehrenreich, H. (2019). Violent aggression predicted by multiple pre-adult environmental hits. *Molecular Psychiatry*, *24*(10), 1549–1564.

Mitkovski, M., Dahm, L., Heinrich, R., Monnheimer, M., Gerhart, S., Stegmüller, J., . . . Ehrenreich, H. (2015). Erythropoietin dampens injury-induced microglial motility. *Journal of Cerebral Blood Flow and Metabolism*, *35*(8), 1233–1236.

Mizuno, Y., McCutcheon, R. A., Brugger, S. P., & Howes, O. D. (2020). Heterogeneity and efficacy of antipsychotic treatment for schizophrenia with or without treatment resistance: a meta-analysis. *Neuropsychopharmacology*, *45*(4), 622–631.

Morishita, E., Masuda, S., Nagao, M., Yasuda, Y., & Sasaki, R. (1996). Erythropoetin receptor is expressed in rat hippocampal and cerebral cortical neurons, and erythropoietin prevents in vitro glutamate-induced neuronal death. *Neuroscience*, *76*(1), 105–116.

Moss, H. B., Chen, C. M., & Yi, H. Y. (2014). Early adolescent patterns of alcohol, cigarettes, and marijuana polysubstance use and young adult substance use outcomes in a nationally representative sample. *Drug and Alcohol Dependence*, *136*(1), 51–62.

Moustafa, A. A., Parkes, D., Fitzgerald, L., Underhill, D., Garami, J., Levy-Gigi, E., . . . Misiak, B. (2018). The relationship between childhood trauma, early-life stress, and alcohol and drug use, abuse, and addiction: An integrative review. *Current Psychology*, 579–584.

Mueser, K. T., Yarnold, P. R., Rosenberg, S. D., Swett, C., Miles, K. M., & Hill, D. (2000). Substance use disorder in hospitalized severely mentally ill psychiatric patients: Prevalence, correlates, and subgroups. *Schizophrenia Bulletin*, *26*(1), 179–192.

Murray, R. M., & Hall, W. (2020). Will Legalization and Commercialization of Cannabis Use Increase the Incidence and Prevalence of Psychosis? *JAMA Psychiatry*.

Nangaku, M., & Eckardt, K. U. (2007). Hypoxia and the HIF system in kidney disease. *Journal of Molecular Medicine*, *85*(12), 1325–1330.

Nielsen, J. V., Thomassen, M., Møllgård, K., Noraberg, J., & Jensen, N. A. (2014). Zbtb20 Defines a Hippocampal Neuronal Identity Through Direct Repression of Genes That Control Projection Neuron Development in the Isocortex. *Cerebral Cortex*, *24*(5), 1216–1229.

Nielsen, J. V., Blom, J. B., Noraberg, J., & Jensen, N. A. (2010). Zbtb20-Induced CA1 Pyramidal Neuron Development and Area Enlargement in the Cerebral Midline Cortex of Mice. *Cerebral Cortex*, *20*(8), 1904–1914.

Noguchi, C. T., Asavaritikrai, P., Teng, R., & Jia, Y. (2007). Role of erythropoietin in the brain. *Critical Reviews in Oncology/Hematology*, *64*(2), 159–171.

Olthuis, J. V., Darredeau, C., & Barrett, S. P. (2013). Substance use initiation: The role of simultaneous polysubstance use. *Drug and Alcohol Review*, *32*(1), 67–71.

Ott, C., Martens, H., Hassouna, I., Oliveira, B., Erck, C., Zafeiriou, M. P., . . . Ehrenreich, H. (2015). Widespread expression of erythropoietin receptor in brain and its induction by injury. *Molecular Medicine*, *21*, 803–815.

Pajonk, F. G., Wobrock, T., Gruber, O., Scherk, H., Berner, D., Kaizl, I., . . . Falkai, P. (2010). Hippocampal plasticity in response to exercise in schizophrenia. *Archives of General Psychiatry*, *67*(2), 133–143.

Park, M. H., Lee, S. M., Lee, J. W., Son, D. J., Moon, D. C., Yoon, D. Y., & Hong, J. T. (2006). ERK-mediated production of neurotrophic factors by astrocytes promotes neuronal stem cell differentiation by erythropoietin. *Biochemical and Biophysical Research Communications*, *339*(4), 1021–1028.

Parmar, K., Mauch, P., Vergilio, J. A., Sackstein, R., & Down, J. D. (2007). Distribution of hematopoietic stem cells in the bone marrow according to regional hypoxia. *Proceedings of the National Academy of Sciences of the United States of America*, *104*(13), 5431–5436.

Pedersen, P. L. (2007). Warburg, me and Hexokinase 2: Multiple discoveries of key molecular events underlying one of cancers' most common phenotypes, the "Warburg Effect", i.e., elevated glycolysis in the presence of oxygen. *Journal of Bioenergetics and Biomembranes*, *39*(3), 211–222.

Pósfai, B., Cserép, C., Orsolits, B., & Dénes, Á. (2019). New insights into microglia–neuron interactions: a neuron's perspective. *Neuroscience*, *405*, 103–117.

Prinz, M., Masuda, T., Wheeler, M. A., & Quintana, F. J. (2021). Microglia and Central Nervous System–Associated Macrophages—From Origin to Disease Modulation. *Annual Review of Immunology*, *39*(1), 251–277.

Qian, D. C., Molfese, D. L., Jin, J. L., Titus, A. J., He, Y., Li, Y., . . . Amos, C. I. (2017). Genome-wide imaging association study implicates functional activity and glial homeostasis of the caudate in smoking addiction. *BMC genomics*, *18*(1), 1–10.

Racz, S. J., Saha, S., Trent, M., Adger, H., Bradshaw, C. P., Goldweber, A., & Cauffman, E. (2016). Polysubstance Use Among Minority Adolescent Males Incarcerated for Serious Offenses. *Child and Youth Care Forum*, *45*(2), 205–220.

Ribbe, K., Friedrichs, H., Begemann, M., Grube, S., Papiol, S., Kästner, A., ... Ehrenreich, H. (2010). The cross-sectional GRAS sample: A comprehensive phenotypical data collection of schizophrenic patients. *BMC Psychiatry*, *10*.

Ruderfer, D. M., Ripke, S., McQuillin, A., Boocock, J., Stahl, E. A., Pavlides, J. M. W., ... Kendler, K. S. (2018). Genomic Dissection of Bipolar Disorder and Schizophrenia, Including 28 Subphenotypes. *Cell*, *173*(7), 1705–1715.e16.

Rybnikova, E., Vataeva, L., Tyulkova, E., Gluschenko, T., Otellin, V., Pelto-Huikko, M., & Samoilov, M. O. (2005). Mild hypoxia preconditioning prevents impairment of passive avoidance learning and suppression of brain NGFI-A expression induced by severe hypoxia. *Behavioural Brain Research*, *160*(1), 107–114.

Santilli, G., Lamorte, G., Carlessi, L., Ferrari, D., Nodari, L. R., Binda, E., ... De Filippis, L. (2010). Mild hypoxia enhances proliferation and multipotency of human neural stem cells. *PLoS ONE*, *5*(1).

Secades-Villa, R., Garcia-Rodríguez, O., Jin, C. J., Wang, S., & Blanco, C. (2015). Probability and predictors of the cannabis gateway effect: A national study. *International Journal of Drug Policy*, *26*(2), 135–142.

Semenza, G. L. (2001). Regulation of hypoxia-induced angiogenesis: A chaperone escorts VEGF to the dance. *Journal of Clinical Investigation*, *108*(1), 39–40.

Semenza, G. L. (1998). Hypoxia-inducible factor 1: Master regulator of O2 homeostasis. *Current Opinion in Genetics and Development*, *8*(5), 588–594.

Semple, D. M., McIntosh, A. M., & Lawrie, S. M. (2005). Cannabis as a risk factor for psychosis: Systematic review. *Journal of Psychopharmacology*, *19*(2), 187–194.

Sirén, A. L., Knerlich, F., Poser, W., Gleiter, C. H., Brück, W., & Ehrenreich, H. (2001). Erythropoietin and erythropoietin receptor in human ischemic/hypoxic brain. *Acta Neuropathologica*, *101*(3), 271–276.

Sirén, A. L., Faßhauer, T., Bartels, C., & Ehrenreich, H. (2009). Therapeutic Potential of Erythropoietin and its Structural or Functional Variants in the Nervous System. *Neurotherapeutics*, *6*(1), 108–127.

Smigielski, L., Jagannath, V., Rössler, W., Walitza, S., & Grünblatt, E. (2020). Epigenetic mechanisms in schizophrenia and other psychotic disorders: a systematic review of empirical human findings. *Molecular Psychiatry*, *25*(8), 1718–1748.

Solovieff, N., Cotsapas, C., Lee, P. H., Purcell, S. M., & Smoller, J. W. (2013). Pleiotropy in complex traits: challenges and strategies. *Nature Reviews Genetics*, *14*(7), 483–495.

Stepniak, B., Papiol, S., Hammer, C., Ramin, A., Everts, S., Hennig, L., ... Ehrenreich, H. (2014). Accumulated environmental risk determining age at schizophrenia onset: A deep phenotyping-based study. *The Lancet Psychiatry*, *1*(6), 444–453.

Strowitzki, M., Cummins, E., & Taylor, C. (2019). Protein Hydroxylation by Hypoxia-Inducible Factor (HIF) Hydroxylases: Unique or Ubiquitous? *Cells*, *8*(5), 384.

Sugawa, M., Sakurai, Y., Ishikawa-Ieda, Y., Suzuki, H., & Asou, H. (2002). Effects of erythropoietin on glial cell development; oligodendrocyte maturation and astrocyte proliferation. *Neuroscience Research*, *44*(4), 391–403.

Toftdahl, N. G., Nordentoft, M., & Hjorthøj, C. (2016). Prevalence of substance use disorders in psychiatric patients: a nationwide Danish population-based study. *Social Psychiatry and Psychiatric Epidemiology*, *51*(1), 129–140.

Treutlein, J., Cichon, S., Ridinger, M., Wodarz, N., Soyka, M., Zill, P., ... Rietschel, M. (2009). Genome-wide Association Study of Alcohol Dependence. *Archives of General Psychiatry*, *66*(7), 773–784.

Tsai, P. T., Ohab, J. J., Kertesz, N., Groszer, M., Matter, C., Gao, J., ... Carmichael, S. T. (2006). A critical role of erythropoietin receptor in neurogenesis and post-stroke recovery. *Journal of Neuroscience*, *26*(4), 1269–1274.

Vairano, M., Russo, C. D., Pozzoli, G., Battaglia, A., Scambia, G., Tringali, G., ... Navarra, P. (2002). Erythropoietin exerts anti-apoptotic effects on rat microglial cells in vitro. *European Journal of Neuroscience*, *16*(4), 584–592.

Van Os, J., Bak, M., Hanssen, M., Bijl, R. V., De Graaf, R., & Verdoux, H. (2002). Cannabis use and psychosis: A longitudinal population-based study. *American Journal of Epidemiology*, *156*(4), 319–327.

Varese, F., Smeets, F., Drukker, M., Lieverse, R., Lataster, T., Viechtbauer, W., ... Bentall, R. P. (2012). Childhood adversities increase the risk of psychosis: A meta-analysis of patient-control, prospective-and cross-sectional cohort studies. *Schizophrenia Bulletin*, *38*(4), 661–671.

Vieira, H. L., Alves, P. M., & Vercelli, A. (2011). Modulation of neuronal stem cell differentiation by hypoxia and reactive oxygen species. *Progress in Neurobiology*, *93*(3), 444–455.

Villa, P., Bigini, P., Mennini, T., Agnello, D., Laragione, T., Cagnotto, A., ... Ghezzi, P. (2003). Erythropoietin selectively attenuates cytokine production and inflammation in cerebral ischemia by targeting neuronal apoptosis. *Journal of Experimental Medicine*, *198*(6), 971–975.

Visscher, P. M., & Yang, J. (2016). A plethora of pleiotropy across complex traits. *Nature Genetics*, *48*(7), 707–708.

Vukovic, J., Colditz, M. J., Blackmore, D. G., Ruitenberg, M. J., & Bartlett, P. F. (2012). Microglia modulate hippocampal neural precursor activity in response to exercise and aging. *Journal of Neuroscience*, *32*(19), 6435–6443.

Wakhloo, D., Scharkowski, F., Curto, Y., Butt, U. J., Bansal, V., Steixner-Kumar, A. A., ... Ehrenreich, H. (2020). Functional hypoxia drives neuroplasticity and neurogenesis via brain erythropoietin. *Nature communications*, *11*(1), 1–12.

Wang, H., Shi, X., Schenck, H., Hall, J. R., Ross, S. E., Kline, G. P., ... Chen, P. (2020). Intermittent Hypoxia Training for Treating Mild Cognitive Impairment: A Pilot Study. *American journal of Alzheimer's disease and other dementias*, *35*, 1–10.

Wang, Y., Zhang, Z. G., Rhodes, K., Renzi, M., Zhang, R. L., Kapke, A., ... Chopp, M. (2007). Post-ischemic treatment with erythropoietin or carbamylated erythropoietin

reduces infarction and improves neurological outcome in a rat model of focal cerebral ischemia. *British Journal of Pharmacology*, *151*(8), 1377–1384.

Watanabe, K., Stringer, S., Frei, O., Umićević Mirkov, M., de Leeuw, C., Polderman, T. J., … Posthuma, D. (2019). A global overview of pleiotropy and genetic architecture in complex traits. *Nature Genetics*, *51*(9), 1339–1348.

White, A., Chan, G. C., Quek, L. H., Connor, J. P., Saunders, J. B., Baker, P., … Kelly, A. B. (2013). The topography of multiple drug use among adolescent Australians: Findings from the National Drug Strategy Household Survey. *Addictive Behaviors*, *38*(4), 2068–2073.

Wolf, A., Agnihotri, S., Micallef, J., Mukherjee, J., Sabha, N., Cairns, R., … Guha, A. (2011). Hexokinase 2 is a key mediator of aerobic glycolysis and promotes tumor growth in human glioblastoma multiforme. *208*(2), 313–326.

Wu, F. F., Zhang, K. L., Wang, Z. M., Yang, Y., Li, S. H., & Wang, J. Q. (2021). Benefit of a single simulated hypobaric hypoxia in healthy mice performance and analysis of mitochondria - related gene changes. *Scientific Reports*, 1–18.

Xie, Z., Ma, X., Ji, W., Zhou, G., Lu, Y., Xiang, Z., … Zhang, L. (2010). Zbtb20 is essential for the speci fi cation of CA1 fi eld identity in the developing hippocampus. *107*(14), 1–6.

Yao, L., Kan, E. M., Lu, J., Hao, A., Dheen, S. T., Kaur, C., & Ling, E. A. (2013). Toll-like receptor 4 mediates microglial activation and production of inflammatory mediators in neonatal rat brain following hypoxia: Role of TLR4 in hypoxic microglia. *Journal of Neuroinflammation*, *10*, 1–21.

Yasuda, S., Arii, S., Mori, A., Isobe, N., Yang, W., Oe, H., … Imamura, M. (2004). Hexokinase II and VEGF expression in liver tumors: correlation with hypoxia-inducible factor-1α and its significance. *Journal of Hepatology*, *40*(1), 117–123.

Yu, X., Shacka, J. J., Eells, J. B., Suarez-Quian, C., Przygodzki, R. M., Beleslin-Cokic, B., … Noguchi, C. T. (2002). Erythropoietin receptor signalling is required for normal brain development. *Development*, *129*(2), 505–516.

Zhu, L. L., Zhao, T., Li, H. S., Zhao, H., Wu, L. Y., Ding, A. S., … Fan, M. (2005). Neurogenesis in the adult rat brain after intermittent hypoxia. *Brain Research*, *1055*(1-2), 1–6.

Zhu, X. H., Yan, H. C., Zhang, J., Qu, H. D., Qiu, X. S., Chen, L., … Gao, T. M. (2010). Intermittent hypoxia promotes hippocampal neurogenesis and produces antidepressant-like effects in adult rats. *Journal of Neuroscience*, *30*(38), 12653–12663.

Appendices

A Co-authored publication: Butt et al. (2021)

Original publication

Butt, U.J., Hassouna, I., Fernandez Garcia-Agudo, L., Steixner-Kumar A. A. et al. (2021). CaMKIIα expressing neurons to report activity-related endogenous hypoxia upon motor-cognitive challenge. International Journal of Molecular Sciences, 22(6), 3164.

Personal contribution

I conducted the scRNA-seq analyses for this paper, provided the respective figures, figure legends and drafted the according passages in the main text. I also contributed to interpretation and discussion of the results.

Article

CaMKIIα Expressing Neurons to Report Activity-Related Endogenous Hypoxia upon Motor-Cognitive Challenge

Umer Javed Butt [1], Imam Hassouna [1], Laura Fernandez Garcia-Agudo [1], Agnes A. Steixner-Kumar [1], Constanze Depp [2], Nadine Barnkothe [1], Matthias R. Zillmann [1], Anja Ronnenberg [1], Viktoria Bonet [1], Sandra Goebbels [2], Klaus-Armin Nave [2] and Hannelore Ehrenreich [1,*

[1] Clinical Neuroscience, Max Planck Institute of Experimental Medicine, 37075 Göttingen, Germany; butt@em.mpg.de (U.J.B.); hassouna@em.mpg.de (I.H.); agudo@em.mpg.de (L.F.G.-A.); steixner@em.mpg.de (A.A.S.-K.); barnkothe@em.mpg.de (N.B.); zillmann@em.mpg.de (M.R.Z.); ronnenberg@em.mpg.de (A.R.); bonet@em.mpg.de (V.B.)

[2] Department of Neurogenetics, Max Planck Institute of Experimental Medicine, 37075 Göttingen, Germany; depp@em.mpg.de (C.D.); sgoebbels@em.mpg.de (S.G.); nave@em.mpg.de (K.-A.N.)

* Correspondence: ehrenreich@em.mpg.de; Tel.: +49-551-389-9628; Fax: +49-551-389-9670

Abstract: We previously introduced the brain erythropoietin (EPO) circle as a model to explain the adaptive 'brain hardware upgrade' and enhanced performance. In this fundamental circle, brain cells, challenged by motor-cognitive tasks, experience functional hypoxia, triggering the expression of EPO among other genes. We attested hypoxic cells by a transgenic reporter approach under the ubiquitous CAG promoter, with Hif-1α oxygen-dependent degradation-domain (ODD) fused to CreERT2-recombinase. To specifically focus on the functional hypoxia of excitatory pyramidal neurons, here, we generated CaMKIIα-CreERT2-ODD::R26R-tdTomato mice. Behavioral challenges, light-sheet microscopy, immunohistochemistry, single-cell mRNA-seq, and neuronal cultures under normoxia or hypoxia served to portray these mice. Upon complex running wheel performance as the motor-cognitive task, a distinct increase in functional hypoxic neurons was assessed immunohistochemically and confirmed three-dimensionally. In contrast, fear conditioning as hippocampal stimulus was likely too short-lived to provoke neuronal hypoxia. Transcriptome data of hippocampus under normoxia versus inspiratory hypoxia revealed increases in CA1 CaMKIIα-neurons with an immature signature, characterized by the expression of *Dcx*, *Tbr1*, *CaMKIIα*, *Tle4*, and *Zbtb20*, and consistent with accelerated differentiation. The hypoxia reporter response was reproduced in vitro upon neuronal maturation. To conclude, task-associated activity triggers neuronal functional hypoxia as a local and brain-wide reaction mediating adaptive neuroplasticity. Hypoxia-induced genes such as EPO drive neuronal differentiation, brain maturation, and improved performance.

Keywords: physiological hypoxia; complex running wheel; hippocampus; scRNA-seq; light-sheet microscopy; Hif-1α; neuronal differentiation; brain maturation; neuron culture; immature neurons

1. Introduction

Erythropoietin (EPO) is a potent hypoxia-inducible growth factor, originally named after its role in hematopoiesis, but later described to have neuroprotective functions in the nervous system [1–3]. 'Brain doping', in the sense of substantially improved maximal exercise performance without altered red blood cell production, has been suspected for a long time to be the main operative force rather than blood doping alone [4]. This was elegantly demonstrated a few years ago in a transgenic mouse line, which constitutively overexpresses human erythropoietin (EPO) exclusively in the brain [5]. However, the mechanisms explaining these dramatic erythropoiesis-independent effects and, in particular, the underlying physiology have remained widely obscure. We previously introduced the brain EPO circle as a working model explaining the adaptive 'brain hardware upgrade' and enhanced performance. In this fundamental regulatory circle, brain cells, challenged

by motor-cognitive tasks, experience functional hypoxia, triggering the local expression of EPO, among other genes [6]. We confirmed functional hypoxic cells by a transgenic reporter approach under the ubiquitous CAG promoter, with the Hif-1α oxygen-dependent degradation-domain (ODD) fused to CreERT2-recombinase [7].

The brain EPO circle matches perfectly with well-established, but mechanistically unexplored, experimental and clinical observations that physical activity and cognitive challenge induce comprehensive brain activation, thereby improving global brain function and increasing brain dimensions [8–10]. We showed that physiological, endogenous hypoxia is likely a respective lead mechanism, regulating neuroplasticity via assimilated gene expression in neurons of the behaving brain [7]. Importantly, targeted deletion of the EPO receptor from pyramidal neurons eliminated the observed improvement in performance [6].

These observations placed pyramidal neurons in the center of our interest and stimulated us to generate a new mouse line using a pyramidal neuronal promoter. The CaMKIIα-CreERT2-ODD::R26R-tdTomato mice presented here allowed us to specifically concentrate on the functional hypoxia of the excitatory pyramidal neurons using immunohistochemistry including light-sheet microscopy (LSM) for three-dimensional views. Additionally, hippocampal single-cell mRNA-seq transcriptome data under normoxia versus inspiratory hypoxia, focusing on CaMKIIα expressing neurons, revealed the first hints of accelerated neurodifferentiation, pointing to enhanced neuroplasticity and brain maturation upon hypoxia.

2. Results and Discussion

2.1. Generation of a New Mouse Line to Report Pyramidal Neuronal Hypoxia

In our previous work [7], we used a transgenic mouse line, driven by the universal CAG promoter (CAG-CreERT2-ODD::R26R-tdTomato, slightly modified from [11]).This reporter line allowed permanent labelling of all cells undergoing transient hypoxia by the expression of a fusion protein, comprised of Hif-1α ODD and tamoxifen-inducible CreERT2. Immunohistochemical analyses identified mainly neurons as reporter-labeled cells, but also certain (much lower) percentages of astrocytes, oligodendrocytes, endothelial cells, and pericytes. Hence, to specifically focus on functional hypoxia of activity-challenged pyramidal neurons, we created CaMKIIα-CreERT2-ODD::R26R-tdTomato mice (Figure 1a).

To characterize these mice, we started out with our previous 'gold standard' of positive control derived from our experience with the CAG-line [7]. We compared mice exposed to intermittent inspiratory hypoxia (6% O_2 for 6 h daily, applied over five days) with mice under inspiratory normoxia (21% O_2) that were handled identically, including five tamoxifen injections as indicated (Figure 1b). This regimen led to very strong staining of the pyramidal neurons already under normoxia and an extreme labelling under hypoxia, as illustrated in Figure 1c. Using corn oil injections alone as a solvent control ('no tamoxifen') to assess the non-induced expression of the transgene ('leakiness' of the tdTomato reporter) led to hardly any labelled cells (Figure 1c; Supplementary Materials-LSM Videos S1 and S2).
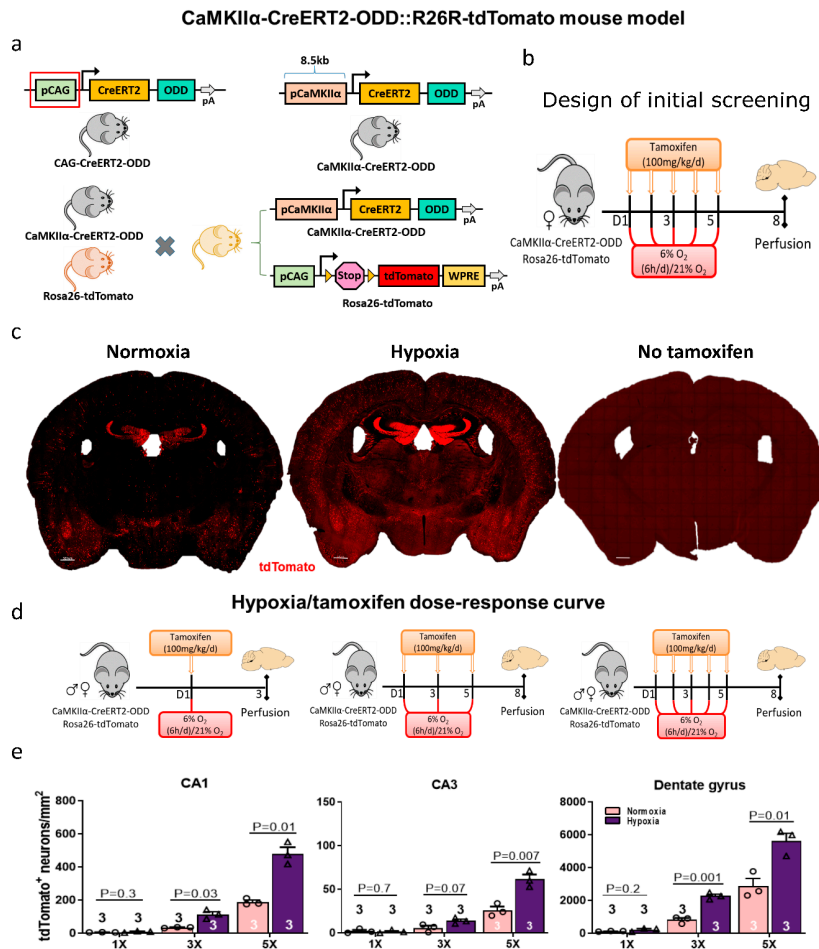
Figure 1. Generation and first characterization of excitatory neuron-specific CaMKIIα-CreERT2-ODD::R26R-tdTomato hypoxia reporter mice. (**a**) Schematic representation of the CAG-CreERT2-ODD construct where the CAG promoter was excised using SpeI and EcoRI restriction enzymes to obtain the vector backbone (CreERT2-ODD-pA). Subsequently, the excitatory neuronal promotor CaMKIIα of 8.5 kb was inserted into CreERT2-ODD-pA to generate the CaMKIIα-CreERT2-ODD-pA vector. Next, the linearized vector was used for the generation of CaMKIIα-CreERT2-ODD expressing transgenic mice. These were crossed with CAG-Rosa26-tdTomato reporter mice. Permanent labelling of hypoxic neurons is achieved via Hif-1α oxygen-dependent degradation domain (ODD) stabilization upon tamoxifen injection. (**b**) Experimental design: For an initial screening, CaMKIIα-CreERT2-ODD::R26R-tdTomato hypoxia reporter mice received tamoxifen five times over five days, each time followed by exogenous hypoxia (6% O_2 for 6 h) versus normoxia (21% O_2), and mice were sacrificed on day eight. (**c**) Representative coronal images of five-times tamoxifen-injected CaMKIIα-CreERT2-ODD::R26R-tdTomato mice under normoxic or hypoxic conditions. The corn oil control ('no tamoxifen') shows only very few tdTomato+ (red) neurons, i.e., minimal tamoxifen-independent Cre-activity. Scale bar represents 500 μm. (**d**) Experimental scheme of the hypoxia/tamoxifen dose response curve in CaMKIIα-CreERT2-ODD::R26R-tdTomato mice. (**e**) Quantification of tdTomato+Ctip2+ double-positive neurons in CA1, CA3 and dentate gyrus from eight-week-old mice of equally distributed mixed gender. Unpaired Student's *t*-test (two-tailed, Welch's corrections) was used for statistical analysis between groups; n numbers given in graphs; error bars indicate standard error of mean (SEM).

2.2. Critical Considerations Regarding Our Model and Proof-of-Concept Testing

The pCaMKIIα-CreERT2-ODD transgene encodes a Cre-fusion protein that is made and immediately inactivated by two independent posttranslational mechanisms, which are both active: (1) The estrogen receptor (ER) domain is chaperoned by heat shock protein Hsp90 and thus the entire fusion protein is maintained inactive in the cytoplasm: Here, no Cre recombination is possible; (2) The ODD domain causes the hydroxylation of the entire fusion protein (by PHD/prolyl-hydroxylase domain proteins, followed by polyubiquitination via the VHL proteins/Von Hippel-Lindau tumor suppressor, leading to proteasomal degradation). Also here, no Cre recombination is possible. Cre recombination only occurs when both inhibitory mechanisms are blocked at the same time, i.e., by the coincidence of tamoxifen (binding to the ER domain and releasing Hsp90) and hypoxia (inactivating PHD and thereby stabilizing CreERT2-ODD). Nuclear Cre activity, even if short and only at a low level, causes the permanent activation of our Rosa26-tdTomato reporter gene by removing a STOP sequence from the DNA upstream of its coding sequence (Figure 1a), rendering the RNA transcript translatable. Consequently, all Cre-recombined cells become stably red labelled (independent of further tamoxifen and/or hypoxia). Thus, we achieved permanent staining of once hypoxic cells.

However, in order to work, a sufficient concentration of Hsp90 as well as of PHD/VHL proteins to match the cellular abundance of CreERT2-ODD are needed. Too much CreERT2-ODD could out-titrate either Hsp90 and/or PHD+VHL proteins and thus result in unspecific Cre activity ('leakiness' of the system). Reassuringly, this is very low in our system as described above (Figure 1c; Supplementary Materials-LSM Videos S1 and S2).

On the other hand, the abundance of neuronally expressed CreERT2-ODD may be critical for the PHD/VHL system to work. When expressed under the control of strong promoters (both, pCAG used in [7], and pCaMKIIα are strong promoters), the ODD domain may out-titrate the abundance of PHD and/or VHL proteins, whose expression level is regulated to exactly match the endogenous Hif proteins. These operate at a much lower abundance level, are not 'inducible' as Hsp90 proteins are, and PHD/VHL out-titration should not cause cellular stress. Therefore, we checked by qPCR whether known target genes of Hif-1α are upregulated under normoxia and without any hypoxia stimulation, simply due to a high-level expression of the ODD domain in transgenic mice. Again reassuringly, the comparative qPCR results for the selected Hif-regulated genes *Vegfa*, *Higdf1a*, and *Epo*, obtained under normoxic conditions from the hippocampal tissue of pCaMKIIα-CreERT2-ODD and pCAG-CreERT2-ODD versus wildtype mice of the same background strain, age, and gender, did not show differences (data not shown).

2.3. Evaluation of a Hypoxia/Tamoxifen Dose–Response Curve

Encouraged by the outcome of these necessary controls, we next performed comparative quantifications of tdTomato+ neurons upon tamoxifen injection immediately before hypoxia, applied either once, thrice, or five times (each 6% O_2 for 6 h), or analogously before normoxia, in cornu ammonis hippocampi (CA1 and CA3), as well as in the dentate gyrus. The quantification results made us select the three-times tamoxifen/hypoxia condition as a suitable titration result, i.e., as the appropriate 'gold standard' of tamoxifen injections to be applied in this particular mouse line (Figure 1d,e).

2.4. Immunohistochemical Characterization of Hypoxic Neurons in Brain and Primary Hippocampal Neuronal Cultures

Figure 2 provides illustrating immunohistochemical images of functional hypoxia, giving examples of tdTomato-stained excitatory neurons in the hippocampus and its subfields, various cortical areas and striatum/corpus callosum. We note the strong tdTomato labelling of hypoxic pyramidal neuronal cell bodies and the abundant neuropil staining in the hippocampus. In particular, mossy fibers in the vicinity of CA3 (stratum lucidum) and granule cell projections in the dentate gyrus are strongly labelled. The whole dentate gyrus reveals densely packed hypoxic neurons with intense fiber staining.
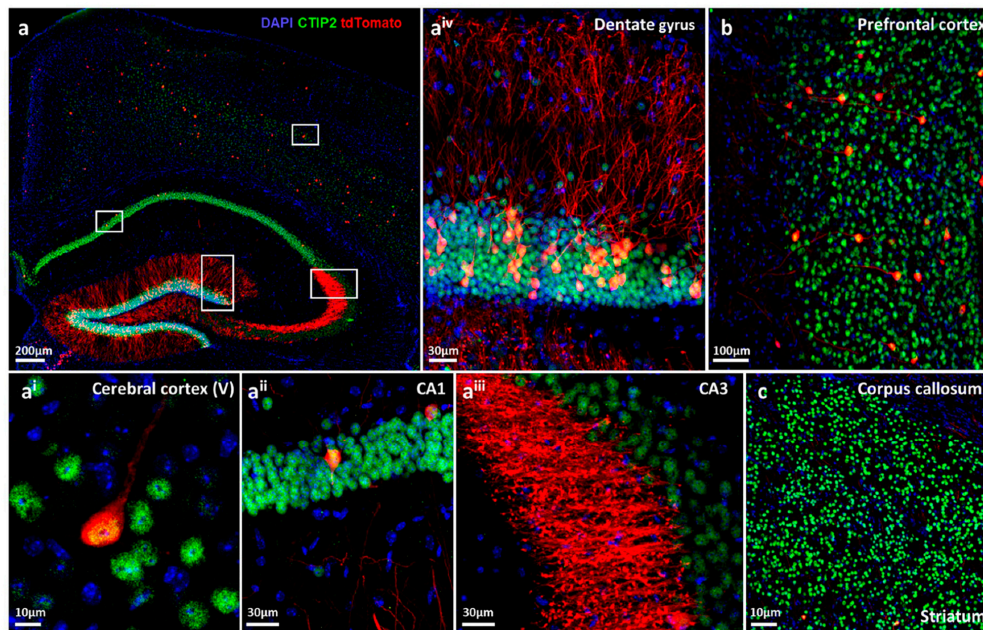
Figure 2. Immunohistochemical characterization of functional hypoxic pyramidal neurons in CaMKIIα-CreERT2-ODD::R26R-tdTomato reporter mice. (**a**) Overview image of an eight-week-old female mouse after exposure to complex running wheel (CRW) showing distinct labelling of neurons with tdTomato fluorescent protein (red), co-immunostained with the neuronal marker Ctip2 (green) and DAPI (blue) as nuclear counterstain. White frames denote magnifications given in **a^i**–**a^{iv}**. (**a^i**) Image of cortical layer V showing a neuron with tdTomato+ and Ctip2+ co-localized signal. (**a^{ii}**) Some cornu ammonis (CA1) pyramidal neurons are tdTomato positive. (**a^{iii}**) In CA3, just a few neuronal cell bodies display the tdTomato signal; however, strong staining is observed in stratum lucidum, rendering neuronal morphological details such as dendritic spines and synapses easily distinguishable at high resolution. (**a^{iv}**) Close-up image of the superior plate of the dentate gyrus, demonstrating densely tdTomato-expressing granular neurons and remarkable labelling of neutropil. (**b**) A subset of neurons in prefrontal cortex and their processes are also tdTomato labelled. (**c**) CaMKIIα expressing tdTomato+ neurons are sparsely present in the striatum. Scale bars represent 200 μm (**a**), 10 μm (**a^i**, **c**), 30 μm (**a^{ii}**, **a^{iii}** and **a^{iv}**), and 100 μm (**b**).

In primary E17 hippocampal neuronal cultures, immediate addition of (Z)-4-hydroxytamoxifen (2 μM) from day in vitro (DIV) 0 onwards, under continuous hypoxia (1% O_2) versus normoxia (21% O_2), revealed tdTomato labelling on DIV16, clearly enhanced under hypoxia. In contrast, no staining was seen on DIV7 (data not shown), indicating that some degree of neuronal maturation is a prerequisite for the activity of the CaMKIIα promoter, and thus for the expression of the CreERT2-ODD fusion protein, leading to permanent labelling of hypoxic cells (Figure 3a–d).
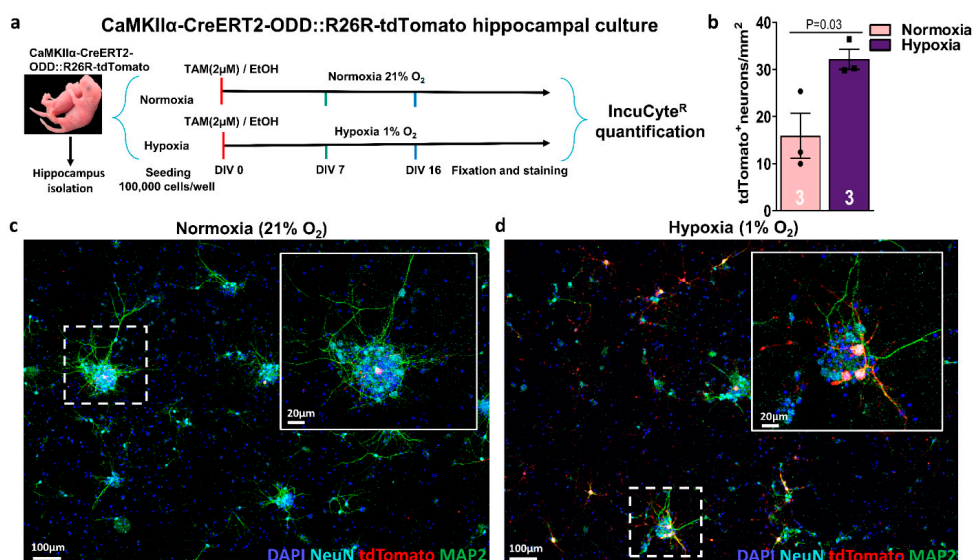
**Figure 3.** Maturing hippocampal neurons from CaMKIIα-CreERT2-ODD::R26R-tdTomato mice respond to hypoxia also in vitro. (**a**) Experimental design: Isolation and culture of hippocampal neurons from E17 pups. (Z)-4-hydroxytamoxifen (2 μM) or solvent control (final EtOH concentration always <0.016%) are added to neuron cultures on day in vitro (DIV)0, followed by incubation in the IncuCyte^R under either normoxia (21% O$_2$) or hypoxia (1% O$_2$) for seven or 16 days, fixation, staining, and quantification. (**b**) Quantification of hypoxic neurons, as visualized by tdTomato+ label, reveals an increase under hypoxia at DIV16. (**c**,**d**) Representative images of hippocampal neurons stained with neuronal markers NeuN (light blue), MAP2 (green) demonstrate co-localization with tdTomato (red), as shown strongly in hypoxic and less prominent in normoxic conditions. DAPI (blue) was used as a nuclear counterstain. Scale bars represent 100 μm in overview and 20 μm in magnified images. Unpaired Student's *t*-test (one-tailed, Welch's corrections) was used for statistical analysis between conditions; n numbers given in graphs; error bars indicate standard error of mean (SEM).

2.5. A Challenging Complex Motor-Cognitive Task but Not a Brief Conditioning Stimulus Induces Functional Neuronal Hypoxia in the Hippocampus

Using complex running wheel (CRW) performance as a challenging motor-cognitive task, a distinct increase in functional hypoxic neurons was assessed immunohistochemically in eight-week-old male and female mice (Figure 4a–c). Particularly in the dentate gyrus, tdTomato labeled neurons were highly abundant under functional hypoxia. Similar to what we observed upon inspiratory hypoxia quantifications (Figure 1e), they were rarer in CA1 and much rarer in CA3. As reported and extensively discussed earlier with the CAG-CreERT2-ODD::R26R-tdTomato mice [7], females displayed distinctly stronger labelling as compared to males (overall gender comparison *p* values CA1: 7.5×10^{-5}, CA3: 0.0034 and dentate gyrus: 0.00035; unpaired Welch's *t*-test, two-tailed).

Fear conditioning does not induce 'functional hypoxia'
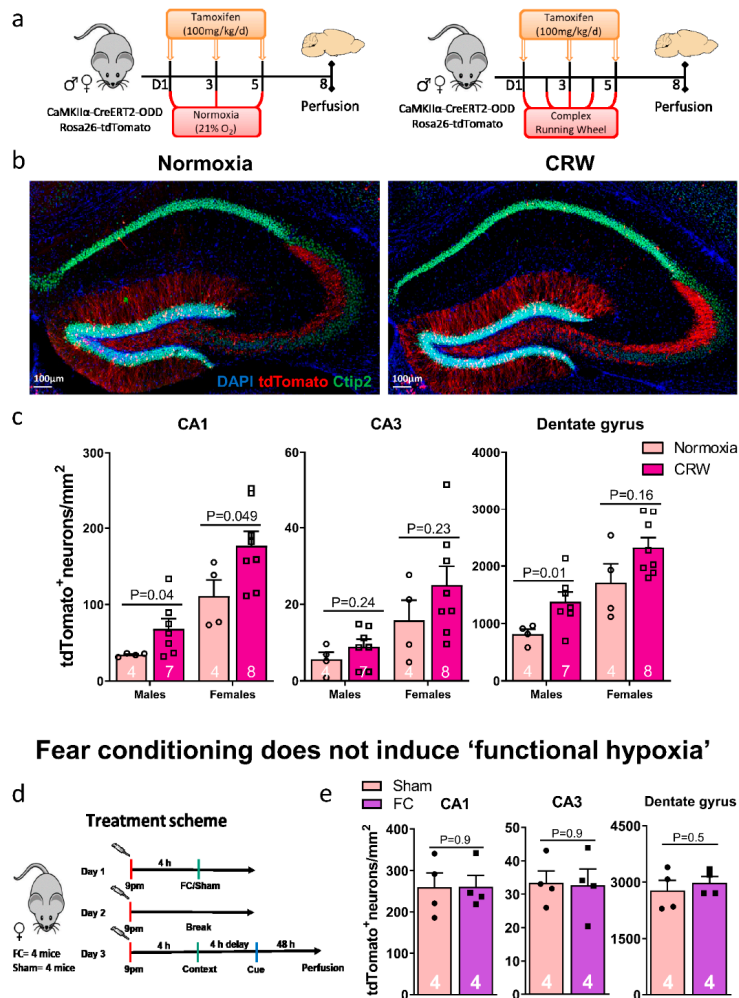
Figure 4. Complex motor-cognitive challenge as inducer of 'functional hypoxia' in the hippocampus. (**a**) Experimental design: mice with no prior training were given free access to complex running wheels (CRW) for five complete days and received tamoxifen injections every other day (three in total). Normoxia mice obtained the same treatment but were kept in standard cages. All mice were perfused on day eight and brains collected for histology. (**b**) Representative hippocampus images from eight-week-old female CRW-exposed and normoxia mice; scale bar 100 μm. (**c**) Quantifications of tdTomato+/Ctip2+ neurons in CA1, CA3, and dentate gyrus revealed an increase upon exposure to CRW in both genders, with normoxia and CRW values considerably more pronounced in females. (**d**) Experimental design of the fear conditioning (FC) pilot experiment (24-week-old females). (**e**) Quantification of tdT+/Ctip2+ neurons in hippocampal CA1, CA3, and dentate gyrus regions of sham and FC mice indicate no noteworthy difference. This is likely due to the FC stimulus being too short-lived to evoke functional hypoxia. Unpaired Student's *t*-test (two-tailed, Welch's corrections); n numbers given in graphs; error bars indicate standard error of mean (SEM).

We next wondered whether a very brief conditioning stimulus, leading to an extended imprinting of a negative memory (in this case, foot shocks in a defined context, also combined with a tone), would equally result in functional hypoxia of the involved hippocampal neurons. In contrast to CRW, however, contextual fear conditioning as hippocampal

stimulus combined with cue memory as primarily amygdala readout was likely too short-lived and 'weak' to provoke detectable neuronal hypoxia in a pilot group of female mice (Figure 4d,e).

Lightsheet microscopy allowed a three-dimensional presentation of stained neurons, with fly-through stacks yielding an ostensive dose-response curve from the nearly negative 'no tamoxifen' condition (lack of substantial non-induced expression of the transgene) to normoxia and to hypoxia (Supplementary Materials-LSM Video S1). In fact, CRW-induced functional neuronal hypoxia was so strong that the tdTomato labeling reached the overall level obtained by inspiratory hypoxia, offering to pool and analyze these two hypoxia conditions together (Figure 5a–c). LSM quantifications under hypoxia (both functional and inspiratory) compared to normoxia (sitting controls) showed a clear trend towards an increase but failed statistical significance due to the considerable mouse-to-mouse variation resulting in a relatively large scatter (Figure 5c; Supplementary Materials-LSM Video S2).
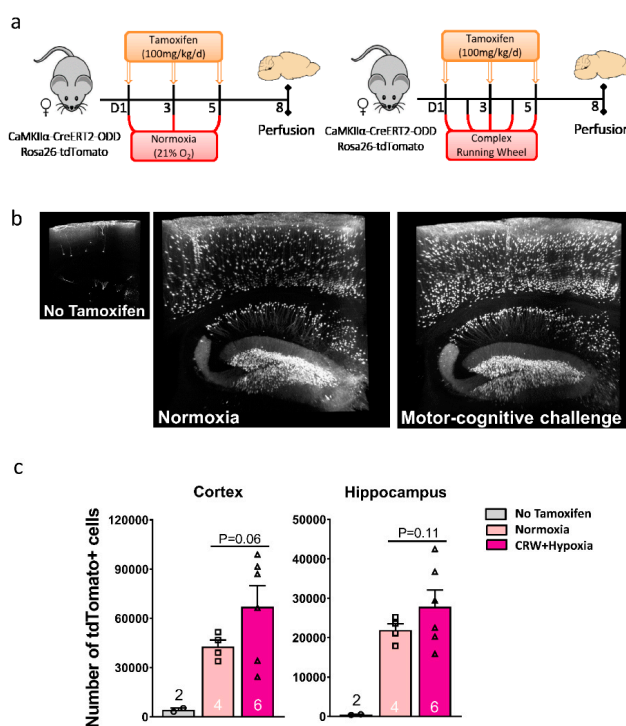
Figure 5. Light-sheet microscopy (LSM) enables 3D presentation of hypoxic neurons in CaMKIIα-CreERT2-ODD::R26R reporter mice. (**a**) Experimental design. (**b**) Illustrative 3D images rendered in maximal intensity modus demonstrate tdTomato+ hypoxic neurons in hippocampus and cortex of female normoxia versus CRW mice; the small image on the left displays a 'no tamoxifen' control brain with very few scattered tdTomato+ neurons. Scale: $1.96 \times 2.28 \times 0.4$ mm. (**c**) LSM quantification of tdTomato+ cells in cortex and hippocampus of eight-week-old female mice show a clear tendency of an equally strong increase under CRW and hypoxia (groups thus pooled) as compared to normoxia, with the 'no tamoxifen' condition being negligible. Unpaired Student's *t*-test (two-tailed, Welch's corrections); n numbers given in graphs; error bars indicate standard error of mean (SEM).

2.6. Transcriptome Data Reveal Profound Regulation of CamkIIα Expressing Neurons Upon Hypoxia vs. Normoxia

We next employed our scRNA-seq dataset of mouse hippocampus (from CAG-CreERT2-ODD::R26R-tdTomato mice) collected upon normoxia (21% O_2) versus inspiratory hypoxia (6% O_2 for six hours/day) for five consecutive days (compare Figure 1b; GSE162079 [7]), to evaluate the hypoxia regulation of all cells expressing the CaMKIIα-promoter. In the first step, we selected all glutamatergic neuronal populations (including mossy fiber cells), known to express *CaMKIIα* [12–15] from the hippocampal dataset and compared the expression levels of *CaMKIIα* under normoxic and hypoxic conditions (Figure 6a). Surprisingly, *CaMKIIα* was consistently upregulated under hypoxia in the excitatory neurons from the three discernible hippocampal regions (CA1, CA3, dentate gyrus). Given that CaMKIIα is known to be a crucial mediator of synaptic plasticity, longterm potentiation as well as memory formation and learning [16–19], this hypoxia-dependent regulation might point to a common pathway that is activated via endogenous functional hypoxia upon neuronal activation and mirrored by exogenous inspiratory hypoxia. In fact, it could very well support our working model of functional hypoxia-induced 'brain hardware upgrade'.

Importantly, neither the overall expression level of *CaMKIIα* nor the strength of upregulation under hypoxia in the three hippocampal regions were indicative of the amount of tdTomato-labelling observed in immunohistochemistry; e.g., the expression of *CaMKIIα* and its upregulation under hypoxia was strongest in CA3 (*CaMKIIα* expression CA3 versus CA1: $p = 1.68 \times 10^{-52}$, logFC = 0.25; CA3 versus the dentate gyrus: $p = 9.96 \times 10^{-9}$, logFC = 0.16), whereas the number of tdTomato-labelled neurons (IHC) was lower in CA3 when compared to CA1 and the dentate gyrus (Figures 1e and 4c). Overall, baseline expression of *CaMKIIα* was high, with 97%, 99%, and 93% of excitatory neurons expressing this gene under normoxia in CA1, CA3, and the dentate gyrus, respectively. Thus, although a certain amount of hypoxia 'over-reporting'—driven by the increased activity of the promoter under hypoxia—cannot be entirely excluded, the regional differences in the strength of hypoxic response we observed with immunohistochemical quantification (tdTomato-labelling) likely reflect true differences in the physiological response of neurons from different hippocampal regions to hypoxia. A systematic error affecting regional differences therefore seems highly unlikely.

In order to further explore the transcriptomic hypoxia response of *CaMKIIα*-neurons, we performed differential expression analyses. Figure 6b depicts the top 20 up- and top 20 downregulated genes under hypoxia after clustering cells and genes by k-means clustering. The major regulated gene clusters included genes of the tubulin (cluster 2) and hemoglobin (cluster 5) family as well as ribosomal genes (cluster 4). Clustering of cells revealed three distinct cell populations with cluster 2 and 3 almost exclusively corresponding to either cells derived from mice exposed to normoxia (cluster 2) or hypoxia (cluster 3). In contrast, cluster 1 was composed of cells from both conditions showing a somewhat 'intermediate' expression of hypoxia-regulated genes, e.g., see gene clusters 2, 4, and 5. The subpopulation of cells, which was derived from mice kept at normoxic conditions but appeared to have a mild hypoxia transcriptome signature, might represent cells that recently underwent physiological functional hypoxia. Notably, these cells were mainly situated in the dentate gyrus, a hippocampal region that harbors a neurogenic niche known to require hypoxia for its functionality [21].
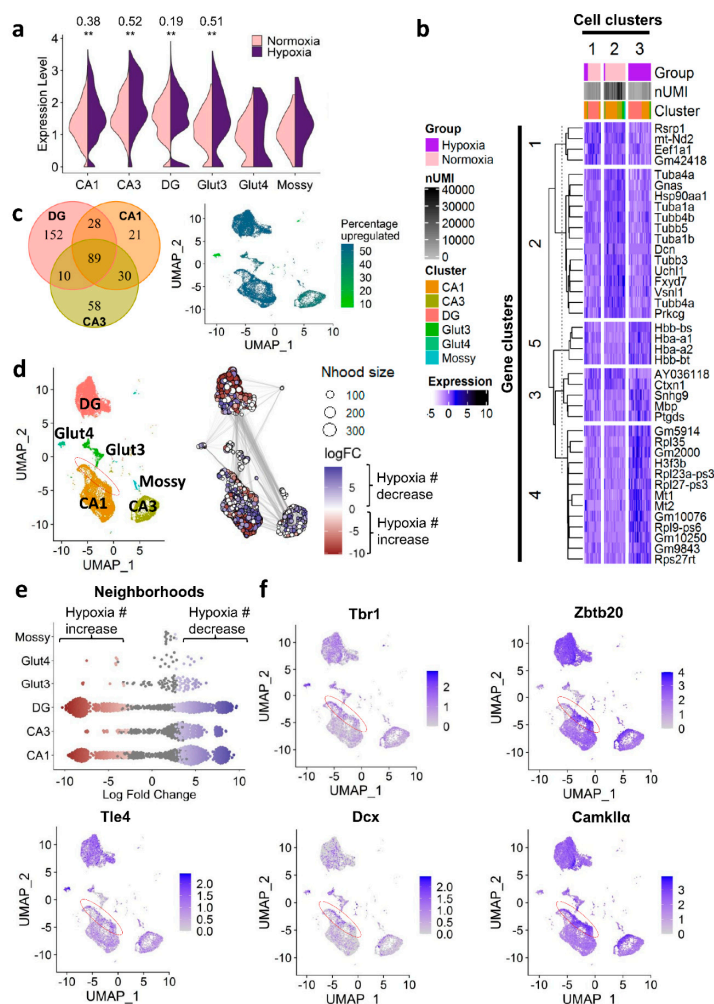
Figure 6. Response of hippocampal excitatory neurons to hypoxia evaluated by scRNA-seq. (**a**) Upregulation of *CaMKIIα* under hypoxia (five days, 6% O_2 for 6 h/day) in excitatory neurons of the hippocampus. (**b**) Heatmap of top 20 upregulated and top 20 downregulated genes under hypoxia. Columns represent cells, rows represent genes. Scaled normalized expression shown. Cells and genes were clustered using the k-means algorithm. Number of unique molecular identifiers per cell: nUMI. (**c**) Left panel: Venn diagram depicting number of shared and uniquely regulated genes under hypoxia amongst excitatory neurons of different hippocampal regions (CA1, CA3, dentate gyrus). All clusters were randomly down-sampled to n = 2296 cells for better comparability. Right panel: Percentage of upregulated genes amongst all hypoxia-regulated genes; |log-fold change| > 0.25, *p*-adj < 0.05, correlation-adjusted Wilcoxon test. (**d**) Differential cell abundance testing with MiloR [20]. Red (= negative logFC) represents a numerical increase upon hypoxia in the respective neighborhood, blue (= positive logFC) indicates a decrease. Region marked in red specifies region of immature and intermediately mature neurons of CA1 increased in number under hypoxia. logFC: log-fold change, Nhood size: neighborhood size. (**e**) Beeswarm plot showing the numerical increases and decreases under hypoxia in the respective neighborhoods of each cell cluster. Red (=negative logFC) indicates an increase under hypoxia, blue (= positive logFC) a decrease. (**f**) Expression of immature and intermediately mature excitatory neuron markers. Red oval indicates again the interesting region denoted in (**d**) with increase in cell abundance upon hypoxia.

In addition, the number of (uniquely) hypoxia regulated genes ($|logFC| > 0.25$, $p_{adj} < 0.05$) was highest in the dentate gyrus. Down-sampling of cells included into differential testing ($n = 2296$, i.e., equal to the size of CA3 as the smallest region) was performed beforehand to avoid differences in the number of detectable, differentially expressed genes due to differences in statistical power (Figure 6c, left panel). This finding points again to a specific and elevated responsivity to hypoxia in the dentate gyrus as compared to CA. In total, 89 genes were equally regulated under hypoxia in CA1, CA3, and the dentate gyrus. As shown in Figure 6c, right panel, the percentage of upregulated genes amongst all regulated genes in CA1 and the dentate gyrus was ~54%, whereas in CA3 the majority of genes was downregulated (44% upregulated). Cluster Glut4, a very small cluster characterized by a high expression of immature neuronal markers such as *Dcx*, *Tbr1*, and *Tle4*, showed a remarkable downregulation of genes with ~93% of all hypoxia differentially expressed genes being downregulated. This cluster is highly similar to the cluster of immature CA1 neurons responding to EPO already six hours after rhEPO administration that we identified earlier [6]. At this point, the physiological relevance of the strongly dampening gene regulatory response in this immature cell subpopulation remains unclear, but certainly will be investigated in future studies.

Next, we investigated numerical abundance changes in the different excitatory neuron populations of the hippocampus using MiloR [20]. This tool allows a fine-grained analysis of numerical abundance shifts under hypoxia by forming neighborhoods of similar cells within each cell cluster and assessing their numerical abundance in each treatment condition. Figure 6d,e show the numerical shifts in each neighborhood. In CA1 and the dentate gyrus, numerically increased (red) as well as numerically decreased (blue) neighborhoods were detected under hypoxia. In contrast, CA3 neurons appeared to primarily respond to hypoxia with a numerical decrease (blue). Interestingly, in the CA1 neurons, there was a small subpopulation of cells located at the rim of the cluster (red oval in Figure 6d), which were increased in number under hypoxia. Inspection of expression markers indicated that these cells were of immature neuronal identity as shown by the high expression of *Tbr1*, *Zbtb20*, *Tle4*, and *Dcx* (Figure 6f). In addition, *CaMKIIα* expression, shown to be important for neuronal maturation in the hippocampus [22], appeared to be elevated in these cells (Figure 6f). Interestingly, previous literature inconsistently reported both negative as well as positive effects of exogenously applied hypoxia on neuronal development, differentiation, and maturation [23–29]. Our current findings indicate a positive, stimulating effect on neuronal differentiation, resulting in an increased number of young neurons in CA1. Importantly, this apparent incongruence of existing findings might not only be due to the different modes and severity of hypoxia application, but also due to a previous lack of more distinct inspections of different neuronal precursor and immature neuron populations in the hippocampus, which we provide here.

2.7. Synopsis of Our Model: Hypoxia as a Fundamental Driving Force of Demand-Oriented Neuroplasticity and the Consequential 'Brain Hardware Upgrade'

In an extensive line of research, we have shown over the last two decades that rhEPO treatment improves cognition and increases brain matter in humans and rodents, both healthy and diseased, but the underlying mechanisms have been unknown for a long time. Just recently, we discovered a fundamental regulatory circle, in which brain networks, challenged by cognitive tasks, drift into 'functional hypoxia' that drives neurodifferentiation and dendritic spine formation via neuronal EPO synthesis [6]. These findings highlight that EPO is not only a crucial mediator of neurogenesis during embryonic life and brain development [30,31], but also pivotal for adult hippocampal neurodifferentiation and neuroplasticity on demand. The neuroprotective and anti-apoptotic effects of EPO, promoting neuronal survival, together with its neurotrophic properties, certainly contribute to the observed enhanced differentiation of local silent precursors and to their undisturbed maturation.

From the discovery of this regulatory EPO circle, driving challenge-induced brain maturation, we moved on to study the hypoxia response of all brain cells [7], and in the

present work specifically of pyramidal neurons, employing our transgenic mouse models pCAG-CreERT2-ODD and pCaMKIIα-CreERT2-ODD, respectively.

In the sense of 'dosis facit venenum', strong oxygen deficit or hypoxia in the brain, as seen after cardiac arrest or in stroke, is definitely a serious state of emergency leading to permanent brain damage. Nevertheless, as shown here, functional hypoxia can be an important signal for growth and a driving force of the 'brain hardware upgrade'.

Hypoxia induces a specific transcriptional program, enabling cells to adapt to lower oxygen levels and/or to inadequate metabolic support. The transcription is to some degree controlled by hypoxia-inducible factors, binding to hypoxia-responsive elements to modulate the expression of many genes, some of which are potent growth factors such as vascular endothelial growth factor (VEGF) or EPO. Newer work, however, has revealed that hypoxia-induced gene transcription is partly Hif-independent [32,33]. Hence, the immunohistochemical findings reported here including LSM are based on Hif mechanisms, and may, therefore, only partly reflect the global cellular hypoxia response. In contrast, our transcriptome data seem to approach the whole hypoxia regulation more fundamentally. Overall, they strongly support the pivotal effects of hypoxia on neuronal differentiation and brain maturation.

Ultimately, moderate hypoxia, at least partly via brain EPO expression, may evolve as a highly promising add-on treatment strategy for neurodevelopmental, neuroinflammatory, and neurodegenerative brain diseases, applicable in the sense of individualized therapeutic approaches to still untreatable conditions.

3. Materials and Methods

3.1. Generation of the CaMKIIα-CreERT2-ODD-pAa Vector

The genetic strategy for the generation of the CaMKIIα-CreERT2-ODD-pA vector is illustrated in Figure 1a. Briefly, the construct consists of the murine CaMKIIα promoter, active in excitatory neurons, which drives the expression of tamoxifen-inducible Cre-recombinase (Cre-ERT2), fused to the oxygen-dependent degradation domain (ODD) of Hif-1α. The latter responds to varying oxygen concentrations. The pCAG-CreERT2-ODD-pA plasmid was kindly provided by Dr. Hashim A Sadek (USA) [11] and slightly modified [7]. In the first step, the CAG promoter was excised by digesting CAG-CreERT2-ODD-pA with SpeI and EcoRI restriction enzymes. In parallel, the CaMKIIα promoter fragment of 8.5 kb was obtained by digesting the CaMKIIα-HA-cEPOR vector [34,35] with XmaI, NdeI, PacI, and NotI restriction enzymes (New England Biolabs, USA). In a second step, this CaMKIIα promoter fragment was ligated upstream into the CreERT2-ODD vector to yield CaMKIIα-Cre-ERT2-ODD-pA.

3.2. CamkIIα-CreERT2-ODD: R26R-tdTomato Transgenic Mice: Generation & Validation

CaMKIIα-Cre-ERT2-ODD-pA was digested with the SfiI and SalI (New England Biolabs, USA) restriction enzymes and the ampicillin selection sequence removed. After gel elusion with the QIAquick gel extraction kit (Qiagen, Venlo, Netherlands), linearized DNA of 11.6 kb was obtained comprising CaMKIIα promoter, inducible Cre-recombinase, and ODD sequence. The linearized DNA was used for pro-nuclear microinjection into fertilized eggs for the production of CaMKIIα-CreERT2-ODD transgenic mice. Litters from the foster mothers were screened for the presence of CaMKIIα and ODD sequence by genotyping as explained below for suitable transgenic founders. CaMKIIα-CreERT2-ODD transgenic mice were maintained on C57BL/6N background (Charles River, MA, USA) and F1 litters carrying the CaMKIIα-CreERT2-ODD transgene were selected and further crossed with C57BL/6N and R26R-tdTomato mice for colony maintenance and to generate the desired heterozygous reporter mice. F2 litters of both genders harboring the CaMKIIα-CreERT2-ODD::R26R-tdTomato transgene were used for the experiments. All transgenic mice showed normal breeding, home cage behavior and life expectancy, and lacked any obvious abnormal phenotype.

3.3. Genotyping

Genotyping polymerase chain reaction (PCR kit, Biozym, Oldendorf, Germany) was performed by using the following primers for *CaMKIIα* promoter, forward: 5′-GGTTCTCCGTTT GCACTCAGGA-3′ and reverse: 5′-CCATGAGTGAACGAACCTGG-3′ and for ODD forward: 5′-GCTGAAGACACAGAAGCAAA-3′ and reverse: 5′-GTGGGTAGGAGATGGAGATG-3′. In the subsequent generation, CaMKIIα-CreERT2-ODD::R26R-tdTomato transgenic F2 offspring, harboring the tdTomato sequence were screened by the following primers: Primer1: 5′TCAATGGGCGGGGGTCGTT3′; Primer2: 5′CTCTGCTGCCTCCTGGCTTCT3′; Primer3: 5′CGAGGCGGATCACAAGCAATA3′. Complete PCR protocols are available on request.

3.4. Mouse Maintenance

All experiments were approved by and conducted in accordance with the regulations of the local Animal Care and Use Committee (Niedersächsisches Landesamt für Verbraucherschutz und Lebensmittelsicherheit, LAVES). CaMKIIα-CreERT2-ODD::R26R-tdTomato mice were kept on the C57BL/6N genetic background, group-housed, maintained in a germ-free and temperature (21 ± 2 °C)-controlled environment on a 12 h light/dark schedule. Adult transgenic mice from F2 generation (seven to eight weeks old) of both genders, harboring the CaMKIIα-CreERT2-ODD::R26R-tdTomato transgene, were used in the experiments unless otherwise stated. Each mouse was single-housed for habituation before the start of the experiment. All mice (normoxia, hypoxia, CRW, 'no tamoxifen') were handled in the same way, and euthanised two days after the last tamoxifen/solvent control injection. See the experimental designs in the figures for details.

3.5. Tamoxifen Preparation

A stock solution of tamoxifen was prepared by mixing 300 mg tamoxifen in 30 mL of corn oil (both Sigma-Aldrich, Darmstadt, Germany) by sonication at 37 °C and stored at 4 °C. To label the hypoxic cells in normoxia, CRW, or hypoxia mice, a working solution of tamoxifen (100 mg/kg) was freshly warmed up, sonicated for 20 min before each application, and injected intraperitoneally (i.p.) as stated in the experimental designs. The 'no tamoxifen' controls received vehicle (corn oil) only.

3.6. Hypoxia Application

Exogenous hypoxia was applied to CaMKIIα-CreERT2-ODD::R26R-tdTomato mice in a small hypoxia chamber (60 cm × 38 cm × 20 cm), custom-designed in cooperation with Coy Laboratory Products (Michigan, USA). The hypoxia chamber is connected to an oxygen sensor, a stage controller and a ceiling fan for constant air circulation. In the hypoxia treatment group, CaMKIIα-CreERT2-ODD::R26R-tdTomato mice received a first dose of tamoxifen (100 mg/kg/d) and were then put into the hypoxia chamber. The ambient oxygen concentration (20.9% O_2) was dropped to 6% O_2 within 15 min, kept for 6 h and then increased back to 20.9% O_2. In the normoxia, CRW, and 'no tamoxifen' group, mice received tamoxifen injections or corn oil, respectively, and were kept in ambient oxygen concentration (20.9% O_2).

3.7. Complex Running Wheel (CRW) Exposure

CRW is a simple, sensitive, and fully computerized voluntary wheel-running task, which is frequently used to detect motor-cognitive and activity impairments in mice [36,37]. The CRW (TSE Systems, Bad Homburg, Germany) is defined by irregularly spaced bars. The locomotor activity and running performance is computer-controlled via Phenomaster software (TSE Systems, Bad Homburg, Germany). Untrained CaMKIIα-CreERT2-ODD::R26R-tdTomato transgenic mice (eight-week-old; both genders) were given tamoxifen injections every other day (Figure 4a) and had continued free access to CRW for five days. On day five, mice were transferred back to standard cages for two days and later perfused.

3.8. Fear Conditioning

Fear conditioning (Med Associates inc, Hertfordshire, United Kingdom) was performed in a single trial (design in Figure 4d) in which, after a 120 s baseline period, mice experienced two paired presentations of a 10 s, 5 kHz, 85 dB tone (conditioned stimulus) and an electrical foot shock for 2 s with an intensity of 0.4 mA (unconditioned stimulus, Context A). The control group (SHAM) consisted of mice exposed to the context only. The contextual memory was assessed 48 h after training (Context A). Trained mice and control mice were observed over 120 s for freezing inside the conditioning chamber. After 4 h, mice were placed in an unfamiliar, new chamber (Context B) and were, after an initial 120 s baseline phase, re-exposed to the tone (CS) to assess cued memory/fear over 120 s.

3.9. Hippocampal Neuronal Culture and Image Acquisition

For the neuronal culture, CaMKIIα-ODD-CreERT2::tdTomato fetuses were extracted from the uterus at approximately embryonic day 17 (E17). Hippocampi were dissected from the brain and the meninges were removed before digestion with 0.05% trypsin for 10 min at 37 °C. Subsequent washes were performed in a neuronal culture medium containing 2% B27 (cat. no. 17504044), 1% GlutaMAX (cat. no. 35050087), and 1% penicillin/streptomycin (cat. no. 15140163) in Neurobasal A (cat. no. 10888022, all from Gibco, Thermo Fisher Scientific, Darmstadt, Germany). Single-cell suspension was obtained by careful dissociation of the tissue with a P200 micropipette. Seeding was conducted using poly-D-lysine (PDL) (Sigma-Aldrich, Darmstadt, Germany)-coated glass coverslips in 24-well plates, in densities of 100,000 cells/well. The same day of the preparation, fresh 2 μM (Z)-4-hydroxytamoxifen (H79049, Sigma-Aldrich, Hamburg, Germany) or an equivalent volume of 99.8% pure ethanol (EtOH) (Honeywell, North Carolina, USA) were prepared and added to the cultured wells. The final EtOH concentration was always <0.016%. Cells were incubated at 37 °C in 5% CO_2, in either normoxia (21% O_2) or hypoxia (1% O_2), for seven or 16 days. Then, fixation was performed with 2% acrolein (Sigma-Aldrich, Darmstadt, Germany) and 3% formaldehyde (Merck, Darmstadt, Germany) in PBS. IncuCyte[R] ZOOM (Sartorius, Ann Arbor, MI, USA) images (1400 × 1400 μm) were taken with a 10× objective using phase contrast and the red fluorescent channel. For the neuronal quantification of tdTomato+ cells, images were processed in IncuCyte[R] ZOOM software with TopHat parameter (radius = 100 μm, threshold red calibrated unit = 0.5) and edge split sensitivity = −10.

3.10. Tissue Preparation and Immunohistochemistry

For tissue harvesting and perfusion, Avertin (Tribromoethanol, Sigma-Aldrich, St Louis, MN, USA, 0.276 mg/g) was used for deep sedation by intraperitoneal injection followed by perfusion with ice cold 0.9% saline solution and 4% formaldehyde (Merck, Darmstadt, Germany). The brains were removed, placed in 4% formaldehyde at 4 °C for 24 h, then cryoprotected in 30% sucrose in phosphate buffered saline (PBS) (Merck, Darmstadt, Germany) at 4 °C for 48 h, finally covered in cryoprotectant (O.C.T.TM Tissue-Tek, Sakura, The Netherlands) and preserved at −80 °C until use. In preparation for immunohistochemistry (IHC), brains were cut into 30-μm-thick coronal sections using a cryostat (Leica, Wetzlar, Germany) and stored floating in a cryoprotective solution (25% ethylene glycol and 25% glycerol in PBS (Sigma-Aldrich, Darmstadt, Germany) at 4 °C. For IHC, five sections (30 μm) from each mouse were washed and blocked for 1 h in 5% horse serum in PBS with 0.5% Triton X-100 (Sigma-Aldrich, Darmstadt, Germany) at room temperature (RT). Primary antibodies were diluted in 3% horse serum (Jackson ImmunoResearch, West Grove, Pennsylvania, USA) in PBS/0.3% Triton X-100 and sections incubated for 48 h at 4 °C, followed by washing and incubation with the respective secondary antibodies for 2 h at RT. For nuclear counterstaining, 4′,6-diamidino-2-phenylindole (DAPI, Sigma, Missouri, United States) was used. The sections were then mounted on SuperFrostPlus slides (ThermoFisher, Darmstadt, Germany) with Aqua-Polymount (Polysciences, Inc. Warrington, PA, USA). For the direct visualization of tdTomato, sections were only counterstained

with nuclear stain (DAPI) and investigated by confocal microscope (Leica TCS SP5-II; Mannheim, Germany). The primary antibodies applied were anti-NeuN (1: 1000, mouse; Millipore, Darmstadt, Germany), and anti-Ctip2 (1: 500, guinea pig; SYSY, Göttingen, Germany). The secondary antibodies used were Alexa488 anti-guinea pig (1: 500, Invitrogen, Darmstadt, Germany), and Alexa647 anti-mouse (1: 500; ThermoFisher, Darmstadt, Germany). For the quantification of NeuN+tdTomato+ co-labelled cells, sequential coronal sections from the dorsal part of hippocampus were taken (coordinates from Bregma: −1.34 to −2.54 mm posterior). Stained sections (30 μm) were imaged using Leica TCS SP5 (Mannheim, Germany), equipped with a 20× objective (NA = 0.70). Hypoxic neurons (Ctip2+tdTomato+) from CA1, CA3, and the dentate gyrus were counted manually by Fiji software (https://imagej.net/Fiji, accessed on 18 February 2021). Representative images of bilateral hippocampi from five sections per mouse were processed/analyzed using Imaris 9.1.0 (www.bitplane.com, accessed on 18 February 2021).

3.11. Light-Sheet Microscopy (LSM)

Whole mount tissue staining and clearing:

To visualize the tdTomato+ cells in the entire brain, we performed LSM in combination with whole mount immune labelling and tissue clearing. Following transcardial perfusion as described above, the brains were removed, post-fixed in 4% PFA overnight and stored in PBS. The brain hemispheres were processed for immune-labelling and tissue clearing following a slightly modified iDISCO protocol [38]. The samples were dehydrated with a methanol/PBS series (50%, 80%, 100%, and 2 × 100%, 1 h, RT) followed by overnight bleaching and permeabilization in a mixture of 5% H_2O_2/20% dimethyl sulfoxide (DMSO) (Sigma-Aldrich, Darmstadt, Germany) in methanol at 4 °C. Samples were retrieved and washed further with methanol at 4 °C for 30 min and −20 °C for 3 h prior to incubation in 20% DMSO in methanol at RT for 2 h. Samples were then rehydrated using a descending methanol/PBS series (80%, 50%, PBS, 1 h each, RT) and further washed with in PBS/0.2% TritonX-100 for 2 h. The samples were then incubated overnight in 0.2% TritonX-100, 20% DMSO, and 0.3 M glycine in PBS at 37 °C and blocked using PBS containing 6% goat serum, 10% DMSO and 0.2% Triton-X100 for two days at 37 °C. The samples were then washed twice in PBS containing 0.2% Tween(r)20 and 10 μg/mL heparin (PTwH) at RT for 1 h and incubated with primary antibody solution (anti-RFP; Rockland # 600-401-379, Pennsylvania, USA; 1: 250 in PTwH/5%DMSO/3% goat serum) for 14 days at 37 °C. After several washes during the day and an additional overnight wash in PTwH, the samples were incubated with secondary antibody solution (goat anti-rabbit Alexa555; ThermoFisher Scientific Darmstadt, Germany; # A-21428; 1: 500 in PTwH/3% goat serum) for seven days at 37 °C. Prior to clearing, the samples were again washed in PTwH (several solution changes during the day) followed by an additional overnight wash. Tissues were dehydrated using an ascending series of methanol/PBS (20, 40, 60, 80, and 2 × 100% 1 h, RT) followed by overnight incubation in a mixture of 33% dichloromethan (DCM) and 66% methanol at RT. Samples were further delipidated by incubation in 100% DCM for 40 min and transferred to pure ethyl cinnamate (Eci; Sigma Aldrich #112372, Darmstadt, Germany) as the clearing agent. The tissues became transparent after 30 min in Eci and were stored at RT until imaging.

LSM and 3D analysis/visualisation:

LSM was performed using a LaVision Ultramicroscope II equipped with a 2× objective, corrected dipping cap and zoom body. Samples were mounted onto the sample holder with the medial surface of the brain hemisphere facing down in order to acquire sagittal images. The holder was placed into the imaging chamber filled with Eci. The images were acquired in mosaic acquisition mode with the following specifications: 5 μm sheet thickness; 20% sheet width; 2x zoom; 4 × 5 tiling; 4 μm z-step size; dual site sheet illumination; 50 ms camera exposure time; 1000 px × 1600 px field of view. Red fluorescence was recorded using 561 nm laser excitation (5 to 10%) and 585/40 emission filters. Images were loaded into Vision4D 3.0 (Arivis) and stitched using the tile sorter setup. Hippocampus and

cortex regions of interests (ROIs) where manually annotated according to the sagittal Allen mouse brain atlas [39]. For this, hippocampus and cortex ROIs were traced manually in a few planes in 2D from which the 3D ROI was extrapolated automatically. Cortex and hippocampus annotations were then cropped with a medial cut-off of approximately 0.4 mm and a lateral cut-off of approximately 4.4 mm (corresponding to the lateral end of the hippocampal formation). Cortex ROIs spanned the dorsal parts of the cortex as defined by anatomical landmarks. Next, tdTomato+ cells per ROI were identified using the blob finder algorithm in Vision4D. Noise was removed by deleting objects with voxel sizes < 10 from the object table. Objects were then critically reviewed, and any additional noise was manually removed from the dataset. The number of tdTomato+ cells per ROI was extracted from the object table and plotted using GraphPad (Prism). For visualisation purposes, a $1300 \times 1400 \times 100$ px field of view spanning the hippocampus and overlaying the cortex was cut out from the original datasets and visualized in the 3D maximal intensity modus. Whole-brain and hippocampal 3D videos as well as 'flythrough' stacks were rendered in Vision4D.

3.12. scRNA-seq

Single-cell RNA sequencing (scRNA-seq) data was obtained and processed as described in detail earlier [7] (GSE162079). For the purpose of the current paper, only excitatory neuron populations known to express *CaMKIIα* were included in the analyses. All analyses were performed using R v4.0.0 [40], except for the MiloR package, which was run in R v4.0.3. Differentially expressed genes between hypoxia and normoxia were identified using the FindMarkers() function with default settings (two tailed correlation-adjusted Mann-Whitney U test, |log-fold change| > 0.25) in Seurat v3.1.5 [41] (please note that the empty brackets indicate the use of respective functions with its default settings). The regional assignment of neuronal clusters was performed using the following markers: *Mpped1* for CA1, *Mndal* for CA3, and *Prox1* for DG. Mossy fiber cells were characterized by the strong expression of *Calb2* [42], while the Glut3 cluster was showing a high expression of *Tshz2*, possibly indicating subicular origin [43]. Glut4 was high in the expression of *Tbr1*, *Dcx*, and *Tle4*, indicating an immature cell state [6]. In order to mitigate power-related differences in the number of detectable differentially expressed genes, clusters were down-sampled to the smallest cluster included in the comparison, i.e., CA3 with $n = 2296$ (Figure 6c, left panel). For easier visualization, a small number of cells located far below on the UMAP2 axis were shifted upwards. The heatmap was created with the ComplexHeatmap package [44]. The Venn diagrams were created with with VennDiagram [45]. The numerical changes under hypoxia versus normoxia were investigated using the MiloR v0.1.0 [20] package. The graph was built using buildGraph($k = 30$, $d = 30$) and neighbourhoods were defined with the same paramaters by makeNhoods() and setting the proportion of randomly sampled graph vertices to prop = 0.2. Distances between the nearest neighbours were calculated with calcNhoodDistance ($d = 30$). Cells per neighbourhood were quanitfied with countCells(). Differential abundance testing was performed with testNhoods(design= ~experimental_group) and the results were visualized after calling buildNhoodGraph() with plotNhoodGraphDA(). On https://github.com/AgnesSteixner/Butt_et_al_Camk2a, accessed on 18 February 2021, analysis scripts are available. Bonferroni-adjusted (Seurat) or false discovery rate-adjusted (MiloR) *p*-values were reported.

3.13. Statistical Analysis

Data obtained for all quantifications were analyzed by Graph Pad Prism 8 (GraphPad Software, Inc. San Diego, CA, USA). The statistical significance was calculated by using an unpaired Welch's *t*-test to compare two groups. A *p* value < 0.05 was considered statistically significant. All bar graphs show means and error bars represent the standard error of mean (SEM).

150

References

1. Brines, M.; Cerami, A. Emerging biological roles for erythropoietin in the nervous system. *Nat. Rev. Neurosci.* **2005**, *6*, 484–494. [CrossRef]
2. Jelkmann, W. Regulation of erythropoietin production. *J. Physiol.* **2011**, *589*, 1251–1258. [CrossRef]
3. Krantz, S.B. Erythropoietin. *Blood* **1991**, *77*, 419–434. [CrossRef]
4. Grasso, G.; Alafaci, C.; Ghezzi, P. Is erythropoietin a worthy candidate for traumatic brain injury or are we heading the wrong way? *F1000Research* **2016**, *5*, 911. [CrossRef] [PubMed]
5. Schuler, B.; Vogel, J.; Grenacher, B.; Jacobs, R.A.; Arras, M.; Gassmann, M. Acute and chronic elevation of erythropoietin in the brain improves exercise performance in mice without inducing erythropoiesis. *FASEB J.* **2012**, *26*, 3884–3890. [CrossRef] [PubMed]
6. Wakhloo, D.; Scharkowski, F.; Curto, Y.; Butt, U.J.; Bansal, V.; Steixner-Kumar, A.A.; Wüstefeld, L.; Rajput, A.; Arinrad, S.; Zillmann, M.R.; et al. Functional hypoxia drives neuroplasticity and neurogenesis via brain erythropoietin. *Nat. Commun.* **2020**, *11*, 1–12. [CrossRef] [PubMed]
7. Butt, U.J.; Steixner-Kumar, A.A.; Depp, C.; Sun, T.; Hassouna, I.; Wüstefeld, L.; Arinrad, S.; Zillmann, M.R.; Schopf, N.; Garcia-Agudo, L.F.; et al. Hippocampal neurons respond to brain activity with functional hypoxia. *Mol. Psychiatry* **2021**, 1–18. [CrossRef]
8. Erickson, K.I.; Hillman, C.; Stillman, C.M.; Ballard, R.M.; Bloodgood, B.; Conroy, D.E.; Macko, R.; Marquez, D.X.; Petruzzello, S.J.; Powell, K.E. Physical Activity, Cognition, and Brain Outcomes: A Review of the 2018 Physical Activity Guidelines. *Med. Sci. Sports Exerc.* **2019**, *51*, 1242–1251. [CrossRef] [PubMed]
9. Kramer, A.F.; Erickson, K.I. Capitalizing on cortical plasticity: Influence of physical activity on cognition and brain function. *Trends Cogn. Sci.* **2007**, *11*, 342–348. [CrossRef]
10. Pajonk, F.-G.; Wobrock, T.; Gruber, O.; Scherk, H.; Berner, D.; Kaizl, I.; Kierer, A.; Müller, S.; Oest, M.; Meyer, T.; et al. Hippocampal Plasticity in Response to Exercise in Schizophrenia. *Arch. Gen. Psychiatry* **2010**, *67*, 133–143. [CrossRef] [PubMed]
11. Kimura, W.; Xiao, F.; Canseco, D.C.; Muralidhar, S.; Thet, S.; Zhang, H.M.; Abderrahman, Y.; Chen, R.; Garcia, J.A.; Shelton, J.M.; et al. Hypoxia fate mapping identifies cycling cardiomyocytes in the adult heart. *Nature* **2015**, *523*, 226–230. [CrossRef]
12. Benson, D.; Isackson, P.; Gall, C.; Jones, E. Contrasting patterns in the localization of glutamic acid decarboxylase and Ca2+ /calmodulin protein kinase gene expression in the rat centrat nervous system. *Neuroscience* **1992**, *46*, 825–849. [CrossRef]
13. Jones, E.; Huntley, G.; Benson, D. Alpha calcium/calmodulin-dependent protein kinase II selectively expressed in a subpopulation of excitatory neurons in monkey sensory-motor cortex: Comparison with GAD-67 expression. *J. Neurosci.* **1994**, *14*, 611–629. [CrossRef]

14. Sík, A.; Hájos, N.; Gulácsi, A.; Mody, I.; Freund, T.F. The absence of a major Ca^{2+} signaling pathway in GABAergic neurons of the hippocampus. *Proc. Natl. Acad. Sci. USA* **1998**, *95*, 3245–3250. [CrossRef] [PubMed]
15. Juárez-Muñoz, Y.; Ramos-Languren, L.E.; Escobar, M.L. CaMKII Requirement for in Vivo Insular Cortex LTP Maintenance and CTA Memory Persistence. *Front. Pharmacol.* **2017**, *8*, 822. [CrossRef] [PubMed]
16. Achterberg, K.G.; Buitendijk, G.H.; Kool, M.J.; Goorden, S.M.; Post, L.; Slump, D.E.; Silva, A.J.; van Woerden, G.M.; Kushner, S.A.; Elgersma, Y. Temporal and region-specific requirements of αCaMKII in spatial and contextual learning. *J. Neurosci.* **2014**, *34*, 11180–11187. [CrossRef] [PubMed]
17. Silva, A.; Stevens, C.; Tonegawa, S.; Wang, Y. Deficient hippocampal long-term potentiation in alpha-calcium-calmodulin kinase II mutant mice. *Science* **1992**, *257*, 201–206. [CrossRef] [PubMed]
18. E Lisman, J.; Schulman, H.; Cline, H.T. The molecular basis of CaMKII function in synaptic and behavioural memory. *Nat. Rev. Neurosci.* **2002**, *3*, 175–190. [CrossRef]
19. Lucchesi, W.; Mizuno, K.; Giese, K.P. Novel insights into CaMKII function and regulation during memory formation. *Brain Res. Bull.* **2011**, *85*, 2–8. [CrossRef] [PubMed]
20. Dann, E.; Henderson, N.; Teichmann, S.; Morgan, M.; Marioni, J. Milo: Differential abundance testing on single-cell data using k-NN graphs. *bioRxiv* **2020**. [CrossRef]
21. Chatzi, C.; Schnell, E.; Westbrook, G.L. Author response: Localized hypoxia within the subgranular zone determines the early survival of newborn hippocampal granule cells. *eLife* **2015**, *4*, 08722. [CrossRef]
22. Yamasaki, N.; Maekawa, M.; Kobayashi, K.; Kajii, Y.; Maeda, J.; Soma, M.; Takao, K.; Tanda, K.; Ohira, K.; Toyama, K.; et al. Alpha-CaMKII deficiency causes immature dentate gyrus, a novel candidate endophenotype of psychiatric disorders. *Mol. Brain* **2008**, *1*, 6. [CrossRef] [PubMed]
23. Vieira, H.L.; Alves, P.M.; Vercelli, A. Modulation of neuronal stem cell differentiation by hypoxia and reactive oxygen species. *Prog. Neurobiol.* **2011**, *93*, 444–455. [CrossRef] [PubMed]
24. Zhu, L.-L.; Wu, L.-Y.; Yew, D.T.; Fan, M. Effects of Hypoxia on the Proliferation and Differentiation of NSCs. *Mol. Neurobiol.* **2005**, *31*, 231–242. [CrossRef]
25. Večeřa, J.; Procházková, J.; Šumberová, V.; Pánská, V.; Paculová, H.; Lánová, M.K.; Mašek, J.; Bohačiaková, D.; Andersson, E.R.; Pacherník, J. Hypoxia/Hif1α prevents premature neuronal differentiation of neural stem cells through the activation of Hes1. *Stem Cell Res.* **2020**, *45*, 101770. [CrossRef] [PubMed]
26. McClendon, E.; Shaver, D.C.; Degener-O'Brien, K.; Gong, X.; Nguyen, T.; Hoerder-Suabedissen, A.; Molnár, Z.; Mohr, C.; Richardson, B.D.; Rossi, D.J.; et al. Transient Hypoxemia Chronically Disrupts Maturation of Preterm Fetal Ovine Subplate Neuron Arborization and Activity. *J. Neurosci.* **2017**, *37*, 11912–11929. [CrossRef] [PubMed]
27. Li, Y.; Zhang, Y.; Liu, X.; Wang, M.; Wang, P.; Yang, J.; Zhang, S. Lutein inhibits proliferation, invasion and migration of hypoxic breast cancer cells via downregulation of HES1. *Int. J. Oncol.* **2018**, *52*, 2119–2129. [CrossRef]
28. Khuu, M.A.; Pagan, C.M.; Nallamothu, T.; Hevner, R.F.; Hodge, R.D.; Ramirez, J.-M.; Garcia, A.J. Intermittent Hypoxia Disrupts Adult Neurogenesis and Synaptic Plasticity in the Dentate Gyrus. *J. Neurosci.* **2018**, *39*, 1320–1331. [CrossRef]
29. Nallamothu, T.; Castro-Rivera, C.; Vera, A.; Garcia, A.J. Changes in Cellular Composition of Dentate Gyrus in Response to Intermittent Hypoxia. *FASEB J.* **2020**, *34*, 1. [CrossRef]
30. Constanthin, P.E.; Contestabile, A.; Petrenko, V.; Quairiaux, C.; Salmon, P.; Hüppi, P.S.; Kiss, J.Z. Endogenous erythropoietin signaling regulates migration and laminar positioning of upper-layer neurons in the developing neocortex. *Development* **2020**, *147*, dev190249. [CrossRef]
31. Noguchi, C.T.; Asavaritikrai, P.; Teng, R.; Jia, Y. Role of erythropoietin in the brain. *Crit. Rev. Oncol.* **2007**, *64*, 159–171. [CrossRef]
32. Lee, P.; Chandel, N.S.; Simon, M.C. Cellular adaptation to hypoxia through hypoxia inducible factors and beyond. *Nat. Rev. Mol. Cell Biol.* **2020**, *21*, 268–283. [CrossRef]
33. Jain, I.H.; Calvo, S.E.; Markhard, A.L.; Skinner, O.S.; To, T.-L.; Ast, T.; Mootha, V.K. Genetic Screen for Cell Fitness in High or Low Oxygen Highlights Mitochondrial and Lipid Metabolism. *Cell* **2020**, *181*, 716–727.e11. [CrossRef]
34. Sargin, D.; El-Kordi, A.; Agarwal, A.; Müller, M.; Wojcik, S.M.; Hassouna, I.; Sperling, S.; Nave, K.-A.; Ehrenreich, H. Expression of constitutively active erythropoietin receptor in pyramidal neurons of cortex and hippocampus boosts higher cognitive functions in mice. *BMC Biol.* **2011**, *9*, 27. [CrossRef]
35. Yoshimura, A.; Longmore, G.; Lodish, H.F. Point mutation in the exoplasmic domain of the erythropoietin receptor resulting in hormone-independent activation and tumorigenicity. *Nat. Cell Biol.* **1990**, *348*, 647–649. [CrossRef] [PubMed]
36. McKenzie, I.A.; Ohayon, D.; Li, H.; De Faria, J.P.; Emery, B.; Tohyama, K.; Richardson, W.D. Motor skill learning requires active central myelination. *Science* **2014**, *346*, 318–322. [CrossRef] [PubMed]
37. Liebetanz, D.; Merkler, D. Effects of commissural de- and remyelination on motor skill behaviour in the cuprizone mouse model of multiple sclerosis. *Exp. Neurol.* **2006**, *202*, 217–224. [CrossRef]
38. Liebmann, T.; Renier, N.; Bettayeb, K.; Greengard, P.; Tessier-Lavigne, M.; Flajolet, M. Three-Dimensional Study of Alzheimer's Disease Hallmarks Using the iDISCO Clearing Method. *Cell Rep.* **2016**, *16*, 1138–1152. [CrossRef] [PubMed]
39. Lein, E.S.; Hawrylycz, M.J.; Ao, N.; Ayres, M.; Bensinger, A.; Bernard, A.; Boe, A.F.; Boguski, M.S.; Brockway, K.S.; Byrnes, E.J.; et al. Genome-wide atlas of gene expression in the adult mouse brain. *Nat. Cell Biol.* **2006**, *445*, 168–176. [CrossRef]
40. R Core Team. *R: A Language and Environment for Statistical Computing*; R Foundation for Statistical Computing: Vienna, Austria, 2020. Available online: https://www.R-project.org (accessed on 18 February 2021).

152

41. Stuart, T.; Butler, A.; Hoffman, P.; Hafemeister, C.; Papalexi, E.; Mauck, W.M.; Hao, Y.; Stoeckius, M.; Smibert, P.; Satija, R. Comprehensive Integration of Single-Cell Data. *Cell* **2019**, *177*, 1888–1902. [CrossRef] [PubMed]
42. Cembrowski, M.S.; Wang, L.; Sugino, K.; Shields, B.C.; Spruston, N. Hipposeq: A comprehensive RNA-seq database of gene expression in hippocampal principal neurons. *eLife* **2016**, *5*, e14997. [CrossRef] [PubMed]
43. Harris, K.D.; Hochgerner, H.; Skene, N.G.; Magno, L.; Katona, L.; Gonzales, C.B.; Somogyi, P.; Kessaris, N.; Linnarsson, S.; Hjerling-Leffler, J. Classes and continua of hippocampal CA1 inhibitory neurons revealed by single-cell transcriptomics. *PLoS Biol.* **2018**, *16*, e2006387. [CrossRef] [PubMed]
44. Gu, Z.; Eils, R.; Schlesner, M. Complex heatmaps reveal patterns and correlations in multidimensional genomic data. *Bioinformatics* **2016**, *32*, 2847–2849. [CrossRef] [PubMed]
45. Chen, H. VennDiagram: Generate High-Resolution Venn and Euler Plots. R Package Version 1.6.20. 2018. Available online: https://CRAN.R-project.org/package=VennDiagram (accessed on 18 February 2021).

B List of publications

List of publications

Wilke, J.H., Hindermann, M., Berghoff, S., Zihsler, S., Arinrad, S., Ronnenberg, A., Barnkothe, N, **Steixner-Kumar, A.A.**, ... & Ehrenreich, H. Autoantibodies against N-methyl-D-aspartate-receptor subunit NR1 modify rather than cause encephalitis. *Submitted.*

Fernandez Garcia-Agudo, L.*, **Steixner-Kumar A.A.***, Curto, Y.*, ... & Ehrenreich H. Counterbalance between adult neurodifferentiation and microglia: role of EPO. *Under review.*

Deutsch, N.R.*, Worthmann, H.*, **Steixner-Kumar, A.A.**, ... & Ehrenreich, H., Weissenborn, K. Autoantibodies against the NMDAR subunit NR1 are associated with neuropsychiatric outcome after ischemic stroke. *Under review*.

Blokland, G.A.M., Grove, J., Chen, C., ... **Schizophrenia Working Group of the Psychiatric Genomics Consortium** ... & Goldstein, J.M. (2021). Sex-Dependent Shared and Non-Shared Genetic Architecture Across Mood and Psychotic Disorders. *Biological Psychiatry, in press*.

Steixner-Kumar, A. A., ... & Ehrenreich, H. (2021). Preadult polytoxicomania – strong environmental underpinnings and first genetic hints. *Molecular Psychiatry*, 1-12.

Butt, U.J., Hassouna, I., Fernandez Garcia-Agudo, L., **Steixner-Kumar, A. A.**, ... & Ehrenreich, H. (2021). CaMKIIα expressing neurons to report activity-related endogenous hypoxia upon motor-cognitive challenge. *International Journal of Molecular Sciences,* 22(6), 3164.

Butt, U. J.*, **Steixner-Kumar, A. A.***, Depp, D.*, ... & Ehrenreich H. (2021). Visualizing functional hypoxia as primary neuronal response to brain activity. *Molecular Psychiatry*, 1-18.

Ehrenreich, H., Wilke, J., **Steixner-Kumar, A.A.** (2020) Spontaneous serum autoantibody fluctuations: To be or not to be. *Molecular Psychiatry*, 1-3.

Kamitaki, N., Sekar, A., Handsaker, R. E., ...**Schizophrenia Working Group of the Psychiatric Genomics Consortium** ... & McCarroll, S. A. (2020). Complement genes contribute sex-biased vulnerability in diverse disorders. *Nature*, 582(7813), 577-581.

Pan, H., **Steixner-Kumar, A. A.**, ...& Ehrenreich, H. (2020) Multiple inducers and novel roles of autoantibodies against the obligatory NMDAR subunit NR1: A translational study from chronic life stress to brain injury. *Molecular Psychiatry*, 1-12.

Wakhloo, D.*, Scharkowski, F.*, Curto, Y.*, Butt, U. J., Bansal, V., **Steixner-Kumar, A. A.**, ... & Ehrenreich, H. (2020) Functional hypoxia drives neuroplasticity and neurogenesis via brain erythropoietin. *Nature communications*, 11(1), 1-12.

Garcia-Agudo, L. F.*, Janova, H.*, Sendler, L. E., Arinrad, S., **Steixner, A.A.** ... & Ehrenreich, H. (2019). Genetically induced brain inflammation by Cnp deletion transiently benefits from microglia depletion. *The FASEB Journal*, 33(7), 8634-8647.

Cross-Disorder Group of the Psychiatric Genomics Consortium (2019). Genomic relationships, novel loci, and pleiotropic mechanisms across eight psychiatric disorders. *Cell*, 179(7), 1469-1482.

Fritz, T.H., Schütte, F., **Steixner, A.**, Contier, O., Obrig, H., & Villringer, A. (2019). Musical meaning modulates word acquisition. *Brain and language*, 190, 10-15.

Fritz, T.H., **Steixner, A.**, Boettger, J., & Villringer, A. (2015). Losing track of time through delayed body representations. *Frontiers in psychology*, 6, 405.

*shared first authorship